Dehydrogenation of Alkanes using Sulfided Metal Catalysts

By

Tayyibah Tahier

Thesis submitted in fulfillment of the requirements for the degree of Doctor of Philosophy

Faculty of Natural Science

Chemistry Department

South African Institute for Advanced Materials Chemistry (SAIAMC)

University of the Western Cape

2021

Supervisor: Prof. Masikana Mdleleni

Co-supervisor: Dr. Ebrahim Mohiuddin

Declaration

I declare that "**Dehydrogenation of Alkanes using Sulfided Metal Catalysts**" is my own, unaided work submitted for the degree of Doctor of Philosophy at the University of the Western Cape, Bellville. It has not been submitted for any degree or examination in any other University, and all sources I have used or quoted have been indicated and acknowledged by means of complete references.

Name: Tayyibah Tahier Date: May 2021

Signature:

Acknowledgments

A special thanks to:

Prof. Masikana Mdleleni and Prof. David Key for their supervision and the opportunity to join the PSFIC research group

Dr. E. Mohiuddin for his excellent supervision, guidance, patience and invaluable mentorship throughout my PhD journey

My friends at SAIAMC, especially from the HYSA research group, for the best conversations, their help, resources and advice in times of distress

PETROSA and NRF for funding

My loved ones for their constant support and motivation

Presentations and Publications

1. Poster presentation (2019), Synthesis, Characterization and Catalytic Testing of Supported Nickel-Sulfided Catalysts for the Dehydrogenation of Propane, MACS 2019: Molecular Aspect of Catalysis by Sulfides, Cabourg, France
2. Tayyibah Tahier, Ebrahim Mohiuddin, David Key, Masikana M. Mdleleni, "*In-depth investigation of the effect of $MgAl_2O_4$ and SiO_2 support on sulfur promoted nickel catalysts for the dehydrogenation of propane"*, Catalysis Today, 2021, doi.org/10.1016/j.cattod.2020.12.028
3. Tayyibah Tahier, Ebrahim Mohiuddin, Alicia Botes, Madelaine Frazenburg, Subelia Botha, Masikana M. Mdleleni, "*Synthesis, characterization and catalytic activity of nickel sulfided catalysts for the dehydrogenation of propane: effect of sulfiding agent and sulfidation temperature"*, Submitted
4. Tayyibah Tahier, Ebrahim Mohiuddin, Alicia Botes, Madelaine Frazenburg, Subelia Botha, Masikana M. Mdleleni, "*Promoted effect of zinc and sulfur on the structural and catalytic properties of bimetallic nickel-zinc catalysts for the dehydrogenation of propane"*, Submitted

Nomenclature

Abbreviation	Description
γ-Al_2O_3	Gamma alumina
BET	Brunauer-Emmett-Teller
DMSO	Dimethyl Sulfoxide
FBD	Fluidized Bed Dehydrogenation
FID	Flame Ionisation Detector
FTIR	Fourier Transform Infrared
FWHM	Full Width at Half Maximum
GC	Gas Chromatography
$MgAl_2O_4$	Magnesium Aluminate
$(NH)_2SO_4$	Ammonium sulfate
$(NH_4)_2S$	Ammonium sulfide
NH_3-TPD	Ammonia-Temperature Programmed Desorption
PDH	Propane Dehydrogenation
SiO_2	Silica
STAR	Steam Active Reforming
STEM	Scanning Transmission Electron Microscopy
TEM	Transmission Electron Microscopy
TGA	Thermogravimetric Analysis
TPR	Temperature Programmed Reduction
WHSV	Weight Hourly Space Velocity
XRD	X-ray Diffraction

Abstract

Light olefins are some of the main raw materials for the petrochemical industry. With the rise in oil prices and increasing demand for olefins, there is an increasing interest in finding cheaper alternatives for processes in the petrochemical industry (PETROSA 2017). Research into the dehydrogenation of light alkanes has received significant attention. This dehydrogenation process represents a route to obtain olefins from inexpensive hydrocarbon feedstocks. The use of inexpensive hydrocarbons as a feedstock in the petrochemical industry could reduce the dependence on oil. Commercially used catalysts based on chromium or platinum have major disadvantages, including the harmful effects of chromium and the high cost of platinum, which limit their application to a certain extent. Therefore, research into developing efficient dehydrogenation systems using environmentally friendly and inexpensive metals have become highly desirable. Sulfide-containing metal catalysts have gained significant research interest for use in the dehydrogenation process and display interesting catalytic activity.

In this research project, three studies were performed in order to investigate the effect of sulfur addition on nickel catalysts for the dehydrogenation of propane to propylene. Firstly, sulfur promoted nickel catalysts supported on $MgAl_2O_4$ and SiO_2 were synthesized to investigate the effect of support material on the catalysts physicochemical properties and catalytic performance in the dehydrogenation of propane. The catalysts were prepared by the impregnation method using ammonium sulfate as the sulfiding agent. The catalysts were evaluated in both the sulfated form, $NiO/MgAl_2O_4$-20wt%SO_4 and NiO/SiO_2-20wt%SO_4, in addition to the reduced form, $Ni/MgAl_2O_4$-20wt%SO_4 and Ni/SiO_2-20wt%SO_4, which contained the sulfided species. The catalysts were characterised by XRD, BET, TEM, TGA, NH_3-TPD, FTIR and TPR techniques to investigate the particle size, surface area, morphology, acidic properties and stability of the catalysts on both $MgAl_2O_4$ and SiO_2 supports.

Structural and textural characterization of the catalysts revealed that $NiO/MgAl_2O_4$-20wt%SO_4 and $Ni/MgAl_2O_4$-20wt%SO_4 displayed highly dispersed particles in comparison to the catalysts on the SiO_2 support. The H_2-TPR analysis showed that the reducibility of the smaller particles on the $MgAl_2O_4$ support was hindered. In addition, the stronger metal-support interactions on $MgAl_2O_4$ enhanced the stability of the catalyst which enables increased activity and facilitated the desorption of olefins, leading to a high selectivity of above 70% for propylene.

The second study involved the investigation of sulfiding nickel catalysts supported on $MgAl_2O_4$, using various sulfiding agents as well as the effect of sulfidation temperatures for the dehydrogenation of propane. The catalysts were prepared by reduction of $NiO/MgAl_2O_4$, followed by sulfidation using $(NH_4)_2SO_4$ (S1), $(NH_4)_2S$ (S2) and DMSO (S3) as the sulfiding agents. The catalysts were sulfided at 200 °C, 400 °C and 550 °C to form $Ni/MgAl_2O_4$-Sx-y, where x and y represent the sulfiding agent and sulfidation temperature, respectively. Physiochemical properties of the catalysts were characterised by XRD, BET, SEM, TEM and TGA to investigate the type of nickel-sulfur species, surface area, morphology, particle size and stability of the catalysts.

Structural and textural properties revealed that the anion present on the sulfiding agent as well as the sulfidation temperature affects the type and strength of the Ni-S species, due to the varying decomposition temperatures of the sulfiding agents. For the S1 catalysts, the SO_4^{2-} ion interacted more with the support to form $MgSO_4$, while the S^{2-} ion on the S2 and S3 catalysts was responsible for the formation of the Ni_3S_2 phase. The sulfidation temperature contributed to the sulfur content(%S) present on each catalyst. Although the catalysts sulfided by S3 contained the least %S, $Ni/MgAl_2O_4$-S3-550 displayed the best catalytic performance as a result of the higher particle dispersion and stronger Ni-S interaction compared to S1 and S2 catalysts.

The third study involved the promotive effect of zinc and sulfur on the structural and catalytic properties of a Ni-Zn bimetallic system for the dehydrogenation of propane. The supported Ni-Zn bimetallic system was prepared by the wetness impregnation method using $Ni(NO_3)_2$ and $Zn(NO_3)_2$ as the metal precursors. The Ni:Zn system was synthesized with varying amounts of each metal according to the following wt% ratios: 13:0, 11:2, 9:4, 6.5:6.5, 4:9, 2:11 and 0:13. The catalysts were characterised by TPR, XRD, BET, and TEM analysis. Structural and textural properties showed that when the ratio of Zn increased to > 4 wt%, the formation of the NiZn alloy was observed.

The promotive effect of Zn was most evident on the 9Ni-4Zn/SiO_2 catalyst, due to the ensemble effect. As the wt% of Zn increased, the particle size decreased and the selectivity toward propylene was improved. The improved catalytic activity for 6.5Ni-6.5Zn/SiO_2, 4Ni-9Zn/SiO_2 and 2Ni-11Zn/SiO_2 was attributed to the formation of the NiZn alloy, with smaller particle size and hydrogenolysis sites that are blocked as a consequence of the strong Ni-Zn interaction. Selectivity toward propylene equalled 49%, 54% and 64% for the 6.5Ni-6.5Zn/SiO_2, 4Ni-9Zn/SiO_2 and 2Ni-11Zn/SiO_2 catalysts compared to 0% for the monometallic 13Ni/SiO_2 catalyst.

In separate experiments, the effect of sulfur addition to the bimetallic system was explored. XRD analysis revealed the presence of the ZnS phase and the absence of the NiZn alloy. In the Ni-Zn bimetallic system, it was found that zinc had a higher affinity for sulfur and caused a repulsive interaction between nickel and sulfur, thereby inhibiting the formation of a nickel-sulfided phase. The selectivity toward propylene increased from 8% for 9Ni-4Zn/SiO_2 to 64% for 9Ni-4Zn/SiO_2-S in the first three minutes of reaction time. Both zinc and sulfur exhibited beneficial geometric and electronic effects, which affect particle size and olefin desorption for improved dehydrogenation activity.

Table of contents

List of tables

CHAPTER 1

CHAPTER 2

CHAPTER 3

CHAPTER 4

CHAPTER 5

List of figures

CHAPTER 1

CHAPTER 2

CHAPTER 3

CHAPTER 4

CHAPTER 5

CHAPTER 1: INTRODUCTION

This chapter outlines the motivations for the work conducted and presented in this thesis. A brief background of this research project will be discussed in this chapter. The rationale for using supported nickel catalysts and the incorporation of sulfur into these catalysts for the dehydrogenation of propane will be given. Two different supports, namely, $MgAl_2O_4$ and SiO_2, were utilized for the catalysts in this study. Various sulfiding agents were used to sulfide the metal catalysts. The properties of these sulfiding agents will be summarised in this chapter. Bimetallic catalysts and the effects of sulfur addition to bimetallic catalysts have been investigated. The aims and objectives of this project are stated at the end of this chapter.

General introduction

Heterogeneous catalysis constitutes more than 80% of the processes in chemical production. The research involved in heterogeneous catalysis aims at the design of clean, energy efficient catalytic processes. This ultimately leads to reduced waste and less by-products.[1] Heterogeneous catalysts are preferred over homogeneous catalysts due to their excellent reusability as well as their chemical stability, thermal stability and ease of recovery. These advantages establish heterogeneous catalysts as environmentally friendly catalysts and appealing to industrial processes. Heterogeneous catalysts have found applications in industry for the dehydrogenation of light alkanes, mainly ethane, propane and butane.[2,3]

Light olefins, such as propylene, are known to have widespread applications in the petrochemical industry and refining. Steam cracking of hydrocarbons and fluid catalytic cracking from crude oil distillation are two main processes for the production of propylene. Approximately 56% of propylene is obtained as a by-product by steam cracking and approximately 33% is produced as a by-product of fluid catalytic cracking. To meet the continuous, growing demand for propylene, the remaining propylene production is required by several on-purpose technologies such as propane dehydrogenation.[3–7]

Compared with the low selectivity of mainstream reactions for light olefin production, in the steam cracking and fluid catalytic cracking processes, propane dehydrogenation can convert one feedstock into a particular olefin, instead of a mixture of products. In 2013, the global demand for propylene was 84 million ton/year up from 65 million ton/year in 2009. It is estimated that the demand will reach 120 million tons annually by 2022. With an increasing demand for propylene, research into alkane dehydrogenation has drawn considerable attention.[3,6,7]

Alkane dehydrogenation is an endothermic, thermodynamically limited process that requires high temperatures and low pressures to obtain substantial yields of alkenes. The dehydrogenation of hydrocarbons involves breaking of two carbon-hydrogen bonds with the simultaneous formation of a hydrogen molecule and an alkene.[8] Furthermore, the high reaction temperatures favour thermal cracking reactions to lighter alkanes and catalyst deactivation by coke formation.[9,10]

The catalytic dehydrogenation of alkanes represent a route desirable to industry since alkenes could be obtained from low-cost saturated hydrocarbons.[10,11] The use of low value hydrocarbons as feedstock in the petrochemical industry could reduce the dependence of oil. However, the activation of alkanes is a challenge and requires an efficient catalyst. It is important to develop a cost effective and efficient process to convert alkanes to olefins. Cr-based and Pt-based catalysts are two commonly used catalysts for dehydrogenation reactions on a commercial scale. Although the performance of these catalysts is satisfactory for industry, the harmful impacts of Cr and high cost of Pt have limited their application to some extent.[5] Alternatively, even with research geared on alternative routes, such as oxidative dehydrogenation, it is difficult to control the extent of oxidation, which leads to large quantities of CO_x and decreased selectivity toward desired olefins. Thus, the major challenge in dehydrogenation processes is to develop a new type of catalyst with cost effective and environmental friendly properties in addition to having excellent catalytic performance in the absence of oxidants.[5]

Transition metals can activate saturated hydrocarbons and for practical purposes, mostly heterogeneous catalysts are used, partly because they can operate at high temperature.[12] Several types of heterogeneous catalysts have been used in industry for the dehydrogenation of light alkanes. Transition metal catalysts, including chromium catalysts and platinum catalysts, are commonly used on a commercial scale. However, it has been shown that carbon-carbon bond insertion is more favourable on thermodynamic grounds than carbon-hydrogen bond insertion over Ni, Co and Fe ions. Although high catalytic activity can be obtained over these metal based catalysts, the reaction exhibits poor selectivity due to aggravated hydrogenolysis reactions, forming methane as the main product instead of the desired alkene.[3,5,10,11] Researchers have since modified and promoted these transition metal catalysts in an attempt to make the catalysts more selective.

An important factor to consider when developing dehydrogenation catalysts is the effect of support, which significantly influences the dispersion, electronic properties of the active components and acid-base properties of the catalysts.[13,14] Interactions between catalytically active metals and supports have been linked to a wide range of physical and chemical observations, which are related to stability, activity and selectivity of the catalysts.[15] The most commonly used catalyst supports in industry include SiO_2 and Al_2O_3.[16] Recently, there has been growing interest in the utilization of magnesium aluminate spinel, $MgAl_2O_4$, as a catalyst support in the field of environmental catalysis, petroleum processing and fine chemicals productions.[21–23] There has not been much reported on the effects of supports on the physicochemical properties of the catalyst.

Sulfur promoted catalysts are a relatively new class of catalysts. Interestingly, sulfur containing compounds have been notoriously known to act as a poison for metal catalysts due to their strong coordinating and adsorptive properties, which usually lead to the blocking of active catalytic sites.[20] Nevertheless, studies have shown that the addition of sulfur to transition metal catalysts to form metal sulfided catalysts, reduces unwanted side reactions, such as hydrogenolysis and cracking, and increases dehydrogenation activity significantly.[4,11]

In general, the promoting effect of sulfur can be understood in two aspects: 1) the geometric effect and 2) the electronic effect. It has been observed that the loss of sulfur during the dehydrogenation reaction is responsible for catalyst deactivation. To replenish the loss of sulfur, continuous sulfidation cycles have been implanted. Hence, the catalyst performance can be maintained at a high level.[11]

There are numerous ways to add sulfur to a catalyst. One way that may appear attractive is to use naturally occurring sulfur in the feedstream as it avoids the cost of purchasing a sulfiding agent. However, the disadvantage of this method is that the catalyst surface will accumulate coke before sulfiding is complete. This would consequently lead to reduced catalyst activity and service life. The cost of reduced catalyst activity and catalyst lifetime far exceeds any savings on sulfiding agents.[21]

In this regard, various sulfiding agents have been used as a source of sulfur on catalysts. The most common sulfiding agent is H_2S gas, however, less toxic, inexpensive sulfur sources have been explored in the literature.[4,22–24] In this project ammonium sulfate, ammonium sulfide and dimethyl sulfoxide (DMSO) have been studied as sulfiding agents for the metal sulfided catalysts. To the best of our knowledge, not much attention has been paid in the literature to the sulfidation temperature on dehydrogenation catalysts. A comparison of the physical and chemical properties of these reagents are displayed in Table 1.1. These reagents are relatively safe, easy to handle and emit some form of sulfur when heated.

Table 1.1: Comparison of physical and chemical properties of $(NH)_2SO_4$, $(NH_4)_2S$ and DMSO

Property	Ammonium Sulfate $(NH)_2SO_4$	Ammonium Sulfide $(NH_4)_2S$	DMSO
Appearance	White crystalline solid	Yellow liquid	Clear liquid
Formula	$H_8N_2O_4S$	H_8N_2S	C_2H_6OS
Sulfur content (wt%/wt)	24	47	41
Decomposition temperature (° C)	250	100	189
Flash point (° C)	N/A	32	87
Odour	Odourless	Rotten eggs	Low odour

In alkane dehydrogenation, additional metals may be introduced to the catalysts containing the active metal serving as promoters. Bimetallic catalysts, which often possess chemical properties that are distinct from their parent metals, may display enhanced performances. Among bimetallic catalysts, Pt-group metals are the most researched catalyst components.[25]

It is well known that the Pt-Sn supported on γ-Al2O3 catalytic system is one of the most efficient catalysts for alkane dehydrogenation. The effect of Sn has been explained in terms of the geometric effect and/or the electronic effect. In terms of the geometric effect, Sn decreases the ensemble size of Pt particles, thereby reducing hydrogenolysis and coking that require large Pt ensembles. For the electronic effect, Sn modifies the electronic density of Pt, due to a positive charge transfer from Sn^{n+} or due to the different electronic structures of Pt-Sn alloys. The catalytic properties of Pt-Sn catalysts depend on the interactions between Pt and Sn, the preparation method, Pt/Sn ratio as well as the Sn state.[26] Nevertheless, during dehydrogenation reactions, the acidity of the alumina support can catalyse undesirable cracking and isomerisation reactions. Hence, a need for selectivity and stability improvements exist.[27,28]

In addition, Zn is commonly added to noble metal catalysts to control catalyst activity and selectivity in a wide range of reactions, including dehydrogenation processes.[26,27,29,30] The Pt-Zn system resembles the Pt-Sn system is some aspects. However, Zn-bimetallic catalysts have not been studied as extensively as the more common Sn-based systems.[31] Platinum and zinc can also form alloy phases (eg. PtZn, Pt_3Zn) of various stoichiometries, which may display distinctive behaviour as compared to the monometallic platinum.[32] The introduction of sulfur on bimetallic Pt catalysts have displayed beneficial effects on various reactions.[33,34]

Much attention has turned to nickel in the field of bimetallic catalysis, since it is cost effective, abundant and displays similar electronic characteristics as platinum. Nickel is known to easily combine with all noble metals and many transition metals.[25] In addition, bimetallic sulfided catalysts have shown promising catalytic abilities for various reactions.[35,36]

Aims and objectives

The aim of this project is to prepare, characterise and evaluate the performance of sulfur promoted nickel-based catalysts for the dehydrogenation of propane to propylene.

The objectives of this research project are listed below:

- Investigate the effect of $MgAl_2O_4$ and SiO_2 supports on sulfur promoted nickel catalysts for the dehydrogenation of propane
- Investigate the effect of $(NH_4)_2SO_4$, $(NH_4)_2S$ and DMSO sulfiding agents and sulfidation temperature on sulfided nickel catalysts for the dehydrogenation of propane
- Investigate the promotive effect of zinc and sulfur addition on the structural and catalytic properties of a bimetallic nickel-zinc catalyst for the dehydrogenation of propane

Literature review

The dehydrogenation of light alkanes has become exceedingly important in recent times. A complete overview of relevant terms and topics obtained from the literature will be discussed in this chapter. Firstly, dehydrogenation will be discussed, considering industrial processes that have been patented and applied as well as the thermodynamics behind dehydrogenation processes. The utilization of platinum and chromium catalysts along with their limitations will be discussed, followed by a review on transition metal catalysts, with a focus on sulfided metal catalysts. The effect of sulfur promotion and support will be detailed. Research performed on bimetallic catalysts is vast and the beneficial properties of using these systems will be explored at the end of this chapter.

1.1 Dehydrogenation of light alkanes

Light olefins, such as propylene or ethylene, continue to serve as a fundamental basis for the chemical industry and refining. Steam cracking and fluid catalytic cracking are the major sources of light olefins. Both processes produce various compounds simultaneously. Variations in the operating conditions can roughly modify the composition of products. However, this may not be sufficient when the demand for one product is higher than the co-products. For example, the demand for propylene is growing faster than ethylene in many geographical areas. In this case, the ability to synthesize a pure product, such as propylene through propane dehydrogenation, can prove more successful than the "multi-product" approach.[6,8]

The dehydrogenation reaction of propane to propylene has an activation energy of ~121 – 143 kJ/mol and is presented by the following equation:

$$C_3H_8 \longleftrightarrow C_3H_6 + H_2$$

The reaction is thermodynamically limited and highly endothermic, which according to Le Chatelier's principle, implies that higher temperatures and lower hydrocarbon partial pressures are needed to favour the forward reaction and attain higher conversions. Temperatures of 550 °C – 750 °C are typically required for the dehydrogenation of C_2-C_4 paraffins to obtain alkane conversions of ≥ 50% at 1 bar.[6]

It is reported that the enthalpy required for the dehydrogenation of alkanes decrease as the chain length becomes longer (**Figure 1.1**). The primary reaction in catalytic dehydrogenation is the formation of mono-olefins from the corresponding alkane feed.[6,8,37–42]

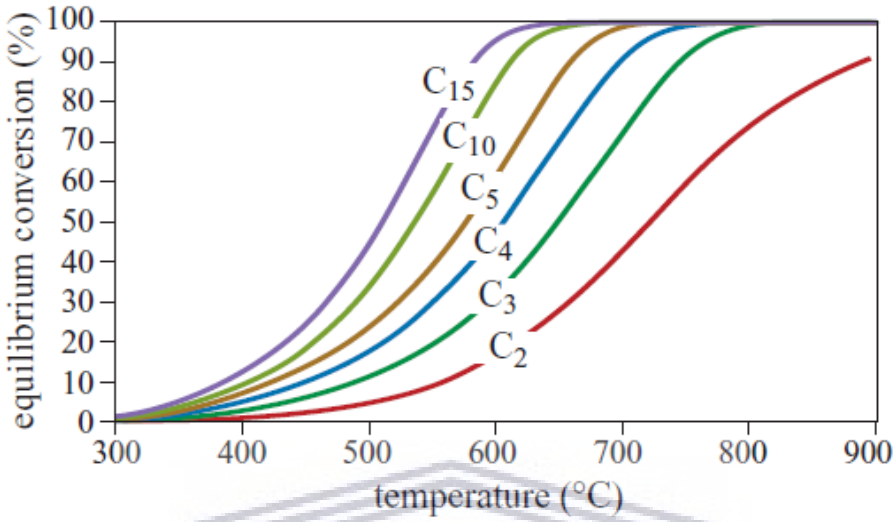

Figure 1.1. Equilibrium conversion in the dehydrogenation of some paraffin at atmospheric pressure.[8]

The most important factor of light alkane dehydrogenation is the energy supply for the endothermic reaction. The C-C bonds in alkanes and olefins are more reactive than C-H bonds, meaning that catalysts which favour C-H cleavage relative to C-C bond cleavage are required to avoid side reactions. In addition, olefins are more reactive than their alkane counterparts, which could further lead to unwanted and secondary reactions. There are three main types of side reactions that can occur; 1) hydrogenolysis, 2) cracking and 3) isomerization.[6,41,43,44]

In hydrogenolysis, a C-C bond within a paraffin is cleaved in the presence of hydrogen, resulting in the formation of two smaller alkane molecules. Cracking also involves the cleavage of a paraffin to form two smaller hydrocarbons, however, in this instance no hydrogen is required. Thermal cracking processes occur at low pressures and high temperatures varying between 600 °C – 850 °C depending on the feedstock being used. This reaction results in the formation of a radical intermediate, which rearrange to form an alkane and an alkene. Catalytic cracking is different in a manner since it requires a catalyst with Bronsted and Lewis acidity and the reaction proceeds by forming a carbocation intermediate, also resulting in the formation of an alkane and an alkene.[6,45,46]

Isomerization can be defined as the rearrangement of atoms within a molecule. For example, during the dehydrogenation of isobutane to isobutene, the alkane could transform to 1- or 2-butene, which could dehydrogenate further to 1,3-butadiene. It is quite complex to optimize dehydrogenation reactions and limit side reactions.[6]

The high temperatures required for a high olefin yield leads to the formation of coke. Consequently, the catalyst deteriorates with time on stream and frequent regeneration of the catalyst is required to maintain catalyst activity. Therefore, the operational conditions in any industrial process should be a compromise between reasonable olefin conversion levels and high selectivity. The production of olefins by the catalytic dehydrogenation of light paraffins should produce high yields of the desired olefins over long periods of time without shutdowns and high operating efficiency. The nature of dehydrogenation reactions can pose a formidable challenge in industry. The focus of research in this field has been to find a method to supply sufficient amounts of heat, owing to the thermodynamic limitations of dehydrogenation reactions, as well as to manage catalyst regeneration cycles.[6,8,38,39]

1.2 Commercial dehydrogenation technologies

The main industrial technologies for the dehydrogenation of light alkanes, such as propane, are Catofin, Oleflex, STAR (Steam Active Reforming), FBD (Fluidized Bed Dehydrogenation) and PDH (Propane Dehydrogenation). A schematic of reactor configurations used in the different industrial technologies are illustrated in **Figure 1.2**.

An efficient reaction system for the industrial application of dehydrogenation of light paraffins should supply a large amount of heat, due to the endothermic nature of dehydrogenation reactions, while simultaneously minimizing the formation of by-products.[47–50] In addition, the system must regenerate the catalyst by removing carbon deposits that accumulate on the catalyst surface. These conditions have urged researchers to develop optimal reactor designs for the industrial application of dehydrogenation reactions. The available commercial processes offer various options with regard to reaction systems, tending to optimize the supply of energy to the system and catalytic cycles.[8,38]

The technical characteristics and limitations of known industrial technologies for the dehydrogenation of light alkanes will be discussed briefly in the following sections. Industrial dehydrogenation technologies can be classified according to catalyst type, composition, reactor design and mode of heat input.[51] Detailed descriptions of the main commercialized technologies are given below and reaction conditions are summarized in Table 1.2.

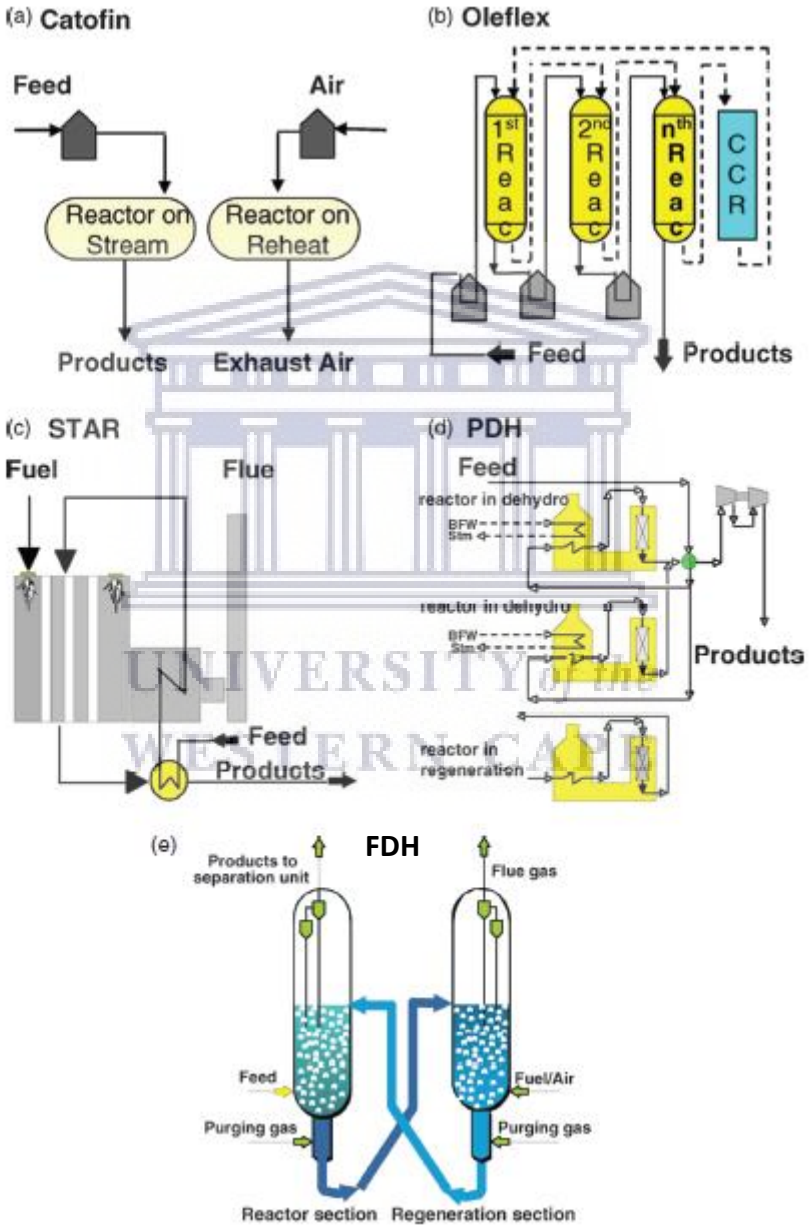

Figure 1.2. Schematic diagram of reactor designs used in various industrial technologies a) Catofin, b) Oleflex, c) STAR, d) PDH and e) FDH[52,53]

1.2.1 Catofin technology

The Catofin process, by CB&I Lummus, is based on the Houdry Catadiene process.[6] This process was extensively employed for the dehydrogenation of isobutane to isobutene. In turn, isobutene was used to produce methyl tertiary butyl ether (MTBE), a fuel additive used to raise the octane number in gasoline. The use of MTBE has decreased in recent years due to environmental concerns. This caused a shift in the use of Catofin process for alternative purposes such as the dehydrogenation of propane.[6,37,54]

The Catofin process consists of multiple parallel adiabatic fixed-bed reactors, where dehydrogenation of propane and catalyst regeneration by decoking are carried out alternatively over roughly 10 minutes for each operation. During the process, the temperature is gradually decreased by the endothermic reaction. The bed temperature is then restored to the original temperature during the exothermic Regen period. Therefore, the process is performed in short, successive dehydrogenation-regeneration cycles.[55,56] The catalyst lifespan is between 2-3 years, whereby the loss in catalyst activity with increasing time on stream is counteracted by increasing the temperature to afford a constant dehydrogenation activity throughout the catalyst lifespan. Typical operating conditions require a temperature range from 587 °C – 647 °C and pressure from 33 kPa – 50 kPa.[6,8,57]

In traditional Catofin processes, the reactor or catalyst bed is purged with hot air during the regeneration cycle in order to reheat the catalyst and remove coke which has been deposited during the dehydrogenation step. However, since the regeneration cycle is short, there is a strong possibility for the formation of a vertical temperature gradient and pressure drop across the catalyst bed, which has adverse effects on the overall yield of the olefin product. Hence, with the hot air flow and combustion of coke as the main heat sources, heat input to the catalyst bed is a critical limiting factor to Catofin dehydrogenation processes.[58]

1.2.2 Oleflex technology

The Universal Oil Products (UOP) Oleflex process consists of three sections: the reactor section; the product recovery section and the catalyst regeneration section. The reactor section is made up of three or more moving bed reactors, charge heater for preheating the hydrocarbon feed, interstage heaters and a feed-effluent gas-gas exchanger. In the product recovery section, the reactor effluents are cooled and compressed, which is then sent to the cryogenic system for hydrogen and hydrocarbon separation or recovery. The catalyst flows at a slow rate, while the reagents flow radially within the various reactors.[38,59]

The Oleflex process consists of intermediate heating stages. The process comprises of a reactor sector as well as a product recovery section.[39,60] The Oleflex process is performed with a moving bed of Pt catalyst in a multi-stage reactor unit. Three or four reactors are required for 40% conversion in the dehydrogenation of propane. This technology requires a high mechanical strength of the catalyst.[61]

1.2.3 Steam Active Reforming (STAR) technology

The STAR dehydrogenation process is currently owned and licensed by Krupp-Uhde.[38] The reactor design is similar to a steam reforming setup that is operated until deactivation of the catalyst occurs as a result of coke formation. The technology consists of a fixed-bed, fire-tube reactor operating at high pressure with steam acting as a diluent to lower the partial pressure of the reactants in order to obtain feasible conversion levels.[8,38,39,62]

1.2.4 Fluidized Bed Dehydrogenation (FBD) technology

The FBD technology, licensed by Snamprogetti-Yarsintez, employs fluidized-bed reactors without diluents and operating at atmospheric pressure.[63] The catalyst circulates continually from the reactor to the regenerator plant and back to the reactor. The heat required for the reaction is provided by a fuel burned directly in the regenerator and then transported to the reactor through the heat capacity supplied by the regenerated catalyst.[8,52] The FBD process is well developed. It is characterized by low capital expenditures, power intensity and low product costs.

However, this process is not promising for the future, as the catalyst(chromium-based) is not environmentally friendly and carcinogenic. An additional problem is the disposal of the spent catalyst and finely divided phases formed in the process.[61]

1.2.5 Propane Dehydrogenation (PDH) technology

The Linde-BASF-Statoil PDH technology has elements in common with the STAR technology, since it uses fixed-bed reactors where the heat of the reaction is supplied by externally burning a fuel.[8] Three of these reactors work in parallel, with two operating in dehydrogenation mode and one in regeneration mode, thereby ensuring a continuous flow of reaction products. The distinctive characteristic of PDH technology is the absence of reagent dilution, which reduces the reactor dimensions and allows for the simple purification of the product.[6,8,38,52]

Table 1.2: Commercial dehydrogenation processes for light alkanes[51]

Technology name	**Catofin**	**Oleflex**	**STAR**	**FBD**	**PDH**
Licensor/Developer	CB&I-ABB Lummus	UOP LLC (Honeywell)	Krupp-Uhde	Yarsintez-Snamprogetti	Linde-BASF-Statoil (Sintef)
Reactor design	Adiabatic fixed-bed	Adiabatic moving bed	DH reactor + adiabatic oxyreactor	Fluidized bed	Isothermal fixed-bed
Catalyst type	Cr_2O_3/Al_2O_3 promoter	$Pt/Sn/Al_2O_3$ promoter	$Pt\text{-}Sn/ZnAl_2O_4$	Cr_2O_3/Al_2O_3 promoter	Cr_2O_3/Al_2O_3 $Pt\text{-}Sn/ZrO_2$
Regeneration mode	Air oxidation	Air oxidation and reduction in H_2	Air oxidation and redcuction in H_2	Air oxidation	Air oxidation
Operation	Cyclic	Continuous	Cyclic	Continuous	Cyclic
Temperature (° C)	565-649	550-620	550-590	535-590	~590
Pressure (bar)	0.3-0.5	2-3	5-6	0.5-1.5	~1
Conversion (%) C3	48-65	25	40	40	30
Selectivity (%) C3	82-87	89-91	89	89	90
Heat import	From catalyst regeneration	Interstage heating	Catalyst tubes placed in furnace	From catalyst regeneration section	Heating of the reactors

1.3 Commercial catalysts

Industrial heterogeneous catalysts can be classified into three major categories according to the metal that acts as the active component: 1) Pt-based catalysts; 2) Cr-based catalysts and 3) other heterogeneous metal catalysts. Although extensive improvements in both Pt-based and Cr-based catalysts and process conditions have been made, catalyst stability and regeneration remain a challenge. Therefore, research into alternative transition metal catalysts has gained considerable attention.[3,64]

1.3.1 Platinum catalysts

The platinum-based catalysts are known for their excellent dehydrogenation activity and ability to form thermally stable dispersions on suitable supports. These catalysts are used widely on a commercial scale for dehydrogenation processes. To modify their catalytic properties, the supported platinum catalysts often contain other inactive metals, such as Sn, Ga or In, which reduce the tendency to form coke. In commercial catalysts, Sn is commonly used as a promoter on Pt catalysts by dividing the Pt particles into smaller ensembles. These Pt-Sn particles reduce coke formation by stabilizing the well dispersed phase of the active component. The addition of Sn to Pt can modify the electronic nature of the Pt atoms, which induces a decrease in adsorption energy of precursors for coke formation. Reactions are modified from hydrogenolysis to dehydrogenation. This is attributed to the different adsorption modes and adsorption energies of the reactants and products over the Pt and Pt-Sn catalysts.[3,40,41,64–66] Liu *et al*. found that strong acid sites of Pt catalysts were partly neutralized or weakened after introducing Sn, which can suppress unwanted side reactions.[64]

Supported Pt-Sn catalysts have been applied in the Oleflex, STAR and PDH technologies.[5] Improving platinum-based catalysts for propane dehydrogenation has been a hot topic for various research studies. It is desirable to obtain the highest possible degree of dispersion for the most efficient use of metal catalysts. This is particularly important for the costly noble metal platinum. The choice of support and reaction conditions, such as co-feeding, are factors taken into consideration in order to have an advantageous effect on the catalytic activity and selectivity toward propylene.[40,67]

Although platinum-based catalysts have been successfully used on an industrial scale for the dehydrogenation of propane, limitations of these catalysts do exist. For example, Pt-Sn catalysts require oxychlorination for regeneration in order to maintain their catalytic properties, since coke burning via simple oxidation results in metal sintering and gradual change of the alloy state of the Pt-Sn catalysts. The oxichlorination requires the use of corrosion-resistant metallurgy for reactor design and an additional process to eliminate corrosive chlorine compounds in the vent gas.[68] Platinum catalysts are expensive and suffer from fast deactivation due to rapid coke formation and sintering at the required high tempeartures.[40,41,65]

1.3.2 Chromium-based catalysts

The beneficial properties of chromium catalysts in dehydrogenation processes have received widespread attention in industry. The chromium-based catalysts are typically composed of chromium oxide dispersed on a porous alumina support, doped with alkali metals. The Cr_2O_3 phase, which constitutes the active component, is present in the catalyst between 10% - 20% by weight. Other supports such as zirconia, silica and magnesium oxide have also been tested for chromium-based catalyst. The CATOFIN and FBD technologies are the two industrial processes which utilize the Cr-based catalysts.[3,9,69–72] However, major challenges associated with this catalytic system are cracking and coking, which have a negative effect on the product selectivity and catalyst stability. The deactivated catalyst must frequently be regenerated while maintaining dehydrogenation activity, which results in the process being complex and expensive.[73]

The dehydrogenation activity of chromium catalysts is ascribed to the unsaturated Cr^{3+} ions.[69,74] With variations in sample properties and treatment conditions, three types of Cr^{3+} ions have been observed: i) redox Cr^{3+} formed from the reduction of Cr^{5+} and Cr^{6+} which is present on oxidized samples, ii) non-redox Cr^{3+} in an amorphous chromia phase that is present in both oxidized and reduced samples, and iii) the Cr^{3+} present in crystalline chromia. The redox Cr^{3+} phase is most abundantly found on alumina-supported catalysts at low chromium contents. The amount of amorphous chromia increases with the total chromium content and the crystalline chromia. It has been suggested that both redox and non-redox Cr^{3+} are active in dehydrogenation reactions, whereas crystalline chromia is less active.

The harmful effects of chromium to humans and the environment is the main reason why research into alternative eco-friendly catalysts has gained considerable attention.[51,69,75] In the case of CrO_x catalysts, the regeneration process via coke combustion cause the incorporation of CrO_x into the Al_2O_3 framework, leading to the gradual loss of accessible catalytically active sites.[68] Previous studies have shown that supported chromia catalysts deactivate during alkane dehydrogenation reactions, due to coke deposition.[76] Shee *et al*. found that regenerated catalysts displayed lower catalytic activity than the corresponding fresh catalysts for light alkane dehydrogenation reactions. Their characterisation studies of the spent and regenerated catalysts indicated that during alkane dehydrogenation a portion of surface accessible Cr(III) species is converted to inaccessible Cr(III) species buried in the alumina matrix. These inactive Cr(III) species could not be converted to higher oxidation states during the regeneration step. It was speculated that the partial irreversible loss of activity is associated with the formation of the Cr(III) species.[76]

1.4 Other heterogeneous metal catalysts

Extensive improvements in both platinum and chromium catalysts and process conditions have been made, however, catalyst stability and regeneration remain a challenge. It is evident that platinum and chromium catalysts will continue to play a major role in the dehydrogenation processes on an industrial scale despite disadvantages, such as the cost of platinum and hazardous effects of chromium, which could limit their applications to some extent.[3,64] Therefore, alternative, transition metal catalysts, with low cost and environmentally friendly characteristics are highly desirable.[3]

The oxidative dehydrogenation of alkanes, an alternative route to dehydrogenation, has been studied widely due to the thermodynamic advantages of this process. Research has been focused on vanadium-based and molybdenum-based catalysts. Attempts have been made to modify the catalyst formula and to select mild oxidants. However, oxidation reactions inevitably occur, which lead to the formation of CO_x and inferior selectivity toward alkenes. Thus, it is difficult to make significant progress using this route. The development of a catalytic system with excellent dehydrogenation performance in the absence of oxidants is important. Nickel-based catalysts have gained considerable attention due to the low cost, abundance of nickel and favourable catalytic performance in dehydrogenation reactions. [11,38,65,77–79]

1.4.1 Metal-sulfided catalysts

Several metal-sulfided catalysts have been investigated for the dehydrogenation of alkanes. Among the transition metal catalysts, Fe-, Co- and Ni-based catalysts are highly active and selective for propane dehydrogenation reactions with co-feeding of H_2S.[4,5,11,22,80,81]

Resasco *et al*. describe the use of heavily sulfided nickel catalysts supported on non-acidic alumina for the dehydrogenation of isobutane to isobutene.[4] It was shown that these catalysts are active and selective for relatively long periods under low hydrogen/hydrocarbon ratios, resulting in an important advantage over existing technologies. The authors studied the effect of adding sulfur, in the form of dimethyl sulfoxide (DMSO), to samples of $Ni/Cs\text{-}Al_2O_3$ and monitoring the catalytic performance in the flow reactor. DMSO was added to the oxidized sample at 200 °C at a sulfur:metal ratio of 1:2, before the temperature was raised to 400 °C. The catalyst was then flushed with H_2 for 30 minutes, purged with N_2, passivated in a 1% O_2 atmosphere and exposed to air.[4]

Figure 1.3 illustrates the variation of the dehydrogenation reaction rates for the sulfided nickel catalyst and the unsulfided platinum catalyst. Over the initial hours on stream, the conversion increased with time, while carbon selectivity toward isobutene remained constant above 90 % (not shown in the graph). It can be noted that there is a higher conversion to isobutene for the nickel sulfided catalyst in comparison to the platinum catalyst. However, an induction period was observed, during which the nickel sulfided catalyst activity increased to a maximum at 10 hours. Data obtained for the unsulfided platinum catalyst showed no induction period and a continuous deactivation of the catalyst.[4]

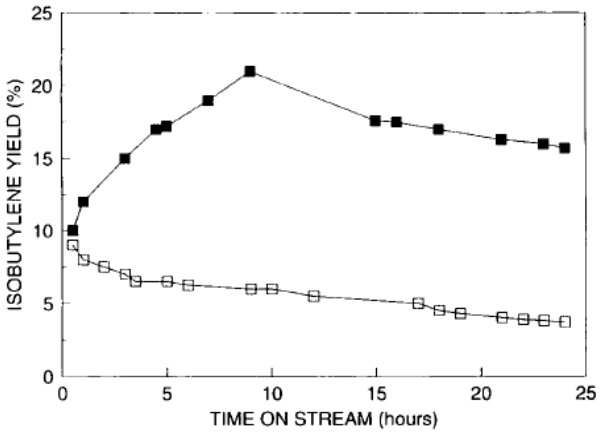

Figure 1.3. Activity of sulfided Ni catalyst (■) *vs.* unsulfided Pt catalyst (□) as a function of TOS.[4]

Wang and co-workers investigated the performance of supported metal sulfides for the dehydrogenation of isobutane to isobutene, with inert silica chosen as the support.[5] A variety of eco-friendly and inexpensive metal oxides, with 13 wt % loading supported on silica were prepared using H_2S/H_2 flow to form the desired sulfided catalysts.[5] The physiochemical properties and dehydrogenation performance of SiO_2-supported metal oxide and corresponding sulfided catalysts are shown in Table 1.3.

The surface area of all the metal oxide catalysts was larger than 220 m^2/g and the pore volume was in the range 0.86-1.01 cm^3/g. Even though the surface area and pore volume of the catalysts decreased slightly after being sulfided, there was no negative effect on the pore structure of the catalyst. Isobutane conversion and selectivity towards isobutene behaved in opposite ways as shown by the results of the unmodified NiO/SiO_2 catalyst, which displayed the highest isobutane conversion and the lowest selectivity. The NiO/SiO_2 catalyst generated a large amount of methane, which is indicative of high activity for C-C bond breaking. After the metal oxides were sulfided with H_2S/H_2, all the catalysts except NiO/SiO_2 revealed improved isobutane conversion. The selectivity toward isobutene was higher than 80 wt % for most of the catalysts, demonstrating the efficient ability of the metal sulfided catalysts for C-H bond activation.[5]

Table 1.3: Physiochemical properties and catalytic performance of SiO_2-supported metal oxide and corresponding metal sulfide catalysts for isobutane dehydrogenation[5]

	oxide catalysts				sulfide catalysts			
	S_{BET},m^2/g	V_p,cm^3/g	$C_{isobutane}$[b], wt%	$S_{isobutene}$[c], wt%	S_{BET},m^2/g	V_p,cm^3/g	$C_{isobutane}$[b], wt%,	$S_{isobutene}$[c], wt%
ZnO/SiO_2	252	1.01	4.2	66.9	249	0.98	28.4	80.6
CuO/SiO_2	248	0.97	3.7	68.6	244	0.93	64.9	84.7
MnO_2/SiO_2	245	0.91	19.1	56.6	240	0.87	62.8	84.5
MoO_3/SiO_2	234	0.87	6.4	66.4	229	0.81	65.2	79.8
Fe_2O_3/SiO_2	239	0.88	13.3	43.5	236	0.84	69.2	86.6
Co_3O_4/SiO_2	225	0.86	14.1	25.3	211	0.71	71.1	87.0
NiO/SiO_2	236	0.88	91.1	7.6	234	0.74	67.0	87.6

[a]Reaction conditions: temp, 560˚C; 4g of catalyst loaded; 14.3 vol % i-C_4H_{10} in nitrogen at a total flow rate of 14 mL min^{-1}. [b]Conversion of isobutane. [c]Selectivity to isobutene, and all the data were obtained at the very beginning of the reaction.

The dehydrogenation performance of industrially relevant catalysts, Cr_2O_3/Al_2O_3 and $Pt\text{-}Sn/Al_2O_3$, were compared with the metal-sulfided catalysts under the same reaction conditions. As listed in Table 1.4, both catalysts were less active in dehydrogenation than most of the sulfided catalysts. To exclude the effect of metal content and support, $13Pt/SiO_2$ and $13Cr_2O_3/SiO_2$ catalysts were prepared and evaluated for isobutane dehydrogenation.

The dehydrogenation performance was not better than that of the industrial catalysts (Table 1.4), which could be due to the weak interaction between the silica support and the active component. The aggregation of Pt particles on $13Pt/SiO_2$ could also contribute to the poor dehydrogenation performance.[5]

Table 1.4: Catalytic performance of commercial catalysts for isobutane dehydrogenation[5]

	$C_{isobutane}$[b], wt%	$S_{isobutene}$[c], wt%
Cr_2O_3/Al_2O_3[d]	54.5	82.4
$Pt\text{-}Sn/Al_2O_3$[e]	49.7	86.2
Cr_2O_3/SiO_2[f]	48.4	84.9
Pt/SiO_2[g]	42.7	78.1

Although the dehydrogenation performance was improved after the metal catalysts were sulfided, the catalytic activity was less stable than that of the commercial catalysts. The deactivation of the catalysts was attributed to the loss of sulfur from the metal catalysts. Furthermore, an online mass spectrometer was used to detect the released gases during isobutane dehydrogenation over the sulfided catalysts. For the sulfided NiO/SiO_2 catalyst, in addition to isobutane, hydrogen and isobutene, H_2S was detected, indicating that sulfur was lost mainly in the form of H_2S gas. To recover the catalytic activity, the spent NiO/SiO_2 catalyst was sulfided by H_2S/H_2 for another 3 hours after an 8 hour reaction. In total, 5 sulfidation-reaction cycles were conducted and the catalytic activity could be recovered after sulfur replenishment.[5]

1.5 Effect of support on catalysts

Catalysts used for the propane dehydrogenation are typically based on supported transition metals. Studied supports include Al_2O_3, TiO_2, ZrO_2, SiO_2, ZSM-5 and MgO for alkane dehydrogenation reactions. Research has shown that the support used for dehydrogenation catalysts has an influence on the dispersion, metal-support electronic effects and activity of the catalyst. It has also been suggested that acid-base properties of supports strongly affect the selectivity toward propylene.[82–89] For example, Shen *et al*. reported that the stability and selectivity of the Ga_2O_3/HZSM-5 catalyst for propane dehydrogenation were enhanced by increasing the Si/Al ratio of HZSM-5 support.[89]

Xu and co-workers reported that Ga_2O_3/ Al_2O_3, Ga_2O_3/ TiO_2 and Ga_2O_3/ ZrO_2 displayed better performance of propane dehydrogenation than Ga_2O_3/ SiO_2 and Ga_2O_3/MgO due to more acid sites in the medium to strong acid-site range.[90] Furthermore, high surface area materials (>200 m^2/g) are preferable supports for metal catalysts. Among the supports mentioned, alumina and silica materials have been reported to increase the efficiency of metal catalysts.[83–89]

Alumina (Al_2O_3) is the most frequently employed catalytic support in the chemical industry. Mesoporous Al_2O_3 has recently been reported as support in several catalyst formulations. The performance of Al_2O_3 support is mainly dependent on its textural properties. Mesoporous Al_2O_3 supports with large surface areas, large pore volumes, applicable surface acidic-basic properties and high thermal stability often enhance catalytic performances. However, research has shown that Al_2O_3 support is susceptible to hydrolysis and phase transitions (leading to the formation of an inactive metal-aluminate species), which occur during thermal breakdown of the ordered structure.[91–94]

For supported nickel catalysts, studies have shown that nickel oxide is the major surface species on most supports, although, species arising from nickel-support interaction may vary depending on the physical and chemical properties of the support.[95] Li *et al*. have stated that the reduction of nickel over supported nickel catalysts is challenging and the equilibrium between NiO and H_2 varies depending on the nickel-support interaction.

This would imply that the nickel-support interaction can be characterized according to the reducibility of the nickel. Previous studies have indicated that nickel supported on alumina is not entirely reduced to the metallic state due to the strong NiO-alumina interaction on the catalyst.[95] Zielinski studied the morphology of nickel/alumina catalysts. It was observed that NiO existed on the support in two states: firstly, as free form NiO and secondly, as fixed form connected with the formation of nickel aluminate (Ni/Al_2O_4).[96] The process of reduction causes a bi-dispersion of small and large nickel crystallites to form on the support. The difficulty of reduction of the supported catalysts arise from the chemical interaction between nickel and the Al_2O_3 support.[95,96]

The interaction between metal oxide and support could be classified into three categories: 1) weak interaction, in which the support only serves as a dispersing agent, 2) solid solution formation and 3) strong interaction or surface compound formation. The interest in nickel/alumina catalysts centres around metal-support interactions, which affect the surface properties of the catalysts. This is a result of the movement of nickel ions into the alumina lattice sites.[96]

Nickel catalysts supported on alumina are susceptible to coke formation due to the acid sites of alumina which promote the deposition of carbon with negative consequences on catalyst stability. One possible strategy to minimize this problem is the modification of the acid-base properties of the catalyst using alkali metals as promoters. As an alkaline earth metal, Mg is extensively used as a promoter on Al_2O_3 support, through the formation of magnesium aluminate spinel ($MgAl_2O_4$).[97–99] The synthesis of the material can be achieved by the reaction of magnesium and aluminium compounds.[100] The $MgAl_2O_4$ spinel was found to increase the basicity of the catalyst, improve dispersion of the nickel on the support, supress the phase transformation to inactive $NiAl_2O_4$ and reduce catalyst deactivation caused by the formation of coke.[94,97] In many of its applications, $MgAl_2O_4$ offers a wide range of desirable characteristics such as high melting point, good mechanical strength and high thermal and chemical stability. This material has been used successfully as support in catalysts for dehydrogenation reactions.[101–103]

As mentioned above, catalytic systems that are based on Al_2O_3 support contain major drawbacks (prone to coke formation and transformation to undesired $NiAl_2O_4$ species). On the other hand, silica (SiO_2) is often used as support for Ni-based catalysts due to its inertness, good thermostability, availability and high surface area.[104,105] The experimental results obtained from Baiker and co-workers showed that the SiO_2 support performed better than Al_2O_3, ZrO_2 and TiO_2 for the oxidative dehydrogenation of ethane.[106,107] SiO_2 is chosen as support since it produces a higher metallic surface area and higher sintering resistance compared to other oxide supports.[108,109]

The initial metal dispersion obtained from the preparation method should be resistant to the operating conditions during catalyst life and possible regeneration treatments that the catalyst could undergo after possible deactivation processes.

The loss of metallic dispersion during the catalyst lifetime or regeneration treatments is mostly due to sintering or solid state reactions between the nickel and the support.[109] Therefore, the properties of SiO_2 make it a suitable choice of support for dehydrogenation reactions.[51,87,110]

Wang reported on the highly selective and stable Ni-Sn/SiO_2 catalyst for isobutane dehydrogenation.[111] Experimental results showed that the selectivity toward isobutene was 90.2% and the conversion of isobutane remained stable at roughly 45% for 120 hours on stream the introduction of hydrogen gas. The dehydrogenation reactivity was completely recovered after regeneration of the spent catalyst. However, the reaction cycle was shortened due to the weak interaction between Ni, Sn and SiO_2 of the catalyst. When the support was changed to Al_2O_3, the Ni species reacted with the support to form the $NiAl_2O_4$ phase, which lead to irreversible catalyst deactivation. With this in mind, the choice of appropriate support, which can avoid the aggregation of surface metallic species, is a key factor for future industrial applications.[65,83,111]

1.6 Influence of sulfur on the catalytic system

Sulfur-containing compounds have commonly been known to act as a catalyst poison for noble metals due to their strong coordinating and adsorptive abilities, which cause them to block active metal sites.[20,112] Poisoning can be classified as reversible or irreversible. For reversible poisoning, catalyst activity is recovered by removing the source of posion or by cleaning the surface of the catalyst through oxidation or steaming. The effect of irreversible poisoning is due to inadequate removal of sulfur that is strongly adsorbed on the catalyst. The loss of catalytic activtity includes decreased cycle lifespan and increased carbon deposition.[113,114]

Some poisons, such as sulfur, are added to catalytic systems as a modifier to improve the performance of a catalyst and increase the selectivity of desired products.[115] For example, platinum catalysts for naphtha reforming are often pre-sulfided to reduce unwanted cracking reactions.

In catalytic reforming, sulfur is added to Pt-Re or Pt-Sn catalysts to enhance the dehydrogenation of alkanes to olefins while poisoning sites responsible for hydrogenolysis or coking reactions.[114,116]

Various metal sulfided catalysts display interesting catalytic activity and have been widely applied in the petroleum industry.[20,117,118] Barbier *et al*. reported that coke formation and sulfur adsorption take place on the same metallic sites.[119] It follows that pre-sulfurisation of catalysts would reduce the extent of coking, resulting in a more stable catalyst.[119]

Metal sulfides are speculated to be the active sites of sulfided catalysts for dehydrogenation. Wang and co-workers evaluated the use of nickel-sulfided catalysts for isobutane dehydrogenation.[22] They reported that the introduction of sulfur to Ni/$MgAl_2O_4$ catalysts promoted the dispersion of nickel particles on the $MgAl_2O_4$ support. The metal-sulfur bond in the sulfided catalysts weakened the interaction between the metal atoms. It was therefore suggested that the effect of sulfur addition to the catalyst can be explained in terms of the geometric effect, which dilute aggregated nickel particles and disintegrates large metallic nickel ensembles that are active for hydrogenolysis reactions. Consequently, this would lead to reduced coking and hydrogenolysis reactions and improved dehydrogenation activity.[11,22]

Ni/$MgAl_2O_4$ catalysts were highly active for isobutane cracking, which lead to the formation of methane, hydrogen and coke. The unmodified NiO catalysts supported on $MgAl_2O_4$ were prepared by wetness impregnation with nickel nitrate. After the introduction of sulfur to the catalyst, unwanted reactions were effectively reduced and the selectivity toward isobutene increased (**Figure 1.4**). It was found that NiO particles became much smaller and better dispersed on the catalyst surface after the catalyst had been sulfided. The sulfur modified Ni/$MgAl_2O_4$ catalysts (Ni/$MgAl_2O_4$-S) were prepared by sequential impregnation of $MgAl_2O_4$ with aqueous ammonium sulfate and nickel nitrate solutions. In addition, Ni/$MgAl_2O_4$ catalysts were also sulfided using H_2S/H_2 gas.[22]

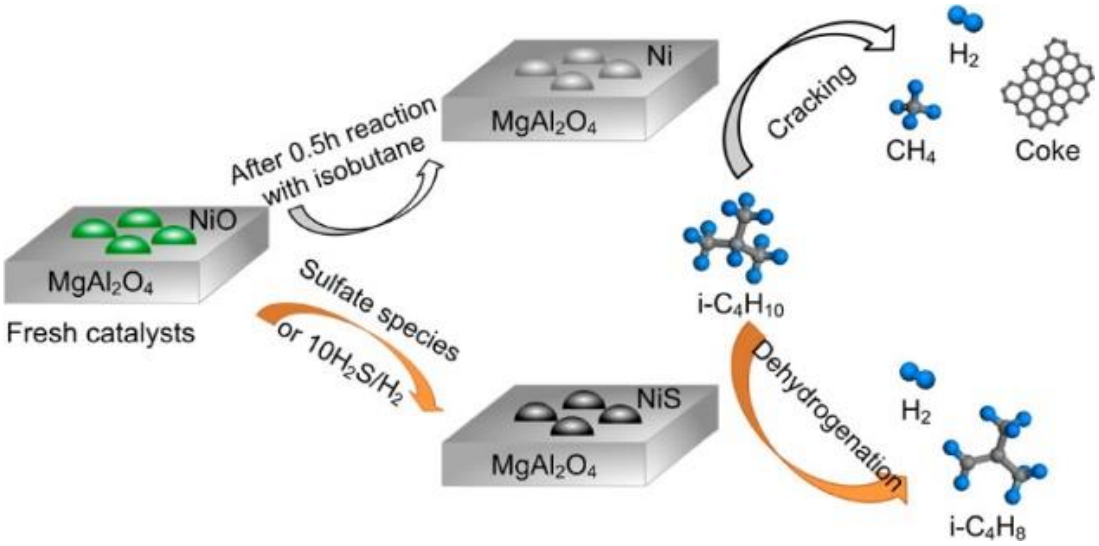

Figure 1.4. Graphical representation showing the effect of sulfur addition on the performance of $Ni/MgAl_2O_4$ catalysts for isobutane dehydrogenation.[22]

Activity test results for $Ni/MgAl_2O_4$-S are shown in **Figure 1.5**. Both isobutane conversion and selectivity toward isobutene increased gradually with time on stream (TOS) in the first 5 hrs of the reaction, suggesting the existence of an induction period for the $Ni/MgAl_2O_4$-S catalyst. It was noted that the Ni-S species, formed during the induction period, was the active phase of the $Ni/MgAl_2O_4$-S catalyst and constituted the active sites for isobutane dehydrogenation along with facilitating the desorption of isobutene from the catalyst.[22]

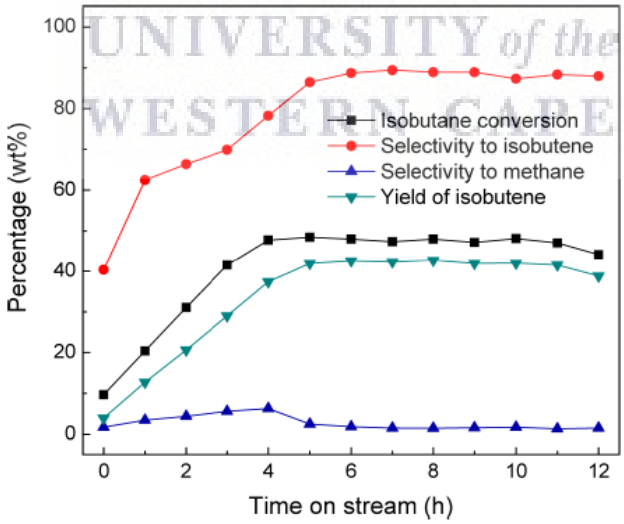

Figure 1.5. Dehydrogenation performance of $13Ni/MgAl_2$-S catalyst.[22]

Additionally, $Ni/MgAl_2O_4$ was sulfided by 10 vol. % H_2S/H_2 and the catalyst was further evaluated. Through sulfiding the catalyst with H_2S/H_2, the induction period disappeared and a relatively high isobutane conversion was observed. This result indicated that the active nickel sulfide species was probably formed during the sulfiding process. Sulfur was consumed from the system and the catalyst activity decreased with TOS. After sulfiding the catalyst again with H_2S/H_2, the catalyst activity was completely recovered, which confirms that the presence of sulfur is necessary for excellent dehydrogenation performance.[22]

Further reasoning for the improved dehydrogenation activity has been recorded.[11] It was reported that the adsorption of isobutene decreased significantly after sulfur treatment for nickel-based catalysts. It was deduced that the addition of sulfur facilitated the desorption of olefins. The interaction between surface metal atoms and adsorbed alkene molecules are weakened by the presence of adjacent sulfur atoms. A possible reason for this phenomenon could be that the higher electron density of nickel atoms, caused by the addition of sulfur, results in higher repulsive interactions with olefins. The addition of sulfur adjusts the electronic properties of nickel atoms, by electron donation and decreased the adsorption heat of olefin and activation energy of its desorption, which enables an increased selectivity toward isobutene. This can be described as the electronic effect of sulfur.[11]

A schematic of the interaction between the isobutane molecule and the catalyst surface before and after sulfiding the catalyst is illustrated in **Figure 1.6**. For the unsulfided metal oxide catalysts, the oxides are easily reduced to the metal atoms during the reaction. A strong interaction between the carbon atoms in isobutane and the metal atoms weaken and break C-C bonds in isobutane, thus leading to the generation of a notable amount of methane. However, with the introduction of sulfur, the aggregated metallic species are diluted and separated, which reduces the possibility for the formation of adjacent carbon-metal bonds in isobutane molecules. In addition, the hydrogen atoms present in isobutane molecules bond with sulfur atoms that neighbour metallic species on the catalyst surface. Consequently, this weaken and break the C-H bonds. As a result, isobutane and hydrogen are released to the gas phase as the final products.[11]

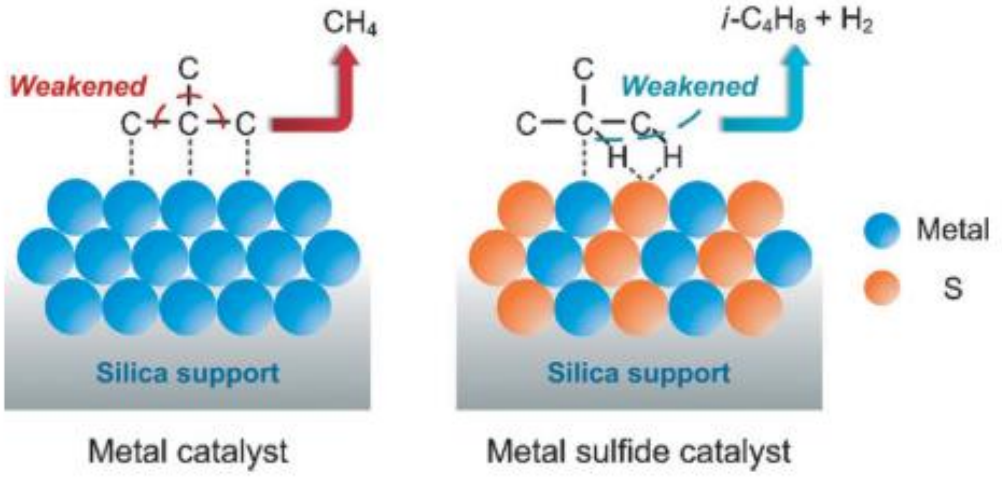

Figure 1.6. Model displaying the interaction between isobutane and the catalyst surface[11]

1.7 Reaction mechanism of sulfur loss

As stated above, the introduction of sulfur affects the catalyst in two ways: the geometric effect (dilution of particles) and the electronic effect (alter electron density of the active metal). The emergence of metal-sulfur species in sulfided metal catalysts seem to fundamentally contribute to the remarkable improvement in the dehydrogenation performance. To better understand the active sites, the reaction mechanism of isobutane dehydrogenation over metal sulfided catalysts has been explored.[11] For example, in the Ni/SiO_2 catalyst, the Ni-S species has a hexagonal structure. Moreover, for hydrodesulfuration reactions, which are catalysed by metal sulfides, the active sites are generally believed to be sulfur vacancies, that is, the co-ordinatively unsaturated sites.[57–59] Therefore, the active Ni atom is speculated to be bonded to three sulfur atoms. Accordingly, a catalytic cycle of sulfide catalysts, including reaction, deactivation and regeneration is proposed in **Figure 1.7**.[45]

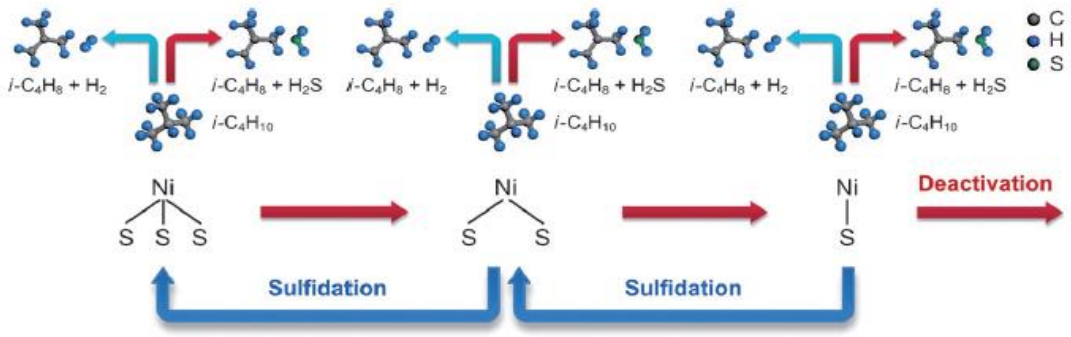

Figure 1.7. Proposed catalytic cycle, including reaction, deactivation and regeneration of the NiS/SiO_2 catalyst for isobutane dehydrogenation[11]

In the above reaction mechanism, an isobutane molecule diffuses to the catalyst surface and dissociatively adsorbs on the unsaturated Ni sites, forming an intermediate species (**Figure 1.8.a**). Through β-hydrogen transfer, a hydrogen molecule is released, leaving a labile intermediate bonded to a π-bonded alkene (**Figure 1.8.b**). In the next step, an isobutene molecule is formed and released from the catalyst surface, while the active centre is regenerated. If the Ni-S bond weakens, H_2S gas is generated and released. The Ni centre is left with one less bonded sulfur, which has a lower dehydrogenation activity (**Figure 1.8.c**). The activity of the spent catalyst is then recovered by sulfur replenishment with H_2S/H_2 gas.[11]

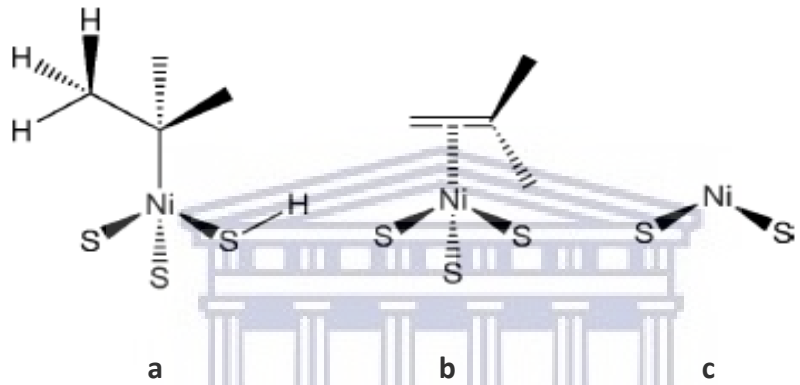

a **b** **c**

Figure 1.8. Intermediate species in the proposed catalytic cycle of isobutane dehydrogenation[11]

1.8 Sulfiding agents

The promotive effects of H_2S used to sulfide metal oxides have been widely studied.[24,117] H_2S is known to decompose to H_2 and S^{2-}, which is the source of sulfur on a range of metal components. However, H_2S is highly toxic and a high corrosion resistance is required for industrial equipment, leading to a high investment cost.[24,83,123] Swift *et al*. pursued the idea of adding H_2S as a sulfiding agent to the butene feed to convert surface nickel to the sulfided state.[124] This reduced the catalyst tendancy to form excessive coke and increased selectivity toward the desired butadiene product. On the other hand, using butanethiol in the feed instead of H_2S gave identical results. The authors suggested that any source of sulfur, which is capable of sulfiding nickel, could be used as the sulfiding agent.[124]

Several alternative sulfiding agents have been used to introduce sulfur into metal sulfided catalysts to improve catalytic activity for dehydrogenation reactions.[4,22,23] For example, dimethyl sulfoxide (DMSO) is a sulfur containing organic solvent used as a sulfiding agent for refineries due to its ease of handling and relatively less toxic properties.[125,126]

The Ni/Al_2O_3 catalysts were sulfided with DMSO by Resasco for the dehydrogenation of isobutane.[4] The catalysts were sulfided by injecting measured quantities of DMSO into the reactor under a stream of hydrogen. As increasing amounts of DMSO were added to the reduced nickel catalyst, they found that both hydrogenolysis and coking rates substantially decreased. As shown in **Figure 1.9**, the carbon content measured after 10 hours on stream (H_2/isobutane ratio of 0.5) dropped from almost 9 g C/g cat. for the unsulfided catalyst to almost 0 g C/g cat. for the catalyst exposed to a S/Ni ratio >0.25. It was also noted that the carbon selectivity toward methane decreased from 100 % to < 4%, thereby highlighting the improved dehyrogenation performance.[4]

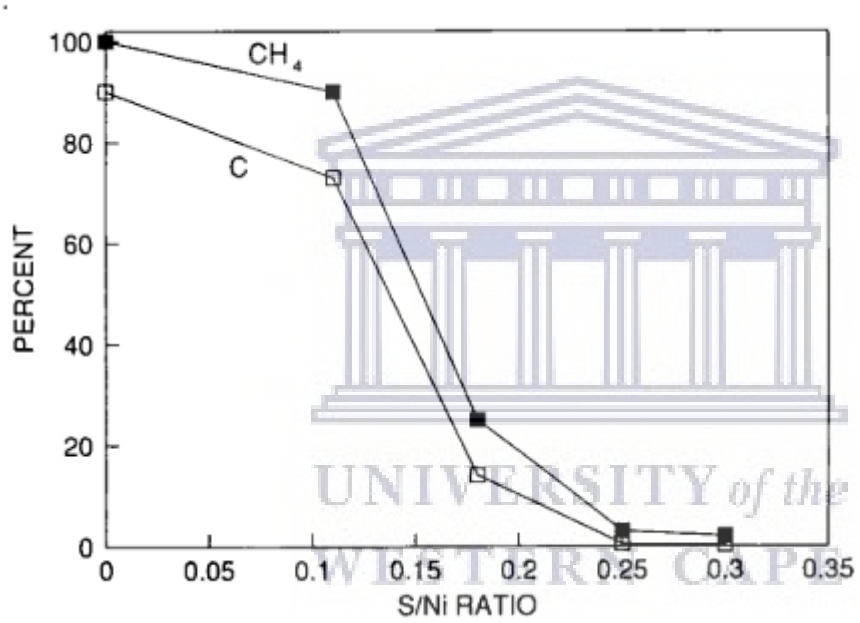

Figure 1.9. Effect of sulfur on isobutane hydrogenaolysis and coking over Ni/Al_2O_3-based catalyst (■) Methane selectivity as measured at 600 °C and H_2/isobutane ratio of ½. (□) Carbon deposited on the catalyst after 10 hours.[4]

Although some weakly bonded sulfur species may have desorbed after the catalyst had been sulfided with DMSO under a hydrogen gas flow, it was reported that most of the sulfur remained on the catalyst. The analysis of one sample which was subjected to a single sulfiding with DMSO at the beginning of the run, indicated a residual sulfur to nickel ratio of 0.2 after 336 hours on stream.

During a separate experiment, using a catalyst with a lower nickel loading, in which H_2S was used as the sulfiding agent and the H_2/isobutane ratio increased to 6, the sulfur content dropped after only 10 hours on stream. These results indicated that the time dependent product distribution was characetrised by a loss of isobutene selectivity and increase in methane with time. The rapid selectivity loss was not observed when DMSO was used as a sulfiding agent and the H_2/isobutane ratio was kept at 2 or less.[4]

In addition, the use of DMSO as a sulfiding agent has been patented and has been used in various industrial processes, including dehydrogenation reactions.[127,128] Elemental sulfur (powder form) is impossible to use in chemical reactions required in petroleum refining. When sulfur is contained in a liquid state such as DMSO, it can be easily utilized for such applications.[129]

The sulfiding of catalysts is further performed in hydrodesulfurization processes. The commercial catalysts for these reactions are often obtained in the form of oxidation, which is presulfided in the reactor by introducing a sulfiding agent to form H_2S in order to transform inactive oxides to sulfides. This conventional procedure, usually named *in situ* presulfidation, subsequently produces the H_2S/H_2 sulfidation atmosphere. However, the long start-up time, usage of posionous sulfiding agents (e.g. CS_2) and equipment corrosion by high concentrations of H_2S in the *in situ* presulfidation process limits the industrial applications in the future.[23,130]

Alternatively, the *ex-situ* presulfidation process proves to be advantageous with lower environmental pollution, shorter activation time and a high sulfidation degree of the active component. Nearly all existing *ex-situ* presulfidation processes were performed by impregnation of the oxides with sulfiding agents such as organic polysulfides or water soluable sulfides.[23,130] Liu and co-workers used ammonium sulfide ($(NH_4)_2S$) as a sulfiding agent to sulfide (*ex-situ*) a $CoMo/Al_2O_3$ catalyst.[23] They speculated that due to the high sulfidation activity of S^{2-}, the transition metals of the catalyst would react with with $(NH_4)_2S$ leading to the full sulfidation of the active components.[23] With this reasoning, $(NH_4)_2S$ was used as a sulfiding agent in this study through a simple sulfiding procedure in low temperature and ambient pressure conditions.

The adsorption of various anions, such as sulfate ions (SO_4^{2-}) onto oxide have been investigated as a means of improving their catalytic activity.[131] Liquids containing sulfur generally possess a pungent, unpleasant odour. The addition of relatively safe ammonium sulfate ($(NH_4)_2SO_4$) to metal catalysts have been explored in research studies.[22,132–134] Wang *et al*. prepared sulfur modified catalysts through the addition of $(NH_4)_2SO_4$ on $Ni/MgAl_2O_4$ and $Mo/MgAl_2O_4$ catalysts for the dehydrogenation of isobutane.[22,133] The catalysts were prepared by sequential wetness impregnation of the $MgAl_2O_4$ support, $(NH_4)_2SO_4$ and the corresponding metal precursors. It was reported that the dehydrogenation performance was significantly improved in comparison to the oxide catalysts.[22,133] For the sulfur modified molybdenum catalyst, $Mo/MgAl_2O_4$-S, XPS data showed features that were characteristic of S^{6+} with binding energy of S 2p at 169 ± 0.2 eV, which suggested the presence of the sulfate species. However, after 2 hours on stream, additional features corresponding to S^{2-} emerged as seen in **Figure 1.10**. These results verified the formation of the active MoS_2 phase.[133]

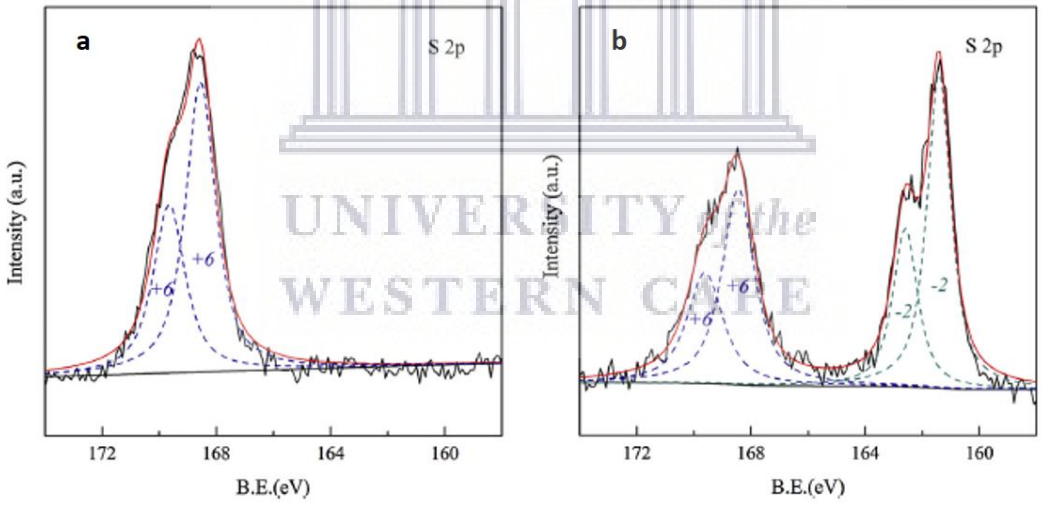

Figure 1.10. XPS spectra of sulfur modified $Mo/MgAl_2O_4$-S a) fresh and b) after 2 hours on stream[133]

In studies perfomed by Watanabe *et al*., they found that transition metal catalysts (Fe, Co, Ni) supported on Al_2O_3, containing sulfate ions, were selective for propane dehydrogenation.[24] Furthermore, Sun *et al*. noted the promotional effects of sulfate.[135] Using such a catalytic system, propylene selectivity improved dramatically and coke deposition was decreased subtstantially by the sulfidation treatment, which involved the addition of ammonium sulfate

to the catalyst support.[135] The loaded sulfate species were reduced to sulfide ions under reaction conditions and then functioned as the active sites for propane dehydrogenation.[24,135]

1.9 Bimetallic sulfided catalysts

The modification of catalyst behaviour of noble metals by the addition of a second metal, able to form bimetallic compounds, is an interesting field in heterogeneous catalysis. For example, the Pt-Sn system supported on alumina is widely used in alkane dehydrogenation reactions, where it exhibits higher activity and stability than monometallic catalysts. Among all bimetallic catalysts, platinum-based metals are the most studied catalyst components.[25,32,64,136] In addition to Sn on Pt catalysts, Zn was found to be a common choice on noble metal catalysts to control the activity and selectivity in a wide range of reactions.[27] Furthermore, understanding the impact of catalyst structure on the activity and selectivity of hydrogenolysis vs. dehydrogenation of hydrocarbons is crucial for the development of improved catalysts. A number of factors are responsible for the structure of bimetallic catalysts.[25,137]

There are many well established methods for preparing bimetallic catalysts. The choice of method depends on the desired surface as well as the bulk structure of the catalyst. The co-impregnation method is used to produce supported bimetallic materials. Alternatively, the sequential impregnation method is adopted to obtain core-shell type materials, where a less active metal core is prepared first and then the active metal component is deposited onto it. Wet impregnation methods are widely applicable as a preparation route for bimetallic catalysts with well-controlled shape, size and composition.[25]

1.9.1 Zinc as a promoter on bimetallic catalyst systems

The presence of Zn has been shown to improve catalytic properties of Pt catalysts in the dehydrogenation of light alkanes, such as propane. The promoting effect of zinc has been attributed to the strong interactions between Zn and Pt, which result in the formation of a PtZn alloy and change in the electronic property of Pt atoms on the catalyst, by donating electron density and weakening the adsorption of $\pi-$bonded alkenes, hence, inhibiting the formation of coke precursors. It has been suggested that Zn displays similar effects to Sn for the modification of Pt catalysts in dehydrogenation reactions.[26,27,138,139]

Moreover, Yu *et al*. have reported that the presence of Zn on Pt/Sn-based catalysts could increase the dispersion of Pt and decrease the electronic density of the Pt metal, which remarkably increased the selectivity of the catalyst for the dehydrogenation of propane to propylene.[29]

1.9.2 Ni-Zn bimetallic catalysts

The high cost and low availability of Pt-group catalysts limit their applications for large scale processes. Therefore, attention has turned toward nickel, which possess similar electronic properties and can perform many of the same reactions as Pt or Pd metals. Nickel is known for its high alloying efficiency with all noble metals and many transition metals, which contributes to the ease of developing a wide range of bimetallic nickel systems for diverse catalytic applications.[25]

Al-ShaikhAli *et. al*. investigated whether bimetallic nickel-based catalysts would exhibit improved dehydrogenation performance of methylcyclohexane (MCH) to toluene (TOL) by coupling the good selectivity of nickel with the high selectivity of a second metal.[137] The bimetallic Ni-Zn catalysts were prepared with various Ni/Zn ratios. The MCH conversion as a function of time for the Ni, $NiZn_{0.1}$ and $NiZn_{0.6}$ samples at 300 °C is shown in **Figure 1.11.a**. The addition of Zn (2 wt%) to the Ni (8 wt%) catalyst lowered conversion of the MCH compared to monometallic Ni, however, the selectivity for toluene improved.[137] The Ni and $NiZn_{0.1}$ catalysts were comparable in their conversion percentages. **Figure 1.11.b** displays the selectivity towards TOL as a function of time under the same reaction conditions. Initially, all the catalysts exhibit improvement in the TOL selectivity. The authors attributed this to reconstruction of the surface active sites that occurred during catalysis.

Reduction of the metals during the reaction was an implausible reason, since the reduction temperature (400 °C) is higher than the reaction temperature. The DFT results from their experiments suggested that the main role of Zn was poisoning of the low-coordinated sites where C-C breaking occurs, which is responsible for hydrogenation. This lead to improved selectivity of the catalyst for dehydrogenation.[137,140]

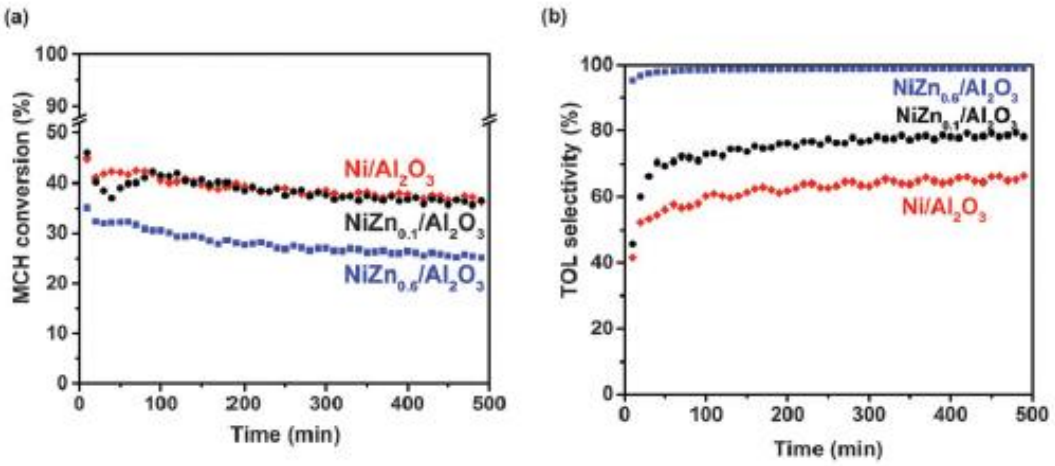

Figure 1.11. a) Conversion of MCH and b) selectivity of TOL as a function of time using Ni/Al_2O_3, $NiZn_{0.1}/Al_2O_3$ (black) and $NiZn_{0.6}/Al_2O_3$ (blue)[137]

1.9.3 Bimetallic sulfided catalysts

In this research project, the promoting effects of sulfur on bimetallic catalysts will be investigated for the dehydrogenation of propane. Depending on the nature of the metal-sulfide and metal-metal interactions, several phenomena can occur when sulfur reacts with a bimetallic catalyst. For some systems, the formation of bimetallic sulfides that display different chemical properties from those of the pure metals are observed.[141,142] In other type of systems, the interaction between sulfur and one of the metals is repulsive, weakening the bimetallic bonds and reducing the "mixing" of the metals. Furthermore, a bimetallic system can exist such that one of the metals increases or promotes the reactivity of the other metal toward sulfur.[141,143]

The introduction of sulfur to bimetallic Pt catalysts have been discussed in the literature.[33,34,144] For example, Dees *et al*. have investigated the influence of sulfur on a Pt/Ir catalyst for hexane/hydrogen reactions.[33] They found that the introduction of sulfur to the catalysts had a beneficial effect on obtaining the desired products.

There was a huge decrease in the selectivity to hydrogenolysis, which was due to a decrease in ensemble size of the free surface metals. Furthermore, sulfur addition decreased the formation of carbonaceous deposits on the metal surface, which consequently increased the selectivity toward the desired reactions.[33]

Ribeiro and co-workers studied the transformation of a bimetallic Pt/Re catalyst into a stable, dehydrogenation-hydrogenation catalyst with the introduction of sulfur to the catalytic system.[34] The increased resistance to deactivation was observed when sulfur was added to the Pt catalysts. However, the monometallic Pt catalyst quickly lost its adsorbed sulfur. It was reported that the catalyst surface could hold sulfur much stronger when the second metal (Re) was present. It was suggested that the presence of sulfur could decrease the rate of catalyst deactivation and it was easier to maintain the sulfur surface concentration in the presence of the Re metal. The stability of the bimetallic catalyst was improved with sulfur, which decreased the hydrogenolysis rate. The Re-S combination acted as a diluent and resulted in small ensembles of Pt that were stable against poisoning by carbon deposition. This stabilization effect arose as a consequence of the smaller Pt particles that cannot build up carbon deposits, since space for large polymeric carbon structures were limited. Thus, the catalyst was stable until the Pt-Re-S moieties lost their sulfur and exposed large patches of Pt-Re, where carbon may be deposited.[34]

1.10 References

1 B. Coq and F. Figueras, *Coord. Chem. Rev.*, 1998, **178–180**, 1753–1783.
2 R. Antony, S. T. David Manickam, P. Kollu, P. V. Chandrasekar, K. Karuppasamy and S. Balakumar, *RSC Adv.*, 2014, **4**, 24820–24830.
3 Y. Zhang, W. Yao, H. Fang, A. Hu and Z. Huang, *Sci. Bull.*, 2015, **60**, 1316–1331.
4 D. E. Resasco, B. K. Marcus, C. S. Huang and V. A. Durante, *J. Catal.*, 1994, **146**, 40–55.
5 G. Wang, C. Li and H. Shan, *ACS Catal.*, 2014, **4**, 1139–1143.
6 J. J. H. B. Sattler, J. Ruiz-Martinez, E. Santillan-Jimenez and B. M. Weckhuysen, *Chem. Rev.*, 2014, **114**, 10613–10653.
7 M. F. Alotibi, B. A. Alshammari, M. H. Alotaibi, F. M. Alotaibi, S. Alshihri, R. M. Navarro and J. L. G. Fierro, *Catal. Surv. from Asia*, 2020, **24**, 1–10.
8 D. Sanfilipo, I. Miracca and F. Trifirò, *Refin. Petrochmicals*, 2007, **2**, 687–700.
9 B. Grzybowska, J. Słoczyński, R. Grabowski, K. Wcisło, A. Kozłowska, J. Stoch and J. Zieliński, *J. Catal.*, 1998, **700**, 687–700.
10 B. M. Weckhuysen and R. A. Schoonheydt, *Catal. Today*, 1999, **51**, 223–232.
11 G. Wang, C. Gao, X. Zhu, Y. Sun, C. Li and H. Shan, *ChemCatChem*, 2014, **6**, 2305–2314.
12 M. R. A. Blomberg, P. E. M. Siegbahn, U. Nagashima and J. Wennerberg, *J. Am. Chem. Soc.*, 1991, **113**, 424–433.
13 G. Wang, X. Zhu, J. Zhang, Y. Sun, C. Li and H. Shan, *RSC Adv.*, 2014, **4**, 57071–57082.
14 P. P. Li, W. Z. Lang, K. Xia, L. Luan, X. Yan and Y. J. Guo, *Appl. Catal. A Gen.*, 2016, **522**, 172–179.
15 I. Ro, J. Resasco and P. Christopher, *ACS Catal.*, 2018, **8**, 7368–7387.
16 J. Guo, H. Lou, H. Zhao, D. Chai and X. Zheng, *Appl. Catal. A Gen.*, 2004, **273**, 75–82.
17 J. Salmones, J. A. Galicia, J. A. Wang, M. A. Valenzuela and G. Aguilar-Rios, *J. Mater. Sci. Lett.*, 2000, **19**, 1033–1037.
18 E. N. Alvar, M. Rezaei and H. N. Alvar, *Powder Technol.*, 2010, **198**, 275–278.
19 M. Tadić, M. Panjan and D. Marković, *Mater. Lett.*, 2010, **64**, 2129–2131.
20 M. R. DuBois, *Chem. Rev.*, 2005, **89**, 1–9.
21 C. D. Roberts, *Hydrocarb. Process.*, 2008, **87**, 1–2.
22 G. Wang, Z. Meng, J. Liu, C. Li and H. Shan, *ACS Catal.*, 2013, **3**, 2992–3001.
23 B. Liu, L. Liu, Y. Chai, J. Zhao, Y. Li, Y. Liu and C. Liu, *Ind. Eng. Chem. Res.*, 2018, **57**, 2041–2049.
24 R. Watanabe, N. Hirata, K. Miura, Y. Yoda, Y. Fushimi and C. Fukuhara, *Appl. Catal. A Gen.*, 2019, **587**, 117238.
25 S. De, J. Zhang, R. Luque and N. Yan, *Energy Environ. Sci.*, 2016, **9**, 3314–3347.
26 C. Yu, H. Xu, Q. Ge and W. Li, *J. Mol. Catal. A Chem.*, 2007, **266**, 80–87.
27 Y. Zhang, Y. Zhou, J. Shi, X. Sheng, Y. Duan, S. Zhou and Z. Zhang, *Fuel Process. Technol.*, 2012, **96**, 220–227.
28 H. Zhu, D. H. Anjum, Q. Wang, E. Abou-Hamad, L. Emsley, H. Dong, P. Laveille, L. Li, A. K. Samal and J. M. Basset, *J. Catal.*, 2014, **320**, 52–62.
29 C. L. Yu, H. Y. Xu, X. R. Chen, Q. J. Ge and W. Z. Li, *J. Fuel Chem. Technol.*, 2010, **38**, 308–312.
30 M. Naseri, F. Tahriri Zangeneh and A. Taeb, *React. Kinet. Mech. Catal.*, 2019, **126**, 477–495.
31 L. Rochlitz, K. Searles, J. Alfke, D. Zemlyanov, O. V. Safonova and C. Copéret, *Chem. Sci.*, 2020, **11**, 1549–1555.
32 J. Silvestre-Albero, J. C. Serrano-Ruiz, A. Sepúlveda-Escribano and F. Rodríguez-Reinoso, *Appl. Catal. A Gen.*, 2005, **292**, 244–251.
33 M. J. Dees and V. Ponec, *J. Catal.*, 1989, **115**, 347–355.
34 F. H. Ribeiro, A. L. Bonivardi, C. Kim and A. Somorjai, *J. Catal.*, 1994, **150**, 186–198.
35 M. Kuhn and J. A. Rodriguez, *Catal. Letters*, 1995, **32**, 345–355.
36 M. Kuhn and J. A. Rodriguez, *J. Catal.*, 1995, 154, 355–363.
37 M. M. Bhasin, J. H. McCain, B. V. Vora, T. Imai and P. R. Pujadó, *Appl. Catal. A Gen.*, 2001, **221**,

397–419.
38 Z. Nawaz, *Rev. Chem. Eng.*, 2015, **31**, 413–436.
39 B. V. Vora, *Top. Catal.*, 2012, **55**, 1297–1308.
40 S. Saerens, M. K. Sabbe, V. V. Galvita, E. A. Redekop, M. F. Reyniers and G. B. Marin, *ACS Catal.*, 2017, **7**, 7495–7508.
41 A. Iglesias-Juez, A. M. Beale, K. Maaijen, T. C. Weng, P. Glatzel and B. M. Weckhuysen, *J. Catal.*, 2010, **276**, 268–279.
42 H. Weyten, J. Luyten, K. Keizer, L. Willems and R. Leysen, *Catal. Today*, 2000, **56**, 3–11.
43 S. Sahebdelfar, M. T. Ravanchi, F. Tahriri Zangeneh, S. Mehrazma and S. Rajabi, *Chem. Eng. Res. Des.*, 2012, **90**, 1090–1097.
44 H. Zhou, J. Gong, B. Xu, L. Yu and Y. Fan, *Appl. Catal. A Gen.*, 2016, **527**, 30–35.
45 N. Rahimi and R. Karimzadeh, *Appl. Catal. A Gen.*, 2011, **398**, 1–17.
46 S. M. Sadrameli, *Fuel*, 2015, **140**, 102–115.
47 S. David Jackson, *Chem. Eng. J.*, 2006, **120**, 119–125.
48 R. Schäfer, M. Noack, P. Kölsch, M. Stöhr and J. Caro, *Catal. Today*, 2003, **82**, 15–23.
49 A. Ricca, F. Montella, G. Iaquaniello, E. Palo, A. Salladini and V. Palma, *Catal. Today*, 2019, **331**, 43–52.
50 R. Hu, X. Li, Z. Sui, G. Ye and X. Zhou, *Chem. Eng. Process. - Process Intensif.*, 2019, **143**, 107608.
51 O. O. James, S. Mandal, N. Alele, B. Chowdhury and S. Maity, *Fuel Process. Technol.*, 2016, **149**, 239–255.
52 D. Sanfilippo and I. Miracca, *Catal. Today*, 2006, **111**, 133–139.
53 P. Bai, D. Liu, P. Wu and Z. Yan, *Rev. Adv. Sci. Eng.*, 2014, **3**, 180–195.
54 W. Won, K. S. Lee, S. Lee and C. Jung, *Comput. Chem. Eng.*, 2010, **34**, 508–517.
55 S. T. Seo, W. Won, K. S. Lee, C. Jung and S. Lee, *Korean J. Chem. Eng.*, 2007, **24**, 921–926.
56 S. Sokolov, M. Stoyanova, U. Rodemerck, D. Linke and E. V. Kondratenko, *J. Catal.*, 2012, **293**, 67–75.
57 T. A. Nijhuis, S. J. Tinnemans, T. Visser and B. M. Weckhuysen, *Chem. Eng. Sci.*, 2004, **59**, 5487–5492.
58 US Pat., 20180029015A1, 2018.
59 M. Farsi, A. Jahanmiri and M. R. Rahimpour, *Asia-Pacific J. Chem. Eng.*, 2013, **8**, 862–869.
60 S. Sahebdelfar, P. M. Bijani, M. Saeedizad, F. T. Zangeneh and K. Ganji, *Appl. Catal. A Gen.*, 2011, **395**, 107–113.
61 R. A. Buyanov and N. A. Pakhomov, *Kinet. Catal.*, 2001, **42**, 64–75.
62 U. Illgen, R. Schäfer, M. Noack, P. Kölsch, A. Kühnle and J. Caro, *Catal. Commun.*, 2001, **2**, 339–345.
63 D. E. Resasco, in *Encyclopedia of Catalysis*, 2002, pp. 1–52.
64 X. Liu, W. Z. Lang, L. L. Long, C. L. Hu, L. F. Chu, Y. J. Guo, P. P. Li, W. Z. Lang, K. Xia, L. Luan, X. Yan and Y. J. Guo, *Chem. Eng. J.*, 2014, **247**, 183–192.
65 Q. Zhu, G. Wang, J. Liu, L. Su and C. Li, *ACS Appl. Mater. Interfaces*, 2017, **9**, 30711–30721.
66 O. A. Bariås, A. Holmen and E. A. Blekkan, *Catal. Today*, 1995, **24**, 361–364.
67 H. A. Benesi and R. M. Curtis, *J. Catal.*, 1968, **10**, 328–335.
68 J. Im and M. Choi, *ACS Catal.*, 2016, **6**, 2819–2826.
69 S. M. K. Airaksinen, M. E. Harlin and A. O. I. Krause, *Ind. Eng. Chem. Res.*, 2002, **41**, 5619–5626.
70 F. Cavani, M. Koutyrev, F. Trifirò, A. Bartolini, D. Ghisletti, R. Iezzi, A. Santucci and G. Del Piero, *J. Catal.*, 1996, **158**, 236–250.
71 D. A. Nazimov, O. V. Klimov, A. V. Saiko, S. N. Trukhan, T. S. Glazneva, I. P. Prosvirin, S. V. Cherepanova and A. S. Noskov, *Catal. Today*, 2020, 1–41.
72 V. Z. Fridman and R. Xing, *Ind. Eng. Chem. Res.*, 2017, **56**, 7937–7947.
73 M. Santhosh Kumar, N. Hammer, M. Rønning, A. Holmen, D. Chen, J. C. Walmsley and G. Øye,

J. Catal., 2009, **261**, 116–128.
74 F. M. Ashmawy, *J. Chem. Soc. Faraday Trans. 1 Phys. Chem. Condens. Phases*, 1980, **76**, 2096–2101.
75 A. B. Gaspar, J. L. F. Brito and L. C. Dieguez, *J. Mol. Catal. A Chem.*, 2003, **203**, 251–266.
76 D. Shee and A. Sayari, *Appl. Catal. A Gen.*, 2010, **389**, 155–164.
77 J. Gao, F. Guan, Y. Zhao, W. Yang, Y. Ma, X. Lu, J. Hou and J. Kang, *Mater. Chem. Phys.*, 2001, **71**, 215–219.
78 R. B. Biniwale, N. Kariya and M. Ichikawa, *Catal. Letters*, 2005, **105**, 83–87.
79 Z. Fan, K. Sun, N. Rui, B. Zhao and C. J. Liu, *J. Energy Chem.*, 2015, **24**, 655–659.
80 W. J. J. Welters, O. H. van der Waerden, H. W. Zandbergen, V. H. J. de Beer and R. A. van Santen, *Ind. Eng. Chem. Res.*, 1995, **34**, 1156–1165.
81 R. Watanabe, N. Hirata, Y. Yoda, Y. Fushimi and C. Fukuhara, *J. Japan Pet. Inst.*, 2020, **63**, 228–237.
82 M. Chen, J. L. Wu, Y. M. Liu, Y. Cao, L. Guo, H. Y. He and K. N. Fan, *Appl. Catal. A Gen.*, 2011, **407**, 20–28.
83 G. Wang, X. Zhu and C. Li, *Chem. Rec.*, 2019, **19**, 1–14.
84 J. Li, J. Li, Z. Zhao, X. Fan, J. Liu, Y. Wei, A. Duan, Z. Xie and Q. Liu, *J. Catal.*, 2017, **352**, 361–370.
85 K. C. Szeto, Z. R. Jones, N. Merle, C. Rios, A. Gallo, F. Le Quemener, L. Delevoye, R. M. Gauvin, S. L. Scott and M. Taoufik, *ACS Catal.*, 2018, **8**, 7566–7577.
86 L. Deng, H. Miura, T. Shishido, S. Hosokawa, K. Teramura and T. Tanaka, *Chem. Commun.*, 2017, **53**, 6937–3940.
87 M. Botavina, C. Barzan, A. Piovano, L. Braglia, G. Agostini, G. Martra and E. Groppo, *Catal. Sci. Technol.*, 2017, **7**, 1690–1700.
88 C. T. Shao, W. Z. Lang, X. Yan and Y. J. Guo, *RSC Adv.*, 2017, **7**, 4710–4723.
89 Z. Shen, J. Liu, H. Xu, Y. Yue, W. Hua and W. Shen, *Appl. Catal. A Gen.*, 2009, **356**, 148–153.
90 B. Xu, B. Zheng, W. Hua, Y. Yue and Z. Gao, *J. Catal.*, 2006, **239**, 470–477.
91 Z. Wang, X. Tian, C. Yang, Y. Zhao and Z. Pi, *J. Nanosci. Nanotechnol.*, 2009, **9**, 6876–6882.
92 C. Márquez-Alvarez, N. Žilková, J. Pérez-Pariente and J. Čejka, *Catal. Rev. - Sci. Eng.*, 2008, **50**, 222–286.
93 P. Minaev, M. Nikulshina, A. Mozhaev, K. Maslakov, R. Boldushevskii and P. Nikulshin, *Fuel Process. Technol.*, 2018, **181**, 44–52.
94 L. P. R. Profeti, E. A. Ticianelli and E. M. Assaf, *Appl. Catal. A Gen.*, 2009, **360**, 17–25.
95 C. Li, Y. W. Chen and C. P. Corporation, *Thermochim. Acta*, 1995, **256**, 457–465.
96 J. Zieliński, *J. Catal.*, 1982, **76**, 157–163.
97 V. R. Bach, A. C. de Camargo, T. L. de Souza, L. Cardozo-Filho and H. J. Alves, *Int. J. Hydrogen Energy*, 2020, **45**, 5252–5263.
98 T. Wu, G. Liu, L. Zeng, G. Sun, S. Chen, R. Mu, S. Agbotse Gbonfoun, Z. J. Zhao and J. Gong, *AIChE J.*, 2017, **63**, 4911–4919.
99 M. L. Dieuzeide, M. Laborde, N. Amadeo, C. Cannilla, G. Bonura and F. Frusteri, *Int. J. Hydrogen Energy*, 2016, **41**, 157–166.
100 A. D. Mazzoni, M. A. Sainz, A. Caballero and E. F. Aglietti, *Mater. Chem. Phys.*, 2003, **78**, 30–37.
101 J. Duan, S. Lu, X. Wang, J. Yin, H. Gao, Z. Su and J. Yang, *IOP Conf. Ser. Earth Environ. Sci.*, , DOI:10.1088/1755-1315/81/1/012028.
102 M. Pudukudy, Z. Yaakob and M. S. Takriff, *Appl. Surf. Sci.*, 2015, **356**, 1320–1326.
103 S. A. Bocanegra, A. D. Ballarini, O. A. Scelza and S. R. de Miguel, *Mater. Chem. Phys.*, 2008, **111**, 534–541.
104 S. S. He, L. Zhang, S. S. He, L. Mo, X. Zheng, H. Wang and Y. Luo, *J. Nanomater.*, 2015, **2015**, 1–8.
105 Q. Zafar, T. Mattisson and B. Gevert, *Energy and Fuels*, 2006, **20**, 34–44.

106 R. Koirala, R. Buechel, S. E. Pratsinis and A. Baiker, *Appl. Catal. A Gen.*, 2016, **527**, 96–108.
107 X. Li, S. Liu, H. Chen, S. Z. Luo, F. Jing and W. Chu, *ACS Omega*, 2019, **4**, 22562–22573.
108 P. H. Blanco, C. Wu, J. A. Onwudili and P. T. Williams, *Appl. Catal. B Environ.*, 2013, **134**–**135**, 238–250.
109 A. Gil, A. Diaz, L. M. Gandia and M. Mantes, *Appl. Catal. A Gen.*, 1994, **109**, 167–179.
110 K. Searles, G. Siddiqi, O. V. Safonova and C. Copéret, *Chem. Sci.*, 2017, **8**, 2661–2666.
111 G. Wang, H. Wang, H. Zhang, Q. Zhu, C. Li and H. Shan, *ChemCatChem*, 2016, **8**, 3137–3145.
112 S. L. Lakhapatri and M. A. Abraham, *Catal. Sci. Technol.*, 2013, **3**, 2755–2760.
113 J. K. Dunleavy, *Platin. Met. Rev.*, 2006, **50**, 110–110.
114 M. Argyle and C. Bartholomew, *Catalysts*, 2015, **5**, 145–269.
115 J. Kobayashi and T. Shimizu, *Bull. Chem. Soc. Japan*, 2000, **73**, 759–763.
116 G. Jacobs, F. Ghadiali, A. Pisanu, C. L. Padro, A. Borgna, W. E. Alvarez and D. E. Resasco, *J. Catal.*, 2000, **191**, 116–127.
117 M. Ziolek, J. Kujawa, O. Saur and J. C. Lavalley, *J. Mol. Catal. A. Chem.*, 1995, **97**, 49–55.
118 Y. Okamoto, K. Nagata, T. Adachi, T. Imanaka, K. Inamura and T. Takyu, *J. Phys. Chem.*, 1991, **95**, 310–319.
119 J. Barbier and P. Marecot, *J. Catal.*, 1986, **102**, 21–28.
120 P. G. Moses, B. Hinnemann, H. Topsøe and J. K. Nørskov, *J. Catal.*, 2009, **268**, 201–208.
121 T. C. Ho and J. M. McConnachie, *J. Catal.*, 2011, **277**, 117–122.
122 H. Wang and E. Iglesia, *J. Catal.*, 2010, **273**, 245–256.
123 Z. Gao, W. Yang, X. Ding, G. Lv and W. Yan, *Appl. Surf. Sci.*, 2018, **436**, 585–595.
124 H. E. Swift, H. Beuther and R. J. Rennard, *Ind. Eng. Chem. Prod. Res. Dev.*, 1976, **15**, 131–136.
125 E. M. Matira, T. C. Chen, M. C. Lu and M. L. P. Dalida, *J. Hazard. Mater.*, 2015, **300**, 218–226.
126 G. Chemical, *Tech. Bull. React.*, **1209**, 1–110.
127 US Pat., 5 489 722, 1996.
128 Y. Labat, *Phosphorus. Sulfur. Silicon Relat. Elem.*, 1993, **74**, 173–194.
129 Gaylord Chemical Company, *Bull. 205*, 2015, **205**, 1–8.
130 B. Liu, L. Liu, Y. Chai, J. Zhao, Y. Li, D. Liu and Y. Liu, 2018, **234**, 1144–1153.
131 F. H. Alhassan, U. Rashid, M. S. Al-Qubaisi, A. Rasedee and Y. H. Taufiq-Yap, *Powder Technol.*, 2014, **253**, 809–813.
132 S. Wang, K. Murata, T. Hayakawa, S. Hamakawa and K. Suzuki, *Catal. Letters*, 1999, **63**, 59–64.
133 G. Wang, N. Sun, C. Gao, X. Zhu, Y. Sun, C. Li and H. Shan, *Appl. Catal. A Gen.*, 2014, **478**, 71–80.
134 Y. N. Sun, Y. N. Gao, Y. Wu, H. Shan, G. Wang and C. Li, *Catal. Commun.*, 2015, **60**, 42–45.
135 Y. Sun, L. Tao, T. You, C. Li and H. Shan, *Chem. Eng. J.*, 2014, **244**, 145–151.
136 B. M. Nagaraja, C. H. Shin and K. D. Jung, *Appl. Catal. A Gen.*, 2013, **467**, 211–223.
137 A. H. Al-Shaikhali, A. Jedidi, L. Cavallo and K. Takanabe, *Chem. Commun.*, 2015, **51**, 12931–12934.
138 Y. Zhang, Y. Zhou, L. Huang, S. Zhou, X. Sheng, Q. Wang and C. Zhang, *Chem. Eng. J.*, 2015, **270**, 352–361.
139 V. J. Cybulskis, B. C. Bukowski, H. T. Tseng, J. R. Gallagher, Z. Wu, E. Wegener, A. J. Kropf, B. Ravel, F. H. Ribeiro, J. Greeley and J. T. Miller, *ACS Catal.*, 2017, **7**, 4173–4181.
140 A. H. Al-Shaikhali, A. Jedidi, D. H. Anjum, L. Cavallo and K. Takanabe, *ACS Catal.*, 2017, **7**, 1592–1600.
141 J. A. Rodriguez, *Prog. Surf. Sci.*, 2006, **81**, 141–189.
142 M. Kuhn, J. A. Rodriguez and J. Hrbek, *Surf. Sci.*, , DOI:10.1016/0039-6028(94)90224-0.
143 J. A. Rodriguez, *Surf. Sci. Rep.*, 1999, **24**, 223–287.
144 C. L. Pieck, P. Marecot and J. Barbier, *Appl. Catal. A Gen.*, 1996, **145**, 323–334.

CHAPTER 2: Experimental

In this chapter, the materials, synthesis and characterisation techniques used for the metal catalysts are described in detail. The techniques used to characterise the catalysts include XRD, BET, TEM, SEM, TGA, TPD, FTIR and TPR analysis. The bench-scale reactor set up used for the evaluation of the catalysts for dehydrogenation is described along with the analysis of hydrocarbon products produced in the catalytic reactions.

2.1 Materials

The following chemicals were used in the study: Silica gel (Davisil Grade 643, Sigma Aldrich), magnesium nitrate hexahydrate (98%-102%, Sigma Aldrich), aluminium nitrate nonahydrate (≥98%, Sigma Aldrich), oxalic acid (99.5%, LabChem), nickel nitrate hexahydrate (≥97%, Sigma Aldrich), zinc nitrate hexahydrate (≥99%, Sigma Aldrich), ammonium sulfate (99%, LabChem), ammonium sulfide solution (20 wt% in H_2O, Sigma Aldrich), dimethyl sulfoxide (ASC reagent ≥99%, Sigma Aldrich) and propane gas. Distilled water is obtained by a house supply that produces Milli-Q water.

Silica gel and $MgAl_2O_4$ were used as supports, silica gel was used without any modification while $MgAl_2O_4$ was synthesised using magnesium nitrate, aluminium nitrate and oxalic acid. Nickel nitrate was used as the metal precursor for the catalysts and zinc was used as the additional metal for the bimetallic catalysts. Ammonium sulfate, ammonium sulfide and dimethyl sulfoxide were used as the sulfiding agents. Propane gas was used as the feed for dehydrogenation reactions.

2.2 Catalyst preparation

Detailed preparation methods of the catalysts are given in the corresponding chapters.

2.3 Characterisation

2.3.1 X-ray Diffraction (XRD) Analysis

X-ray diffraction analysis (XRD) was used to determine the various components present in the catalysts by phase analysis. The XRD powder patterns were recorded using a BRUKER AXS D8 Advance (Cu-Kα radiation λKα1 = 1.5406 Å) 40 kV running from 5 – 90 ° in the 2θ range. Moreover, using the Scherrer equation (1), the crystallite size (D, nm) of the catalysts were calculated:

$$D = 0.9\,\lambda / \beta \cos\theta_B$$

where λ is the wavelength of X-ray radiation, β is the full width at half maximum (FWHM) of the diffraction peak and θ_B is the Bragg diffraction angle.

2.3.2 Brunauer-Emmett-Teller (BET) Surface Area

The surface area measurements and porosity analysis were determined by N_2 adsorption/desorption isotherms at -196 °C using the Micromeritics 3 FLEX analyzer. Approximately 0.3 g of sample was degassed overnight at 150 °C with a constant flow of nitrogen gas over the sample to remove atmospheric moisture from the sample. The specific surface areas and pore volumes of the samples were determined by the BET and BJH methods.

2.3.3 Transmission Electron Microscopy (TEM) and Scanning Transmission Electron Microscopy (STEM)

Transmission electron microscopy (TEM) images were obtained on a high resolution Tecnai F20. All samples were loaded on a copper grid and carbon coated before imaging. A ZEISS MERLIN SEM instrument was used for STEM imaging and x-ray mapping of samples. The setting for the imaging and energy dispersive x-ray spectroscopy (EDS) spectrometer was at a working distance of 9.5 mm with beam strength of 20 kV and probe current of 10 nA, using the backscattered electron detector. Samples were prepared by mounting the catalyst evenly on carbon tape and sputter coated with gold at 10 mm and 10 nm, respectively. STEM detector was used at a 20 kV beam strength and 250 pA probe current with a working distance of 4 mm. Samples were prepared by 10 x dilution, then pipetted onto the TEM grid and air dried.

Urinyl acetate was used for negative staining and samples were left to dry in darkness before loading onto a STEM stub and into the MERLIN SEM instrument.

2.3.4. Thermogravimetric Analysis (TGA)

Thermogravimetric analysis (TGA) was performed on a simultaneous analyzer (STA) 8000 to investigate the thermal stability of the catalysts. Approximately 0.03 g of sample was placed in the sample holder. The sample was then heated at a ramp rate of 10 °C/min from 30 °C – 1000 °C under a flow of argon gas. For the analysis of spent catalysts, samples were heated using the same temperature program without any gas flow.

2.3.5. NH_3-Temperature Programmed Desorption (NH_3-TPD)

The acidic properties, such as the quantity and strength of acid sites, in the catalysts were determined using the Micromeritics Autochem II by temperature programmed desorption of ammonia (NH_3-TPD). For each test, 0.025 g of sample was loaded into the reactor tube, degassed at 500 °C for 20 minutes under a 30 ml/min flow of helium gas and allowed to cool to 120 °C. The sample was then exposed to 5% NH_3 and the NH_3 was adsorbed at 120 °C for 30 minutes at a flow rate of 15 ml/min. Subsequently, helium was allowed to flow over the sample to remove any physically adsorbed NH_3. Ultimately, desorption was measured at a heating rate of 10 °C/min under helium flowing at a rate of 25 ml/min with the temperature increasing from 100 °C – 900 °C. The amount of desorbed NH_3 was calculated from the area under the TPD curve.

2.3.6. Fourier transform infrared (FTIR) spectroscopy

Fourier transform infrared (FTIR) spectroscopy was used to analyse the structural changes of the modified sulfided catalysts. The spectroscopic analysis was carried out using a Perkin Elmer UATR two FTIR spectrometer. Prior to FTIR analysis, samples were heated to 400 °C for 2 hours under a flow of nitrogen gas to remove any surface impurities and moisture. Approximately 10 mg of the catalyst was placed on the Attenuated Total Reflectance (ATR) diamond crystal and the force gauge was gently applied on the sample. The spectra were recorded at ambient room temperature in the wavenumber range 400 – 4000 cm^{-1} by collecting 100 scans at a 4 cm^{-1} resolution.

2.3.7. Temperature Programmed Reduction (TPR)

The reduction temperatures of the catalysts were measured using H_2 temperature programmed reduction (TPR). Roughly 0.025 g was placed in the sample holder followed by the preparation of a cold trap. The gases, argon and hydrogen, which are blended in a fixed proportion of 10 H_2-Ar, flowed through the sample at a rate of 50 ml/min and a baseline reading was established by the detector at room temperature. The temperature was then raised from 25 °C– 900 °C at a ramp rate of 10 °C/min. When the critical temperature was reached, H_2 atoms in the gas mixture reacted with the sample, forming H_2O, which was removed from the gas stream using the cold trap.

2.3.8. Gas Chromatography (GC) Analysis

Gas products were analysed offline by gas chromatography (GC) analysis. The detailed characteristics of the GC used for analysis of gas products are given in Table 2.1 below

Table 2.1: Properties of the GC method used for gas hydrocarbon analysis

Instrument	Bruker 450 GC	
Column	BR-Alumina-Na_2SO_4 50m x 0.53mm ID x 10µm (C_1-C_6)	
Detector	FID	
Temperature	375°C	
Gas	Helium	
GC injection program		
Injection temperature	220°C	
GC column pneumatics		
Middle FID	12psi	
Oven temperature program		
Rate (°C/minute)	**Final temperature (°C)**	**Hold time (minute)**
8	50	10
	190	2.5

2.4. Catalyst evaluation

2.4.1. Reactor setup

The dehydrogenation of propane was carried out using the unmodified and sulfur modified catalyst. The diagram of the reactor setup is shown in **Figure 2.1**. A bench scale quartz fixed bed reactor (12 mm diameter) was used and the catalyst was supported with quartz wool. The heater was placed into the reactor with the thermocouple placed next to the catalyst. The temperature of the reactions was maintained using a temperature control box. The top and bottom end of the heater was packed with quartz wool to prevent heat from escaping and to maintain a constant temperature. The outlet of the reactor was connected to a round bottom flask, which served as a collection vessel for the products obtained during the experiments. The sprout of the round bottom flask was connected to a vent line. The gas products were collected by attaching a Tedlar bag to the sprout of the flask. The flow rates throughout the experiments were measured using a flow bubble meter that could be connected to the sprout of the round bottom flask. A Teflon tube was connected to the source of propane feed, which was then connected to the inlet of the reactor. The amount of feed and N_2 diluent entering the reactor was regulated using a mass flow controller.

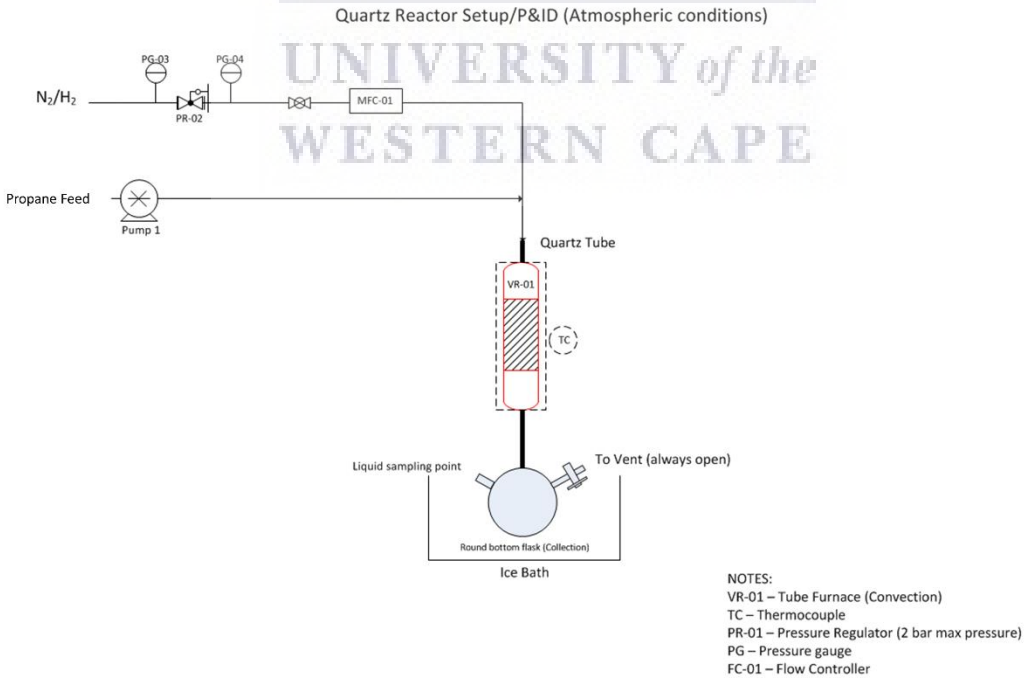

Figure 2.1. Diagram showing reactor setup

2.4.2. Experimental procedure

The performance of the catalysts in this study were tested for the dehydrogenation of propane gas. Approximately 1 g of catalyst was loaded into the fixed bed reactor. The propane feed and N_2 diluent was pumped at a rate of 30 ml/min which equals a weight hourly space velocity (WHSV) of 1.8 hr^{-1}. The reaction was performed at a temperature of 600 °C and atmospheric pressure. The experiments were conducted for 120 minutes. Products were analysed on an offline Bruker 450 GC equipped with a BR-Alumina/Na_2SO_4 column (C_1 – C_6), coupled to a flame ionization detector (FID).

2.4.3. Product analysis

The gas products obtained from the dehydrogenation of propane were collected in Tedlar bags and were analysed on an offline GC. To identify the components of the gas produced a gas standard obtained from PETROSA was used to calibrate the GC. A trace of the gas calibration is shown in **Figure 2.2** below. The gas calibration shows the products obtained in the C1-C5 range. In addition, the GC was calibrated with pure propane gas which was used as feed in all the reactions. This was done to identify the retention time at which it elutes in order to determine the percentage of propane gas conversion. A trace of pure propane gas is shown in **Figure 2.3**.

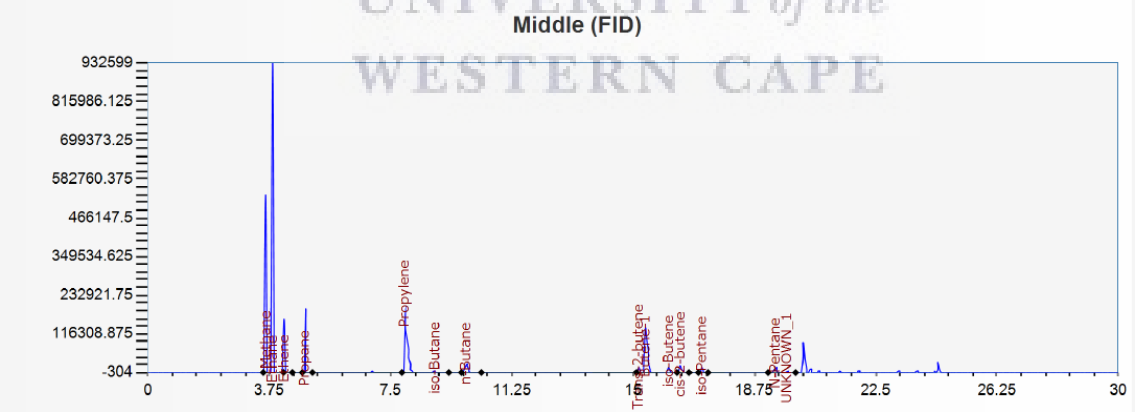

Figure 2.2. GC trace of the calibration gas used to identify gaseous hydrocarbon products

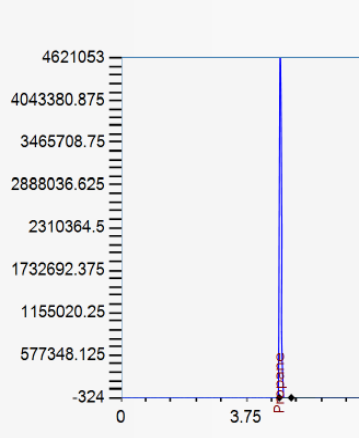

Figure 2.3. GC trace of the calibration of propane gas feed

2.4.4. Mass balance calculations

The calculations used to determine the mass balance, conversion and selectivity are shown in the equations that follow. Mass balance calculations of 90 – 100% were accepted as satisfactory. The calibration of the gas components was carried out with a gas standard from PETROSA of known composition containing the compounds shown in the calibration trace in Figure 2.4. The moles of each of the components present in the calibration gas was calculated using the following equation:

$$n_{c,out} = \frac{Ac}{Ac,cal} \times X_{c,cal} \times F_{out} \times t$$

Where A_c is the GC integrated area of component c, $A_{c,cal}$ is the area of the component c in the calibration gas, $X_{c,cal}$ is the mole fraction of the component c in the calibration gas, F_{out} is the total reactor exit stream mol/s and t is the total mass balance time.

The mass of the gas component was calculated as:

$$m_{c,out} = n_{c,out} \times M_c$$

Where M_c is the molar mass of component c.

The product selectivity for the hydrocarbons was calculated for component x_i as follows:

$$\%\ Product\ selectivity = \frac{mass\ component\ xi}{\sum xi} \times 100$$

Mass balances were obtained using the above analysis and calculations:

$$\%\ Mol\ balance = \frac{nFeed(in) - nGas(out)}{nFeed(in)} \times 100$$

Conversion of propane gas was determined by the equation:

$$\%\ Propane\ conversion = \frac{Feed(in) - Feed(out)}{Feed(in)} \times 100$$

2.5 References

1 M. Y. Nassar, I. S. Ahmed and I. Samir, *Spectrochim. Acta - Part A Mol. Biomol. Spectrosc.*, 2014, **131**, 329–334.

CHAPTER 3: In-depth investigation of the effect of $MgAl_2O_4$ and SiO_2 support on sulfur promoted nickel catalysts for the dehydrogenation of propane

3.1 Introduction

Light olefins are among the most important and versatile feedstocks in the petrochemical and fine chemical industries. With an increasing demand for olefins, processes for alkane dehydrogenation have gained considerable attention, solely because they provide a potential route to obtain olefins from low cost saturated hydrocarbons.[1–8] Although the selective activation of C-C and C-H bonds proves to be a challenge, attributing to the stable nature of alkanes, transition metals can activate saturated hydrocarbons.[3] The production of olefins by alkane dehydrogenation is being practised commercially, however, due to the highly endothermic nature of the reaction, high temperatures are required to achieve economically attractive yields.[9] Under these severe conditions, undesirable side reactions such as cracking and hydrogenolysis are inevitable. In addition, coke is rapidly formed at these elevated temperatures, which lead to catalyst deactivation and the catalytic processes generally require regeneration of the catalysts.[10] Pt and Cr based catalysts are commonly used industrial catalysts. However, the high cost of Pt and hazardous effects of Cr limit their application to some extent.[2,11–14]

Nickel based catalysts may be used as an alternative in dehydrogenation reactions, since these metal species are known to be active in various reactions, such as hydrogenation, water-gas shift and steam reforming of methane and ethanol.[11,12,15,16] Resasco *et al*. showed that nickel catalysts displayed high catalytic activity but low selectivity toward olefins in isobutane dehydrogenation. Instead, cracking reactions occurred at a rapid rate, with methane and coke being generated in relatively large quantities.[17] Wang and co-workers found that various sulfided catalysts, prepared either by impregnation with sulfate or sulfided with H_2S, displayed promising performance in alkane dehydrogenation.[12,18] It was found that the introduction of sulfur on nickel oxide catalysts decreases coking and increases the dehydrogenation activity of the catalysts significantly, despite sulfur being known to poison catalysts.[12,18] The promoting effects of sulfur can be explained in terms of two aspects.

The first is the geometric effect, which dilute aggregated metal species, thereby inhibiting C-C bond rupture. The second aspect is an electronic effect to facilitate alkene desorption, leading to increased selectivity of products.[2]

Furthermore, the effect of the nature of support plays a significant role in the performance of catalysts.[16,19] Interactions between catalytically active metals and supports have been linked to a wide range of physical and chemical observations, which is related to stability, activity and selectivity of the catalysts.[20] Generally, a support with a high surface area is imperative for nickel dispersion and improving thermal stability, thereby providing more active sites as well as decreasing deactivation over time due to sintering.[16] The most commonly used catalyst supports in industry include SiO_2 and Al_2O_3.[21] Due its excellent thermostability, availability, relatively high surface area and inertness, SiO_2 is widely used for preparing supported nickel based catalysts.[16,22] Recently, there has been growing interest in the utilization of magnesium aluminate spinel, $MgAl_2O_4$, as catalyst support in the field of environmental catalysis, petroleum processing and fine chemicals productions.[23] $MgAl_2O_4$ offers a combination of desirable properties such as chemical inertness, high thermal stability and increased coke resistance.[21,24,25] The addition of alkaline earth-metals to γ-Al_2O_3 reduces the acidity of the support and therefore the formation of undesirable by-products. These promoters are usually added to the support to improve the dispersion of the metal catalyst and to prevent the formation of an inactive metal-aluminate phase. Some studies have shown that the addition of MgO to Al_2O_3 improves the performance of nickel based catalysts in reactions and that the $MgAl_2O_4$ spinel inhibits the phase transformation to $NiAl_2O_4$ spinel and thus stabilizes the nickel crystallites in the catalyst.[26]

Metal sulfide materials are a relatively new class of dehydrogenation catalysts. Although they have been prepared on various supports, not much attention has been paid to the effects of supports on the physicochemical properties of the catalyst such as textural properties, particle size, acidity and metal support interactions and its relation to activity, selectivity and stability of the catalysts. In this study, an in-depth investigation on the dehydrogenation of propane over sulfur promoted nickel-based catalysts supported on $MgAl_2O_4$ and SiO_2 is performed. The catalysts have been characterized using various analytical techniques to determine the structural and electronic properties of the catalysts, which are important for understanding the activity, selectivity and stability in dehydrogenation reactions.

3.2 Experimental

3.2.1 Raw materials

The following chemicals were used in the study: Silica gel (Davisil Grade 643, Sigma Aldrich), magnesium nitrate hexahydrate (98%-102%, Sigma Aldrich), aluminium nitrate nonahydrate (≥98%, Sigma Aldrich), oxalic acid (99.5%, LabChem), nickel nitrate hexahydrate (≥97%, Sigma Aldrich), ammonium sulfate (99%, LabChem) and propane gas. Distilled water is obtained by a house supply that produces Milli-Q water.

3.2.2 Catalyst preparation: synthesis of $MgAl_2O_4$ support, supported NiO catalysts and sulfur modified catalysts

The synthesis of $MgAl_2O_4$ was performed using a sol-gel combustion method proposed by Nassar and co-workers.[27] An aqueous solution (30 ml) of $Mg(NO_3)_2.6H_2O$ (4 g, 15.6 mmol) was added to a stirring solution (50 ml) of $Al(NO_3)_2.9H_2O$ (12 g, 31.2 mmol) and the reaction was heated to 60 °C, while stirring for 10 minutes. To the hot stirring mixture, oxalic acid dissolved in distilled water was added and the reaction was heated to 80 °C while stirring for a further 60 minutes. The solution formed a gel, upon heating and stirring at 120 °C. The gel was heated in an oven at 200 °C for 2 hours to give a dry, white mass, which was then ignited in an electric furnace at 350 °C for 10 minutes. The produced powder was ground and calcined at 700 °C for 4 hours to give the final $MgAl_2O_4$ product.

The loading of Ni by weight was 13 wt% Ni for all catalysts. Nickel oxide catalysts supported on $MgAl_2O_4$ and SiO_2 were prepared by incipient wetness impregnation using $Ni(NO_3)_2.6H_2O$ as the metal precursor. After impregnation of the supports, the catalysts were dried at 140 °C overnight and calcined at 700 °C in air for 2 hours and 6 hours for the catalysts supported on $MgAl_2O_4$ and SiO_2, respectively to convert them to the oxide form.

The sulfur modified catalysts were prepared with loadings of 20wt% SO_4^{2-} (Ni:S, 1:1). The sulfur catalysts were obtained by sequential impregnation of the supports with aqueous $Ni(NO_3)_2.6H_2O$ and $(NH_4)_2SO_4$ solutions respectively. After impregnation, the catalysts were dried at 140 °C overnight and calcined at 700 °C in air for 2 hours on the $MgAl_2O_4$ support and 4 hours on the SiO_2 support.[12,16]

3.3 Results and Discussion

3.3.1 Structural and textural properties of modified and unmodified catalysts

The X-ray diffraction (XRD) patterns of NiO-based catalysts supported on $MgAl_2O_4$ and SiO_2 are shown in **Figure 3.1** below. The reflections corresponding to the $MgAl_2O_4$ phase occur at 19°, 31°, 45°, 59° and 65° 2θ angles. The diffraction peaks corresponding to $MgAl_2O_4$ can be indexed to the cubic spinel structure of the $MgAl_2O_4$ support.[27] The possibility of intermediate products have not been detected in the support, as indicated by the absence of peaks in the XRD pattern corresponding to products such as MgO and Al_2O_3, which consequently confirm the single phase of the as-synthesised $MgAl_2O_4$ support. An amorphous peak at 2θ 22° is present for SiO_2, which is typical for this material.[28] The peaks present in the 2θ regions 37°, 43°, 63°, 75° and 79° correspond to NiO dispersed on the $MgAl_2O_4$ and SiO_2 supports, respectively.

The peaks in the 2θ region 20 - 35° correspond to $NiSO_4$ species on both the $NiO/MgAl_2O_4$-20wt%SO_4 and NiO/SiO_2-20wt%SO_4 catalysts.[29] Peaks matching $MgSO_4$ are present in the XRD pattern of $NiO/MgAl_2O_4$-20wt%SO_4, indicating that SO_4^{2-} reacted with both the nickel particles and the $MgAl_2O_4$ support. Peaks matching NiO are present at 2θ 43° and 63° in $NiO/MgAl_2O_4$-20wt%SO_4, which could indicate that not all the NiO particles have been sulfated on the $MgAl_2O_4$ support. The possibility of hydrated $NiSO_4.6H_2O$ was detected on the NiO/SiO_2-20wt%SO_4 catalyst. XRD analysis provides evidence that $NiO/MgAl_2O_4$ and NiO/SiO_2 were both successfully modified using $(NH_4)_2SO_4$ as the sulfiding agent, however, it was noted through elemental analysis (supplementary material A, Table S1) that the ratio of Ni:S was not equal to 1:1 (20wt% SO_4) on both $NiO/MgAl_2O_4$-20wt%SO_4 and NiO/SiO_2-20wt%SO_4 samples.

The crystallite size of nickel-based particles was calculated using the Scherrer equation. The peak at 2θ 37°, was used to calculate the crystallite size of unsupported NiO and was equal to 26 nm. The corresponding peak in the 2θ region of 37° was used to calculate the crystallite size of NiO in the XRD patterns of $NiO/MgAl_2O_4$ and NiO/SiO_2 and was equal to 7 nm and 16 nm, respectively.

This drastic change in the crystallite size of NiO was expected on both supports, while the crystallite size of NiO supported on $MgAl_2O_4$ decreases significantly, implying that the NiO particles could be better dispersed on the $MgAl_2O_4$ support compared to the SiO_2 support. The crystallite size of $NiSO_4$ on $NiO/MgAl_2O_4$-20wt%SO_4 and NiO/SiO_2-20wt%SO_4 are 16 nm and 27 nm, respectively. These results suggest that $NiSO_4$ could consist of smaller particles on the $MgAl_2O_4$ support.

The XRD patterns of the reduced catalysts, $Ni/MgAl_2O_4$-20wt%SO_4 and Ni/SiO_2-20wt%SO_4 showed the presence of the Ni_3S_2 phase, which is the primary species of sulfur in the catalyst. However, for $Ni/MgAl_2O_4$-20wt%SO_4, it was found that sulfur interacted with the MgO in the support to form the $MgSO_4$ phase. This was not the case for Ni/SiO_2-20wt%SO_4 due to the inert nature of the silica support. The crystallite size of Ni_3S_2 was calculated, using the Scherrer equation, as 13 nm on the $Ni/MgAl_2O_4$-20wt%SO_4 catalyst. For Ni/SiO_2-20wt%SO_4, the crystallite size of Ni_3S_2 was calculated to 24 nm. The difference in peak intensity and crystallite size of the sulfur-modified catalysts, obtained from XRD analysis, suggest that the particles are much larger on the SiO_2 support in comparison to the $MgAl_2O_4$ support, which could consist of smaller particles with better dispersive properties.

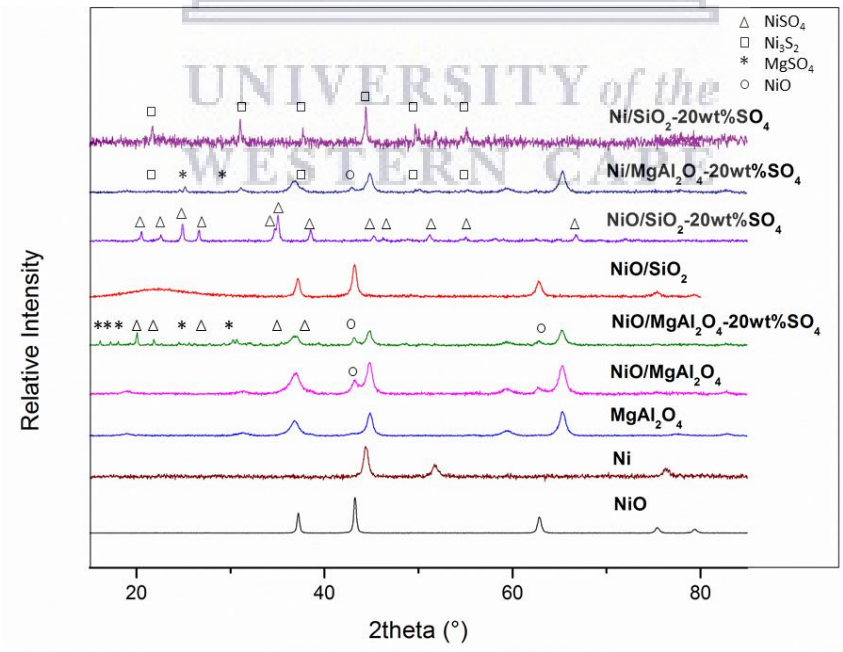

Figure 3.1. XRD patterns of NiO, Ni, $MgAl_2O_4$ and sulfur modified Ni-based catalysts supported on $MgAl_2O_4$ and SiO_2

Nitrogen adsorption-desorption isotherms of the catalysts are shown in **Figure 3.2.a** and **Figure 3.2.b** below. All the samples display type IV isotherms and type H_1 hysteresis loops, which is indicative of mesopores present in the catalysts.[30,31]

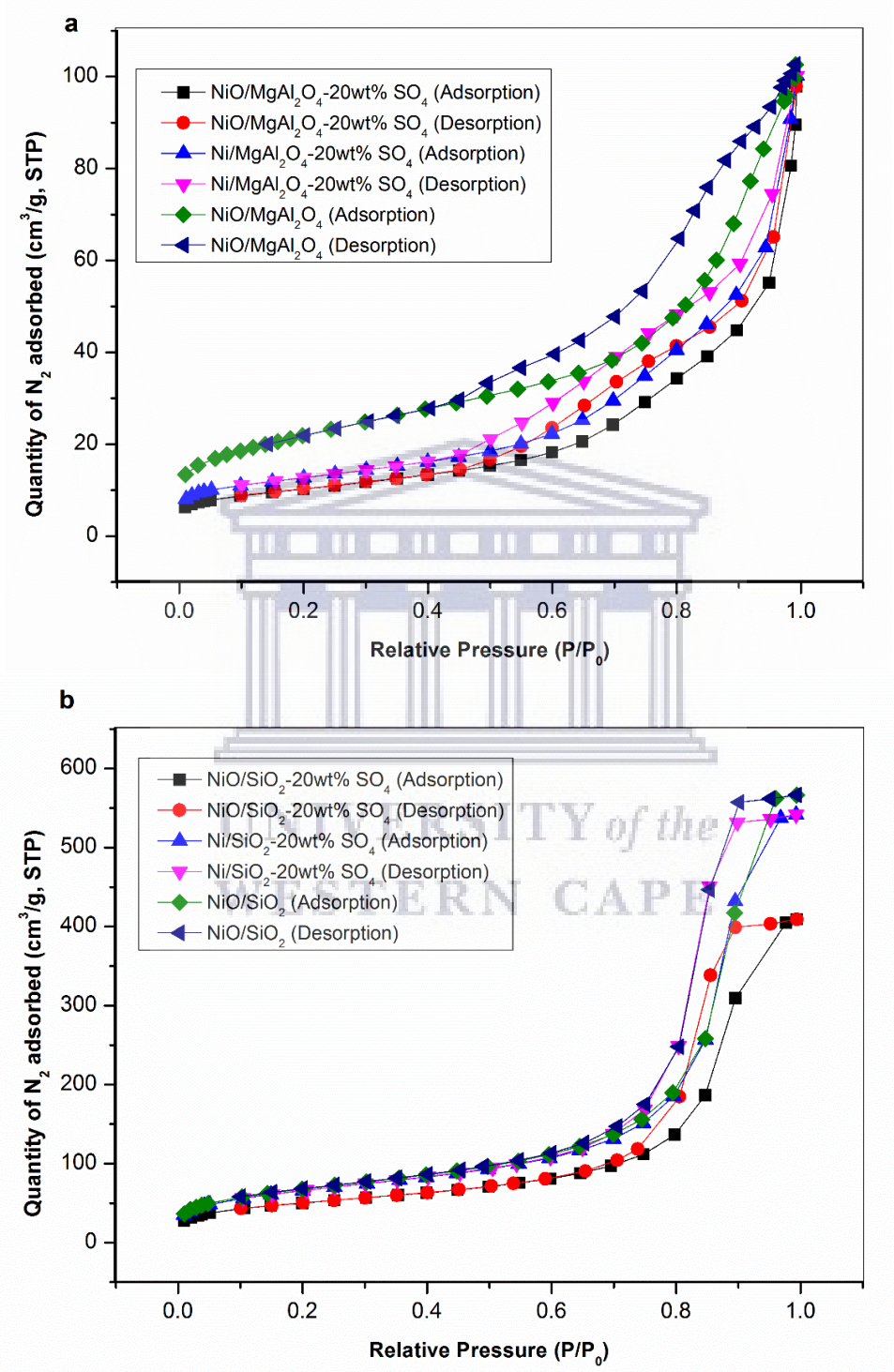

Figure 3.2. N_2 adsorption-desorption isotherms of unmodified and sulfur modified catalysts supported on a) $MgAl_2O_4$ and b) SiO_2

Table 3.1 contains a summary of the BET surface area and the crystallite size of the Ni species in the various catalysts on the $MgAl_2O_4$ and SiO_2 supports. The $NiO/MgAl_2O_4$ and NiO/SiO_2 catalysts displayed surface areas of 79 m^2/g and 236 m^2/g, respectively. It was noted that doping both $MgAl_2O_4$ and SiO_2 with 13 wt% nickel had no significant effect on the surface area of the pure support, indicating that the pores of the support are not blocked by the metal species. The surface area decreased to 36 m^2/g and 179 $m^2/$ for the $NiO/MgAl_2O_4$-20wt%SO_4 and NiO/SiO_2-20wt%SO_4 catalysts, respectively. The decrease in surface area could imply that the addition of SO_4^{2-} cause the nickel species to aggregate to some extent. These results contrast those found in the literature, whereby the effect of the sulfate anion on metal oxide catalysts, reduces grain sizes and increases the surface area.[32] This could be due to small sulfated particles clustering together to form agglomerates and contributing to an increase in crystallite size, accompanied by a decrease in surface area as observed in the BET results.

Interestingly, the reduced catalysts containing Ni_3S_2 particles, $Ni/MgAl_2O_4$-20wt%SO_4 and Ni/SiO_2-20wt%SO_4, showed an increase in surface area, compared to the sulfated catalysts, equal to 45 m^2/g and 236 m^2/g, respectively. The increase in surface area upon reduction could be due to change in particle size upon reduction of the catalysts, as observed by XRD analysis.

Table 3.1: Surface area and crystallite size of supported catalysts

Sample	**S_{BET} (m^2/g)**	**Crystallite size of Ni species (nm)** [a]
$MgAl_2O_4$	82	-
$NiO/MgAl_2O_4$	79	7 (NiO)
$NiO/MgAl_2O_4$-20wt%SO_4	36	16 ($NiSO_4$)
$Ni/MgAl_2O_4$-20wt%SO_4	45	13(Ni_3S_2)
SiO_2	240	-
NiO/SiO_2	241	16 (NiO)
NiO/SiO_2-20wt%SO_4	179	27 ($NiSO_4$)
Ni/SiO_2-20wt%SO_4	236	24 (Ni_3S_2)

[a] Calculated from XRD.

3.3.2 Morphology

The dispersion of nickel and sulfur over $MgAl_2O_4$ and SiO_2 supports can be seen through electron mapping images shown in **Figure 3.3** below. Visual evidence of SO_4^{2-} interacting with $MgAl_2O_4$ can be observed in $NiO/MgAl_2O_4$-20wt%SO_4 (**Figure 3.3.a**). Furthermore, sulfur particles seem denser on the reduced $Ni/MgAl_2O_4$-20wt%SO_4 catalyst than the $NiO/MgAl_2O_4$-20wt%SO_4 catalyst as observed in **Figure 3.3.b** below. Large clusters of $NiSO_4$ particles were observed on NiO/SiO_2-20wt%SO_4 (**Figure 3.3.c**). The absence of $NiSO_4$ clusters on $NiO/MgAl_2O_4$-20wt%SO_4 could propose that the sulfated complex is better dispersed on the $MgAl_2O_4$ support. Electron mapping of individual nickel atoms and sulfur atoms can be found in Figure S1.1 and Figure S1.2 in the supplementary material A, for both $NiO/MgAl_2O_4$-20wt%SO_4 and NiO/SiO_2-20wt%SO_4 catalysts, respectively.

TEM analysis was used to measure particle size of the sulfur modified catalysts. The nickel particles are depicted in each image by arrows in **Figure 3.4**. The sulfated catalysts, $NiO/MgAl_2O_4$-20wt%SO_4 and NiO/SiO_2-20wt%SO_4, consisted of localised clusters as seen in **Figure 3.4.a** and **Figure 3.4.b**, respectively. The particle size distribution of the four catalysts are shown in **Figure 3.5**. The average size of these clusters were measured using the program ImageJ and were equal to 20 nm and 59 nm for $NiO/MgAl_2O_4$-20wt%SO_4 and NiO/SiO_2-20wt%SO_4, respectively. The range of particle size for the reduced catalysts were 3 – 9 nm for the $Ni/MgAl_2O_4$-20wt%SO_4 catalyst and 4 – 12 nm for the NiO/SiO_2-20wt%SO_4 catalyst. These results are consistent with BET, which indicate that the sulfated catalysts had a lower surface area than the reduced $Ni/MgAl_2O_4$-20wt%SO_4 and Ni/SiO_2-20wt%SO_4 catalysts containing Ni_3S_2 species. It was proposed that perhaps the reduced catalysts disintegrate into smaller particles or that there could be a wider range of particle sizes as seen in TEM images.

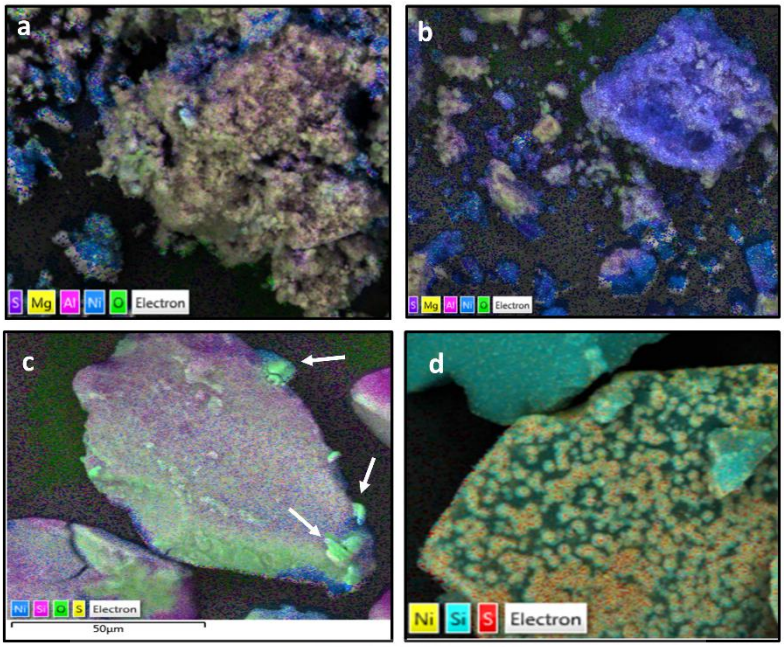

Figure 3.3. X-ray mapping of a) $NiO/MgAl_2O_4$-20wt%SO_4, b) $Ni/MgAl_2O_4$-20wt%SO_4, c) NiO/SiO_2-20wt%SO_4 and d) Ni/SiO_2-20wt%SO_4 catalysts

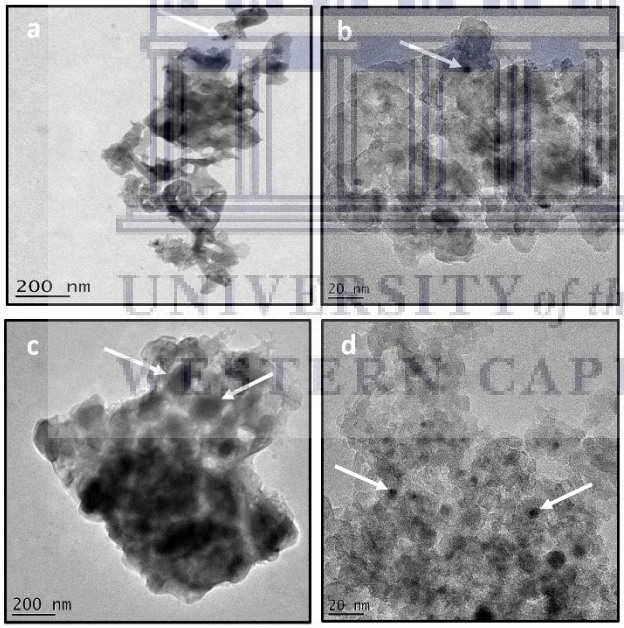

Figure 3.4. TEM images of a) $NiO/MgAl_2O_4$-20wt%SO_4, b) $Ni/MgAl_2O_4$-20wt%SO_4, c) NiO/SiO_2-20wt%SO_4 and d) Ni/SiO_2-20wt%SO_4 catalysts

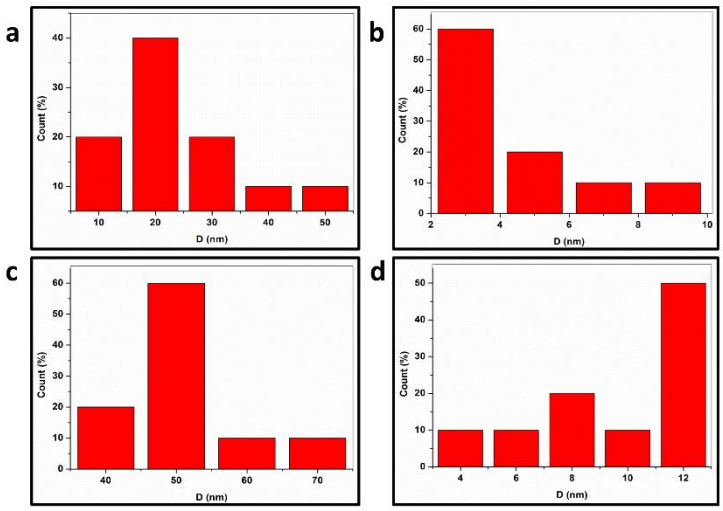

Figure 3.5. Particle size distribution of nickel species on a) NiO/$MgAl_2O_4$-20wt%SO_4, b) Ni/$MgAl_2O_4$-20wt%SO_4, c) NiO/SiO_2-20wt%SO_4 and d) Ni/SiO_2-20wt%SO_4 catalysts

3.3.3 Thermal stability of the sulfated catalysts supported on $MgAl_2O_4$ and SiO_2

Thermogravimetric analysis (TGA) of the sulfated catalysts was carried out to study the thermal stability of the nickel sulfate on the $MgAl_2O_4$ and SiO_2 supported catalysts. The TGA profiles of the NiO/$MgAl_2O_4$-20wt%SO_4 and NiO/SiO_2-20wt%SO_4 catalysts showed two mass loss steps as shown in **Figure 3.6**. The first step, which occurs in the range 30 – 200 °C, was attributed to the mass loss of physically adsorbed water molecules on the catalysts. The mass loss of water was 8% and 17% for NiO/$MgAl_2O_4$-20wt%SO_4 and NiO/SiO_2-20wt%SO_4, respectively. The mass loss at the higher temperatures i.e. 700 °C and 800 °C, was assigned to the decomposition of the sulfate groups on NiO/SiO_2-20wt%SO_4 and NiO/$MgAl_2O_4$-20wt%SO_4, respectively.[33] The wt% mass loss was equal to 17% and 12% for the NiO/SiO_2-20wt%SO_4 and NiO/$MgAl_2O_4$-20wt%SO_4 catalysts, respectively.

The TGA results confirmed that nickel sulfate on both supports would be thermally stable under the given reactions conditions used in the catalytic evaluation. However, the difference in sulfate decomposition temperatures show that sulfate decomposes at a higher temperature on $MgAl_2O_4$ than SiO_2 support, which could be due to stronger sulfate-nickel interactions as well as sulfate-support interactions (evidenced from XRD information as $MgSO_4$) on the $MgAl_2O_4$ support in comparison to that of the SiO_2 support.

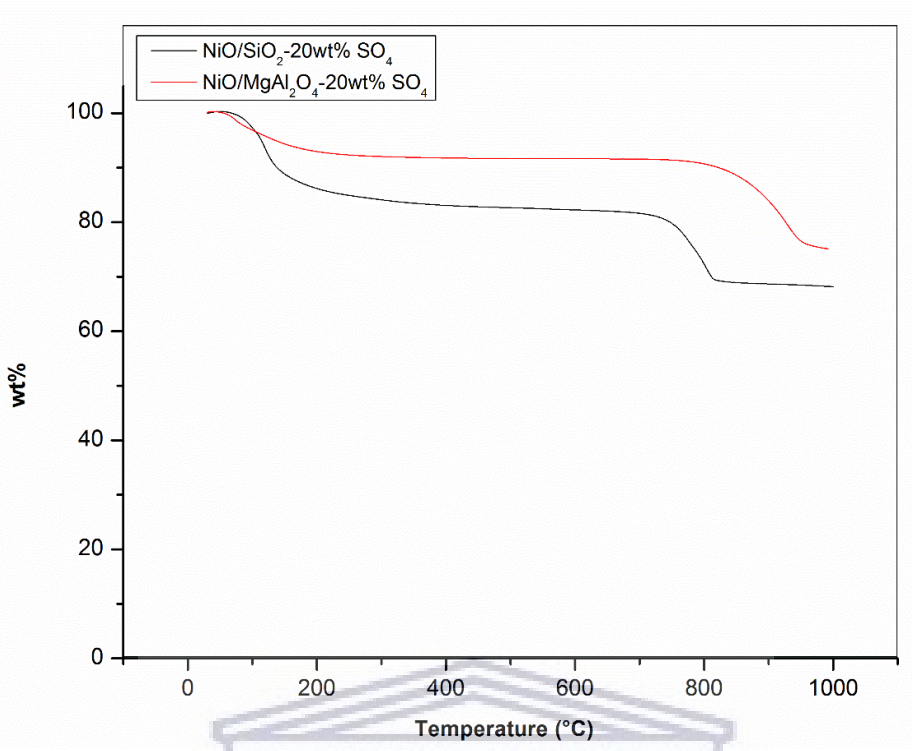

Figure 3.6. TGA profiles of $NiO/MgAl_2O_4$-20wt%SO_4 and NiO/SiO_2-20wt%SO_4 catalysts

The acidic properties of a catalyst are important in determining the catalytic activity and selectivity of a catalyst. The temperature programmed desorption of ammonia (NH_3-TPD) experiments were conducted in order to obtain the acidic properties of the catalysts. The desorption profiles are shown in **Figure 3.7**. Low temperature peaks are assigned to weak acid sites, while high temperature peaks are assigned to strong acid sites.[34] The TPD profile of the unmodified $NiO/MgAl_2O_4$ showed the absence of acid sites. The sulfur modified $NiO/MgAl_2O_4$-20wt%SO_4 catalyst contained a peak at 200 °C, indicating the presence of weak acid sites. A shoulder peak is found at 520 °C, which indicates the presence of strong acid sites. Furthermore, two peaks were observed in the high temperature domain. The first peak occurred at 710 °C and the second peak was found at 850 °C as seen in **Figure 3.7.a**, indicating the onset of thermal decomposition as indicated by TGA analysis. Similarly, the $Ni/MgAl_2O_4$-20wt%SO_4 catalyst contained a peak at 700 °C, which was attributed to the desorption of sulfate from the catalyst in the form of $MgSO_4$ species as indicated by XRD analysis, which shows that sulfate species is present in the reduced catalyst.

The catalysts supported on SiO_2 (**Figure 3.7.b**) contained no peaks in the low temperature domain, which was an indication that no weak acid sites were present for the catalysts. After the introduction of sulfur, strong acid sites were formed, as indicated by the shoulder peak found in the region of 485 °C. The peak at 700 °C was assigned to decomposition of the sample, which was confirmed by TGA analysis. Table 3.2 summarises the quantity of acid sites found on both $MgAl_2O_4$ and SiO_2 supports. It was observed that the sulfated catalyst supported on $MgAl_2O_4$ contained more acid sites than that of the NiO/SiO_2-20wt%SO_4 catalyst, in both the low temperature range and high temperature range. Furthermore, the $Ni/MgAl_2O_4$-20wt%SO_4 catalyst contained a sulfur desorption peak which was absent in the TPD profile of the Ni/SiO_2-20wt%SO_4 catalyst. This could imply that the sulfur content was higher in $Ni/MgAl_2O_4$-20wt%SO_4 than Ni/SiO_2-20wt%SO_4, since there is additional sulfur interaction with the $MgAl_2O_4$ support.

Table 3.2: Acidic properties of sulfur modified and unmodified Ni-based catalysts

Catalyst	Acidity Temp (°C)	Quantity (µmol/g)
$NiO/MgAl_2O_4$	-	-
$NiO/MgAl_2O_4$-20wt%SO_4	200	1569
	520	212
$Ni/MgAl_2O_4$-20wt%SO_4	-	-
NiO/SiO_2	-	-
NiO/SiO_2-20wt%SO_4	485	36
Ni/SiO_2-20wt%SO_4	-	-

The TPD results indicate an increase in the acid sites of the catalysts after sulfur promotion for the catalysts supported on both $MgAl_2O_4$ and SiO_2 support. This observation is consistent with results obtained by Jin and co-workers.[35,36] It was reported that the generation of the strong acidity by the introduction of sulfur is due to the formation of the surface sulfur complex on the catalysts. Moreover, it was suggested that the strong electron attracting ability of a sulfur compound, like S=O, to accept electrons from a basic molecule, such as NH_3, is the primary factor to generate highly acidic properties.[35,37]

The acid site is the Ni(II) cation whose acidic strength is enhanced by the induction effect of S=O in the sulfur catalyst. It was noted that the acidity disappeared upon reduction for the $Ni/MgAl_2O_4$-20wt%SO_4 and Ni/SiO_2-20wt%SO_4 catalysts. This could imply that the primary source of acidity is due to the SO_4^{2-} species on the $MgAl_2O_4$ support. It has been reported by Nagase and co-workers that the oxidized state of sulfate is necessary for the generation of acidity on catalysts.[37] No peaks were observed in the high temperature range of the TPD plot for Ni/SiO_2-20wt%SO_4, which could imply that no sulfur is desorbed from the catalyst. The loss of acidity arise from the removal of surface oxygens bridged to both nickel and sulfur in the catalyst.[37,38]

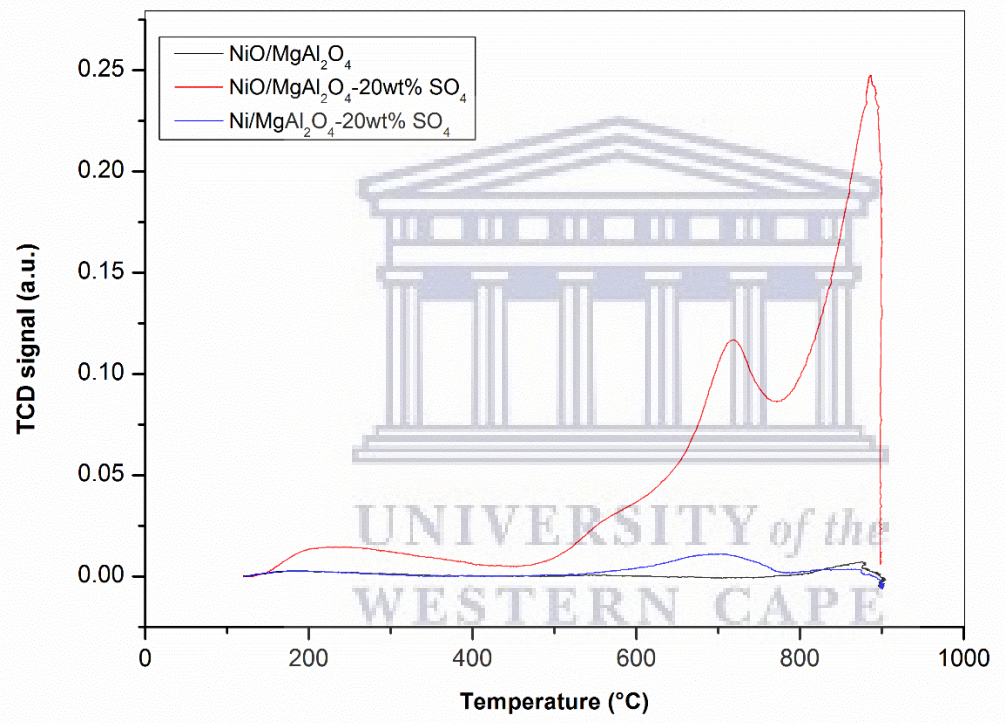

Figure 3.7. a) TPD profile of unmodified and modified NiO catalysts supported on $MgAl_2O_4$

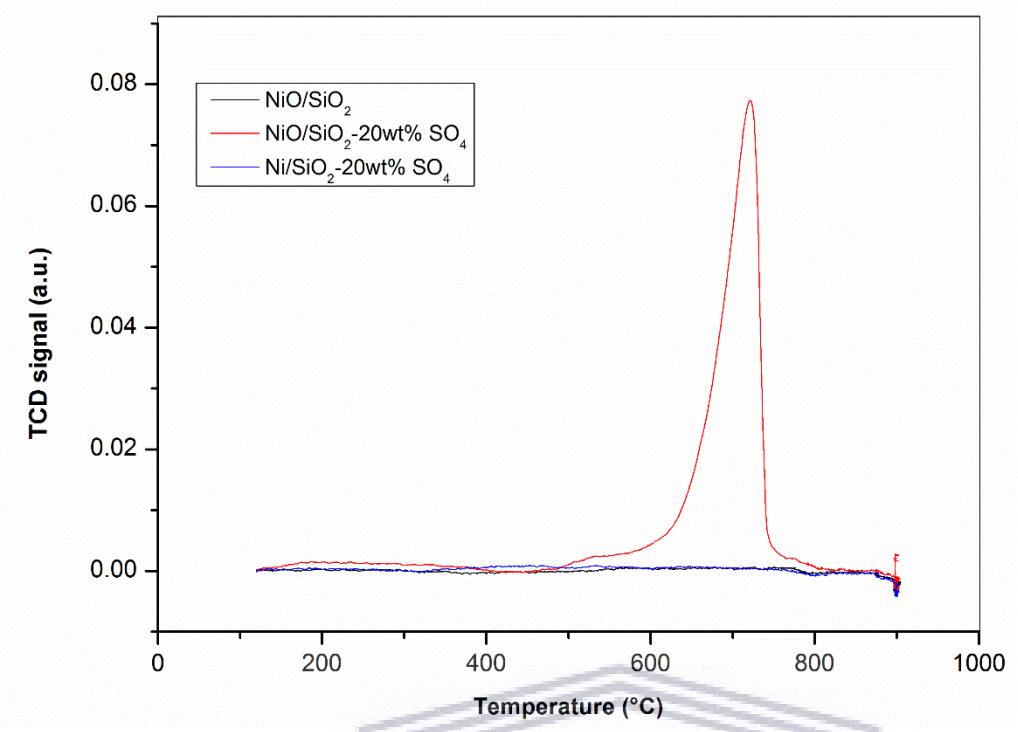

Figure 3.7. b) TPD profile of unmodified and modified NiO catalysts supported on SiO_2

As it has been suggested, a sulfur complex like S=O may be responsible for the acidity generated in the catalysts. Infrared spectroscopy has been used to confirm the nature of the sulfur species present on the different supports. FTIR analysis indicated the presence of the surface sulfur complex, consisting of covalent S-O double bonds present on the sulfur promoted nickel oxide catalysts (**Figure 3.8**). The $NiO/MgAl_2O_4$-20wt%SO_4 catalyst displayed four absorption bands at 1260 cm^{-1} 1180 cm^{-1}, 1100 cm^{-1} and 1060 cm^{-1}, respectively. A chelating bidentate complex usually has four absorption bands in the regions of 1240-1230 cm^{-1}, 1125-1090 cm^{-1}, 1035-995 $cm^{-1}$and 960-940 cm^{-1}, which are assigned to the asymmetric and symmetric stretching frequencies of S-O bonds.[39] This indicates that the sulfur species present in the $NiO/MgAl_2O_4$-20wt%SO_4 catalyst coordinates in a chelating bidentate fashion to the nickel metal. Additionally, the IR absorption bands at 712 cm^{-1} can be assigned to the bending mode of Al^{3+} occupied in the spinel. The bands at 615 cm^{-1} correspond to the spinel type structure of the $MgAl_2O_4$ support, which are associated with lattice vibrations of tetra- and octahedrally coordinated metal ions.[40]

The NiO/SiO_2-20wt%SO_4 catalyst displayed peaks at 1167 cm^{-1}, 1090 cm^{-1}, 1000 cm^{-1} and 832 cm^{-1}, 691 cm^{-1}, 618 cm^{-1} and 465 cm^{-1}, respectively. According to Yamaguchi *et. al*., if SO_4^{2-} in metal sulfates, such as $NiSO_4$, coordinates to Ni(II) through two of its oxygen atoms, a chelating or bridged bidentate complex is formed. A bridged bidentate complex also has four absorption bands at 1195-1160 cm^{-1}, 1110-1105 cm^{-1}, 1035-1030 cm^{-1} and 990-960 cm^{-1}, which are assigned to the stretching frequencies of the S-O bonds in the complex.[39] These values are in close range with the values obtained for the NiO/SiO_2-20wt%SO_4 catalyst. This suggests that the sulfur present in the NiO/SiO_2-20wt%SO_4 catalyst, coordinates to the metal in a bridging bidentate fashion. The absorption bands at 691 cm^{-1} and 618 cm^{-1} correlates to the anti-symmetric and symmetric stretching modes of Si-O-Si of the support, respectively. The band at 465 cm^{-1} is assigned to bending vibrations of Si-O-Si that is present in the SiO_2 support.[41]

Therefore, it is shown that the bonding in the sulfur complex is different on the two supports possibly resulting in differing electronic effects. It has been reported that the highest frequency in the chelating bidentate complex is higher than that of the bridged bidentate complex, which is consistent with the results obtained for the $NiO/MgAl_2O_4$-20wt%SO_4 and NiO/SiO_2-20wt%SO_4 catalysts. It has been noted in previous studies that bridging bidentate species desorb at low temperatures in TPD experiments, while chelating bidentate species desorb at more moderate temperatures. This is consistent with the observation from the TPD analysis and implies that the different bonding modes on the support might have an effect on the acidity of the catalysts.[39,42]

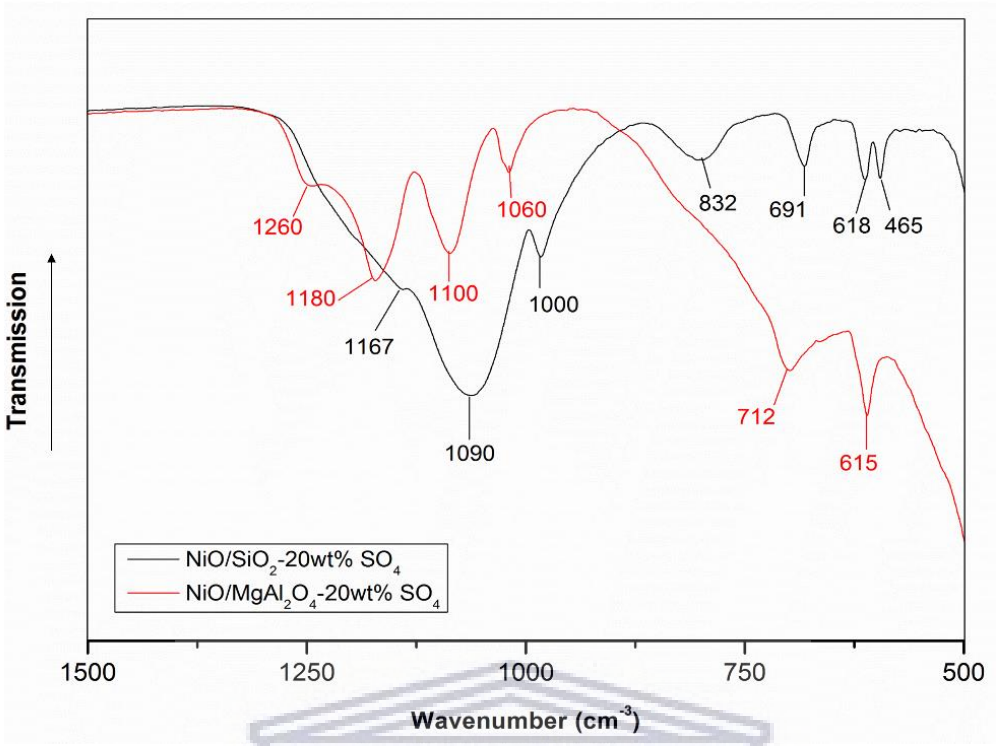

Figure 3.8. FTIR spectra of $NiO/MgAl_2O_4$-20wt%SO_4 and NiO/SiO_2-20wt%SO_4 catalysts

Temperature programmed reduction (TPR) analysis was used to characterize the reducibility of the unsulfated and sulfated nickel-supported catalysts. The TPR results for the unsulfated catalysts are presented in **Figure 3.9.a**. The TPR profile for NiO/SiO_2 shows that the catalyst reduces at 340 °C, which is typical for NiO-based catalysts. A shoulder peak is commonly found at high temperatures for supported NiO catalysts, indicating nickel-support interaction.[15] In this case, a small peak occurred at 470 °C which could be due to NiO interacting with the SiO_2 support.[43] A similar trend was observed for the $NiO/MgAl_2O_4$ catalyst. The first peak occurred at 550 °C, while a smaller peak at 650 °C was present, indicating that NiO had some interaction with the $MgAl_2O_4$ support.[44–46] The second peak for $NiO/MgAl_2O_4$ occurred at a higher temperature than that of NiO/SiO_2, indicating that the interaction between the metal and $MgAl_2O_4$ is stronger than the NiO-SiO_2 interaction, since reduction occurred at a higher temperature.

The strong interaction between the nickel and the $MgAl_2O_4$ support could form the $NiAl_2O_4$ phase, although this is difficult to determine as this phase overlaps with the $MgAl_2O_4$ phase in the XRD analysis. The particle size of NiO calculated from the XRD patterns indicated that the Ni(II) crystallite size on $NiO/MgAl_2O_4$ is smaller than NiO/SiO_2, which is further inferred by TPR analysis, since $NiO/MgAl_2O_4$ reduces at 550 °C due to the smaller crystallites that require a higher temperature to be reduced.[47] It has been reported previously that the structural and physiochemical properties of supported metal sulfates differ compared to bulk metal sulfates due to metal-support interactions, which has been observed in our study as well.[48]

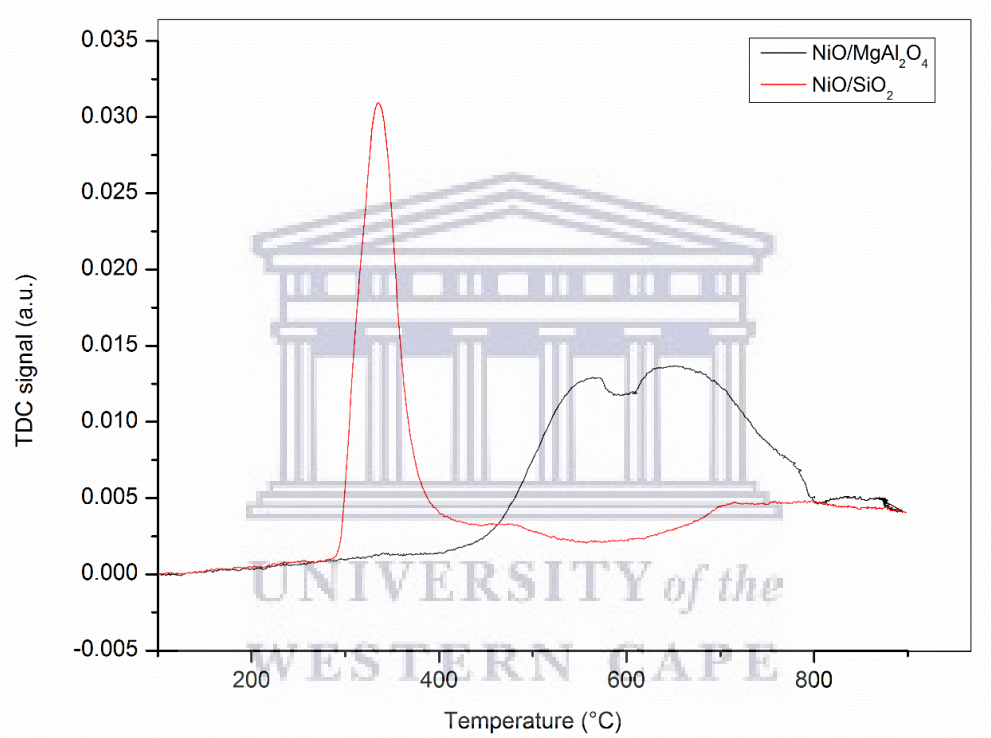

Figure 3.9. a) TPR profiles of unsulfated NiO catalysts supported on $MgAl_2O_4$ and SiO_2

Figure 3.9.b shows the TPR profiles of the sulfur modified catalysts on the different supports. Two peaks were observed for $NiO/MgAl_2O_4$-20wt%SO_4, the first peak, occurring at 400 °C could be due to the reduction of NiO, which was still present on the catalyst after sulfur modification as shown in the XRD results. The second peak occurred at 600°C and can be ascribed to the reduction of the sulfated species, $NiSO_4$ and $MgSO_4$, on the catalyst. Furthermore, it was noted that the peak at 650 °C in the TPR profile of $NiO/MgAl_2O_4$ was absent in the sulfated catalyst, which could indicate that any Ni-Al_2O_4 interactions is negligible in the sulfated catalyst.

The NiO/SiO_2-20wt%SO_4 catalyst displayed a split peak that occurred at a higher temperature than the unmodified catalyst on the SiO_2 support. The starting reduction temperature of $NiSO_4$ occurs at 340 °C, which is in accordance with the onset of the peak found in the TPR profile (Figure 3.9.b). The reduction of $NiSO_4$ is a one-step process according to the equation below.[49]

$$3NiSO_4 + 10H_2 \longrightarrow Ni_3S_2 + SO_2 + 10H_2O$$

An online mass spectrometer was connected to the TPR autochem to investigate whether the reduction of NiO/SiO_2-20wt%SO_4 followed the one-step process or whether any intermediate species were formed. Mass spectrometry showed the absence of peaks at 34 amu and 64 amu up to 435 °C (Figure S1.3), corresponding to H_2S or SO_2, respectively. However, the presence of H_2O was detected. The XRD analysis of NiO/SiO_2-20wt%SO_4 reduced at 435 °C (Figure S1.4) confirmed that the sample contained no intermediate phase. Hence, a possibility for the split peak could be due to reduction of Ni^{2+} and SO_4^{2-} ions on the surface of the catalyst at 435 °C, while the bulk reduction of the catalyst occurs at 500 °C.

TPR analysis indicates that NiO/SiO_2-20wt%SO_4 has a higher H_2-consumption, since this catalyst contains only $NiSO_4$, while the sulfur promoted catalyst supported on $MgAl_2O_4$ contains traces of NiO, $MgSO_4$ and $NiSO_4$ peaks as seen in the XRD patterns of $NiO/MgAl_2O_4$-20wt%SO_4 and NiO/SiO_2-20wt%SO_4 (**Figure 3.1**). Furthermore, the higher reduction temperature of $NiO/MgAl_2O_4$-20wt%SO_4 could be due to smaller, $NiSO_4$ particles on the catalyst as indicated by XRD and TEM analysis leading to stronger metal-support interactions which suppress reducibility.

Table 3.3: H_2-consumption of sulfur promoted catalysts on $MgAl_2O_4$ and SiO_2

Catalyst	T_{max} (°C)	H_2-consumption (µmol/g)
$NiO/MgAl_2O_4$-20wt%SO_4	400 600	584 7636
NiO/SiO_2-20wt%SO_4	435 500	12122

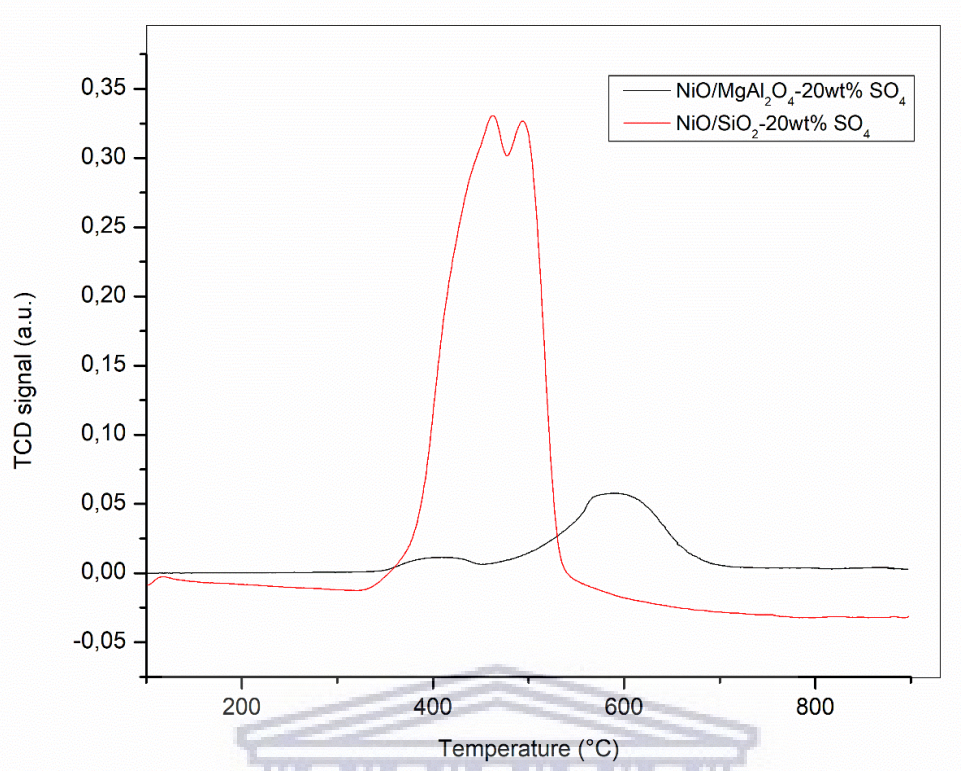

Figure 3.9. b) TPR profiles of sulfated NiO catalysts supported on $MgAl_2O_4$ and SiO_2

3.3.4. Catalytic performance

The catalysts $NiO/MgAl_2O_4$-20wt%SO_4 and NiO/SiO_2-20wt%SO_4, which contain the $NiSO_4$ phase, were evaluated for the dehydrogenation of propane. In separate experiments, the fresh catalysts $NiO/MgAl_2O_4$-20wt%SO_4 and NiO/SiO_2-20wt%SO_4 were reduced under a flow of H_2 gas at 50 ml/min to form the reduced catalysts, $Ni/MgAl_2O_4$-20wt%SO_4 and Ni/SiO_2-20wt%SO_4, both containing Ni_3S_2, which were then tested for the dehydrogenation of propane. **Figure 3.10** shows the conversion of propane towards the main products, over the sulfate-based and sulfide-based catalysts.

The conversion % of propane increased in the following order $NiO/MgAl_2O_4$-20wt%SO_4 (35%) < $Ni/MgAl_2O_4$-20wt%SO_4 (46%) < Ni/SiO_2-20wt%SO_4 (50%) < NiO/SiO_2-20wt%SO_4 (54%) at three minutes of the reaction time. It was noted that after the initial 3 minutes on stream, the $Ni/MgAl_2O_4$-20wt%SO_4, Ni/SiO_2-20wt%SO_4 and NiO/SiO_2-20wt%SO_4 catalysts showed a significant decrease in propane conversion to approximately 30%, while $NiO/MgAl_2O_4$-20wt%SO_4 increased to above 40% and remained fairly stable for 2 hours on stream. The $NiO/MgAl_2O_4$-20wt%SO_4 catalyst displayed an induction period, indicating that the active phase of $NiO/MgAl_2O_4$-20wt%SO_4 might be present after 30 minutes of the reaction time.

Previous studies have shown by XPS analysis that the S^{2-} species is present after completion of the reaction indicating that the SO_4^{2-} species is transformed to a NiS species which is the active phase of the dehydrogenation catalyst.[12] In our study, $Ni/MgAl_2O_4$-20wt%SO_4 and Ni/SiO_2-20wt%SO_4 contain the Ni_3S_2 phase and are therefore already in the active form. Interestingly, the NiO/SiO_2-20wt%SO_4 containing $NiSO_4$ shows the same conversion or slightly higher than the Ni_3S_2 catalysts. This may be due to the catalyst being quickly reduced to Ni_3S_2 i.e. within the first three minutes compared to the $NiO/MgAl_2O_4$-20wt%SO_4 catalyst. The TPR analysis indicated that the reducibility of $NiO/MgAl_2O_4$-20wt%SO_4 to Ni_3S_2 was suppressed due to stronger metal support interactions and therefore an activation period is observed.

Additionally, $NiO/MgAl_2O_4$-20wt%SO_4 was subjected to a 30 minute reaction time, followed by XRD analysis of the spent catalyst for this reaction. The XRD profile showed that Ni_3S_2 species was present in the catalyst after 30 minutes and corresponded to an increase in conversion after this time. Activation periods are common in heterogeneous catalysis and some possible causes of activation are the formation of active carbon species, the creation of surface defects and an increase in active surface area.[17] The observed increase in activity in the $NiO/MgAl_2O_4$-20wt%SO_4 and NiO/SiO_2-20wt%SO_4 catalysts may be due to the increase in active surface area as the catalyst is reduced to Ni_3S_2 and this is confirmed by the BET results. Furthermore, the higher activity on the $MgAl_2O_4$ support could be ascribed to the smaller particle sizes of the sulfur modified nickel species on the catalysts, hence a better dispersion of the active phase. This may increase the exposure of the catalytically active Ni-S moiety. Therefore, the structural characteristics such as size and surface area of the nickel sulfide particles as well as reducibility seem to influence the catalytic activity.

The selectivity of the four catalysts at 30 minutes on stream is shown in **Figure 3.11** below. The $NiO/MgAl_2O_4$-20wt%SO_4 and $Ni/MgAl_2O_4$-20wt%SO_4 catalysts displayed the highest selectivity toward propene of about 70% which increased to almost 80% after 2 hours on stream, indicating that the catalyst supported on $MgAl_2O_4$ has a better dehydrogenation activity than both NiO/SiO_2-20wt%SO_4 and Ni/SiO_2-20wt%SO_4 catalysts. Methane, ethane, ethene and C4 paraffins were additional products that were produced as shown in **Figure 3.11**. The selectivity toward methane and that of the C2-C4 products, suggests that possibly cracking and hydrogenolysis occur as secondary reactions. In addition, there were less secondary reactions on the $MgAl_2O_4$ support possibly due to a higher desorption rate of propylene, which could be due to stronger electronic effects of the metal-support interactions in comparison to nickel-silica.

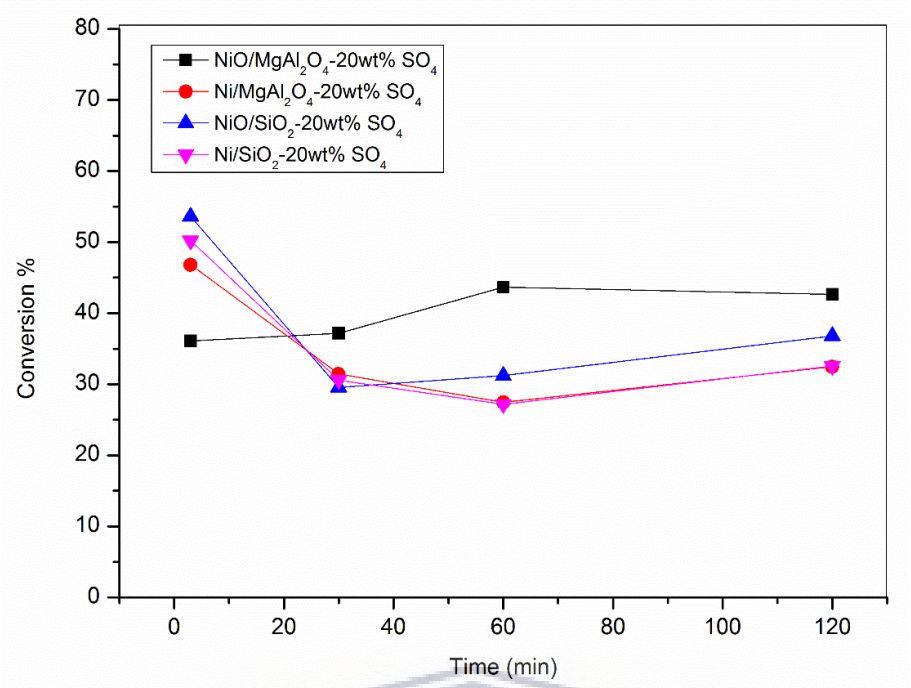

Figure 3.10. Conversion % of sulfur modified Ni-based catalysts supported on $MgAl_2O_4$ and SiO_2 with reduction (Ni/support-20wt%SO_4) and without reduction (NiO/support-20wt%SO_4)

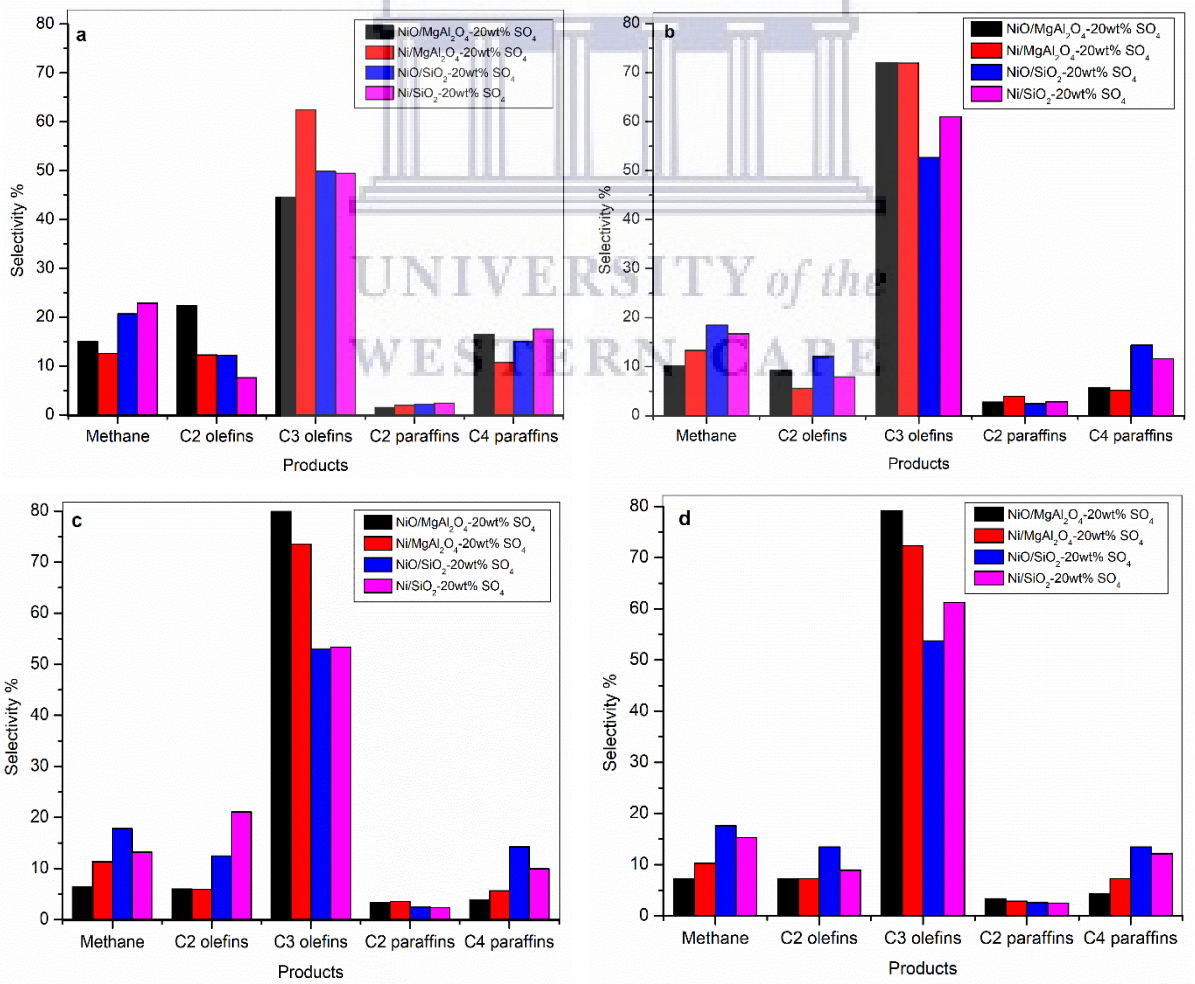

Figure 3.11. Selectivity % of sulfur modified Ni-based catalysts supported on $MgAl_2O_4$ and SiO_2 at a) 3 minutes b) 30 minutes c) 60 minutes and d) 120 minutes

It was observed that after 2 hour reactions, sulfur was present in the form of Ni_3S_2 particles in all the spent catalysts as shown in **Figure 3.12**. Therefore, it can be implied that the sulfur modified nickel catalysts exhibit high stability characteristics, with regard to retaining sulfur on the catalysts.

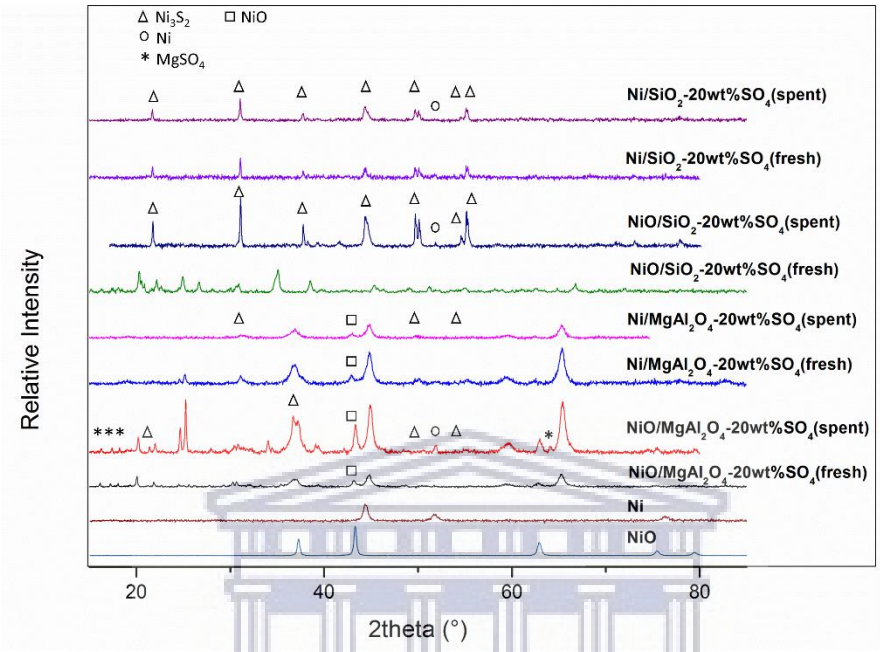

Figure 3.12. XRD profile of fresh and spent sulfur modified catalysts supported on $MgAl_2O_4$ and SiO_2

The $NiO/MgAl_2O_4$-20wt%SO_4 catalyst was evaluated for 7 hours to investigate catalyst activity and catalyst deactivation over an extended period of time. **Figure 3.13.a** shows that the conversion of propane increased during the activation period and gradually decreases after 180 minutes on stream. The reason for the decline in propane conversion could be due to the loss of sulfur from the catalyst.[50] This trend was observed for both $NiO/MgAl_2O_4$-20wt%SO_4 and NiO/SiO_2-20wt%SO_4 as seen in the results for the spent catalysts in **Figure 3.13.b**.

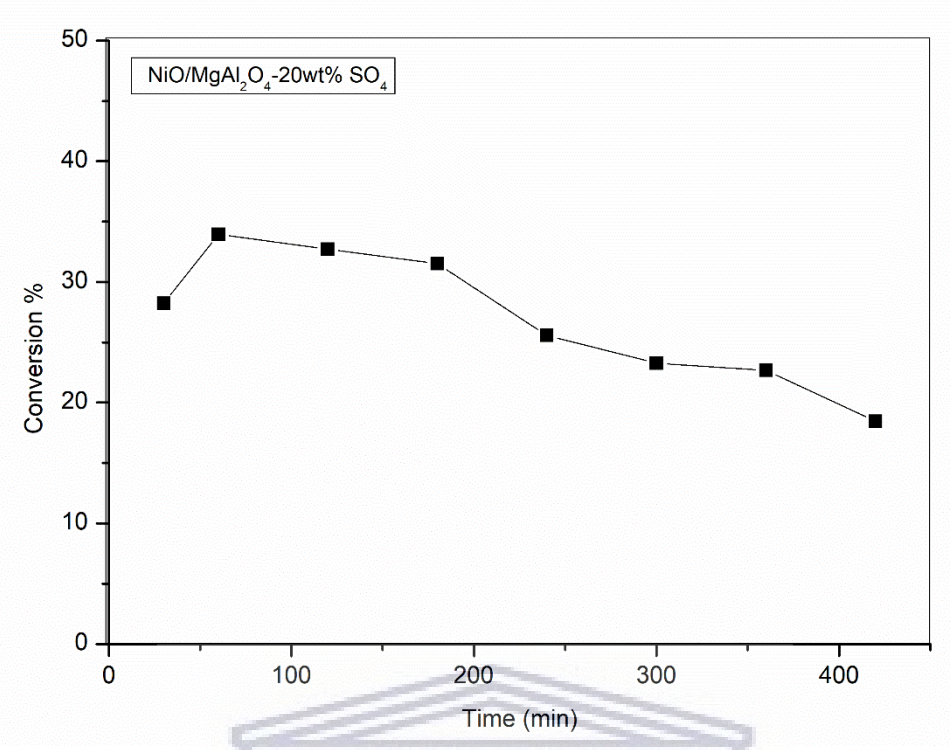

Figure 3.13. a) Conversion % of $NiO/MgAl_2O_4$-20wt%SO_4 over 7 hours on stream

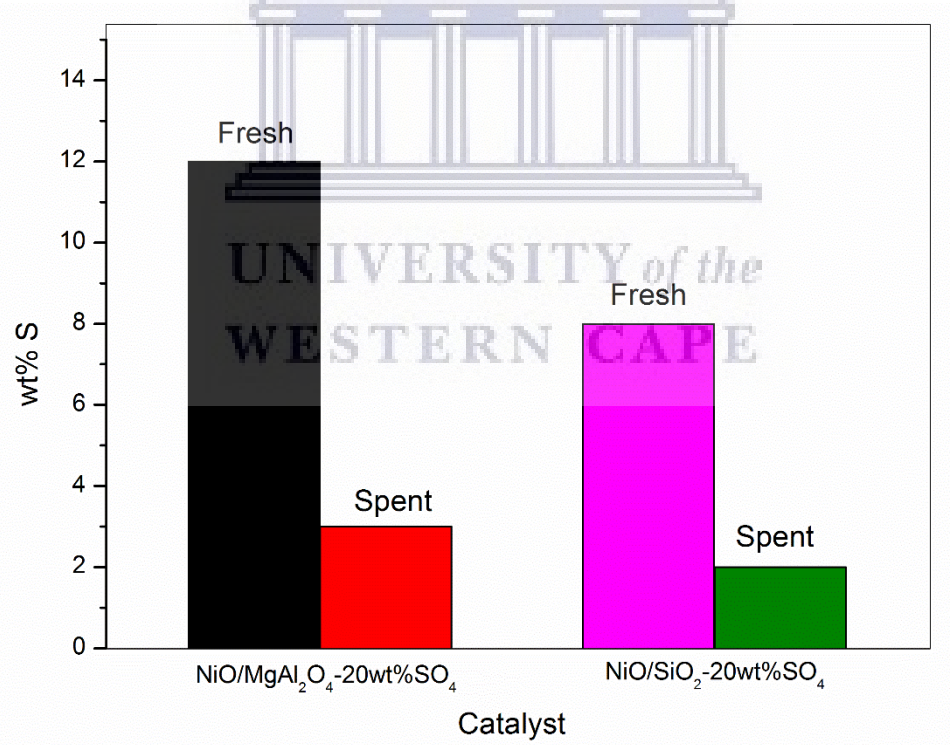

Figure 3.13. b) EDS results of fresh and spent $NiO/MgAl_2O_4$-20wt%SO_4 and NiO/SiO_2-20wt%SO_4 catalysts

The selectivity toward the various products is shown in **Figure 3.13.c** and further confirms the excellent dehydrogenation activity toward the desired propylene product over 7 hours. Although there is a decrease in conversion from about 35% to 20% at the end of the reaction, interestingly, only a slight decrease in selectivity to propylene was noted. This occurred concurrently with a slight increase in methane selectivity possibly due to hydrogenolysis reactions over nickel particles, as sulfur is lost.

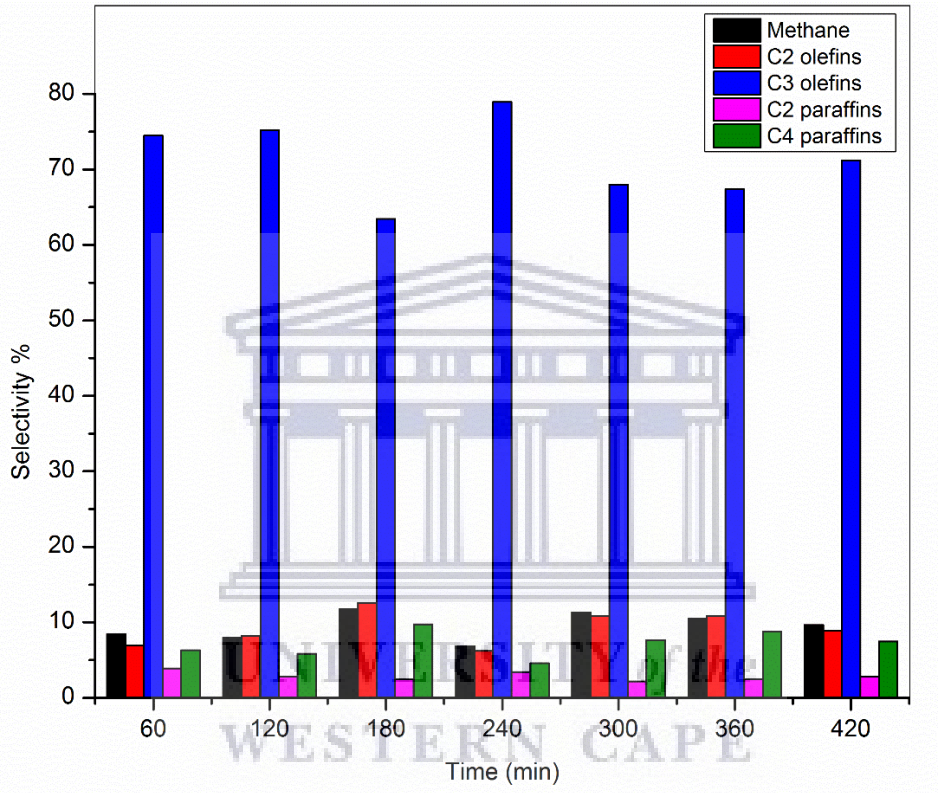

Figure 3.13. c) Selectivity % of $NiO/MgAl_2O_4$-20wt%SO_4 over 7 hours on stream

3.4. Conclusion

Nickel oxide catalysts supported on $MgAl_2O_4$ and SiO_2 were successfully sulfated using ammonium sulfate as the sulfiding agent, to form $NiO/MgAl_2O_4$-20wt%SO_4 and NiO/SiO_2-20wt%SO_4 (both containing $NiSO_4$). In separate experiments, the sulfated catalysts were reduced to form $Ni/MgAl_2O_4$-20wt%SO_4 and Ni/SiO_2-20wt%SO_4, which contained the sulfided species (Ni_3S_2). Structural and textural characterization of the catalysts revealed that sulfur promoted nickel species supported on $MgAl_2O_4$ displayed smaller particles with a higher dispersion in comparison to the particles on the SiO_2 support.

STEM analysis showed that the $NiSO_4$ and Ni_3S_2 particles formed localised clusters on the SiO_2 support. These clusters were effectively absent on the $MgAl_2O_4$ support. Furthermore, it was revealed that the bonding of sulfur varies on the two supports. Sulfate is bonded as a chelating bidentate ligand on $MgAl_2O_4$ and a bridging bidentate ligand on the SiO_2 support, which has an effect on the acidic properties of the catalyst. The metal-support interaction were stronger on the $MgAl_2O_4$ support as indicated by TPR analysis. Whereby, peaks occurring at higher temperatures on $NiO/MgAl_2O_4$-20wt%SO_4 corresponded to the decomposition of sulfur, which contributes to the stability of the catalyst, since the loss of sulfur is associated with the deactivation of the catalysts.

Catalytic evaluation of the sulfate-based and sulfide-based catalysts supported on $MgAl_2O_4$ and SiO_2 showed that the catalyst supported on $MgAl_2O_4$ had a higher activity which was ascribed to the smaller particle size of the active species with a larger exposed area of Ni-S moeities, a stronger metal-support interaction, which results in a high electronic effect and facilitates the desorption of the products leading to a high selectivity of above 70% for propylene.

3.5 References

1 Y. Zhang, W. Yao, H. Fang, A. Hu and Z. Huang, *Sci. Bull.*, 2015, **60**, 1316–1331.
2 G. Wang, C. Gao, X. Zhu, Y. Sun, C. Li and H. Shan, *ChemCatChem*, 2014, **6**, 2305–2314.
3 M. R. A. Blomberg, P. E. M. Siegbahn, U. Nagashima and J. Wennerberg, *J. Am. Chem. Soc.*, 1991, **113**, 424–433.
4 B. M. Weckhuysen and R. A. Schoonheydt, *Catal. Today*, 1999, **51**, 223–232.
5 G. Bekmukhamedov, A. Mukhamed'yarova, S. Egorova and A. Lamberov, *Catalysts*, 2016, **6**, 162.
6 E. J. Jang, J. Lee, H. Y. Jeong and J. H. Kwak, *Appl. Catal. A Gen.*, 2019, **572**, 1–8.
7 M. Bayat and M. R. Rahimpour, *J. Taiwan Inst. Chem. Eng.*, 2014, **45**, 2906–2919.
8 I. Amghizar, L. A. Vandewalle, K. M. Van Geem and G. B. Marin, *Engineering*, 2017, **3**, 171–178.
9 H. Xiong, S. Lin, J. Goetze, P. Pletcher, H. Guo, L. Kovarik, K. Artyushkova, B. M. Weckhuysen and A. K. Datye, *Angew. Chemie - Int. Ed.*, 2017, **56**, 8986–8991.
10 J. Im and M. Choi, *ACS Catal.*, 2016, **6**, 2819–2826.
11 Q. Zhu, G. Wang, J. Liu, L. Su and C. Li, *ACS Appl. Mater. Interfaces*, 2017, **9**, 30711–30721.
12 G. Wang, Z. Meng, J. Liu, C. Li and H. Shan, *ACS Catal.*, 2013, **3**, 2992–3001.
13 S. M. K. Airaksinen, M. E. Harlin and A. O. I. Krause, *Ind. Eng. Chem. Res.*, 2002, **41**, 5619–5626.
14 A. B. Gaspar, J. L. F. Brito and L. C. Dieguez, *J. Mol. Catal. A Chem.*, 2003, **203**, 251–266.
15 C. Li, Y. W. Chen and C. P. Corporation, *Thermochim. Acta*, 1995, **256**, 457–465.
16 S. S. He, L. Zhang, S. S. He, L. Mo, X. Zheng, H. Wang and Y. Luo, *J. Nanomater.*, 2015, **2015**, 1–8.
17 D. E. Resasco, B. K. Marcus, C. S. Huang and V. A. Durante, *J. Catal.*, 1994, **146**, 40–55.
18 G. Wang, N. Sun, C. Gao, X. Zhu, Y. Sun, C. Li and H. Shan, *Appl. Catal. A Gen.*, 2014, **478**, 71–80.
19 C. T. Shao, W. Z. Lang, X. Yan and Y. J. Guo, *RSC Adv.*, 2017, **7**, 4710–4723.
20 I. Ro, J. Resasco and P. Christopher, *ACS Catal.*, 2018, **8**, 7368–7387.
21 J. Guo, H. Lou, H. Zhao, D. Chai and X. Zheng, *Appl. Catal. A Gen.*, 2004, **273**, 75–82.
22 Q. Zafar, T. Mattisson and B. Gevert, *Energy and Fuels*, 2006, **20**, 34–44.
23 J. Salmones, J. A. Galicia, J. A. Wang, M. A. Valenzuela and G. Aguilar-Rios, *J. Mater. Sci. Lett.*, 2000, **19**, 1033–1037.
24 E. N. Alvar, M. Rezaei and H. N. Alvar, *Powder Technol.*, 2010, **198**, 275–278.
25 M. Tadić, M. Panjan and D. Marković, *Mater. Lett.*, 2010, **64**, 2129–2131.
26 L. P. R. Profeti, E. A. Ticianelli and E. M. Assaf, *Appl. Catal. A Gen.*, 2009, **360**, 17–25.
27 M. Y. Nassar, I. S. Ahmed and I. Samir, *Spectrochim. Acta - Part A Mol. Biomol. Spectrosc.*, 2014, **131**, 329–334.
28 S. Musić, N. Filipović-Vinceković and L. Sekovanić, *Brazilian J. Chem. Eng.*, 2011, **28**, 89–94.
29 F. Jin, H. Long, W. Song, G. Xiong, X. Guo and X. Wang, *Energy and Fuels*, 2013, **27**, 3394–3399.
30 P. P. Li, W. Z. Lang, K. Xia, L. Luan, X. Yan and Y. J. Guo, *Appl. Catal. A Gen.*, 2016, **522**, 172–179.
31 S. He, C. Sun, H. Du, X. Dai and B. Wang, *Chem. Eng. J.*, 2008, **141**, 284–289.
32 V. R. Pradhan, J. W. Tierney, I. Wender and D. E. Herrick, *Energy and Fuels*, 1991, **5**, 712–720.
33 F. H. Alhassan, U. Rashid, M. S. Al-Qubaisi, A. Rasedee and Y. H. Taufiq-Yap, *Powder Technol.*, 2014, **253**, 809–813.
34 S. Moon, H. J. Chae and M. B. Park, *Appl. Catal. A Gen.*, 2018, **553**, 15–23.
35 T. Jin, T. Yamaguchi and K. Tanabe, *J. Phys. Chem.*, 1986, **90**, 4794–4796.
36 G. A. H. Mekhemer, *Colloids Surfaces A Physicochem. Eng. Asp.*, 2006, **274**, 211–218.
37 Y. Nagase, T. Jin, H. Hattori and T. Yamaguchi, *Bull. Chem. Soc. Japan*, 1985, **58**, 916–918.

38 K. Tanabe and T. Yamaguchi, *Design of sulfur-promoted solid superacid catalyst*, 1989, vol. 44.
39 T. Yamaguchi, T. Jin and K. Tanabe, *J. Phys. Chem.*, 1986, **90**, 3148–3152.
40 S. Tripathy and D. Bhattacharya, *J. Asian Ceram. Soc.*, 2013, **1**, 328–332.
41 R. Antony, S. T. David Manickam, P. Kollu, P. V. Chandrasekar, K. Karuppasamy and S. Balakumar, *RSC Adv.*, 2014, **4**, 24820–24830.
42 S. Ordóñez, E. Díaz, M. León and L. Faba, *Catal. Today*, 2011, **167**, 71–76.
43 B. Mile, D. Stirling, M. A. Zammitt, A. Lovell and M. Webb, *J. Catal.*, 1988, **114**, 217–229.
44 Z. Mosayebi, M. Rezaei, A. B. Ravandi and N. Hadian, *Int. J. Hydrogen Energy*, 2012, **37**, 1236–1242.
45 D. S. Park, Z. Li, H. Devianto and H. I. Lee, *Int. J. Hydrogen Energy*, 2010, **35**, 5673–5680.
46 N. Nakamura, R. Takahashi, S. Sato, T. Sodesawa and S. Yoshida, *Phys. Chem. Chem. Phys.*, 2000, **2**, 4983–4990.
47 J. F. Da Costa-Serra, R. Guil-López and A. Chica, *Int. J. Hydrogen Energy*, 2010, **35**, 6709–6716.
48 J. R. Sohn and W. C. Park, *Korean J. Chem. Eng.*, 2002, **19**, 580–586.
49 F. Habashi, S. A. Mikhail and K. V. Van, *Can. J. Chem.*, 1976, **54**, 3646–3650.
50 G. Wang, C. Li and H. Shan, *ACS Catal.*, 2014, **4**, 1139–1143.

CHAPTER 4: Synthesis, characterisation and catalytic activity of nickel sulfided catalysts for the dehydrogenation of propane: effect of sulfiding agent and sulfidation temperature

4.1 Introduction

With an increasing demand for olefins, processes for alkane dehydrogenation have gained considerable attention. The dehydrogenation of light alkanes serves as a fundamental reaction for the petrochemical industry and refining, since it is a selective process used to produce short-chain alkenes. Two common types of industrial catalysts have been developed and patented for this reaction, namely, chromia-based catalysts and platinum-based catalysts. However, both catalysts suffer from drawbacks, including the high cost of platinum and toxic effect of chromium, which limit their application to some extent. [1–7] In recent years, sulfided metal catalysts have gained considerable attention in the academic and patent literature.[8–11] For example, sulfided nickel catalysts have been identified as an alternative type of catalyst in dehydrogenation reactions. Wang *et al*. found that the introduction of sulfur on nickel oxide catalysts decreased coking and increased the dehydrogenation activity of the catalysts significantly.[4,8] Transition metal sulfides are usually prepared by direct sulfiding of a metal salt or by decomposition of a sulfur-containing precursor.[12]

The promotive effect of H_2S on metal oxides have been widely studied.[13,14] H_2S is decomposed to H_2 and S^{2-}, which is the source of sulfur on a range of metal components. However, H_2S is highly toxic and a high corrosion resistance is required for industrial equipment leading to a high investment cost.[13,15,16] Various alternative sulfiding agents have been used in order to introduce sulfur into metal sulfided catalysts to improve catalytic activity for dehydrogenation reactions.[4,17,18]

Wang *et al*. prepared sulfur modified catalysts through the addition $(NH_4)_2SO_4$ on $Ni/MgAl_2O_4$ and $Mo/MgAl_2O_4$ catalysts for the dehydrogenation of isobutane.[4,19] The adsorption of various anions, such as sulfate ions onto oxides have been investigated as a means of improving their catalytic activity.[20] The addition of relatively safe ammonium sulfate to metal catalysts have been explored in previous research studies.[4,19,21,22]

Liu and co-workers used $(NH_4)_2S$, as a sulfiding agent, to sulfide a $CoMo/Al_2O_3$ catalyst. They speculated that due to the high sulfidation activity of S^{2-} the transition metals of the catalyst would react with with $(NH_4)_2S$ leading to the full sulfidation of the active components.[17] With this reasoning, $(NH_4)_2S$ was used as a sulfiding agent in their study through a simple sulfiding procedure in low temperature and ambient pressure conditions. Furthermore, DMSO is a sulfur containing organic solvent used as a sulfiding agent for refineries due to its ease of handling and relatively less toxic properties.[23,24] The Ni/Al_2O_3 catalysts were sulfided with DMSO by Resasco for the dehydrogenation of isobutane.[18] Three different procedures have been reported for the conventional sulfiding of oxidic catalyst precursors: 1) reduction followed by sulfiding of the reduced catalyst, 2) simultaneous reduction and sulfiding and 3) sulfiding followed by reduction. The first two routines are more typically applied, where H_2 is used for the *in situ* reduction.[25,26]

Furthermore, Yu *et al*. studied the intrinsic effect of various anion precursors on nickel catalysts.[27] It was reported that the properties of the anions might affect the dispersion of particles during drying, calcination and reduction of the catalyst. It has been suggested that the anion might be involved in modifying catalytic behaviours of the catalyst. This could be due to the different anions, that have different properties and distinct decompostion temperatures. The anion will interact with the nickel cation or the support in various ways, which could potentially affect the dispersion of the nickel species, reduction of the nickel oxide and the interaction of the nickel with the support. Therefore, a fundamental understanding about the effects of precusor anions on the catalyst is required for the development of effective catalysts.[27] In our study, we investigate the effect of sulfides with various precursors, hence containing different anions, on the dispersion, particle size and phase of nickel-sulfide. Moreover, the decomposition of the sulfiding agent is important to determine which sulfiding agent is most effective in the sulfidation of the nickel catalyst.

Previous studies demonstrate that catalyst textural properties and catalytic performance were greatly influenced by treatment conditions such as sulfidation temperature on catalysts for hydrodesulfurization reactions.[28–30] Jiang *et al*. found that Mo-based catalysts sulfidation depended on temperature.[28] They reported that lower sulfidation temperatures (< 500 °C) had little effect on the catalyst morphology or catalytic activity and catalytic stability increased when sulfidation temperature was > 500 °C.[28]

Farag and co-workers reported complete sulfidation to a highly crystalline MoS_2-2H structure at 800 °C and sulfidation at 400 °C produced an amorphous MoS_2 state.[29] Therefore, it is clearly observed from literature that temperature can influence the degree of sulfidation, catalyst morphology and catalytic activity. However, to the best of our knowledge, not much attention has been paid to the sulfidation temperature on dehydrogenation catalysts. For this study we compare the effect of three sulfiding agents, containing different anions, namely, $(NH_4)_2SO_4$ (S1), $(NH_4)_2S$ (S2) and DMSO (S3) for the sulfidation of Ni/$MgAl_2O_4$ catalyst. These sulfiding agents decompose at 250 °C, 100 °C and 189 °C for S1, S2 and S3, respectively. Herein, we investigate the effect of the sulfiding agent and sulfidation temperature on the morphology, textural properties and catalytic activity of the sulfided catalysts. Initially, NiO/$MgAl_2O_4$ catalysts were reduced to Ni/$MgAl_2O_4$ before being sulfided to Ni/$MgAl_2O_4$-Sx-y, where x represents the sulfiding agent and y represents the temperature at which sulfidation took place.

4.2 Experimental

4.2.1 Raw materials

The following chemicals were used in the study: Magnesium nitrate hexahydrate (98%-102%, Sigma Aldrich), aluminium nitrate nonahydrate (≥98%, Sigma Aldrich), oxalic acid (99.5%, LabChem), nickel nitrate hexahydrate (≥97%, Sigma Aldrich), ammonium sulfate (99%, LabChem), ammonium sulfide (20wt%, Sigma Aldrich), DMSO (≥99.9%, Sigma Aldrich) and propane gas. Distilled water is obtained by a house supply that produces Milli-Q water.

4.2.2 Catalyst preparation: Synthesis of $MgAl_2O_4$ support, supported Ni catalysts and sulfur modified catalysts

The synthesis of $MgAl_2O_4$ was performed according to our previous work and adapted by Nassar and co-workers.[31,32] The targeted loading of Ni by weight was 13 wt% for all catalysts. Nickel oxide catalysts supported on $MgAl_2O_4$ was prepared by wetness impregnation using $Ni(NO_3)_2.6H_2O$ as the metal precursor. After impregnation of the supports, the catalysts were dried at 140 °C overnight and calcined at 700 °C in air for 2 hours. The catalyst was then reduced under a flow of H_2 (50 ml/min) at 600 °C for 5 hours.

Sulfur modified Ni/$MgAl_2O_4$ catalysts were prepared using three different sulfiding agents: $(NH_4)_2SO_4$ (S1), $(NH_4)_2S$ (S2) and DMSO (S3). The sulfiding agents were utilized without dilution for catalyst sulfidation. The molar ratio of Ni:S is 1:5 for each sulfiding agent. The catalysts were loaded into the reactor, sulfided with the calculated amount of sulfiding agent under a flow of nitrogen (50 ml/min) at 200 °C, 400 °C and 550 °C for 3 hours.

4.3 Results and Discussion

4.3.1 Structural and textural properties of the sulfided catalysts

The X-ray diffraction (XRD) pattern of Ni/$MgAl_2O_4$ is shown in **Figure 4.1.a** below. The reflections corresponding to the $MgAl_2O_4$ phase occur at 19°, 31°, 37°, 45°, 56°, 59°, 65° and 77° 2θ angles. The diffraction peaks corresponding to $MgAl_2O_4$ can be indexed to the cubic spinel structure of the $MgAl_2O_4$ support.[31] The possibility of intermediate products have not been detected in the support, as indicated by the absence of MgO and Al_2O_3 peaks, which consequently confirm the single phase of the as-synthesised $MgAl_2O_4$ support. The peak present at 52° 2θ is associated with the reduced Ni metal on the catalyst. The peaks present in the 2θ regions 43° and 63° correspond to NiO which was not fully reduced during the reduction step of the catalyst. According to MATCH software, using semi-quantitative phase analysis, the % of NiO still present on the catalyst was 6.4%. The Scherrer equation was applied to calculate the particle size at 52° 2θ of the unmodified Ni and was equal to 35 nm.

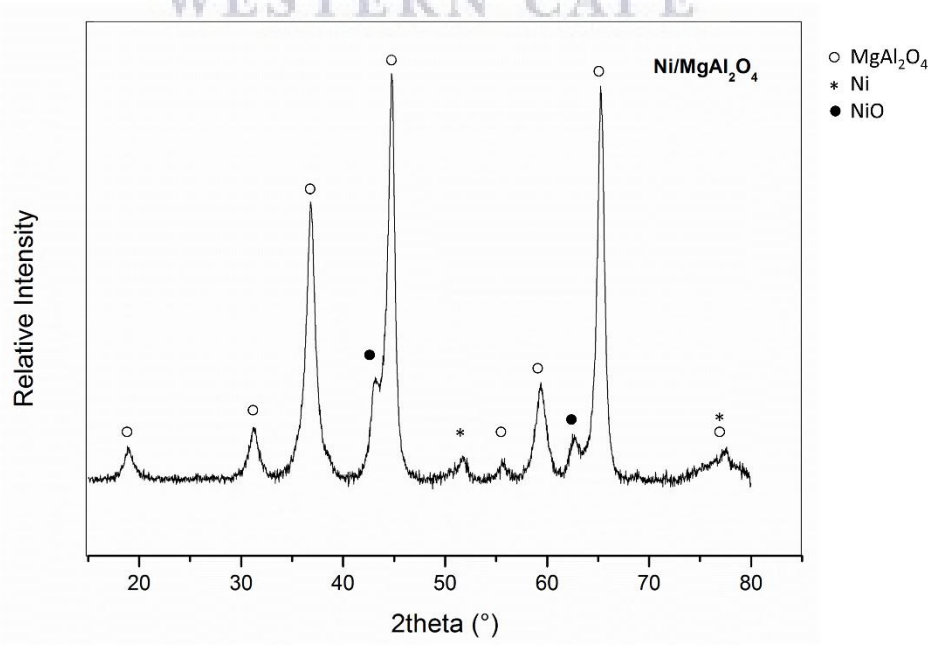

Figure 4.1. a) XRD pattern of Ni/$MgAl_2O_4$

The XRD patterns of $Ni/MgAl_2O_4$ sulfided with $(NH_4)_2SO_4$ (S1) to form $Ni/MgAl_2O_4$-S1-y, where y is the temperature of sulfidation, is shown in **Figure 4.1.b**. At 200 °C, the XRD pattern of $Ni/MgAl_2O_4$-S1-200 matched that of $(NH_4)_2SO_4$, with traces of reduced Ni and the $MgAl_2O_4$ support. At sulfidation temperatures of 400 °C and 550 °C, the XRD pattern of $Ni/MgAl_2O_4$-S1-400 and $Ni/MgAl_2O_4$-S1-550, contain peaks corresponding to $MgSO_4$, indicating that the SO_4^{2-} anion from the sulfiding agent has a stronger interaction with the support than the Ni metal on the catalyst. As seen in the XRD patterns of all three catalysts that were sulfided with $(NH_4)_2SO_4$, the presence of nickel-sulfur species were absent or the intensity was insufficient to be detected by XRD analysis. The % of unreacted Ni with sulfur is 2%, 11% and 5% for $Ni/MgAl_2O_4$-S1-200, $Ni/MgAl_2O_4$-S1-400 and $Ni/MgAl_2O_4$-S1-550 catalysts, detected by MATCH software. This could imply that there is more interaction between sulfur and the $MgAl_2O_4$ support in $Ni/MgAl_2O_4$-S1-400 and $Ni/MgAl_2O_4$-S1-550 catalysts, leading to a higher % of unreacted Ni metal.

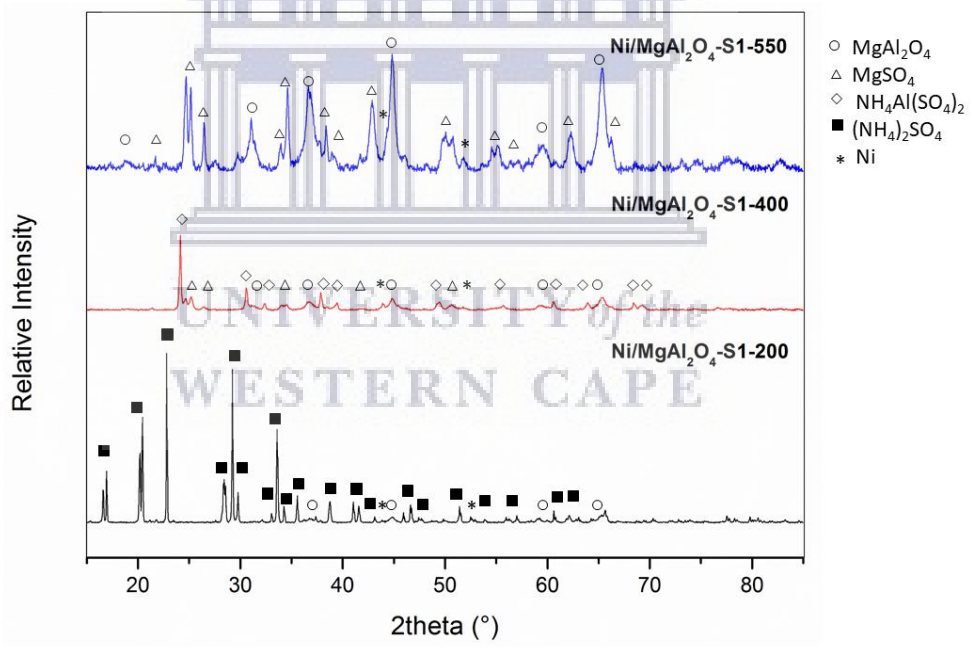

Figure 4.1. b) XRD pattern of $Ni/MgAl_2O_4$-S1 sulfided at 200 °C, 400 °C and 550 °C

The XRD patterns of $Ni/MgAl_2O_4$ sulfided with $(NH_4)_2S$ (S2) to form $Ni/MgAl_2O_4$-S2-y, where y is the temperature of sulfidation, is shown in **Figure 4.1.c**. For the $Ni/MgAl_2O_4$-S2-200 catalyst, the peaks present in the 2θ regions 30 °, 34°, 53° and 56° correspond to NiS on the catalyst. Studies have shown that nickel-sulfide can exist as several phases. The reaction of nickel and sulfur at temperatures between 177 °C – 477 °C under steady state conditions could produce the NiS, Ni_3S_2, Ni_6S_5 and NiS_2 phases.

The formation of a specific nickel-sulfide phase depends on various factors, such as the role of starting precursors and temperature.[33,34] The $Ni/MgAl_2O_4$-S2-400 and $Ni/MgAl_2O_4$-S2-550 catalysts contained Ni_3S_2 phase after sulfidation. It can be noticed that when using the $(NH_4)_2S$ precursor nickel sulfides are easily formed at all temperatures compared to the $(NH_4)_2SO_4$ sulfiding agent.

Furthermore, an increase in sulfidation temperature resulted in the formation of a different nickel-sulfur species compared to the lower temperature of 200 °C indicating that the sulfidation temperature could influence the type of nickel-sulfur species that form. It was noted that as the sulfidation temperature is increased, the NiO peak disappears and there is an increase in the metal sulfided phases (Ni_3S_2 and NiS) when using $(NH_4)_2S$ as the sulfiding agent. The % of unreacted Ni according to MATCH is 1% and 0.5% for $Ni/MgAl_2O_4$-S2-200 and $Ni/MgAl_2O_4$-S2-400 catalysts. This could suggest that $(NH_4)_2S$ is an effective sulfiding agent, as complete sulfidation can be obtained at low temperatures, which is probably due to the low decomposition temperature of $(NH_4)_2S$ and the presence of the S^{2-} ion on of $(NH_4)_2S$. The S^{2-} ion is known to be involved in the formation of nickel-sulfide species, which is the active phase for dehydrogenation.[4] The crystallite size of nickel-sulfur particles was calculated using the Scherrer equation. The peak at 53° was used to calculate the crystallite size of NiS and was found to be equal to 9 nm.

The peaks present in the 2θ regions 21 °, 50° and 55° correspond to Ni_3S_2 on the $Ni/MgAl_2O_4$-S2-400 and $Ni/MgAl_2O_4$-S2-550 catalysts. The crystallite size of Ni_3S_2 on $Ni/MgAl_2O_4$-S2-400 and $Ni/MgAl_2O_4$-S2-550 was calculated using the peak at 55° and equalled 11 nm and 12 nm, respectively. The crystallite sizes of nickel sulfides are smaller compared to the unsulfided nickel.

This indicates the sulfur acts as a structural promoter and reduces the particle size of nickel. However, the crystallite sizes although still smaller than pure nickel, do increase in size with the increase in sulfidation temperature as expected.

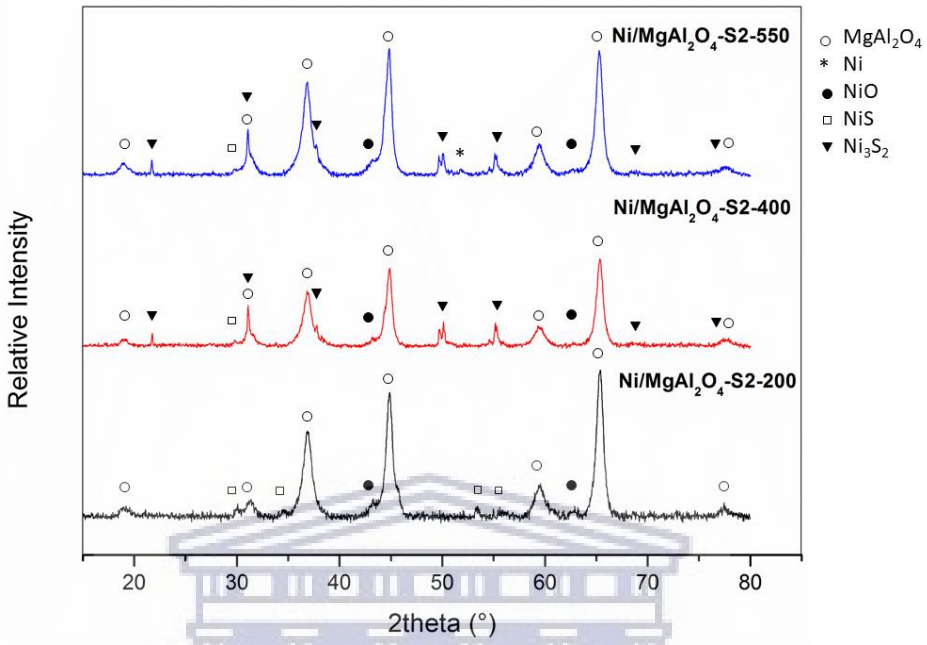

Figure 4.1. c) XRD pattern of $Ni/MgAl_2O_4$-S2 sulfided at 200 °C, 400 °C and 550 °C

The XRD patterns of the catalysts sulfided with DMSO (S3) to form $Ni/MgAl_2O_4$-S3-y, where y is the temperature of sulfidation, is shown in **Figure 4.1.d** below. The catalysts sulfided at the three temperatures all contained peaks corresponding to the presence of a Ni-S_x species in the form of the Ni_3S_2 phase. In addition, the presence of NiO was also observed which seems to be slightly more prevalent compared to catalysts sulfided with agents S1 and S2. According to MATCH, the % NiO present on $Ni/MgAl_2O_4$-S3-200, $Ni/MgAl_2O_4$-S3-400 and $Ni/MgAl_2O_4$-S3-550 is 6.4%, 6% and 3.7%, respectively. This indicates that not all the metallic nickel was sulfided by DMSO. The % NiO present on the $Ni/MgAl_2O_4$-S3-200 and $Ni/MgAl_2O_4$-S3-400 catalysts was also more than the unmodified catalyst.

Furthermore, the EDS data (Table 4.1) show that the catalysts sulfided with DMSO contained the least %S compared to the catalysts sulfided with $(NH_4)_2SO_4$ and $(NH_4)_2S$ as sulfiding agents. This could be due to the loss of sulfur by H_2S gas. The S-O bond of DMSO (chemical formula C_2H_6OS) is weak, thus DMSO can easily be reduced to CH_3SH. With further increase in temperature CH_3SH bonds will break and some H_2S gas will be produced.[36]

It was speculated that some of the oxygen lost from DMSO may oxidize the reduced Ni, hence a combination of the smaller presence of sulphur and availability of oxygen may have led to an increased amount of NiO on the sulfided catalysts. The peak at 2θ 55 ° corresponding to Ni_3S_2 was barely visible on the S3 catalysts. It would appear that Ni_3S_2 particles were highly dispersed on the surface of $Ni/MgAl_2O_4$-S3 catalysts and could therefore not be detected by XRD analysis.

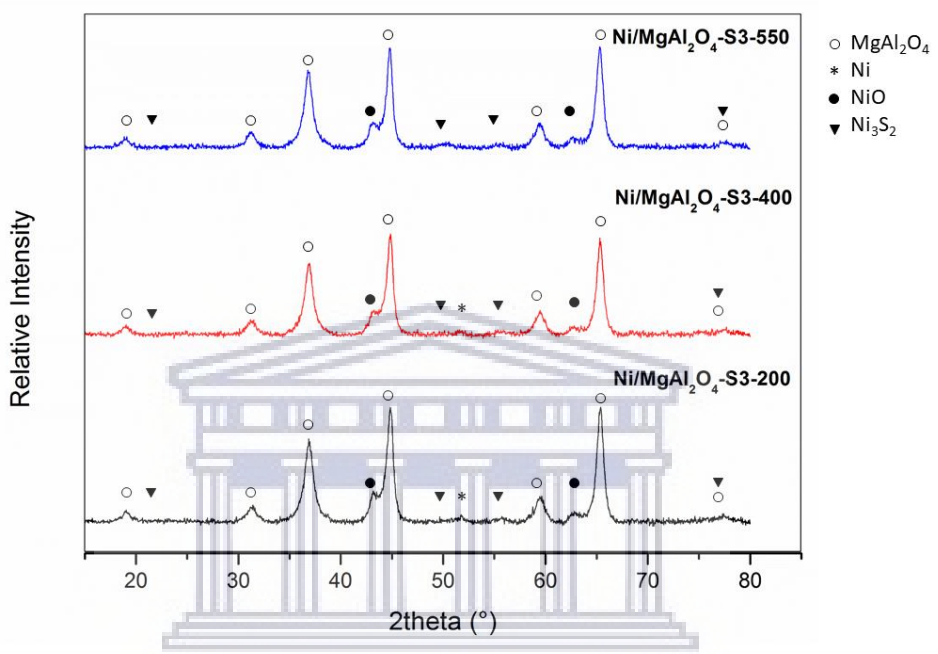

Figure 4.1. d) XRD pattern of $Ni/MgAl_2O_4$-S3 sulfided at 200 °C, 400 °C and 550 °C

The various sulfiding agents as well as sulfidation temperature influence the Ni-S species formed, crystallite size and degree of sulfidation. The sulfur in $(NH_4)_2SO_4$ (S1) interacts mostly with the support, as indicated by the peaks corresponding to $MgSO_4$. Under the reaction conditions in our study, the $(NH_4)_2SO_4$ did not reduce to a sulfide phase as with $(NH_4)_2S$ (S2) and DMSO (S3). For S2 and S3 catalysts, the Ni_3S_2 phase is present at sulfiding temperatures of 400 °C and 550 °C. The crystallite size of Ni_3S_2 increased with an increase in temperature, for the S2 sulfiding agent. The formation of NiS at low sulfidation temperature and Ni_3S_2 at high sulfidation temperature could be due to the reduction of the nickel-sulfided species at the higher temperature according to the equations listed below.[35]

1) $7NiS + 2e^- \longrightarrow Ni_7S_6 + S^{2-}$

2) $3Ni_7S_6 + 8e^- \longrightarrow 7Ni_3S_2 + 4S^{2-}$

These results are consistent with those found in the literature. Increasing temperatures usually cause the sintering of metal particles. The crystallites move over the support and collide to form larger particles.[37–39] As reaction temperature increases so does the crystallite size of a given material.

The % of unreacted Ni decreased with an increase in temperature for both S2 and S3 sulfiding agents, which could indicate increased decomposition of the sulfiding agents, hence an increase in the nickel-sulfur phase. Evidence given by EDS analysis highlights the increase in wt% S with an increase in sulfidation temperature, implying increased decomposition from low to high temperature conditions. This is consistent with previous studies that show complete sulfidation of catalysts is likely to occur at higher temperatures.[28–30] The exception to the trend is S1, which could be due to loosely bound sulfur being lost with an increase in sulfidation temperature.

Table 4.1: EDS data showing wt% S on catalysts sulfided at 200 °C, 400 °C and 550 °C

$Ni/MgAl_2O_4$ sulfiding conditions:	**200 °C**	**400 °C**	**550 °C**
$(NH_4)_2SO_4$ (S1)	33.7	24	12.87
$(NH_4)_2S$ (S2)	9.42	13.81	18.17
DMSO (S3)	2.55	3.18	5.91

4.3.2 Thermal stability of sulfided catalysts

Thermogravimetric analysis (TGA), shown in **Figure 4.2**, was performed on S1, S2 and S3 catalysts to determine which sulfiding agent was the best for sulfiding the Nickel supported catalyst as well as the strength of the sulfur interaction with the catalyst. As sulfidation temperature increased from 200 °C – 550 °C, the sulfur loss from the catalyst decreased, indicating a stronger nickel-sulfur interaction as a consequence of the higher sulfidation temperature. This trend was observed for the S1 and S2 catalysts, while S3 catalysts showed no wt% mass loss, suggesting that sulfur has the strongest interaction with the catalysts sulfided with DMSO.

The TGA profile of Ni/$MgAl_2O_4$-S1-200 is typical for $(NH_4)_2SO_4$, with multiple mass loss steps. The wt% loss at the higher temperatures i.e. above 600 °C, was assigned to the decomposition of the sulfate groups on Ni/$MgAl_2O_4$-S1-400 and Ni/$MgAl_2O_4$-S1-550, respectively.[20] The results obtained from TGA correlate with EDS data, which show that Ni/$MgAl_2O_4$-S1-200 catalyst had the highest sulfur content, with a total mass loss of 75% due to decomposition of the ammonium sulfate. This was followed by wt% mass loss of Ni/$MgAl_2O_4$-S1-400 (23%) > Ni/$MgAl_2O_4$-S1-550 (20%) > Ni/$MgAl_2O_4$-S2-200 (10%) > Ni/$MgAl_2O_4$-S2-400 (6%) > Ni/$MgAl_2O_4$-S2-550 (5%).The mass loss observed at approximately 800 °C, could be associated with the loss of sulfur from the catalysts.[40]

TGA data shows that loosely bound sulfur, with mass loss occurring < 200 °C were present on the catalysts sulfided with $(NH_4)_2SO_4$. The sulfur interaction with the catalyst was stronger using $(NH_4)_2S$ as the sulfiding agent, compared to $(NH_4)_2SO_4$, and the interaction strengthened with an increase in sulfidation temperature as observed for the smaller wt% mass loss on S2 catalysts. The catalysts sulfided with DMSO showed no losses of loosely bound sulphur. This is most likely due to the smaller amount of sulphur on the catalyst which interacts strongly with the nickel particles. Interestingly, DMSO is identified as the most stable, further highlighting the strong nickel-sulfur interaction using this sulfiding agent, due to no or negligible mass loss at temperatures as high as 800 °C. TGA analysis clearly highlights DMSO as an excellent sulfiding agent resulting highly stable metal sulphide species.

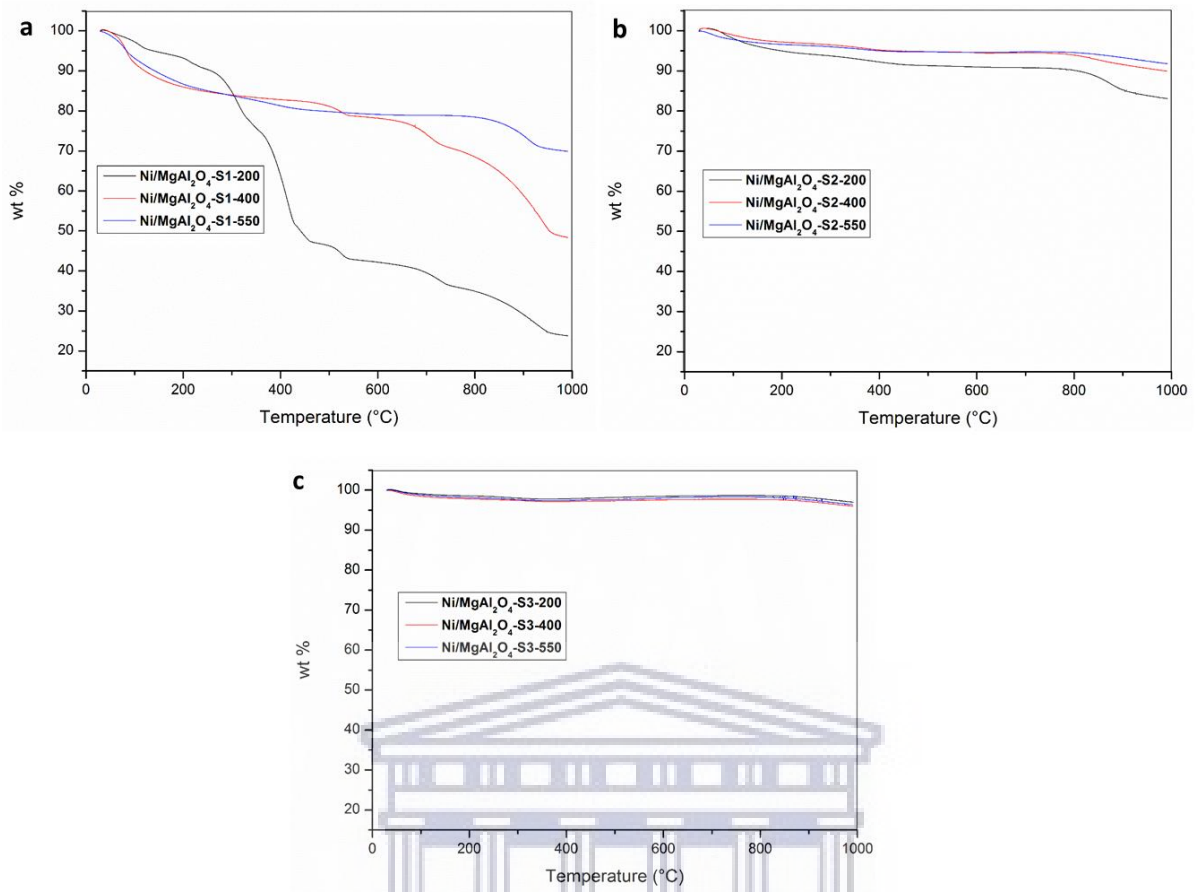

Figure 4.2. TGA profiles of catalysts sulfided with a) $(NH_4)_2SO_4$, b) $(NH_4)_2S$ and c) DMSO at 200 °C, 400 °C and 550 °C

4.3.3 Morphology

SEM analysis was used to determine the morphology and dispersion of NiS_x particles on the support material. The morphology of the catalysts sulfided with $(NH_4)_2SO_4$ (S1), $(NH_4)_2S$ (S2) and DMSO (S3) at 200 °C, 400 °C and 550 °C can be observed from the SEM micrographs shown in **Figure 4.3**. The morphology of the catalysts sulfided with S1 (**Figure 4.3.1**) varied gradually from low sulfidation temperature to high sulfidation temperature. The appearance of Ni/$MgAl_2O_4$-S1-200 (**Figure 4.3.1.a**) composed of needle-like agglomerates, which could be due to the catalyst consisting of $(NH_4)_2SO_4$ as indicated by XRD analysis. The surface of the Ni/$MgAl_2O_4$-S1-400 (**Figure 4.3.1.b**) catalyst is characterized by floccules, which could be attributed to some decomposition of $(NH_4)_2SO_4$ on the catalyst. When the sulfidation temperature is increased to 550 °C, the flocculant-shaped surface morphology disappeared, as observed for the Ni/$MgAl_2O_4$-S1-550 catalyst (**Figure 4.3.1.c**).

This result could indicate that the catalyst is loose and porous with an increase in sulfidation temperature.[41] Additionally, at 550 °C, the $(NH_4)_2SO_4$ sulfiding agent could be completely decomposed, with enhanced dispersion of particles and interaction with the $MgAl_2O_4$ support to form $MgSO_4$ as shown by XRD analysis.

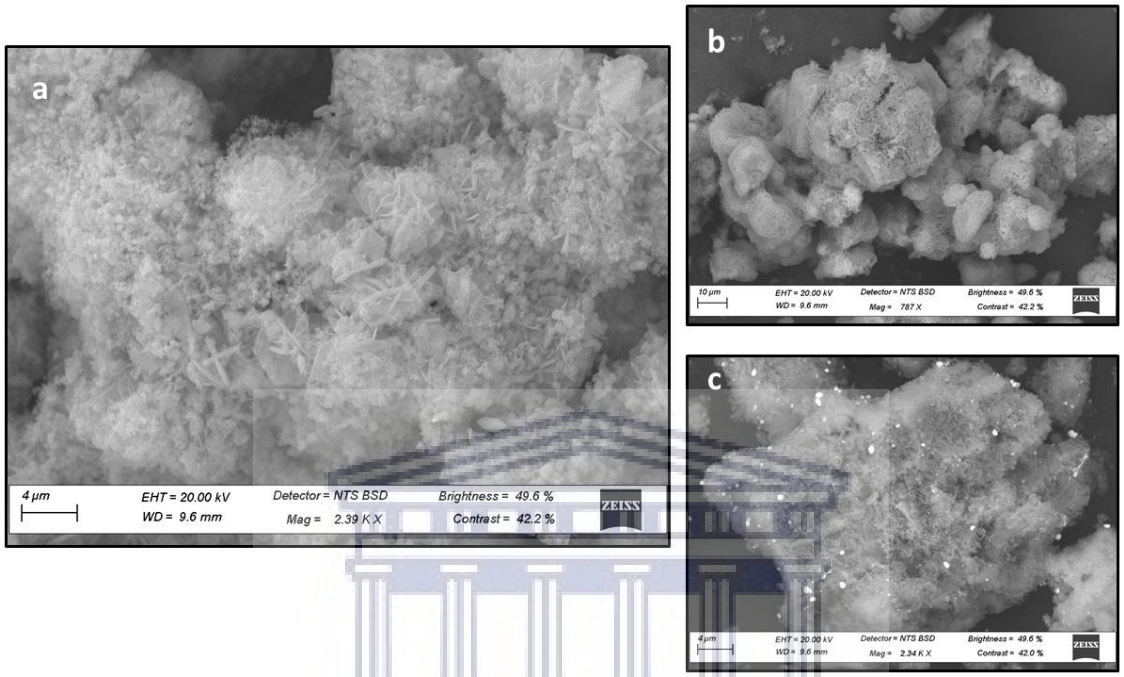

Figure 4.3.1. SEM images of a) Ni/$MgAl_2O_4$-S1-200, b) Ni/$MgAl_2O_4$-S1-400 and c) Ni/$MgAl_2O_4$-S1-550

Figure 4.3.2 displays the surface morphology of catalysts sulfided with S2 as the sulfiding agent. It was observed that a coating was present on the catalyst, which became more prominent with an increase in sulfidation temperature, which could possibly be due to the increased decomposition of the sulfiding agent. The "coating" was not uniformly distributed over the support but rather appeared as agglomerations indicating a lower dispersion of nickel-sulfide species when using the $(NH_4)_2S$ sulfiding agent. According to the literature, nickel sulfide prepared by the addition of $(NH_4)_2S$ to a nickel salt, usually contains a non-stoichiometric excess of sulfur.[42] The data obtained from EDS show that in fact, the %S on the catalysts increased with sulfidation temperature, thereby correlating with the result obtained from SEM. Nickel sulfide is a complex compound with various valence states and it is difficult to obtain nickel sulfide with pure phase, uniform size and structural morphology.[42] The excess sulfur could react with the nickel to form the dense areas of aggregated nickel-sulfided species as seen in the SEM images.

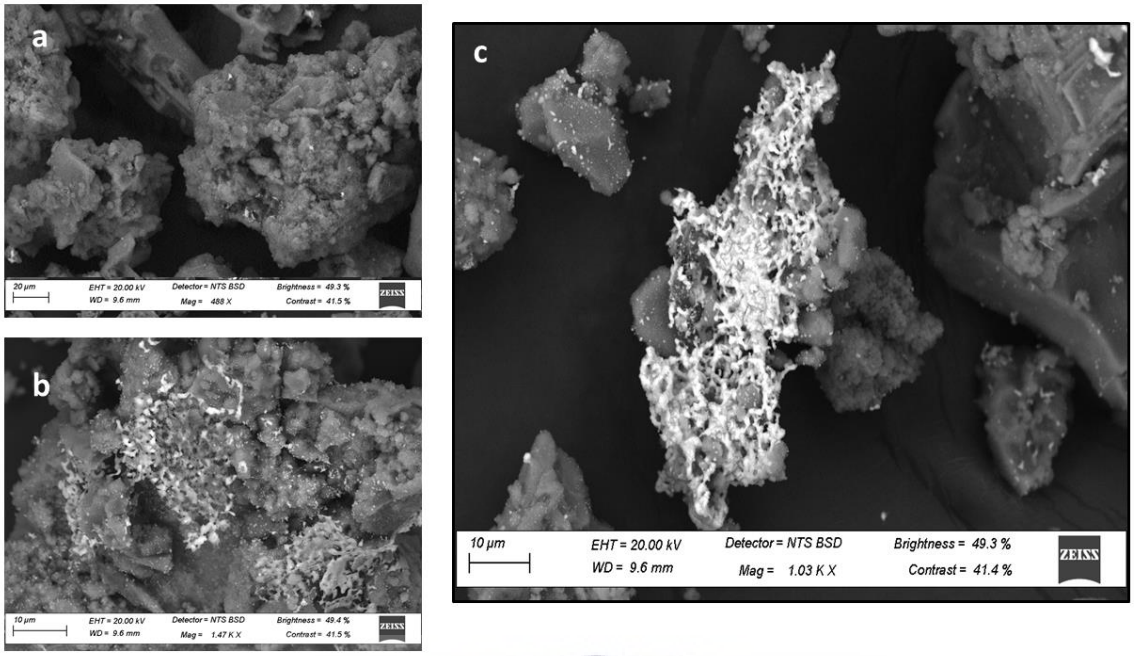

Figure 4.3.2. SEM images of a) Ni/$MgAl_2O_4$-S2-200, b) Ni/$MgAl_2O_4$-S2-400 and c) Ni/$MgAl_2O_4$-S2-550

The surface morphology of Ni/$MgAl_2O_4$ sulfided with S3 at the various temperatures is shown in **Figure 4.3.3** below. The Ni/$MgAl_2O_4$-S3-550 catalyst consist of distinctive, clusters of small particles with a spherical morphology, which is suspected to be Ni_3S_2 particles, absent from the catalysts sulfided with S1 and S2 sulfiding agents. This morphology is consistent at all sulfidation temperatures for S3 catalysts.

It is clear from SEM imaging that the morphology of the catalysts is affected by the type of sulfiding agent. The morphology changes with an increase in temperature, in particular for $(NH_4)_2SO_4$ sulfiding agent, however, for DMSO the morphology is maintained at all sulfiding temperatures. The increase in sulfidation temperature from 200 °C – 550 °C seem to result in a more uniform distribution of particles for S1 and S3, however with S2 larger clusters of particles are observed. Furthermore, SEM analysis provide evidence that the sulfiding agents produce distinct morphologies. For example, S1 consists of closely packed particles, S2 is distinguished by the appearance of the "coating" on the catalyst surface due to agglomeration of NiS_x particles and S3 is composed of aggregates of small spherical particles. The dense coating of nickel-sulfided complexes that is observed for the S2 catalysts is absent in the catalyst sulfided with DMSO.

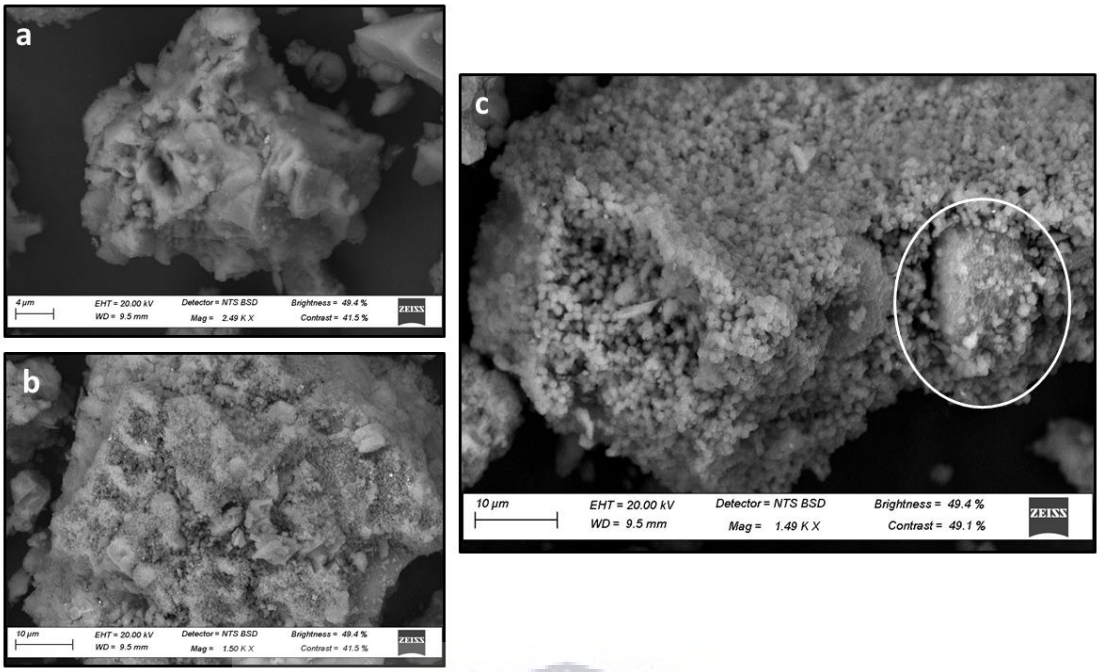

Figure 4.3.3. SEM images of a) Ni/$MgAl_2O_4$-S3-200, b) Ni/$MgAl_2O_4$-S3-400 and c) Ni/$MgAl_2O_4$-S3-550

To gain more information about the level of dispersion of nickel and sulfur over the $MgAl_2O_4$ support electron mapping of the sulfided catalysts were conducted and the images shown in **Figure 4.4**. The sulfur on Ni/$MgAl_2O_4$-S1-200 (**Figure 4.4.a**) seems to be present as a thick mass over the catalyst. This is noticed by the map of sulfur (green), which shows sulfur to be dense and well dispersed on the support. This is due to the $(NH_4)_2SO_4$ crystals that completely cover the support. EDS analysis also confirmed the high sulfur content of 33%, the highest of all compared catalysts.

Visual evidence of sulfur interacting with $MgAl_2O_4$ can be observed in Ni/$MgAl_2O_4$-S1-400 and Ni/$MgAl_2O_4$-S1-550 (**Figure 4.4.b** and **Figure 4.4.c**). There is a greater interaction with Mg than with Ni as evidenced by the electron maps of the elements. This is consistent with XRD analysis, which indicated the presence of $MgSO_4$ for the Ni/$MgAl_2O_4$-S1-400 and Ni/$MgAl_2O_4$-S1-550 catalysts. In industry, the $MgAl_2O_4$ spinel can be used as a sulfur-transfer catalyst in fluid catalytic cracking units for SO_x emission control and it has been reported that sulfur oxide species have a high reactivity with $MgAl_2O_4$ spinel. Gerle and co-workers found that the chemical reaction of $MgAl_2O_4$ with sulfur oxides to form $MgSO_4$ occurred between reaction temperatures of 400 °C –800 °C.[44,45] This result corresponds with our system, where the $MgSO_4$ phase was present at sulfidation temperatures of 400 °C and 500 °C.

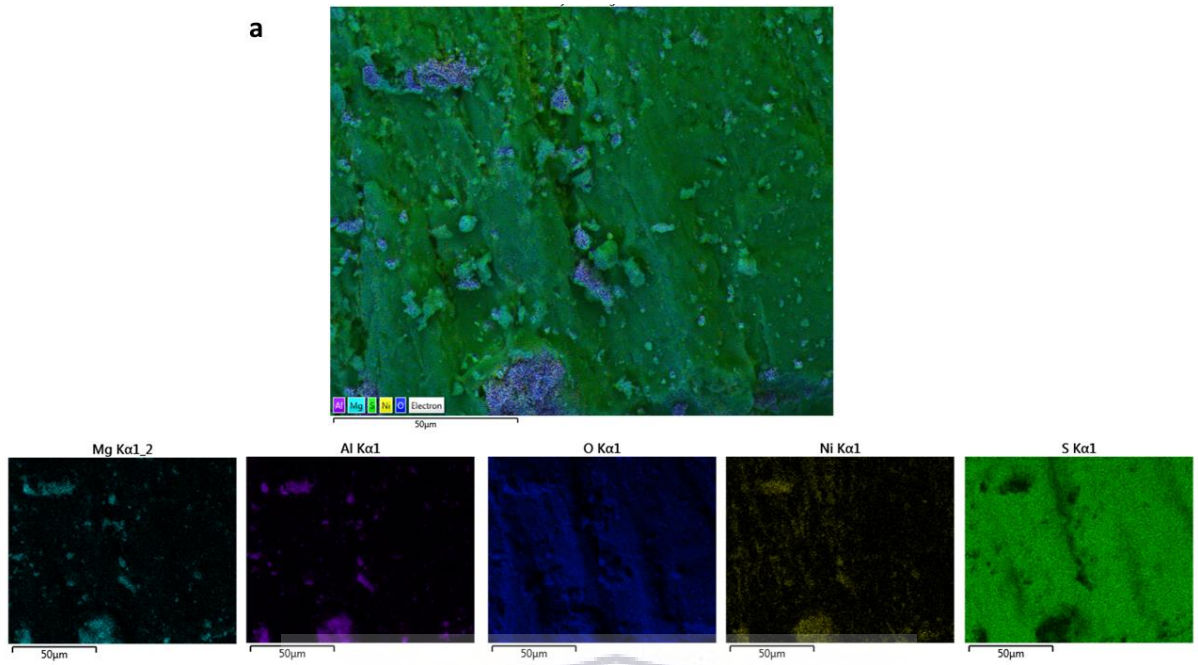

Figure 4.4. a) X-ray mapping of Ni/$MgAl_2O_4$-S1-200

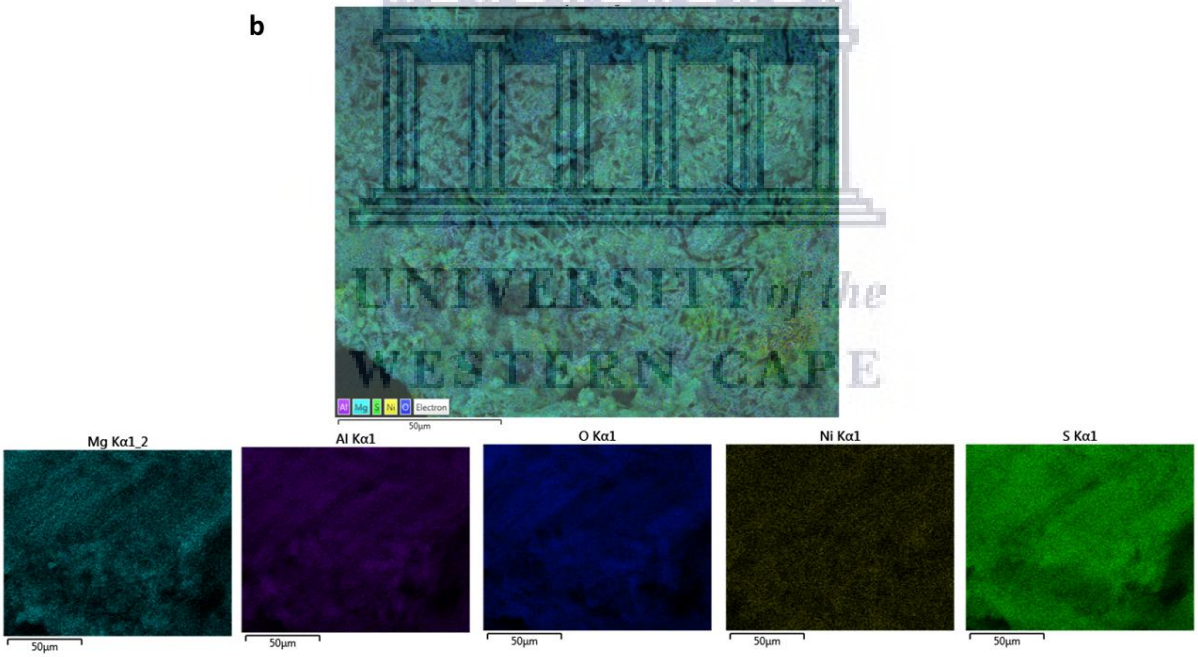

Figure 4.4. b) X-ray mapping of Ni/$MgAl_2O_4$-S1-400

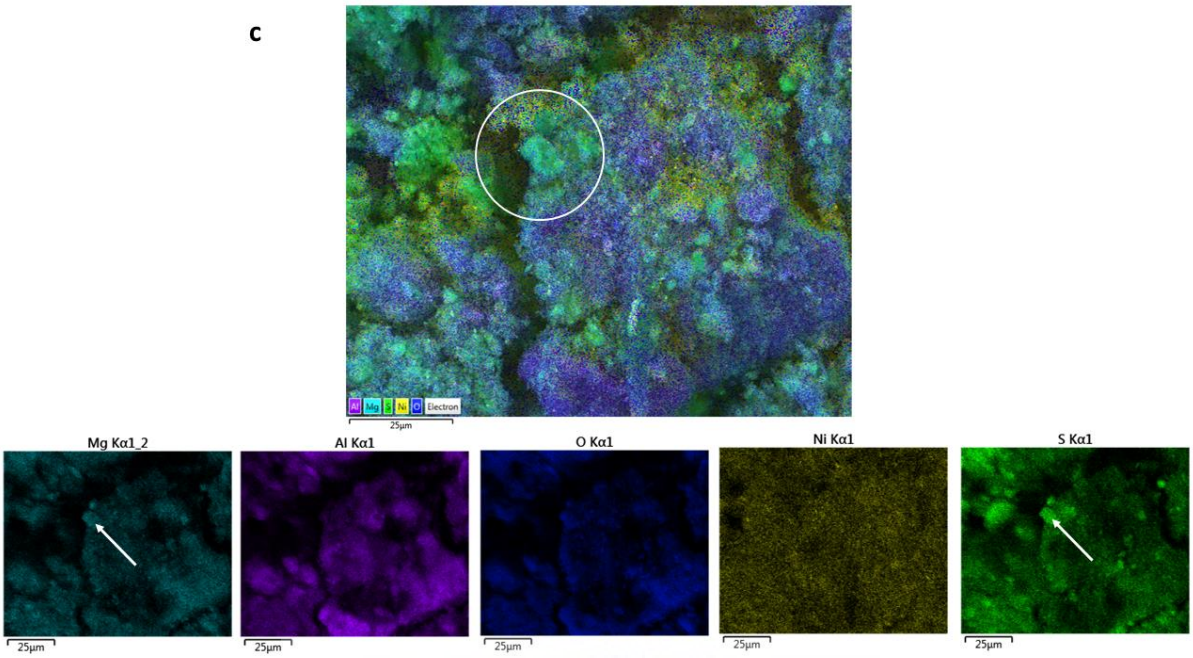

Figure 4.4. c) X-ray mapping of Ni/$MgAl_2O_4$-S1-550

The electron mapping images for S2 catalysts (**Figure 4.5**) indicate that the "coating" observed from SEM analysis could be attributed to nickel-sulfided particles that are distributed on the catalyst. The %S is equal to 9.42%, 13.81% and 18.17% for Ni/$MgAl_2O_4$-S2-200, Ni/$MgAl_2O_4$-S2-400 and Ni/$MgAl_2O_4$-S2-550, respectively, as indicated from EDS analysis.

It is suggested that the amount of nickel-sulfided species increase with an increase in sulfidation temperature (**Figure 4.5.a**, **Figure 4.5.b** and **Figure 4.5.c**) due to greater decomposition of the sulfiding agent. The electron maps of the individual elements confirm a greater interaction with Ni and S compared to S1, however aggregates of Ni and S are present on the support with a low dispersion.

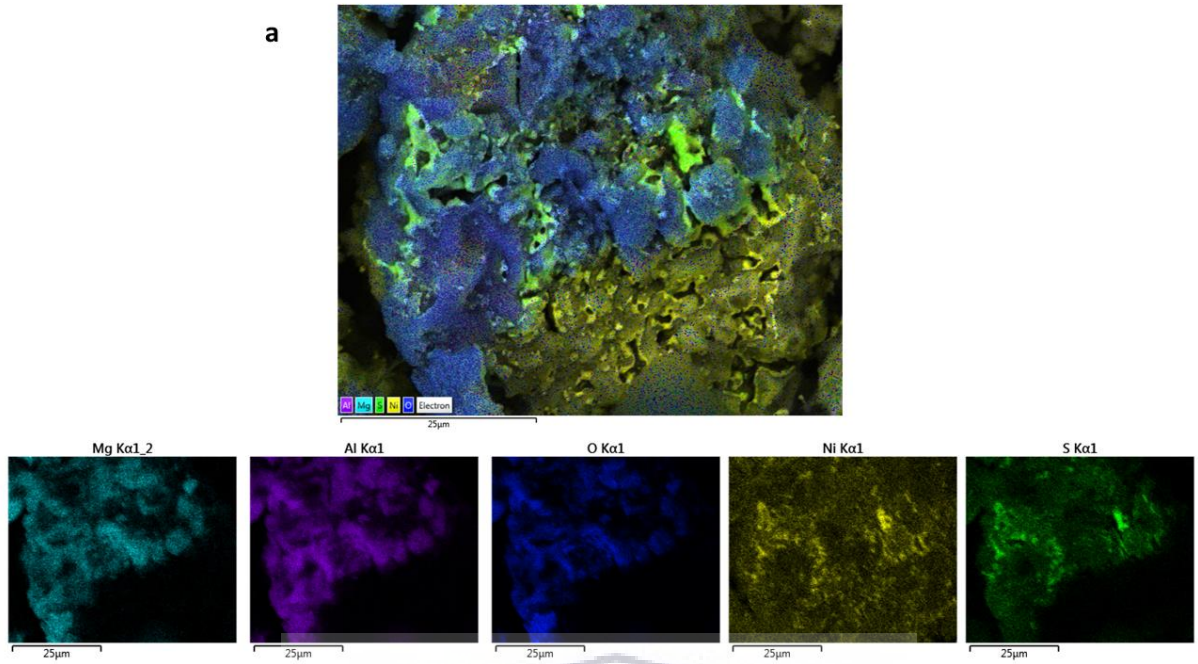

Figure 4.5. a) X-ray mapping of Ni/$MgAl_2O_4$-S2-200

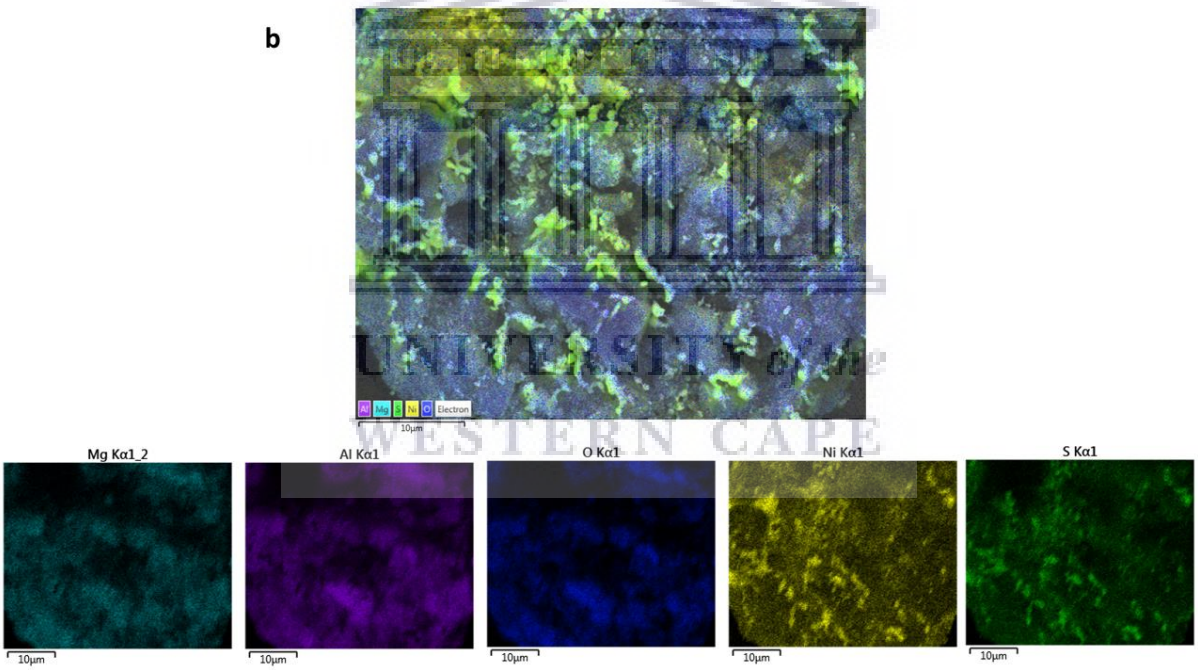

Figure 4.5. b) X-ray mapping of Ni/$MgAl_2O_4$-S2-400

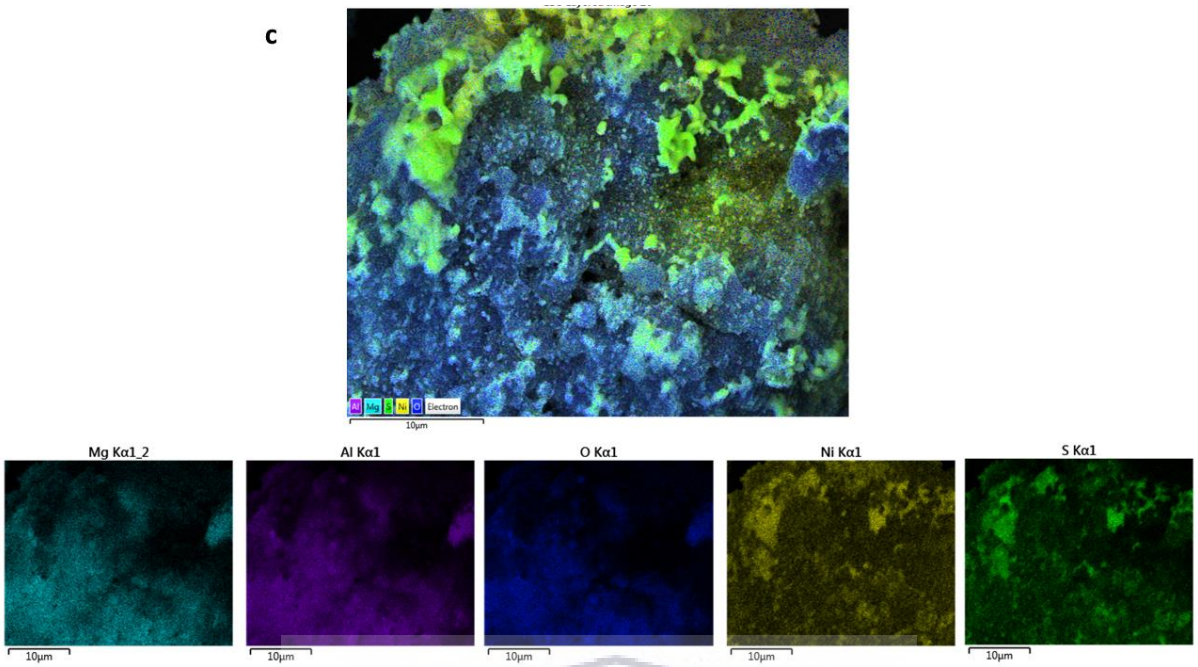

Figure 4.5. c) X-ray mapping of Ni/$MgAl_2O_4$-S2-550

Figure 4.6 shows the electron mapping of the catalysts sulfided with DMSO. Both the nickel and sulfur particles are evenly dispersed on the Ni/$MgAl_2O_4$-S3-200 (**Figure 4.6.a**) and Ni/$MgAl_2O_4$-S3-400 (**Figure 4.6.b**) catalysts with some clusters of nickel-sulfided species forming on the Ni/$MgAl_2O_4$-S3-550 catalyst as indicated by the white arrows in **Figure 4.6.c**.

DMSO has been used previously in the preparation of highly dispersed silica-supported nano-copper heterogeneous catalysts and dispersible palladium nanoparticles. The advantages of using DMSO was attributed to i) sufficient interaction with the surface of the metal nanoparticles to effectively stabilize nanoparticle dispersion and ii) the absence of agglomeration.[46,47] In our study, overall sulfiding with DMSO at all temperatures led to a high dispersion of nickel and sulfur compared to the S1 and S2 catalysts, correlating well with the results obtained from XRD analysis. The high dispersion may be due to a stronger interaction between Ni and S as sulfur acts as a structural promoter and reduces the nickel particle size.

The sulfur content of S3 however, is much lower compared to S1 and S2 as shown in the EDS results. The interaction between nickel and sulfur on the catalysts sulfided with DMSO seem to have a high consistency, high dispersion and small particle size which could be promising for catalytic activity.

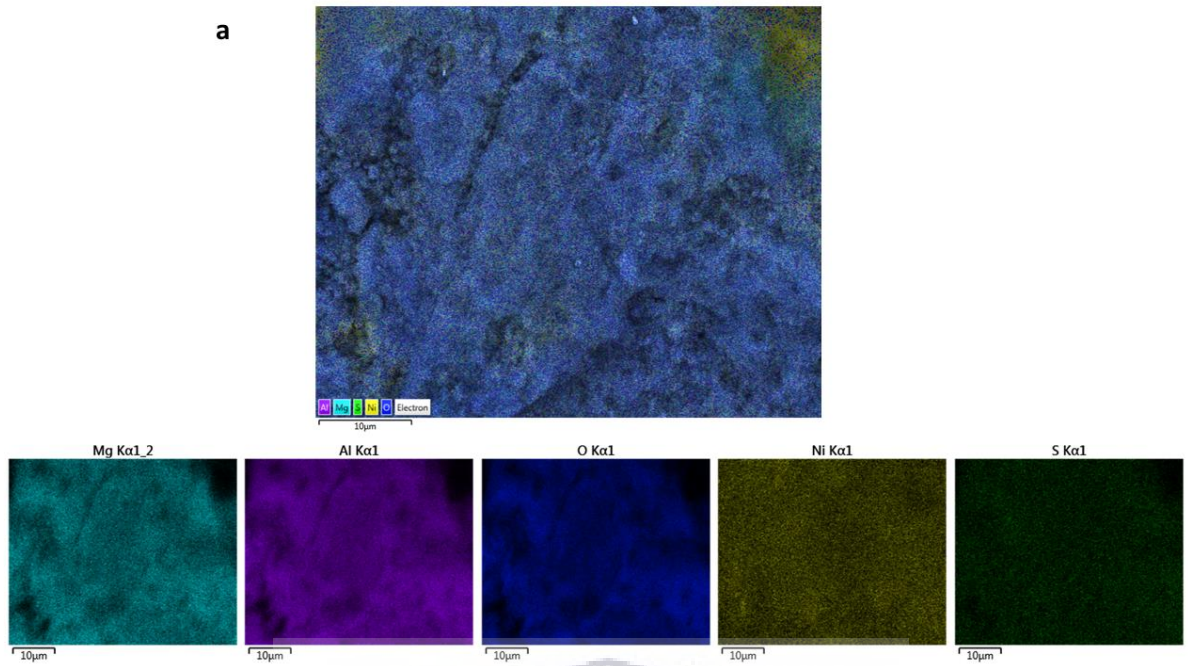

Figure 4.6. a) X-ray mapping of Ni/$MgAl_2O_4$-S3-200

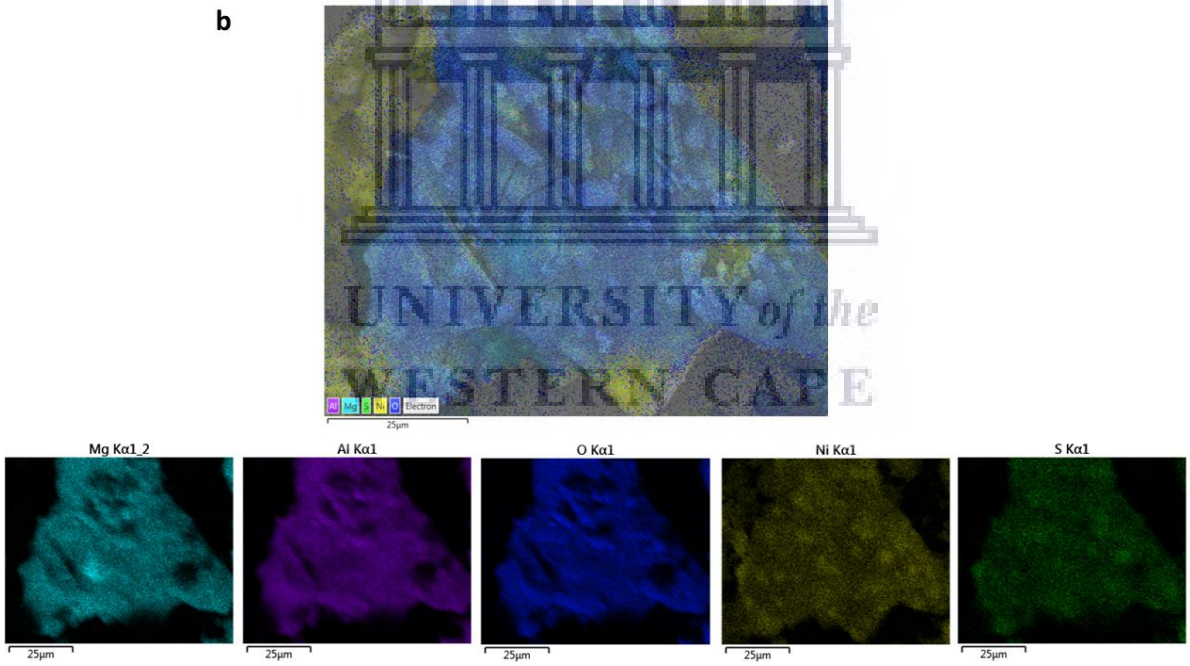

Figure 4.6. b) X-ray mapping of Ni/$MgAl_2O_4$-S3-400

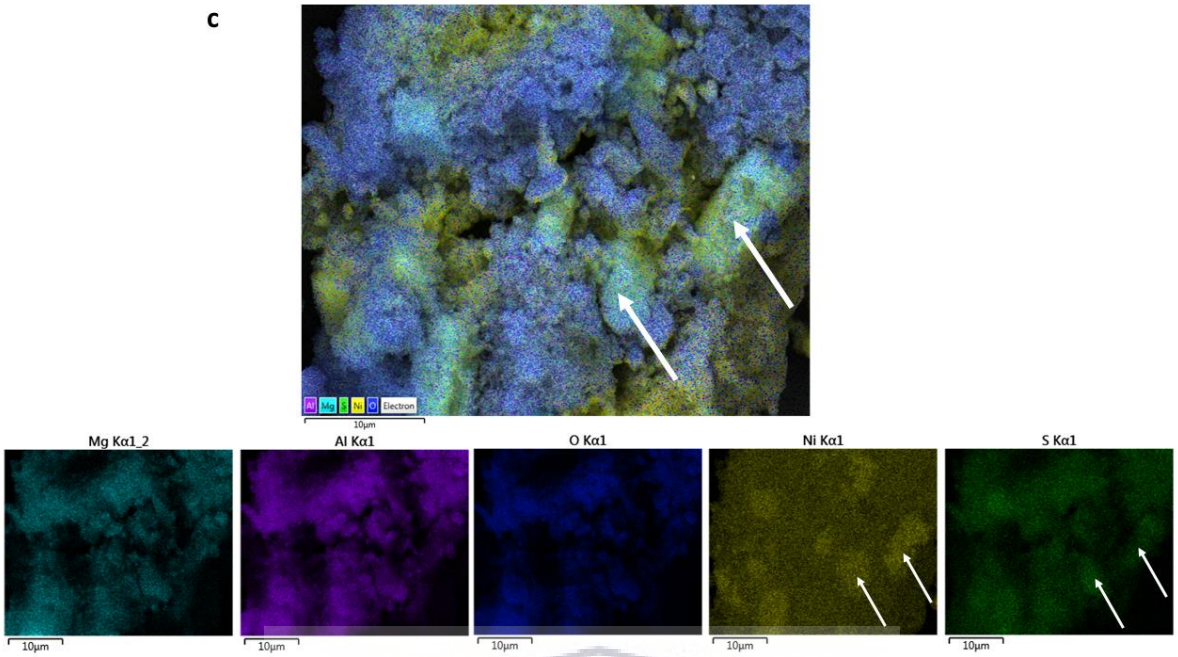

Figure 4.6. c) X-ray mapping of Ni/$MgAl_2O_4$-S3-550

SEM and electron mapping indicated that the surface morphology and dispersion varies when using S1, S2 and S3 sulfiding agents. The sulfur content on the S1 catalysts contained the highest %S, which was densely distributed as seen for Ni/$MgAl_2O_4$-S1-200 and Ni/$MgAl_2O_4$-S1-400 catalysts. For Ni/$MgAl_2O_4$-S1-550, the sulfiding agent is decomposed, as suggested from SEM analysis and sulfur interacts strongly with the $MgAl_2O_4$ support, seen in **Figure 4.4.c**. The same trend is observed for S2 catalysts, where the increase in sulfidation temperature could lead to higher decomposition of the sulfiding agent.

The presence of nickel and sulfur clusters grow and increase at the sulfidation temperature of 550 °C for Ni/$MgAl_2O_4$-S2-550 and there is evidence of strong nickel-sulfur interactions present on the catalyst. The catalysts sulfided with S3 at 200 °C, 400 °C and 550 °C have the "best" dispersion compared to S1 and S2 sulfiding agents. For the Ni/$MgAl_2O_4$-S3-550 catalyst, the nickel and sulfur form small clusters less dense than S2 catalysts, indicating strong nickel-sulfur interactions at this sulfidation temperature. Since the catalysts sulfided at 550 °C showed improved dispersion and strong sulfur interactions, this could imply that the optimum temperature for sulfidation is 550 °C for all three sulfiding agents.

TEM analysis was used to measure particle size of the catalysts. Firstly, the unmodified catalyst (Figure S2.1), contained large particles measuring 59 nm. There was an expected decrease in particle size with the addition of sulfur, due to the geometric effect, which dilutes aggregated Ni sites on the catalyst and dissociates large Ni ensembles responsible for hydrogenolysis reactions.[48] The sulfided nickel particles are depicted in each image by white arrows. For the S1 catalysts (**Figure 4.7**), nickel-sulfur species was not present in the XRD analysis, due to the sulfiding agent $(NH_4)_2SO_4$ present on the surface of the catalyst (low temperatures-200 °C) and interacting mostly with the Mg in the support (high temperatures-550 °C). It was observed that there was a wider particle size distribution for $Ni/MgAl_2O_4$-S1-400 and $Ni/MgAl_2O_4$-S1-550 compared to the $Ni/MgAl_2O_4$-S1-200 catalyst (**Figure 4.8**). The particle sizes of the catalysts sulfided at 200 °C, 400 °C and 550 °C was calculated from the program Image J to be 5 nm, 11 nm, 9 nm, respectively. The increase in temperature led to an increase in particle size.

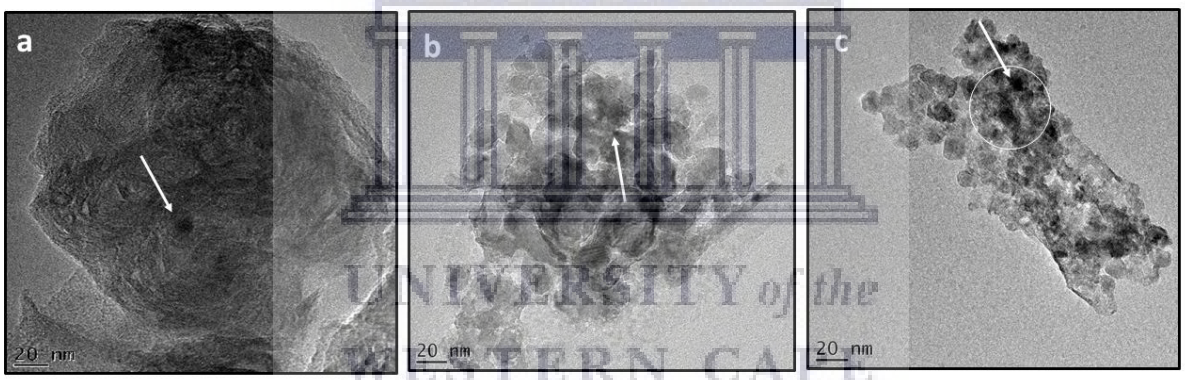

Figure 4.7. TEM images of $Ni/MgAl_2O_4$ sulfided with $(NH_4)_2SO_4$ (S1) at a) 200 °C, b) 400 °C and c) 550 °C

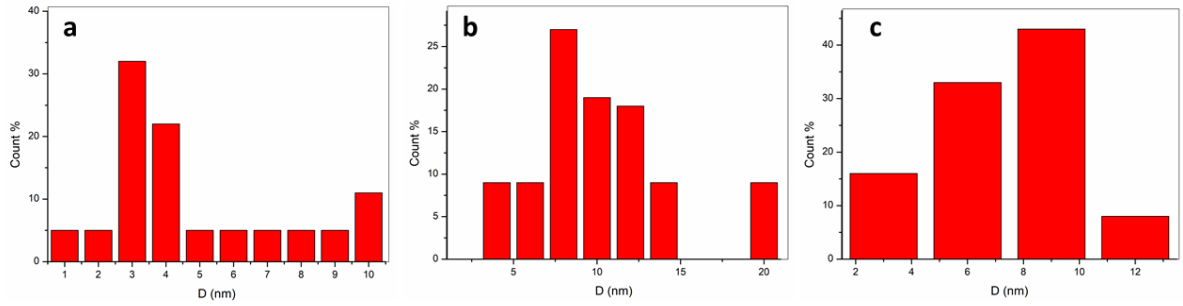

Figure 4.8. Particle size distribution of $Ni/MgAl_2O_4$ sulfided with $(NH_4)_2SO_4$ (S1) at a) 200 °C, b) 400 °C and c) 550 °C

The TEM imaging and particle size distribution for S2 catalysts is shown in **Figure 4.9** and **Figure 4.10**, respectively. The particle cluster size for Ni/$MgAl_2O_4$-S2-200, Ni/$MgAl_2O_4$-S2-400, Ni/$MgAl_2O_4$-S2-550 was calculated as 11 nm, 17 nm and 48 nm, respectively. The images for Ni/$MgAl_2O_4$-S2-400 and Ni/$MgAl_2O_4$-S2-550 show that the catalysts consisted of small particles clustered together. As sulfidation temperature increased the interaction of the Ni and S particles increased as well as sulfur content, leading to the formation of larger sized and increased number of clusters (Ni_3S_2) as seen from the TEM images (**Figure 4.9.c**). This correlates with the results from SEM analysis and electron imaging, showing that the nickel sulfided particles become more dense with an increase in sulfidation temperature.

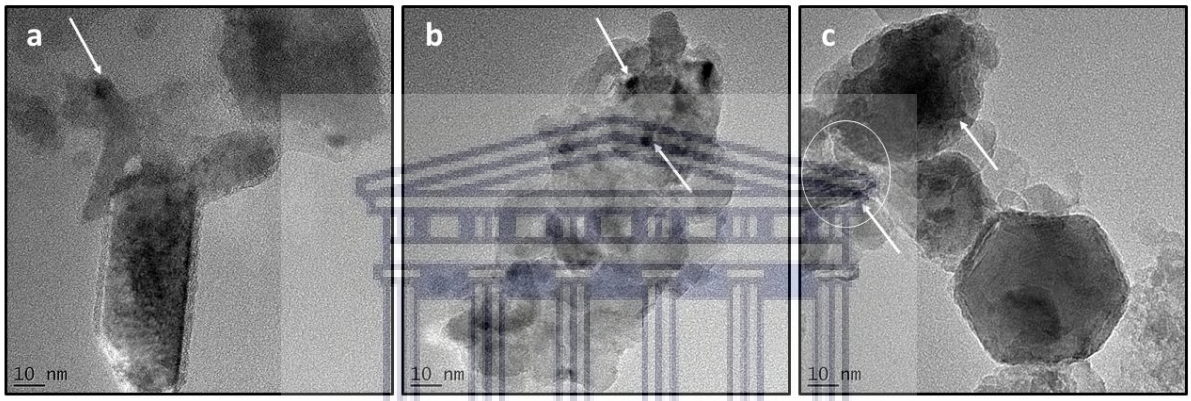

Figure 4.9. TEM images of Ni/$MgAl_2O_4$ sulfided with $(NH_4)_2S$ (S2) at a) 200 °C, b) 400 °C and c) 550 °C

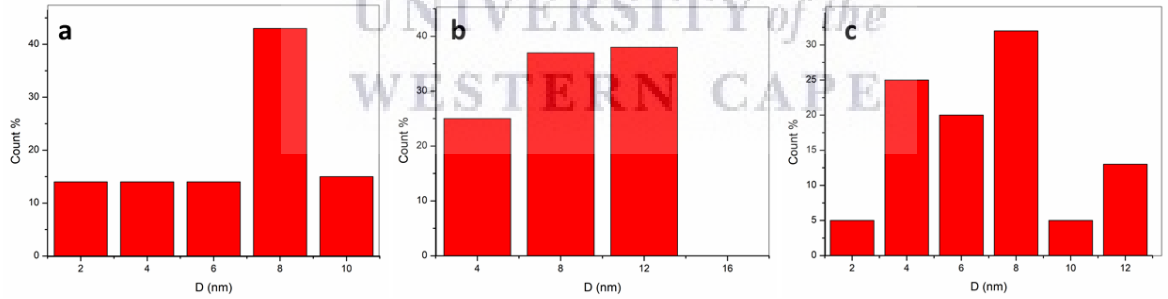

Figure 4.10. Particle size distribution of Ni/$MgAl_2O_4$ sulfided with $(NH_4)_2S$ (S2) at a) 200 °C, b) 400 °C and c) 550 °C

The TEM imaging and particle size distribution for S3 catalysts is shown in **Figure 4.11** and **Figure 4.12**, respectively. The TEM images show that the catalyst sulfided with DMSO displays the best dispersion of the nickel particles. Particle size for Ni/$MgAl_2O_4$-S3-200, Ni/$MgAl_2O_4$-S3-400, Ni/$MgAl_2O_4$-S3-550 was calculated as 6 nm, 11 nm and 15 nm.

The same trend was observed for the catalyst sulfided with $(NH_4)_2S$ as the sulfiding agent. It was observed that Ni/$MgAl_2O_4$-S2-400 and Ni/$MgAl_2O_4$-S2-550 had a similar particle size to that of Ni/$MgAl_2O_4$-S3-550. However, the particles were better dispersed on Ni/$MgAl_2O_4$-S3-550 compared to the S2 catalysts. The strongest interaction between nickel and sulfur occur in S3 catalysts as indicated by TGA. The beneficial geometric effects of sulfur that dilute the aggregated metal particles, causing the increased dispersion, is most notable in S3 catalysts. Since the interactions of Ni and S increase with sulfidation temperature (200 °C, 400 °C and 550 °C), we would expect that Ni/$MgAl_2O_4$-S3-550 has the highest dispersion of particles on the catalyst.

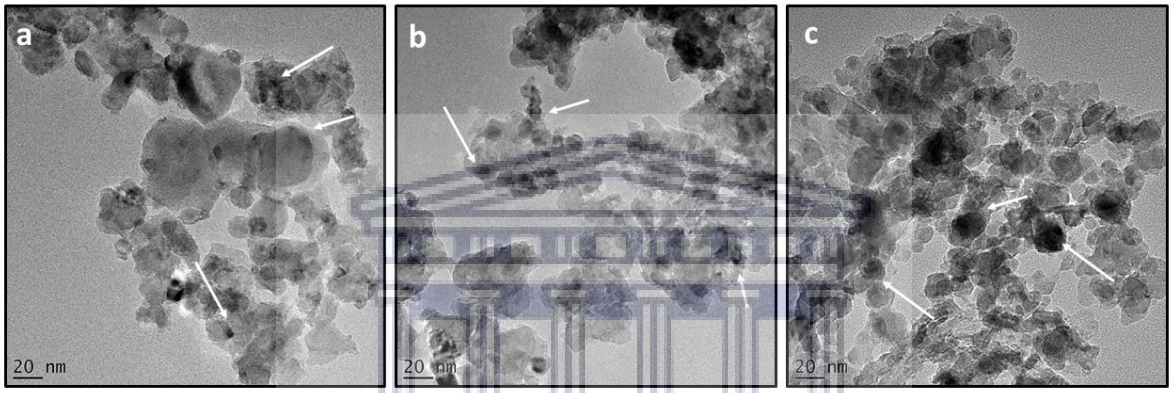

Figure 4.11. TEM images of Ni/$MgAl_2O_4$ sulfided with DMSO (S3) at a) 200 °C, b) 400 °C and c) 550 °C

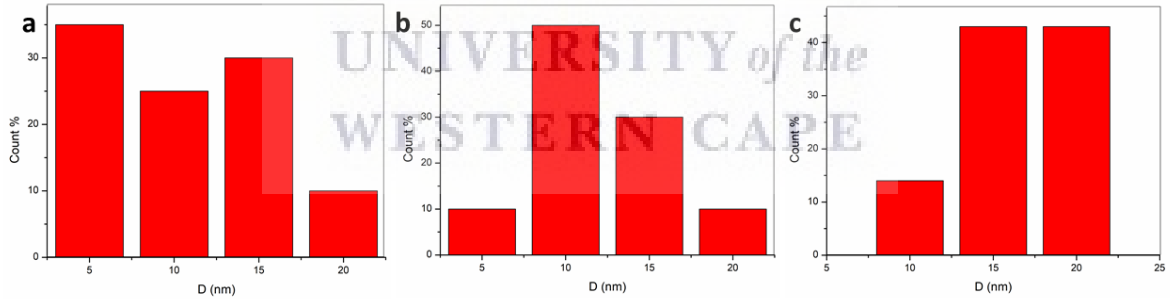

Figure 4.12. Particle size distribution of Ni/$MgAl_2O_4$ sulfided with DMSO (S3) at a) 200 °C, b) 400 °C and c) 550 °C

Nitrogen adsorption-desorption isotherms of the catalysts sulfided with $(NH_4)_2SO_4$, $(NH_4)_2S$ and DMSO, at 200 °C, 400 °C and 550 °C are shown in **Figure 4.13.a**, **Figure 4.13.b** and **Figure 4.13.c**, respectively. All the catalysts, with the exception of Ni/$MgAl_2O_4$-S1-200, display type IV isotherms and type H_1 hysteresis loops, which is indicative of mesopores present in the catalysts.[49,50] The largest decrease in surface area observed for the Ni/$MgAl_2O_4$-S1-200 could be due to the covering of $(NH_4)_2SO_4$ crystals on the surface and within the pores of the support.

An increase in surface area is observed with an increase in sulfidation temperature for S1 catalysts, which is consistent with the findings from SEM analysis that indicated a change in morphology to a more porous structure with an increase in sulfidation temperature. This could be due to the decomposition of $(NH_4)_2SO_4$ and reduction of pore blockages caused by sulfur.[51] The surface areas of the S1 catalysts at higher temperatures were also the largest compared to the other sulfiding agents.

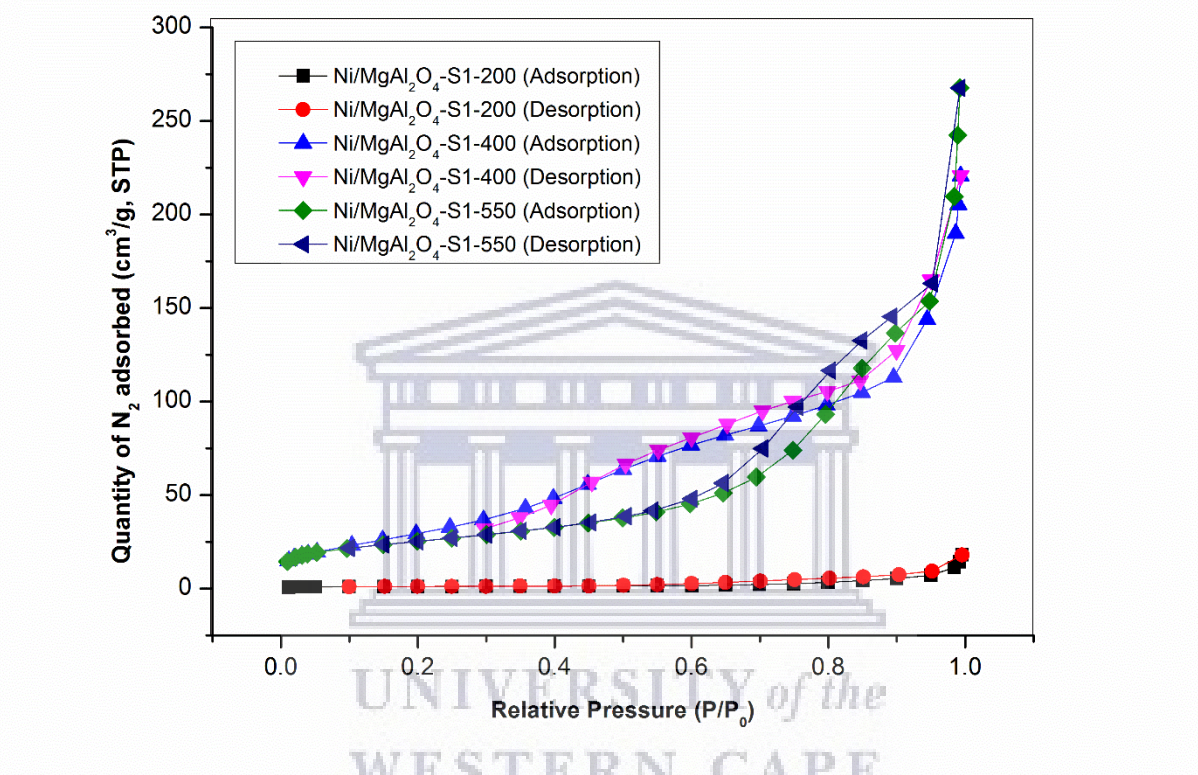

Figure 4.13. a) N_2 adsorption-desorption isotherms of $Ni/MgAl_2O_4$ sulfided with $(NH_4)_2SO_4$ (S1) at various temperatures

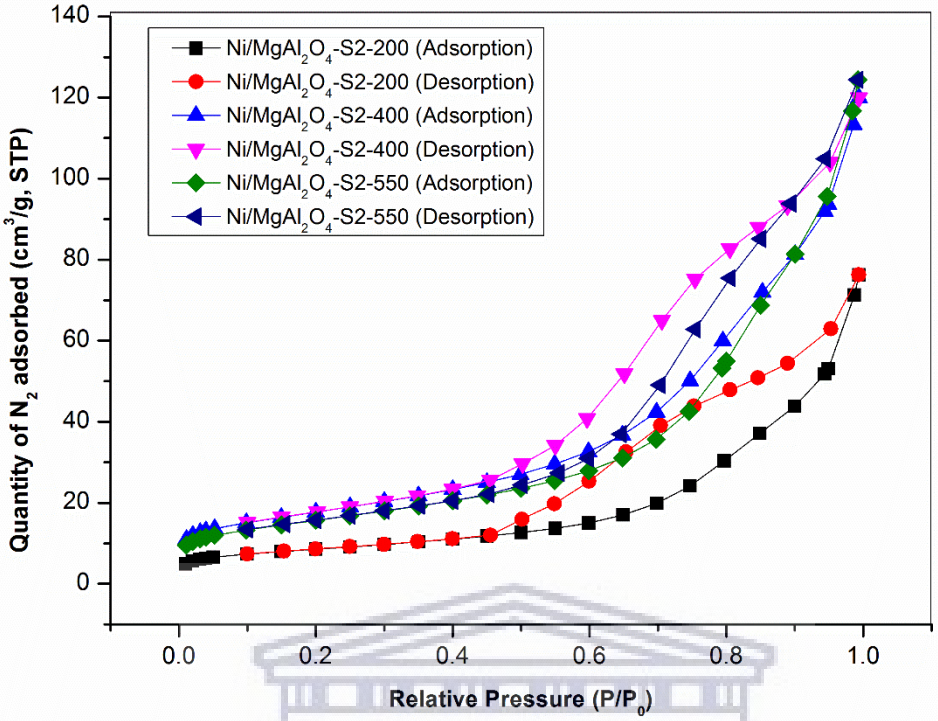

Figure 4.13. b) N_2 adsorption-desorption isotherms of $Ni/MgAl_2O_4$ sulfided with $(NH_4)_2S$ (S2) at various temperatures

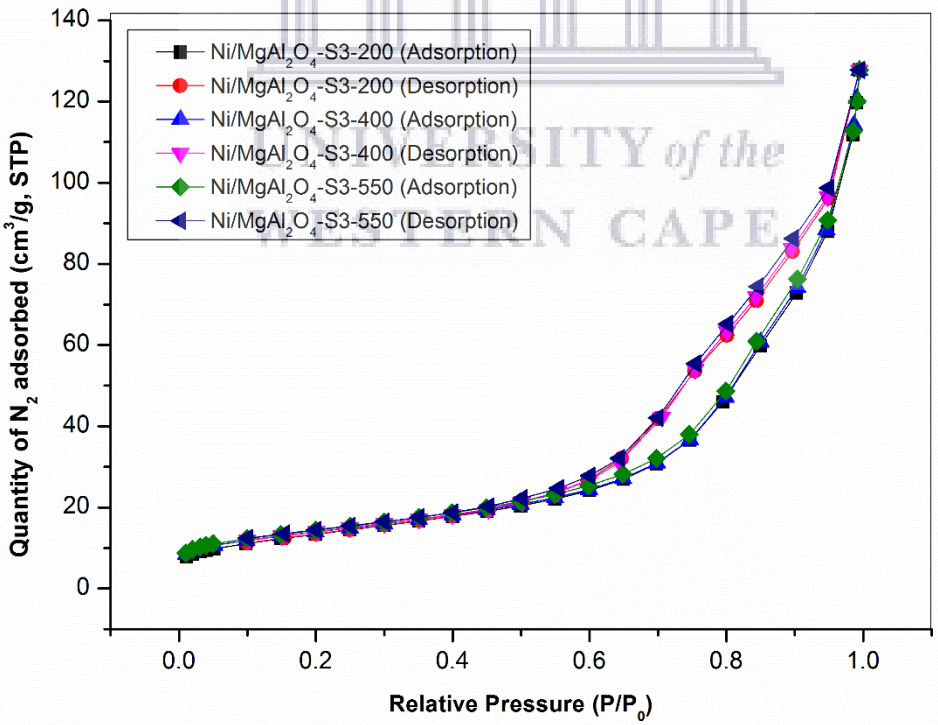

Figure 4.13. c) N_2 adsorption-desorption isotherms of $Ni/MgAl_2O_4$ sulfided with DMSO (S3) at various temperatures

The N_2-physisorption results for the catalysts are displayed in Table 4.2. The S1 catalysts showed the highest surface area of 90-120 m^2/g compared to S2 and S3 catalysts. The surface areas increased for the S2 catalysts as the sulfiding temperature increased above 200 °C. This could be due to the difference in surface areas of the NiS and Ni_3S_2 species observed at different sulfiding temperatures. The surface areas of the catalysts sulfided with DMSO, however, all had the same surface area likely due to the high dispersion observed at all sulfiding temperatures. The N_2 physisorption studies indicate that differences in the textural properties, in particular the surface areas are obtained when using different sulfiding agents. This was dependent on the decomposition of the sulfiding agent in which temperature has an effect as well as dispersion of Ni-S species on the catalyst.

Table 4.2: Surface area, pore volume, pore size and crystallite size of supported catalysts

Sample	**S_{BET} (m^2/g)**	**Pore volume (cm^3/g)**	**Pore size (nm)**	**Crystallite size (nm) Ni_3S_2**
$MgAl_2O_4$	85	0.190	7.9	-
$Ni/MgAl_2O_4$	58	0.156	9.2	-
$Ni/MgAl_2O_4$-S1-200	4	0.022	22.4	-
$Ni/MgAl_2O_4$-S1-400	119	0.340	8.3	-
$Ni/MgAl_2O_4$-S1-550	90	0.400	16	-
$Ni/MgAl_2O_4$-S2-200	30	0.119	14	17
$Ni/MgAl_2O_4$-S2-400	63	0.188	11	16
$Ni/MgAl_2O_4$-S2-550	56	0.194	12	22
$Ni/MgAl_2O_4$-S3-200	49	0.200	14	22
$Ni/MgAl_2O_4$-S3-400	50	0.200	15	19
$Ni/MgAl_2O_4$-S3-550	51	0.200	15	23

4.3.4 Catalytic performance

The catalysts sulfided with $(NH_4)_2SO_4$, $(NH_4)_2S$ and DMSO at the various temperatures were evaluated for the dehydrogenation of propane. The conversion % of propane and selectivity % toward the various products for the catalyst sulfided with $(NH_4)_2SO_4$ is shown in **Figure 4.14** and **Figure 4.15**, respectively. The initial conversion % of propane for the S1 catalysts increased in the following order: Ni/$MgAl_2O_4$-S1-200 (26%), Ni/$MgAl_2O_4$-S1-550 (37%) and Ni/$MgAl_2O_4$-S1-400 (51%) at three minutes of the reaction time. The S1 catalysts follow a trend of increasing stability with time, which could be due to the formation of Ni_3S_2 as the reaction proceeds due to reduction of $(NH_4)_2SO_4$ by propane. The presence of an active Ni_3S_2 was confirmed by XRD analysis of the spent catalysts at 120 minutes (Figure S2.2). The S1-400 and S1-550 which both have higher initial conversions, then decreased slightly after 30 min TOS and then remained stable for the length of the reaction time.

Regarding selectivity of the catalysts, it was noted that as the reaction progressed, more C2 olefins were being produced with time on stream. The major side products for the reaction were CH_4, C_2H_4 and C_2H_6 indicating that hydrogenolysis as well as cracking reactions occur. The selectivity of Ni/$MgAl_2O_4$-S1-400 and Ni/$MgAl_2O_4$-S1-550 toward propylene was higher than Ni/$MgAl_2O_4$-S1-200. For example, at 3 minutes, the selectivity toward propylene was 76% and 72% for Ni/$MgAl_2O_4$-S1-400 and Ni/$MgAl_2O_4$-S1-550, respectively. While Ni/$MgAl_2O_4$-S1-200 displayed a selectivity of 65% at 3 minutes. As indicated by XRD analysis, Ni/$MgAl_2O_4$-S1-400 and Ni/$MgAl_2O_4$-S1-550 contained the least amount of unreacted Ni species. This could be the reason for the improved selectivity in addition to stronger metal-sulfur bonds being formed, as indicated by TGA results, which facilitates the desorption of propylene.

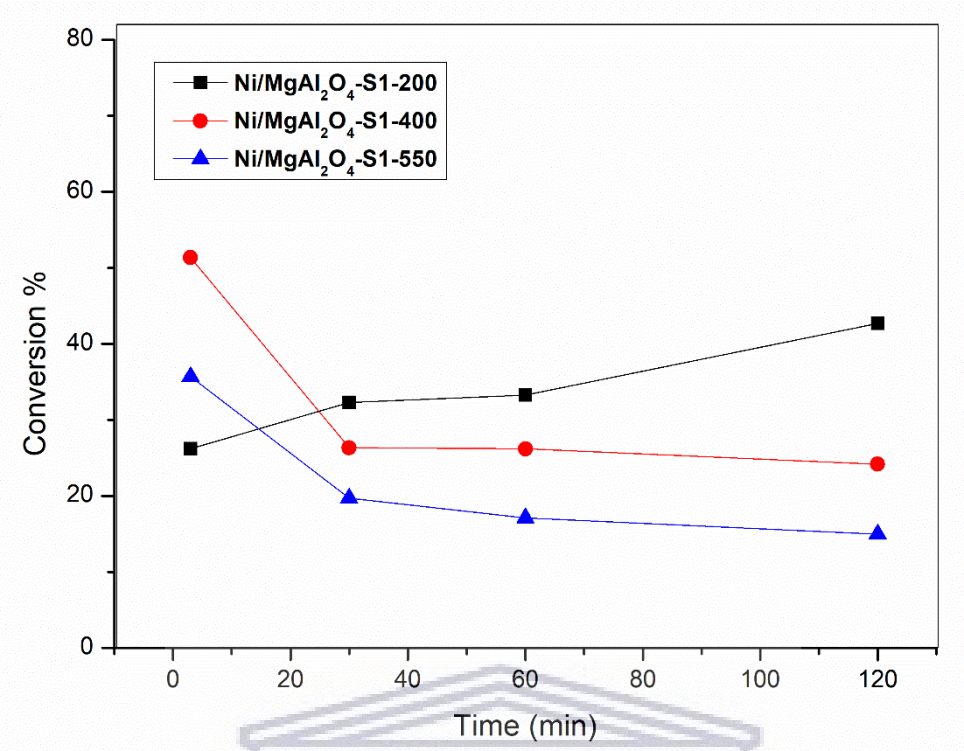

Figure 4.14. Conversion % of $Ni/MgAl_2O_4$ sulfided with $(NH_4)_2SO_4$ at a) 200 °C, b) 400 °C and c) 550°C

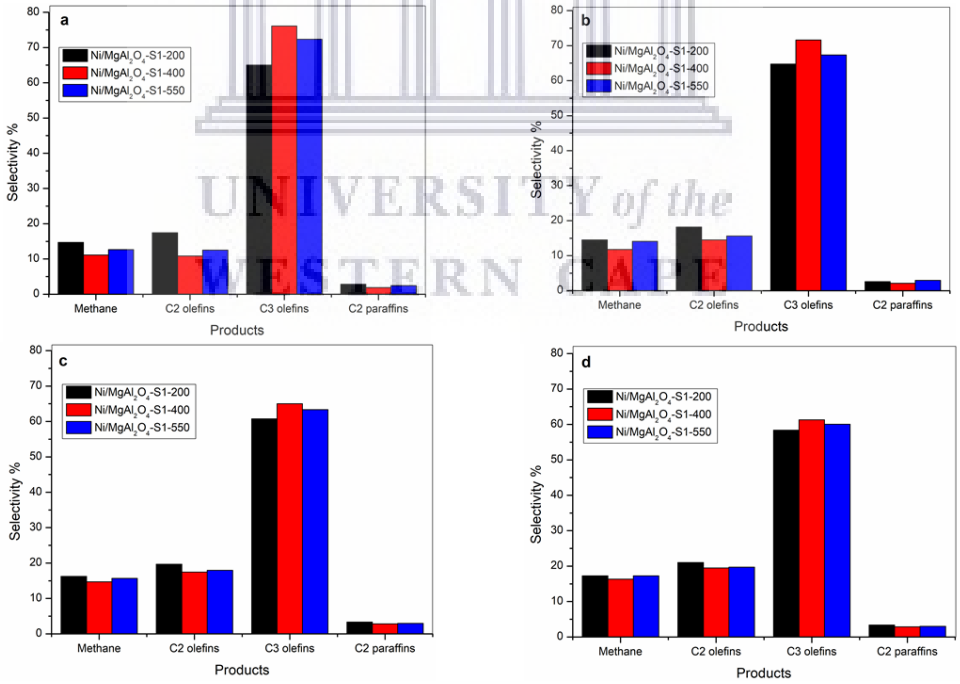

Figure 4.15. Selectivity % of $Ni/MgAl_2O_4$ sulfided with $(NH_4)_2SO_4$ at a) 3 min, b) 30 min, c) 60 min and d) 120 min

In the case of the catalysts sulfided with $(NH_4)_2S$, the catalyst activity decreased over time (**Figure 4.16**). The S1 catalysts showed a decrease in the conversion between 3 – 30 min (S1-400 and S1-550), followed by these catalysts being stable up to 120 minutes. This contrasts with S2 catalysts, whereby the catalysts are stable up to 60 minutes, followed by a decrease in conversion of propane. This contrast could be due to the phases present in the catalyst. Since fresh S2 catalysts contain NiS and Ni_3S_2, the initial conversion and stability is high and activity gradually decreases as sulfur may be lost from the catalyst. However, the presence of Ni_3S_2 is only present in the spent S1 catalysts as the S1catalysts experience an induction phase which results in increase in conversion and stability as the Ni_3S_2 phase forms during the reaction due to reduction by hydrogen. The conversion % at 3 minutes were in close range: Ni/$MgAl_2O_4$-S2-200 (50%), Ni/$MgAl_2O_4$-S2-400 (50%) and Ni/$MgAl_2O_4$-S2-550 (43%).

Overall, the catalyst activity is noticed to decrease with increase in sulfidation temperature. It is possible that the decrease in activity is a result of increase in particle size and lower dispersion as shown by the TEM and SEM analyses which was observed when the sulfidation temperature was increased. The catalysts sulfided with $(NH_4)_2S$ showed excellent selectivity toward propylene, ~78% for Ni/$MgAl_2O_4$-S2-200, Ni/$MgAl_2O_4$-S2-400 and Ni/$MgAl_2O_4$-S2-550, indicating a high dehydrogenation activity of the catalyst as observed from **Figure 4.17**. This could be due to stronger nickel-sulfur bonds and better desorption of olefins, due to a higher electronic effect on S2 catalysts compared to S1. Furthermore, S2 catalysts contains the S^{2-} species, which is part of the active phase (Ni_3S_2) for dehydrogenation.

Wang and co-workers reported that the introduction of sulfur facilitated the desorption of olefins, by weakening the interaction between the surface metal atoms and the adsorbed alkene molecules.[48] One reason is that the introduction of sulfur caused a higher electron density on the surface atoms and led to more repulsive interactions with the olefins. It was proposed that sulfur addition i.e. the presence of S^{2-} adjusted the electronic properties of Ni atoms, altered the nature of the surface species and decreased the adsorption heat of olefins as well as the activation energy of its desorption, thereby leading to a higher dehydrogenation activity.[4,48]

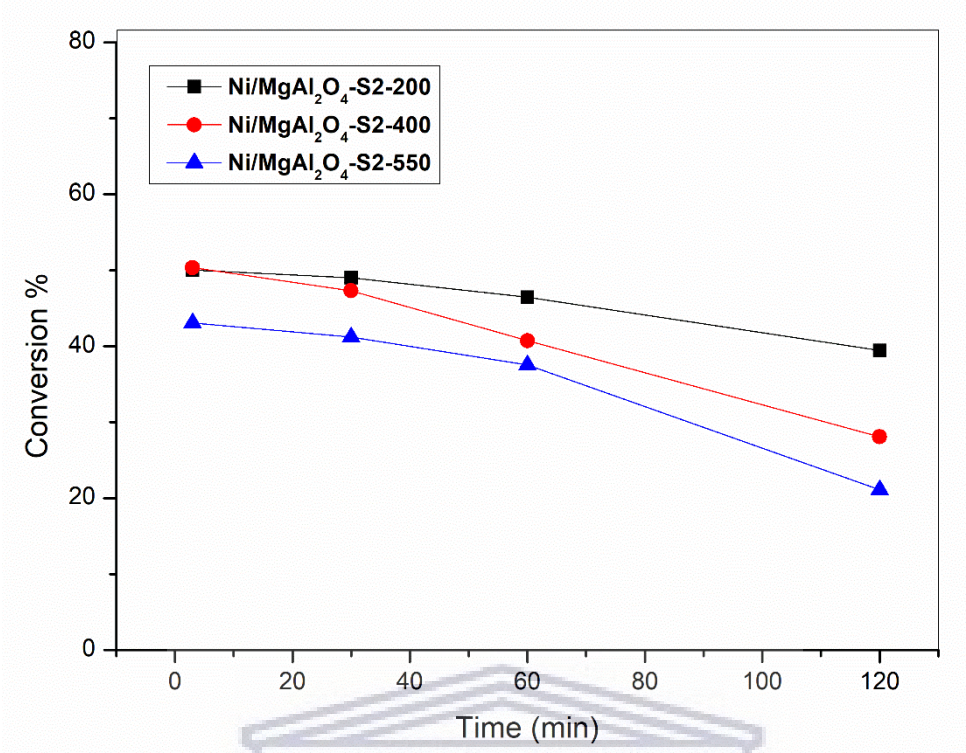

Figure 4.16. Conversion % of $Ni/MgAl_2O_4$ sulfided with $(NH_4)_2S$ at a) 200 °C, b) 400 °C and c) 550°C

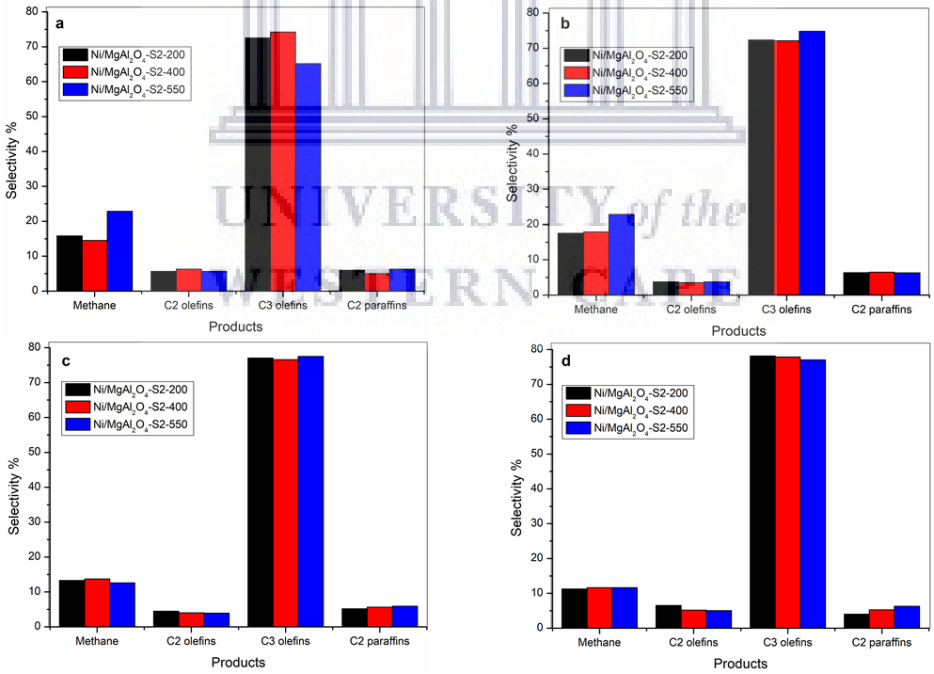

Figure 4.17. Selectivity % of $Ni/MgAl_2O_4$ sulfided with $(NH_4)_2S$ at a) 3 min, b) 30 min, c) 60 min and d) 120 min

The dehydrogenation activity for the catalysts sulfided with DMSO is shown in **Figure 4.18** and **Figure 4.19**. The conversion of propane for the S3 catalysts was in the following order: $Ni/MgAl_2O_4$-S3-400 (36%) < $Ni/MgAl_2O_4$-S3-200 (37%) < $Ni/MgAl_2O_4$-S3-550 (45%) in the first 3 minutes. The $Ni/MgAl_2O_4$-S3-550 catalyst displayed the highest stability compared to all the catalysts including the catalysts sulfided with $(NH_4)_2SO_4$ and $(NH_4)_2S$ as the sulfiding agents. The conversion of propane for $Ni/MgAl_2O_4$-S3-550 was 46%, the highest conversion value of all catalysts at 120 minutes. The enhanced stability of the S3 catalyst is likely due to the highest dispersion of Ni-S_x species as observed by SEM elemental mapping compared to S1 and S2 catalysts. Although sulfidation with DMSO resulted in the lowest wt% sulfur content, the high dispersion and small particle size may have resulted in the strong interaction between the metal and sulfur, thereby enhancing stability and preventing sulfur loss from the catalyst.

EDS analysis of the spent catalysts (**Figure 4.20**) further confirmed that S3 showed the lowest loss of sulfur compared to S1 and S2. The stability of the $Ni/MgAl_2O_4$-S3-550 catalyst could also be due to suppression of the release of S^{2-} in the metal sulfide, which is important for achieving stable dehydrogenation performance.[52] The TGA profile of S3 catalysts confirm the excellent stability of nickel-sulfur bonds when compared to S1 and S2. The increase in conversion with temperature for the S3 catalysts may be correlated with the slightly higher content of sulfur on the $Ni/MgAl_2O_4$-S3-550 catalyst compared to the $Ni/MgAl_2O_4$-S3-200 and $Ni/MgAl_2O_4$-S3-400 catalysts. This increase in activity may be attributed to the higher content of sulfur increasing the electronic charge distribution on the catalyst, thus acting as an electronic promoter.

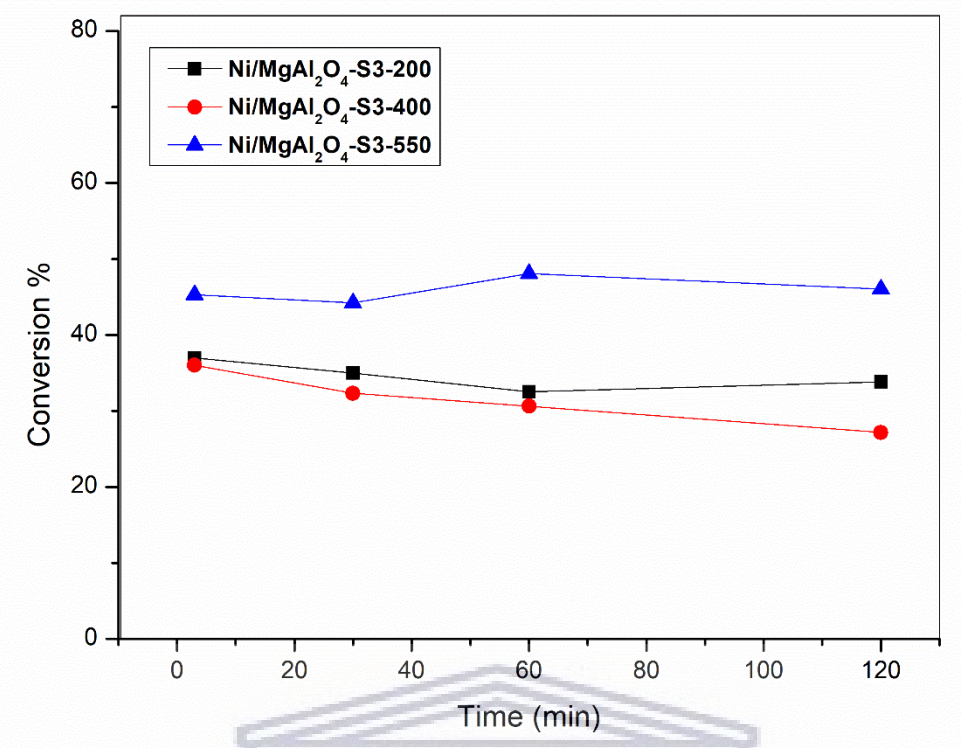

Figure 4.18. Conversion % of $Ni/MgAl_2O_4$ sulfided with DMSO at a) 200 °C, b) 400 °C and c) 550°C

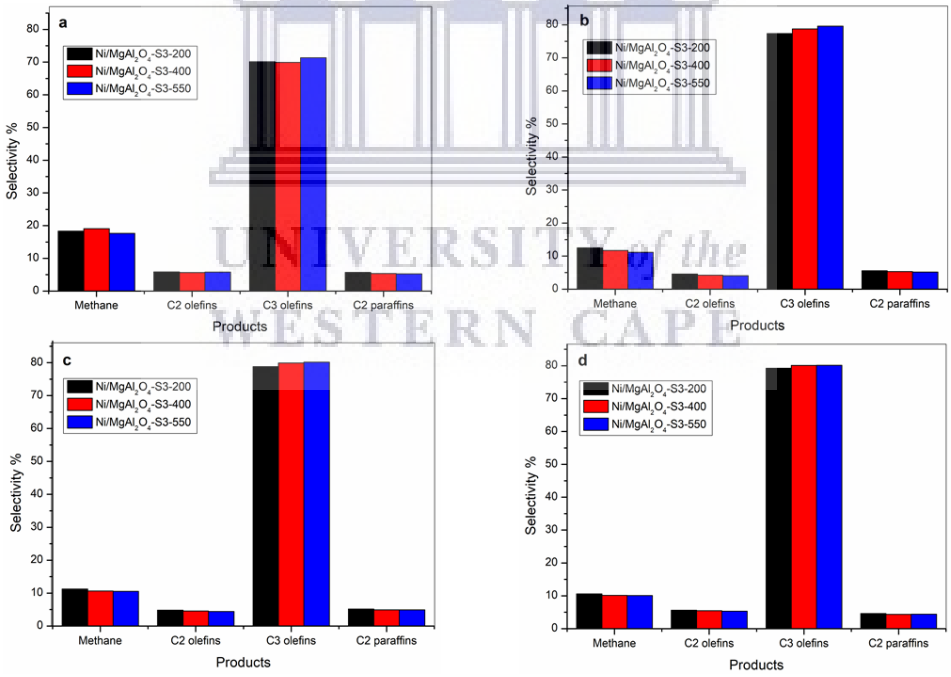

Figure 4.19. Selectivity % of $Ni/MgAl_2O_4$ sulfided with DMSO at a) 3 min, b) 30 min, c)60 min and d) 120 min

Figure 4.20 shows that sulfur is lost after 2 hours of reaction time by the decrease in %S on the spent catalysts. The S3 catalysts although having the lowest sulfur content also showed the least loss of sulfur compared to S1 and S2 catalysts. This indicates a strong interaction between the metal and sulfur, confirmed by TGA, possibly due the higher dispersion observed. The difference in catalytic activity between S1, S2 and S3 catalysts could be due to the strength of the sulfur bonds to the metal. Furthermore, the difference in decomposition of the sulfiding agent at different temperatures, i.e. either 200 °C, 400 °C or 550 °C may lead to different sulfur contents which change the net electronic charge distribution that affects the activity of the catalyst. Thus, the amount of sulfur present a stronger metal-sulfur bond could lead to an enhanced activity and stability as shown for the $Ni/MgAl_2O_4$-S3-550 catalyst.

It was noted that S1 catalysts (containing the SO_4^{2-} ion) had a higher selectivity toward C2 compared to S2 and S3 catalysts (containing the S^{2-} ion), indicative of more cracking reactions. It is known that the SO_4^{2-} ion promotes acidity on dehydrogenation catalysts. It has previously been reported that cracking reactions occur on dehydrogenation catalysts containing higher acid site density in comparison to moderate acid site density.[22,53] This is consistent in our study, whereby S1 contained the highest wt% S in the form of the SO_4^{2-} as indicated by XRD analysis and electron mapping imaging. For the catalysts sulfided with $(NH_4)_2S$ and DMSO, although a high dehydrogenation activity existed, side products (CH_4, C_2H_4 and C_2H_6) were observed, an indication that propane cracking and propane hydrogenolysis reactions were not completely eliminated.[52]

The selectivity of the catalysts sulfided with DMSO to propene however were still high, comparable with the S2 catalysts. Interestingly, it showed the best selectivity toward propane as the reaction proceeded. The selectivity increased to as high as 80% at 120 minutes of the reaction time, highlighting the beneficial effect of high dispersion of sulfur on the catalyst. The enhanced stability of the catalyst resulted in the high selectivity to propene with time on stream. The high dispersion may have also resulted in sulfur reducing the nickel ensemble size and blocking sites responsible for the hydrogenolysis as the lowest methane selectivity was observed for the S3 catalysts.

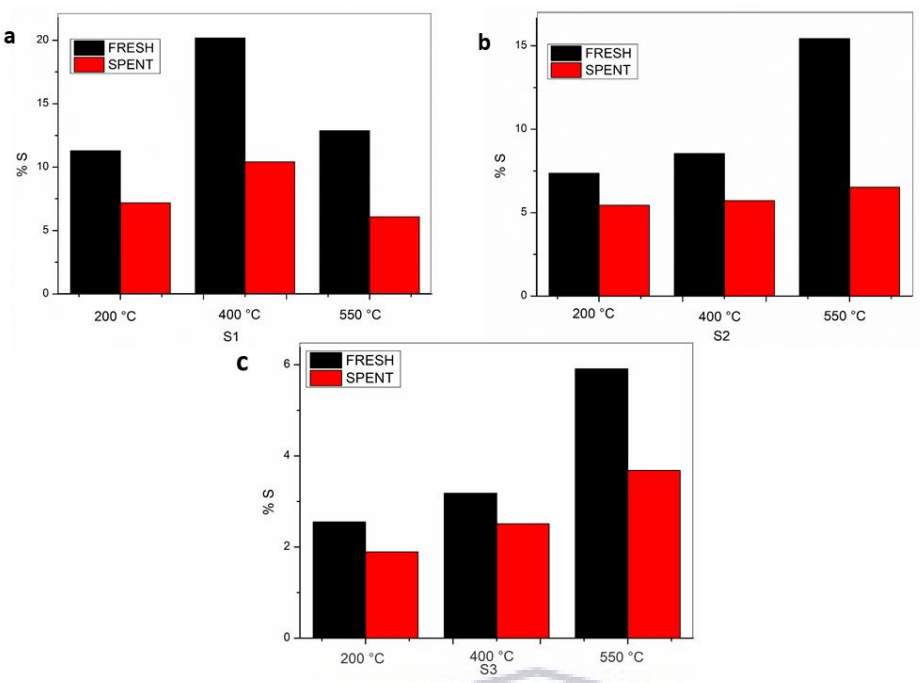

Figure 4.20. EDS data of a) S1 catalysts b) S2 catalysts and c) S3 catalysts at sulfidation temperatures of 200 °C, 400 °C and 550 °C

4.4 Conclusion

Nickel catalysts supported on $MgAl_2O_4$ were successfully prepared using $(NH_4)_2SO_4$ (S1), $(NH_4)_2S$ (S2) and DMSO (S3). The catalysts were sulfided at 200 °C, 400 °C and 550 °C. For S1 catalysts, Ni/$MgAl_2O_4$-S1-200 contained the highest percentage of unreacted Ni with sulfur and peaks associated with nickel-sulfur phases were absent, according to XRD analysis. For the Ni/$MgAl_2O_4$-S1-400 and Ni/$MgAl_2O_4$-S1-550 catalysts, decomposition of the sulfiding agent increased with temperature above the decompsition temperature of 250 °C leading better sulfur dispersion and interaction with the catalyst. XRD analysis displayed peaks for $MgSO_4$, indicating a stronger interaction between the support and SO_4^{2-} ion of the sulfiding agent when the temperature was increased.

$Ni/MgAl_2O_4$-S2-200, $Ni/MgAl_2O_4$-S2-400 and $Ni/MgAl_2O_4$-S2-550 catalysts contained NiS and Ni_3S_2, while $Ni/MgAl_2O_4$-S3-200, $Ni/MgAl_2O_4$-S3-400 and $Ni/MgAl_2O_4$-S3-550 catalysts contained only the Ni_3S_2 phase indicating sulfiding agent as sulfiding conditions such as temperature may influence the NiS_x phase formed. Although $Ni/MgAl_2O_4$-Sx-y catalysts were reduced prior to sulfidation, S3 catalysts contained the presence of NiO, which disappeared with an increase in sulfidation teperature. This could indicate that the sulfiding agent decomposed to a higher extent at the elevated temperatures of 400 °C and 550 °C compared to the sulfidation temperature of 200 °C. Furthermore, it was noted that the increase in sulfidation temperature resulted in an increase in crystallite size of the nickel-sulfided particles, which could be due to sintering that commonly occurs at higher temperatures.

SEM analysis showed that the morphology of the catalysts were distinct with respect to sulfiding agent and sulfidation temperature. Electron mapping images confirmed the strong interaction between $MgAl_2O_4$ and S, with visual evidence of $MgSO_4$ as seen in $Ni/MgAl_2O_4$-S1-400 and $Ni/MgAl_2O_4$-S1-550 catalysts. The S2 catalysts displayed the presence of a "coating" that became more apparent with an increase in sulfidation temperature resulting in a low dispersion. This coating was attributed to Ni_3S_2, highlighting the strong interaction between nickel and sulfur with an increase in temperature, as observed from TGA.

The S3 catalysts showed the catalysts had the lowest sulfur content and best dispersion compared to S1 and S2 catalysts, for $Ni/MgAl_2O_4$-S3-200, $Ni/MgAl_2O_4$-S3-400 and $Ni/MgAl_2O_4$-S3-550 catalysts indicating the type of sulfiding agent and sulfiding conditions used may influence dispersion of NiS_x species. However, $Ni/MgAl_2O_4$-S3-550 showed the strongest interaction of nickel and sulfur, visible by clusters of Ni_3S_2 on the catalyst surface. TEM analysis indicate that the particle size on S1 catalysts did not have a significant change with increasing sulfidation temperature. S3 catalysts displayed improved dispersion, with clusters of smaller particles, highlighting the geometric effect of sulfur.

The sulfided catalysts were then tested for the dehydrogenation of propane. The $Ni/MgAl_2O_4$-S1-400 and $Ni/MgAl_2O_4$-S1-550 catalysts performed better than $Ni/MgAl_2O_4$-S1-200, since the former catalysts contained less unreacted Ni and had a higher impact by sulfur as the decomposition was more efficient at higher temperatures. The catalysts seemed to undergo an induction period , in particular $Ni/MgAl_2O_4$-S1-200, as the $(NH_4)_2SO_4$ crystals were reduced to Ni_3S_2 during the reaction. The conversion % for S2 catalysts were~ 50% with a selectivity toward propylene equal to ~ 78%. This could be due to Ni_3S_2 present on the catalyst being the active phase, promoting better interaction between nickel and sulfur as sulfur content increased with higher sulfiding temperatures. The high propene selectivities were attributed to increased desorption of olefins due to sulfur interaction with the Ni metal. The $Ni/MgAl_2O_4$-S3-550 catalyst showed the highest conversion of propane and selectivity toward propylene by at 120 minutes of the reaction. This catalyst displayed the best overall performance compared to all the catalysts, which could be attributed to the high dispersion of metal sulfide species which led to strong Ni-S interactions and ultimately higher activity, selectivity and enhanced stability.

By sulfiding catalysts at 200 °C, 400 °C and 550 °C, the findings show that the sulfiding agent (containing the different anions) and the sulfidation conditions (temperature) has an influence on the catalyst structural and textural properties in terms of decomposition and sulfur content which affect morphology, particle size, dispersion and Ni-S interaction. The catalytic performance was shown to be most dependent on Ni-S interaction and particle dispersion of which the best results were obtained with DMSO (S3). DMSO used as a sulfiding agent improved conversion, increased selectivity to propene (80%) and enhanced stability especially when a high sulfiding temperature (550 °C) was utilized.

4.5 References

1 M. M. Bhasin, J. H. McCain, B. V. Vora, T. Imai and P. R. Pujadó, *Appl. Catal. A Gen.*, 2001, **221**, 397–419.
2 Z. Nawaz, *Rev. Chem. Eng.*, 2015, **31**, 413–436.
3 Q. Zhu, G. Wang, J. Liu, L. Su and C. Li, *ACS Appl. Mater. Interfaces*, 2017, **9**, 30711–30721.
4 G. Wang, Z. Meng, J. Liu, C. Li and H. Shan, *ACS Catal.*, 2013, **3**, 2992–3001.
5 S. M. K. Airaksinen, M. E. Harlin and A. O. I. Krause, *Ind. Eng. Chem. Res.*, 2002, **41**, 5619–5626.
6 A. B. Gaspar, J. L. F. Brito and L. C. Dieguez, *J. Mol. Catal. A Chem.*, 2003, **203**, 251–266.
7 A. Farjoo, F. Khorasheh, S. Niknaddaf and M. Soltani, *Sci. Iran.*, 2011, **18**, 458–464.
8 G. Wang, C. Li and H. Shan, *ACS Catal.*, 2014, **4**, 1139–1143.
9 E. Cheng, L. McCullough, H. Noh, O. Farha, J. Hupp and J. Notestein, *Ind. Eng. Chem. Res.*, 2020, **59**, 1113–1122.
10 WO Patent 2017162427A1, 2017, 1.
11 US005468710A, 1995.
12 R. R. Chianelli, M. Daage and M. J. Ledoux, *Adv. Catal.*, 1994, **40**, 177–232.
13 R. Watanabe, N. Hirata, K. Miura, Y. Yoda, Y. Fushimi and C. Fukuhara, *Appl. Catal. A Gen.*, 2019, **587**, 117238.
14 M. Ziolek, J. Kujawa, O. Saur and J. C. Lavalley, *J. Mol. Catal. A. Chem.*, 1995, **97**, 49–55.
15 G. Wang, X. Zhu and C. Li, *Chem. Rec.*, 2019, **19**, 1–14.
16 Z. Gao, W. Yang, X. Ding, G. Lv and W. Yan, *Appl. Surf. Sci.*, 2018, **436**, 585–595.
17 B. Liu, L. Liu, Y. Chai, J. Zhao, Y. Li, Y. Liu and C. Liu, *Ind. Eng. Chem. Res.*, 2018, **57**, 2041–2049.
18 D. E. Resasco, B. K. Marcus, C. S. Huang and V. A. Durante, *J. Catal.*, 1994, **146**, 40–55.
19 G. Wang, N. Sun, C. Gao, X. Zhu, Y. Sun, C. Li and H. Shan, *Appl. Catal. A Gen.*, 2014, **478**, 71–80.
20 F. H. Alhassan, U. Rashid, M. S. Al-Qubaisi, A. Rasedee and Y. H. Taufiq-Yap, *Powder Technol.*, 2014, **253**, 809–813.
21 S. Wang, K. Murata, T. Hayakawa, S. Hamakawa and K. Suzuki, *Catal. Letters*, 1999, **63**, 59–64.
22 Y. N. Sun, Y. N. Gao, Y. Wu, H. Shan, G. Wang and C. Li, *Catal. Commun.*, 2015, **60**, 42–45.
23 E. M. Matira, T. C. Chen, M. C. Lu and M. L. P. Dalida, *J. Hazard. Mater.*, 2015, **300**, 218–226.
24 G. Chemical, *Tech. Bull. React.*, **1209**, 1–110.
25 B. W. Hoffer, J. A. Moulijn, F. Devred, P. J. Kooyman, A. D. van Langeveld, R. L. C. Bonné, C. Griffiths and C. M. Lok, *J. Catal.*, 2002, **209**, 245–255.
26 B. W. Hoffer, R. L. C. Bonné, A. D. Van Langeveld, C. Griffiths, C. M. Lok and J. A. Moulijn, *Fuel*, 2004, **83**, 1–8.
27 Z. Yu, X. Hu, P. Jia, Z. Zhang, D. Dong, G. Hu, S. Hu, Y. Wang and J. Xiang, *Appl. Catal. B Environ.*, 2018, **237**, 538–553.
28 M. Jiang, B. Wang, J. Lv, H. Wang, Z. Li, X. Ma, S. Qin and Q. Sun, *Appl. Catal. A Gen.*, 2013, **466**, 224–232.
29 H. Farag, *Energy and Fuels*, 2002, **16**, 944–950.
30 Y. Okamoto, A. Kato, Usman, N. Rinaldi, T. Fujikawa, H. Koshika, I. Hiromitsu and T. Kubota, *J. Catal.*, 2009, **265**, 216–228.
31 M. Y. Nassar, I. S. Ahmed and I. Samir, *Spectrochim. Acta - Part A Mol. Biomol. Spectrosc.*, 2014, **131**, 329–334.
32 T. Tahier, E. Mohiuddin, D. Key and M. M. Mdleleni, *Catal. Today*, , DOI:10.1016/j.cattod.2020.12.028.
33 S. H. Yu and M. Yoshimura, *Adv. Funct. Mater.*, 2002, **12**, 277–285.
34 W. Li, S. Wang, L. Xin, M. Wu and X. Lou, *J. Mater. Chem. A*, 2016, **4**, 7700–7709.
35 C. Jin, L. Zhou, L. Fu, J. Zhu, D. Li and W. Yang, *J. Power Sources*, 2017, **352**, 83–89.
36 W. Wang, S. Y. Wang, Y. L. Gao, K. Y. Wang and M. Liu, *Mater. Sci. Eng. B Solid-State Mater.*

Adv. Technol., 2006, **133**, 167–171.
37 Y. Qu, H. Yang, N. Yang, Y. Fan, H. Zhu and G. Zou, *Mater. Lett.*, 2006, **60**, 3548–3552.
38 D. G. Mustard and C. H. Bartholomew, *J. Catal.*, 1981, **67**, 186–206.
39 J. Sehested, A. Carlsson, T. V. W. Janssens, P. L. Hansen and A. K. Datye, 2001, **209**, 200–209.
40 Y. U. Jeong and A. Manthiram, *Inorg. Chem.*, 2001, **40**, 73–77.
41 G. Li, X. Xiong, L. Wang, L. Che, L. Wei, H. Cheng, X. Zou, Q. Xu, Z. Zhou, S. Li and X. Lu, *Metals*, 2019, **9**, 1-15
42 G. N. Schrauzer and V. Mayweg, *J. Am. Chem. Soc., 1962*, **84**, 3221.
43 Y. L. Wang, X. Q. Wei, M. B. Li, P. Y. Hou and X. J. Xu, *Appl. Surf. Sci.*, 2018, **436**, 42–49.
44 A. Gerle, J. Piotrowski and J. Podwórny, 2016, **10**, 25–31.
45 J. A. Wang and C. L. Li, *Appl. Surf. Sci.*, 2000, **161**, 406–416.
46 P. Veerakumar, M. Velayudham, K. L. Lu and S. Rajagopal, *Catal. Sci. Technol.*, 2011, **1**, 1512–1525.
47 J. Liu, N. Ruffini, P. Pollet, V. Llopis-Mestre, C. Dilek, C. A. Eckert, C. L. Liotta and C. B. Roberts, *Ind. Eng. Chem. Res.*, 2010, **49**, 8174–8179.
48 G. Wang, C. Gao, X. Zhu, Y. Sun, C. Li and H. Shan, *ChemCatChem*, 2014, **6**, 2305–2314.
49 P. P. Li, W. Z. Lang, K. Xia, L. Luan, X. Yan and Y. J. Guo, *Appl. Catal. A Gen.*, 2016, **522**, 172–179.
50 S. He, C. Sun, H. Du, X. Dai and B. Wang, *Chem. Eng. J.*, 2008, **141**, 284–289.
51 K. Wijayanti, S. Andonova, A. Kumar, J. Li, K. Kamasamudram, N. W. Currier, A. Yezerets and L. Olsson, *Appl. Catal. B Environ.*, 2015, **166–167**, 568–579.
52 R. Watanabe, N. Hirata, Y. Yoda, Y. Fushimi and C. Fukuhara, *J. Japan Pet. Inst.*, 2020, **63**, 228–237.
53 P. Taghavinezhad, M. Haghighi and R. Alizadeh, *Korean J. Chem. Eng.*, 2017, **34**, 1346–1357.

CHAPTER 5: Promoted effect of zinc and sulfur on the structural and catalytic properties of bimetallic nickel-zinc catalysts for the dehydrogenation of propane

5.1 Introduction

There is a growing interest in the catalytic dehydrogenation of light alkanes, such as propane, due to the increase in demand for light olefins, which are fundamental building blocks for processes in the chemical and petrochemical industry.[1–5] Pt or Pt-Sn systems are widely used in light alkane dehydrogenation reactions, where these catalysts exhibit higher activity and stability than monometallic catalysts. The high cost and low availability of Pt limit their applications for large scale processes to some extent.[6,7] Much attention has turned toward nickel, which possess similar electronic properties and can perform many of the same reactions as Pt or Pd. Nickel is known for its high alloying efficiency with all noble metals and many transition metals, which contributes to the ease of developing a wide range of bimetallic nickel systems for diverse catalytic applications.[8–10] Various promoters, including S, Sn or Zn have been added to nickel catalysts to reduce the effects of hydrogenolysis and enhance geometric and electronic properties.[11–13]

Several suggestions have been made to explain the promoting effect of Sn on Pt catalysts. Increased dispersion or formation of favourable ensemble size of Pt have been attributed to the geometric effect of Sn.[1,11,14–17] In addition to Sn on Pt-based catalysts, Zn was found to be a common promoter of choice on noble metal catalysts to control the activity and selectivity in a wide range of reactions. The presence of Zn is known to improve the performance of Pt catalysts in the dehydrogenation of propane. The enhancing effect of Zn has been ascribed to the strong interactions between the Zn and Pt metals, leading to the formation of a PtZn alloy and modifying the electronic property of Pt atoms on the catalyst, by donating electron density and weakening the adsorption of $\pi-\text{bonded}$ alkenes, hence, inhibiting the formation of coke precursors. It has been suggested that Zn display similar effects to Sn for the modification of Pt catalysts in dehydrogenation reactions.[18–21]

Zinc is an abundant, non-toxic metal that has gained interest as the second component in a bimetallic system for propane dehydrogenation. However, Zn-bimetallic catalysts have not been studied as extensively as the more common Sn-based systems.[22]

Furthermore, the understanding of sulfur interaction with bimetallic catalysts is an important topic in several areas of heterogeneous catalysis. Catalysts that combine noble and late-transition metals are extremely sensitive to sulfur poisoning. On the other hand, when a catalyst is sulfided, several beneficial effects can take place. As previously discussed, the introduction of sulfur on catalysts has been found to reduce coke formation and increase catalytic activity. Research has been published explaining the phenomena that could occur when sulfur interacts with a bimetallic surface. Firstly, the formation of bimetallic sulfides that exhibit different chemical properties compared to the corresponding pure metal. Secondly, the interaction between sulfur and one of the metals in the bimetallic system could be repulsive, with sulfur weakening the bimetallic bonds and reducing the mixing of metals. Lastly, a bimetallic system could exist whereby one of the metals promotes the reactivity of the other toward sulfur.[9,23–25]

In previously reported studies, NiZn bimetallic catalysts supported on Al_2O_4 have been utilized for the dehydrogenation of methylcyclohexane (MCH).[8,26] The bimetallic NiZn catalysts were prepared by varying Ni/Zn ratios. The addition of Zn (2 wt%) to the Ni (8 wt%) catalyst lowered conversion of the MCH compared to monometallic Ni, however, the selectivity for toluene improved.[8] The authors attributed this to reconstruction of the surface active sites that occurred during catalysis. The DFT results from their experiments suggested that the main role of Zn was poisoning of the low-coordinated sites where C-C breaking occurs, which is responsible for hydrogenolysis. This led to improved selectivity of the catalyst for dehydrogenation.[8,26]

In this work, we investigate the effect of the Ni-Zn ratio on the structural and catalytic properties of bimetallic catalysts and whether the effect of sulfur addition on the bimetallic catalytic system could further enhance selectivity to propylene in the dehydrogenation of propane.

5.2 Experimental

5.2.1 Raw materials

The following chemicals were used in the study: Silica gel (Davisil Grade 643, Sigma Aldrich), nickel nitrate hexahydrate (≥97%, Sigma Aldrich), zinc nitrate hexahydrate (≥99%, Sigma Aldrich), DMSO (≥99.9%, Sigma Aldrich) and propane gas. Distilled water is obtained by a house supply that produces Milli-Q water.

5.2.2 Catalyst preparation: Synthesis of bimetallic Ni-Zn/SiO_2 catalysts

Ni-Zn catalysts supported on SiO_2 were prepared by wetness impregnation using $Ni(NO_3)_2.6H_2O$ and $Zn(NO_3)_2.6H_2O$ as the metal precursors. An aqueous solution of $Ni(NO_3)_2.6H_2O$ was added dropwise to the support, followed by dropwise addition of an aqueous solution of $Zn(NO_3)_2.6H_2O$ to the support solution. The final solution, containing the support and both metal precursors were heated at 80 °C with continuous stirring of the solution. After impregnation of the support, the catalysts were dried at 140 °C overnight and calcined at 550 °C in air for 5 hours to convert them to the oxide form. The catalysts were prepared with the following wt% of Ni and Zn: 13Ni/SiO_2, 11Ni-2Zn/SiO_2, 9Ni-4Zn/SiO_2, 6.5Ni-6.5Zn/SiO_2, 4Ni-9Zn/SiO_2, 2Ni-11Zn/SiO_2 and 13Zn/SiO_2. The catalysts were then reduced under a H_2 atmosphere at 600 °C for 6 hours.

The sulfur modified bimetallic catalysts were prepared by using DMSO as the sulfiding agent, with a ratio of Ni:S is 1:5. The reduced catalysts were loaded onto the reactor, sulfided with the calculated amount of sulfiding agent under a flow of nitrogen (50 ml/min) 550 °C for 3 hours.

5.3 Results and Discussion

5.3.1 Structural and textural properties of bimetallic catalysts

The monometallic and bimetallic catalysts were reduced at 600 °C and then subjected to X-ray diffraction (XRD) analysis. The XRD patterns of the various catalysts supported on SiO_2 is shown in **Figure 5.1** below. The reflections corresponding to Ni metal occur at 44°, 52° and 76° 2θ angles. ZnO was present on the $13Zn/SiO_2$ catalyst indicating that not all the ZnO was reduced at 600 °C.

With the addition of the second metal, Zn < 6.5 wt%, the diffraction peaks of the nickel phase is observed. However, there is a slight shift in these diffraction peaks to lower 2θ values. With the decrease of Ni content from 11 wt% Ni to 9 wt% Ni, the diffraction peaks of the bimetallic catalysts is found at lower 2θ values for $11Ni\text{-}2Zn/SiO_2$ and $9Ni\text{-}4Zn/SiO_2$ catalysts, with a 0.9% and 1.8% shift in the Ni metal peak, respectively. This can be explained in terms of the lattice substitution effect. Since the ionic radius of Zn (0.6 – 0.9 Å) is larger than that of Ni ions (0.49 Å), the Zn atoms substitute the Ni atoms in the lattice, which could result in an increased unit cell volume. The lattice substitution effect has been reported in the literature and is a common cause for a shift in 2θ values observed for bimetallic catalysts.[28,29] Thus, at Zn loadings less than 6.5 wt% only a single phase is observed which is likely to be a solid solution of Ni and Zn.

When the wt% of Zn is increased to 6.5 wt% there is an emergence of a new peak at 47° 2θ, which corresponds to NiZn. This implies that when the ratio of Ni:Zn is 1:1 (Table S3.1), there is a possibility of a Ni-Zn alloy formation. This could be the case for the $4Ni\text{-}9Zn/SiO_2$ catalyst and $2Ni\text{-}11Zn/SiO_2$ catalyst as the peak at 47° 2θ is observed in these diffractograms. With an increase in Zn on the catalysts, the formation of the Ni-Zn alloy is more probable. The % of NiZn on $6.5Ni\text{-}6.5Zn/SiO_2$ and $4Ni\text{-}9Zn/SiO_2$ according to MATCH software is 39% and 71%, respectively. At lower Zn content, the Zn atoms substitute the Ni atoms in the Ni structure, however, from the Ni:Zn ratio of 1:1, we observe the formation of a Ni-Zn alloy, which is confirmed with the presence of the new diffraction peak.

Zhang and co-workers showed that small ZnO particle size (< 8 nm) promotes the dispersion of Ni on Zn, which will directly form the Ni-Zn alloy during calcination.[30] When 11 wt% Zn is added to the catalyst as in the case of 2Ni-11Zn/SiO_2, the presence of free Ni metal was not detected and the catalyst is solely composed of a NiZn alloy. It was noted that the intensities of the metal diffraction peaks in 6.5Ni-6.5Zn/SiO_2, 4Ni-9Zn/SiO_2 and 2Ni-11Zn/SiO_2 were weaker than the intensities of the 11Ni-2Zn/SiO_2 and 9Ni-4Zn/SiO_2 catalysts, which might be due to better dispersion and smaller particle size of the metal species on the former three catalysts.

The crystallite size of Ni and NiZn particles were calculated using the Scherrer equation for the peak at 2θ ~44° and 47°, respectively. The crystallite sizes of the particles are summarized in Table 5.1. At an increased Ni:Zn molar ratio, the Ni crystallite size is smaller than the monometallic 13Ni/SiO_2 catalyst. Furthermore, it was noted that with an increase in the Zn loading from the ratio of 1 and greater, the NiZn crystallite size decreases, highlighting Zn as a structural promoter on the catalyst. Meng and co-workers suggest that there is a strong synergetic effect between Zn-based and Ni-based species to form a well dispersed sample when the molar ratio of Zn/Ni is as low as 0.4 in the sample.[31] These results support the data presented by Zhang and co-workers, which indicate that the presence of small ZnO particles promote dispersion of Ni and facilitate the formation of the Ni-Zn alloy with small particle size.[30]

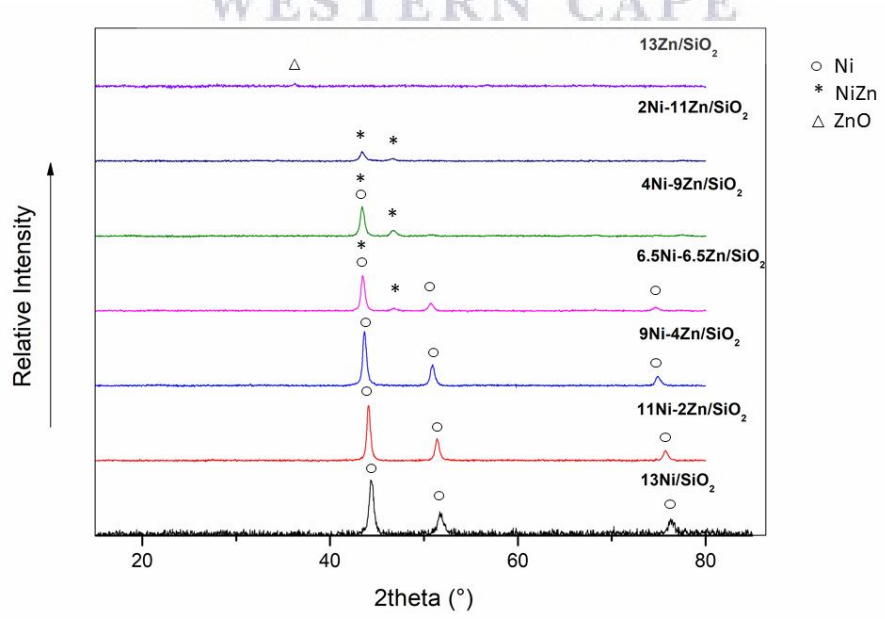

Figure 5.1. XRD pattern of bimetallic catalysts supported on SiO_2

Nitrogen adsorption-desorption isotherms of the bimetallic catalysts are shown in **Figure 5.2**. All the samples display type IV isotherms and type H_1 hysteresis loops, which is indicative of mesopores present in the catalysts.[32,33]

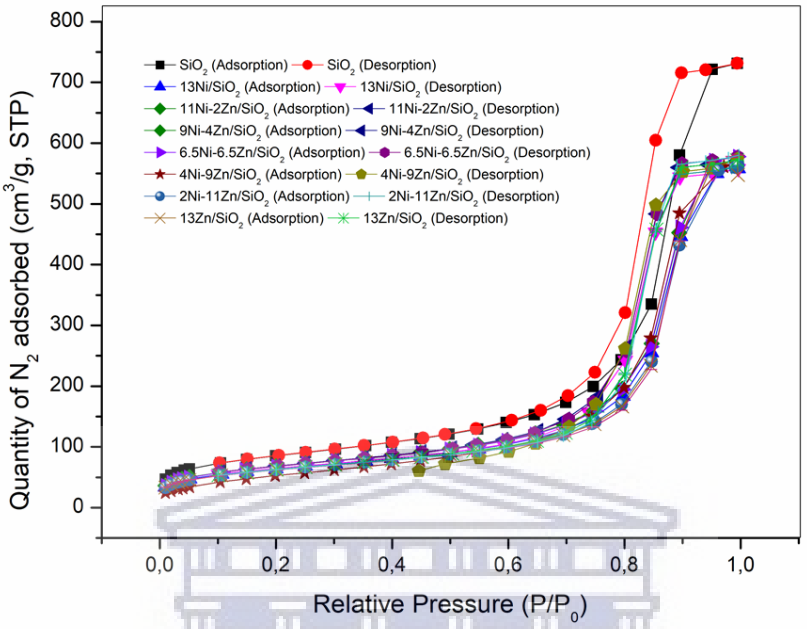

Figure 5.2. N_2 adsorption-desorption isotherms of catalysts

Table 5.1 contains a summary of the BET surface area and the crystallite size of the Ni species in the catalysts on the SiO_2 support. The surface area increased with the addition of Zn to the monometallic 13Ni/SiO_2 catalysts, as seen by results obtained for the 11Ni-2Zn/SiO_2 (244 m^2/g) and 9Ni-4Zn/SiO_2 (241 m^2/g) catalysts. There was a noticeable decrease of surface area from 244 m^2/g for 11Ni-2Zn/SiO_2 to 200 m^2/g for the 6.5Ni-6.5Zn/SiO_2 catalyst. The significant loss in surface area after the addition of 6.5 wt% Zn could possibly be ascribed to metal species that entered the pores and the extent of pore obstruction led to the reduction in surface area.[34,35] The surface area increased from 200 m^2/g for 6.5Ni-6.5Zn/SiO_2 to 224 m^2/g and 225 m^2/g for 4Ni-9Zn/SiO_2 and 2Ni-11Zn/SiO_2, respectively. This slight increase in surface area could be due to change in the particle size of the metals. There was negligible difference of surface area between 4Ni-9Zn/SiO_2, 2Ni-11Zn/SiO_2 and 13Zn/SiO_2 catalysts possibly due to the similar sizes of particles present in these catalysts.

Table 5.1: Surface area, pore size and crystallite size of catalysts

Sample	S_{BET} (m^2/g)	Pore size (nm)	Crystallite size Ni (nm)	Crystallite size NiZn (nm)
SiO_2	303	14	-	-
13Ni/SiO_2	230	14	20	
11Ni-2Zn/SiO_2	244	13	18	-
9Ni-4Zn/SiO_2	241	14	15	-
6.5Ni-6.5Zn/SiO_2	200	13	13	11
4Ni-9Zn/SiO_2	224	14	-	3
2Ni-11Zn/SiO_2	225	15	-	3
13Zn/SiO_2	223	15	-	

5.3.2 Reducibility of the bimetallic catalysts

Temperature programmed reduction (TPR) analysis was used to determine the reducibility of the catalysts. The TPR results for the monometallic oxides and bimetallic oxides are presented in **Figure 5.3**. The TPR profile for 13NiO/SiO_2 shows that the catalyst reduces at 350 °C, which is typical for NiO-based catalysts. A shoulder peak is commonly found at high temperatures for supported NiO catalysts, indicating nickel-support interaction.[36] In this case, a small peak occurred at 480 °C which could be due to NiO interacting with the SiO_2 support.[37] The reducibility of ZnO can be seen from the TPR curve of the 13ZnO/SiO_2 catalyst. One small peak was observed at approximately 800 °C, due to the partial reduction of ZnO, since the ZnO phase is present on the 13ZnO/SiO_2 catalyst as seen from XRD analysis. Previous studies have shown the difficulty in fully reducing ZnO samples and that the complete reduction of ZnO to Zn could require temperatures above 800 °C.[38–40]

The TPR profiles for the bimetallic oxide catalysts displayed an evident shift to higher temperatures with an increase in Zn content. The 11NiO-2ZnO/SiO_2 catalyst contained a peak at 400 °C and 550 °C, while the 9NiO-4Zn/SiO_2 catalyst contained a peak at 400 °C and 600 °C. As indicated in previous studies on NiZn compounds, Ni species could exist in three states, namely i) loosely attached to Zn (400 °C), ii) strongly attached to ZnO (550 °C) and iii) doped into the ZnO lattice (~ 650 °C).[41]

For our catalysts, the peak at 400 °C and 550 °C could be attributed to Ni weakly interacting to Zn as well as Ni strongly attached to Zn, respectively. Since crystallite NiO was absent from the bimetallic oxides (Figure S3.1), the reduction peaks could not be associated with the reduction of NiO on the samples. As the wt% of Zn increases, the reducibility of the catalyst is decreased, suggesting the formation of the Ni-Zn alloy that reduces at a higher temperature.

When the ratio of Zn to Ni is equal to one and above, a single peak is observed in the TPR profiles with the disappearance of the shoulder peak. The peak can be found at 570 °C, 590 °C and 600 °C for the 6.5Ni-6.5Zn/SiO_2, 4Ni-9Zn/SiO_2 and 2Ni-11Zn/SiO_2 catalysts, respectively. The high temperature peaks could be assigned to Ni-based metal alloys formed with another metal. The appearance of a one-step reduction peak for the bimetallic catalysts, could indicate the formation of bimetallic alloy during the reduction process. As shown in XRD analysis, the appearance of the NiZn phase is present for the 6.5Ni-6.5Zn/SiO_2, 4Ni-9Zn/SiO_2 and 2Ni-11Zn/SiO_2 catalysts, which correlates with the result obtained from TPR, suggesting the formation of a NiZn alloy. In the 6.5Ni-6.5Zn/SiO_2 catalyst, Ni and Zn may exist in a similar homogeneous oxide structure which could lead to the single step reduction with the broad peak.[42–44] It was noted that the TPR peaks become smaller as the Ni content decreases and it is possible that this is due to the reduction of Ni in the NiZn bimetallic phase. From XRD analysis it was observed that although the 6.5Ni-6.5Zn/SiO_2 catalyst contained the NiZn alloy, some Ni metal was still present. With a decrease in Ni, only the NiZn phase is present, which correlates with the high temperature peaks (close to 600 °C) in the TPR profile.

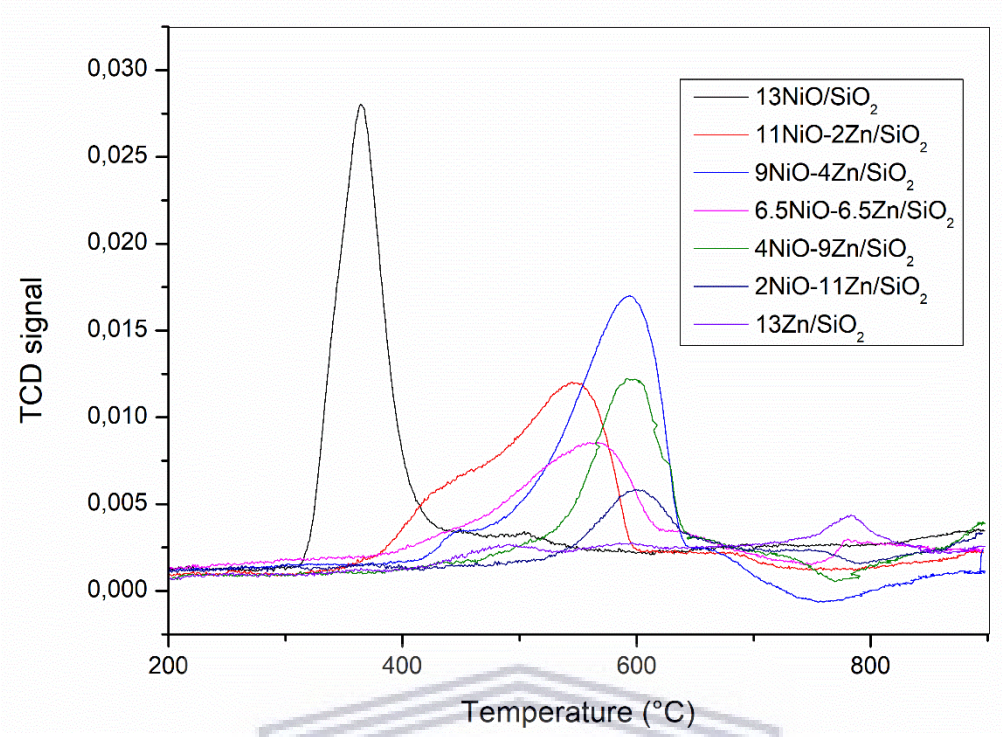

Figure 5.3. TPR profile of monometallic and bimetallic oxide catalysts

5.3.3 Morphology

Transmission electron microscopy (TEM) analysis was used to investigate the particle morphology and size distribution of the catalysts. **Figure 5.4** displays the TEM images of the monometallic and bimetallic catalysts. The 13Ni/SiO_2 catalyst (**Figure 5.4.a**) and 11Ni-2Zn/SiO_2 (**Figure 5.4.b**) catalyst both consist of large, clustered particles. **Figure 5.4.c** shows that 9Ni-4Zn/SiO_2 consists of smaller spherical particles that form agglomerates. It is evident that when the ratio of Ni:Zn is 1:1 as in the case of 6.5Ni-6.5Zn/SiO_2 (**Figure 5.4.d**), the agglomerates begin to break up into smaller particles compared to 9Ni-4Zn/SiO_2 catalyst. As the Zn content increases a reduction in particle size is clearly observed and therefore it can be said that Zn acts as a structural promoter reducing particle size and increasing dispersion.

The metal particles begin segregating further for the 4Ni-9Zn/SiO_2 (**Figure 5.4.e**) and 2Ni-11Zn/SiO_2 (**Figure 5.4.f**) catalysts, indicating smaller particles and better dispersion on the catalysts. It is suggested that the particles on 4Ni-9Zn/SiO_2 and 2Ni-11Zn/SiO_2 which are smaller than those observed on the 6.5Ni-6.5Zn/SiO_2 have a lesser effect on the surface area resulting in a higher surface area when compared to 6.5Ni-6.5Zn/SiO_2 as shown in Table 5.1. This result is further supported by XRD analysis indicating smaller crystallite sizes for 6.5Ni-6.5Zn/SiO_2, 4Ni-9Zn/SiO_2 and 2Ni-11Zn/SiO_2 catalysts.

Compared to the 13Ni/SiO_2 monometallic catalyst, the 13Zn/SiO_2 catalyst consists of small, well dispersed ZnO particles (**Figure 5.4.g**) From XRD analysis it was noted that the ZnO phase was challenging to identify, which could be due to the small particle size observed from TEM analysis.

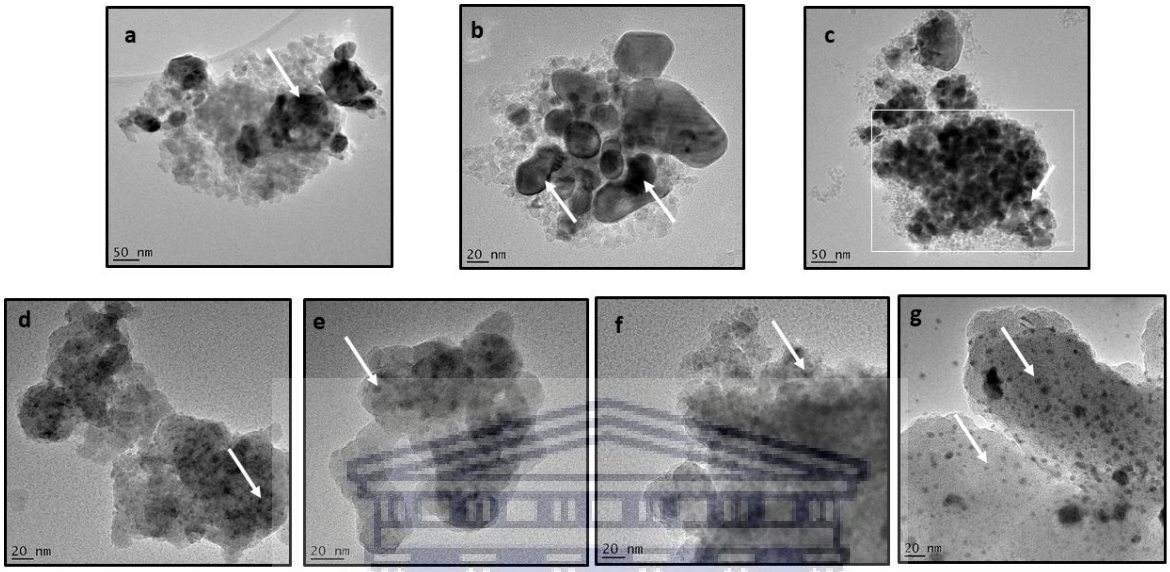

Figure 5.4. TEM images of a) 13Ni/SiO_2 b) 11Ni-2Zn/SiO_2 c) 9Ni-4Zn/SiO_2 d) 6.5Ni-6.5Zn/SiO_2 e) 4Ni-9Zn/SiO_2 f) 2Ni-11Zn/SiO_2 and g) 13Zn/SiO_2 catalysts

The particle size distribution of the catalysts is shown in **Figure 5.5**. The average particle size of the catalysts decreased in the following order 13Ni/SiO_2 (27 nm) > 11Ni-2Zn/SiO_2 (21 nm) > 9Ni-4Zn/SiO_2 (15 nm) > 6.5Ni-6.5Zn/SiO_2 (5.9 nm) > 4Ni-9Zn/SiO_2 (6.2nm) > 2Ni-11Zn/SiO_2 5.7nm) > 13Zn/SiO_2 (4.3 nm). The particle size of the nickel bimetallic catalysts was smaller than the monometallic 13Ni/SiO_2 catalyst.

This result is consistent with XRD analysis and supported with the literature, involving Ni-based bimetallic catalysts.[45] The monometallic 13Zn/SiO_2 catalyst showed a significant difference in particle size compared to 13Ni/SiO_2 catalyst as observed from the particle size distribution. The particle size of ZnO on SiO_2 have been reported in the range 2 nm – 4 nm, which is in close agreement with our values.[46] TEM analysis confirmed the improved dispersion of the metal species with the introduction of the second metal.

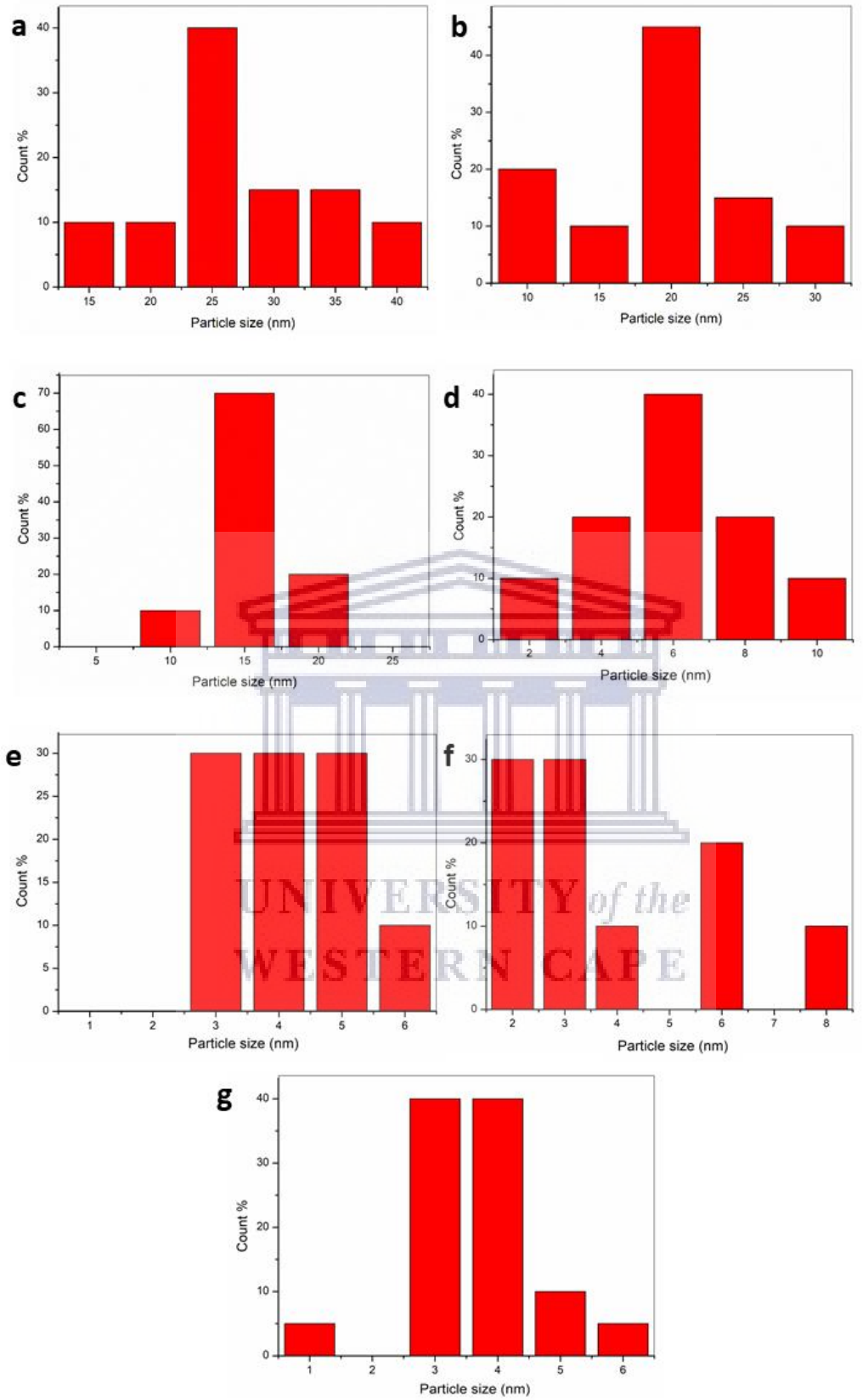

Figure 5.5. Particle size distribution of a) 13Ni/SiO_2 b) 11Ni-2Zn/SiO_2 c) 9Ni-4Zn/SiO_2 d) 6.5Ni-6.5Zn/SiO_2 e) 4Ni-9Zn/SiO_2, f) 2Ni-11Zn/SiO_2 and g) 13Zn/SiO_2

5.3.4 Catalytic Performance of bimetallic catalysts

The monometallic and bimetallic catalysts were evaluated for the dehydrogenation of propane. **Figure 5.6** shows the conversion % of propane for the monometallic and bimetallic catalysts on the SiO_2 support. The monometallic 13Ni/SiO_2 catalyst had a 100 % conversion of the propane feed, however, the selectivity was 100% toward methane (**Figure 5.7**). This could be a result of the rapid hydrogenolysis reactions, generating methane and coke, since the breakage of C-C bonds occurs preferentially over nickel catalysts. The conversion dropped dramatically to 0% after an hour as the catalyst was completely coked. Studies from the literature support the observation that large aggregated nickel ensembles, which is the active sites for hydrogenolysis, could lead to increased cracking reactions and coking of the catalyst, which is the main reason for catalyst deactivation.[10,12,47,48]

On the other hand, the monometallic 13Zn/SiO_2 displayed a 13% propane conversion and improved selectivity toward propylene. The XRD analysis of the monometallic 13Zn/SiO_2 catalyst showed the presence of ZnO on the catalyst, indicating the partial reduction of the catalyst, however, literature has shown that ZnO supported on SiO_2 is active for the dehydrogenation of propane, as in the case of our study.[40]

Analysis of the bimetallic catalytic results showed that at 3 minutes of reaction time, the 11Ni-2Zn/SiO_2 catalyst had a 100% conversion of propane with nearly 100 % selectivity toward methane. This was maintained for the complete time on stream and is an improvement when compared to the monometallic Ni catalyst. From this study, it is suggested that the ratio of Zn to Ni on the 11Ni-2Zn/SiO_2 catalyst is insufficient to promote desirable dehydrogenation results for the bimetallic catalyst and to significantly reduce hydrogenolysis reactions. However, 2 wt% Zn did have some effect in reducing coking as methane is obtained throughout the reaction. Therefore, although the catalyst was not active for dehydrogenation, the addition of Zn to 11Ni-2Zn/SiO_2 improved the catalyst stability and hindered coke formation. A further increase of Zn to 4 wt% resulted in a remarkable drop in conversion to ~40%. The product distribution also changed significantly as products besides methane were detected such as C2 olefins and C2 paraffins as well as C3 olefins. This indicates that additional reactions, such as cracking and dehydrogenation had occurred.

The selectivity of chemical reactions taking place on a solid catalyst is often controlled by "ensemble" effects where ensemble refers to a group of active sites responsible for a particular reaction.[49] Reactions such as hydrogenolysis require a large amount of active sites and occur on large ensembles of free Ni sites. The reaction may be suppressed by poisoning or removing a fraction of these sites. In this case, addition of Zn to Ni to form a bimetallic catalyst causes the Ni ensemble size to decrease thereby removing active sites as observed by the decrease in particle size as well as Zn blocking active sites at which hydrogenolysis occurs. Thus, selectivity to hydrogenolysis decreases while allowing reactions such as dehydrogenation that require smaller ensembles to increase. Therefore, Zn may be said to induce geometric effects similar to the addition of Sn in Pt/Sn dehydrogenation catalysts.

The addition of 4 wt% loading of Zn is the lowest content at which dehydrogenation of propane is promoted. The effect of Zn loading on the conversion % of propane showed that increasing the ratio of Zn on Ni:Zn to > 4wt% improved the initial conversion at 3 minutes, which could be due to the decrease in particle size and increase in dispersion of the bimetallic catalysts with the increased addition of Zn as observed from TEM analysis. The conversion of propane was observed for the following catalysts: 9Ni-4Zn/SiO_2 (39%) < 2Ni-11Zn/SiO_2 (40%) < 6.5Ni-6.5Zn/SiO_2 (44%) < 4Ni-9Zn/SiO_2 (47%). The catalysts generally showed the same stability that did not vary much with increasing Zn loading although the 4Ni-9Zn/SiO_2 which had the highest initial conversion also showed the most deactivation i.e. from conversion of 47% to 10%.

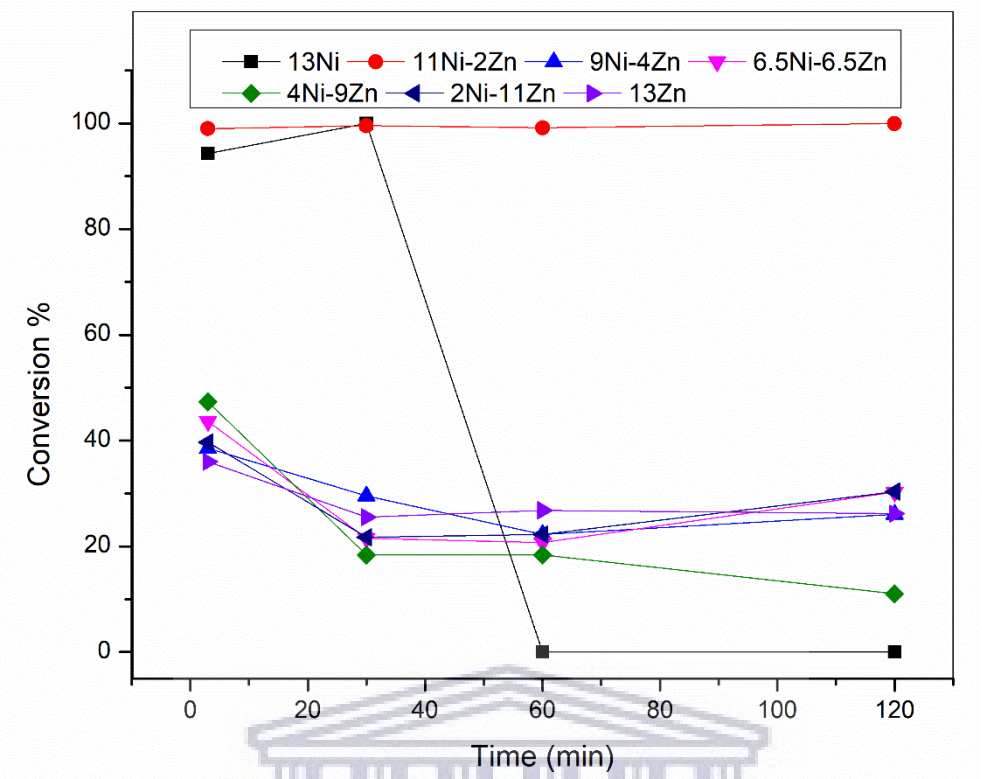

Figure 5.6. Conversion % of monometallic (13Ni/SiO_2 and 13Zn/SiO_2) and bimetallic catalysts supported on SiO_2

The selectivity toward the various products is depicted in **Figure 5.7**. The selectivity results show that the 11Ni-2Zn/SiO_2 catalyst had a 99 % selectivity toward methane. When the ratio of Zn to Ni increased, the dehydrogenation activity increased significantly for the 9Ni-4Zn/SiO_2, 6.5Ni-6.5Zn/SiO_2, 4Ni-9Zn/SiO_2 and 2Ni-11Zn/SiO_2 catalysts starting at the first 3 minutes of reaction time. The selectivity toward propene increased in the following order at 3 minutes 11Ni-2Zn/SiO_2 (0.8%) < 9Ni-4Zn/SiO_2 (8%) < 6.5Ni-6.5Zn/SiO_2 (49%) < 4Ni-9Zn/SiO_2 (59%) < 2Ni-11Zn/SiO_2 (63%). The beneficial effects of the Ni:Zn ratio and addition of Zn became evident for the 9Ni-4Zn/SiO_2 catalyst, compared to 11Ni-2Zn/SiO_2 at 3 minutes. Although the selectivity toward propene increased further for 6.5Ni-6.5Zn/SiO_2, 4Ni-9Zn/SiO_2 and 2Ni-11Zn/SiO_2, the values were similar. At the end of the 2 hour reaction, the 6.5Ni-6.5Zn/SiO_2 catalyst had the highest selectivity toward propylene (60%) followed by 2Ni-11Zn/SiO_2 (58%) and 4Ni-9Zn/SiO_2 (56%).

Since the XRD analysis show that these three catalysts contain the NiZn alloy and TEM analysis showed improved dispersion and smaller particle size, this could imply that perhaps the NiZn alloy is responsible for the enhanced selectivity and dehydrogenation activity. In the case of a NiZn alloy, it is well established experimentally and theoretically that there is a transfer of electrons from Zn to Ni leading to increased electron density on the Ni metal.[50] The significant reduction in cracking reactions is observed on the 9Ni-4Zn/SiO_2 catalyst, highlighting the effect of Zn addition on the nickel catalyst. This increase in electron density on the Ni metal, due to the addition of Zn, could lead to more repulsive interactions with the olefins and facilitate the desorption of olefins, thereby allowing the increase in dehydrogenation activity that was observed. This is similar to the effect of sulfur addition on nickel catalysts.[6]

Increasing the content of Zn, up to and more than the Ni:Zn ratio of 1:1, lead to the formation of the NiZn alloy. The formation of the alloy is more desirable as it is likely that there is a better interaction between Ni and Zn, which may result in enhanced transfer of electron density that facilitates desorption of alkenes and ultimately better dehydrogenation activity. Anaam and co-workers studied NiZn for the selective dehydrogenation of methylcyclohexane to toluene.[8,26] It was reported that the addition of Zn on a Ni catalyst improved the selectivity of methylcyclohexane to toluene by preferentially occupying low coordination sites on the Ni surface which facilitates C-H cleavage rather than C-C cleavage.[8,26,53] Therefore it is possible that Zn in addition to ensemble or geometric effects may also act as an electronic promoter.

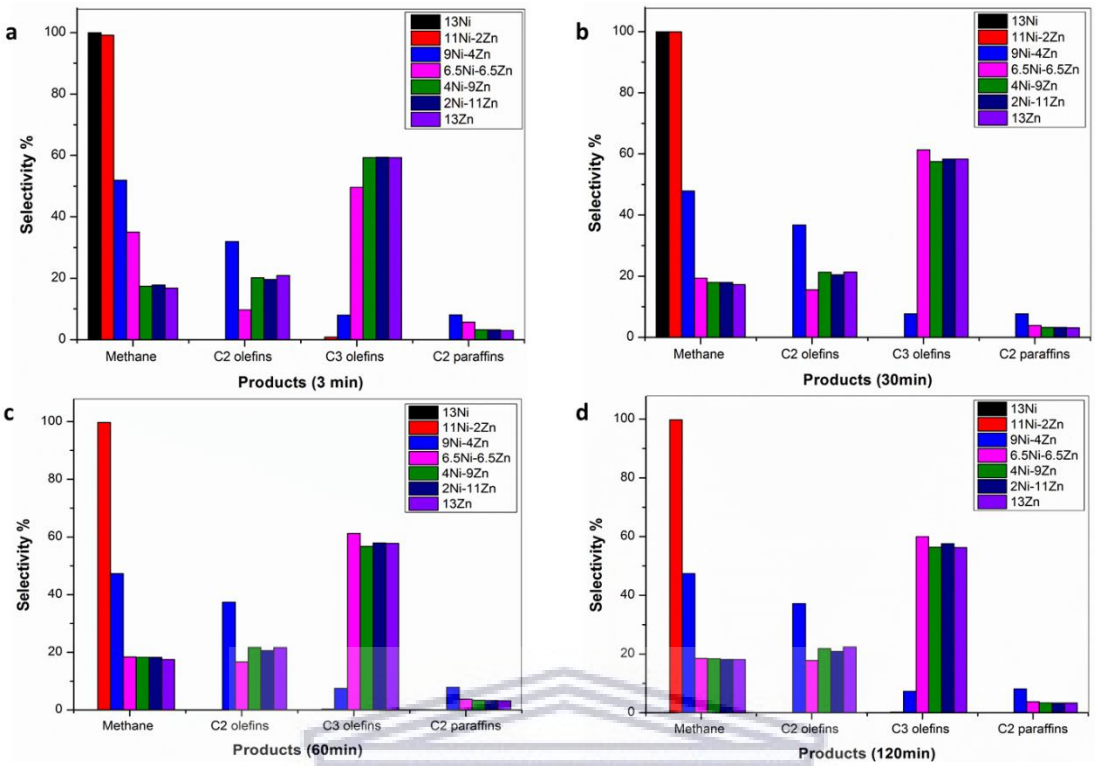

Figure 5.7. Selectivity % of monometallic (13Ni/SiO_2 and 13Zn/SiO_2) and bimetallic catalysts supported on SiO_2 toward the various products at a) 3 min, b) 30 min, c) 60 min and d) 120 min

5.4 Sulfided Bimetallic Catalysts

5.4.1 Preparation of sulfided bimetallic catalysts

The 9Ni-4Zn/SiO_2 and 6.5Ni-6.5Zn/SiO_2 catalysts were sulfided with DMSO to investigate whether the introduction of sulfur would influence the catalytic properties of the bimetallic catalysts with different structural compositions, i.e. 9Ni-4Zn/SiO_2 containing substituted Zn atoms in Ni framework and 6.5Ni-6.5Zn/SiO_2 containing the NiZn alloy. The method of sulfidation was performed as discussed in Chapter 5 (section 5.2.2). The resulting ratio of Ni:Zn:S can be found in Table S3.2 of the supplementary material. The catalysts were loaded into the reactor, sulfided with the calculated amount of sulfiding agent (DMSO) under a flow of nitrogen (50 ml/min) at 550 °C for 3 hours.

5.4.2 Structural and textural properties of sulfided bimetallic catalysts

The XRD analysis of the sulfided bimetallic catalysts, 9Ni-4Zn/SiO_2-S and 6.5Ni-6.5Zn/SiO_2-S is shown in **Figure 5.8**. The observed diffraction peaks in the 2θ region of 28.8°, 48.3° and 57° are attributed to the crystalline planes of the ZnS phase.[54] The peaks at 44° and 52° correspond to Ni in both catalysts. Depending on the nature of the metal-sulfur or metal-metal interactions, various phenomena can occur when sulfur reacts with a bimetallic surface. For example, the formation of a bimetallic sulfide with chemical properties different to the pure metal, or one of the metals increases or promotes the reactivity of the other metal toward sulfur. In other systems the interaction between sulfur and one metal may be repulsive leading to weakening of metal-metal bonds and lastly alloy formation leads to lower affinity for sulfur of both metals.[55]

In our system, we notice that after sulfidation the appearance of the ZnS phase for both 9Ni-4Zn/SiO_2-S and 6.5Ni-6.5Zn/SiO_2-S catalysts, however, no Ni-S phase is observed only metallic Ni. It could be that Zn has a higher affinity for sulfur and therefore the formation of ZnS is preferred over the NiS species. It has been reported in the literature that ZnO has a higher affinity for sulfur species compared to Ni, for samples containing Ni, Zn and sulfur species.[56]

The relative stabilities of the admetal (Zn) can have a direct impact on whether the Ni sulfide is formed.[55] Interestingly, in the 6.5Ni-6.5Zn/SiO_2-S catalyst the peaks corresponding to the NiZn alloy in the XRD pattern have disappeared. This may indicate that in this NiZn bimetallic system there is a repulsive interaction between sulfur and Ni. This led to the loss of the NiZn alloy as the bonds between the metals weaken causing metal segregation. Similar effects were reported for a ZnPt bimetallic system.[57] It was reported that although there is a net charge transfer toward platinum in Zn-Pt bonds which should facilitate sulfidation of Pt the conditions for noticing a promotional effect of the admetal (Zn) on platinum sulfides was insufficient.[55] Thus, similar effects may be occurring when using Zn in this system in that the Ni-S phase does not form. Since sulfur has a high propensity to interact with Zn, a further possibility could be that Zn is being extracted from the alloy by sulfur. Evidence of this is given by the formation of ZnS, as seen from XRD analysis.

The crystallite size of Ni and ZnS were calculated using the Scherrer equation for the peak at 2θ 44° and 47°, respectively. The crystallite size of Ni decreased from 15 nm to 11 nm with the introduction of sulfur, as observed for the 9Ni-4Zn/ SiO_2-S catalyst. The crystallite size of Ni on 6.5Ni-6.5Zn/SiO_2-S (14 nm) remained the same upon sulfidation when compared to the unsulfided catalyst (13 nm). The crystallite size of ZnS equalled 18 nm and 17 nm for 9Ni-4Zn/ SiO_2-S and 6.5Ni-6.5Zn/SiO_2-S, respectively.

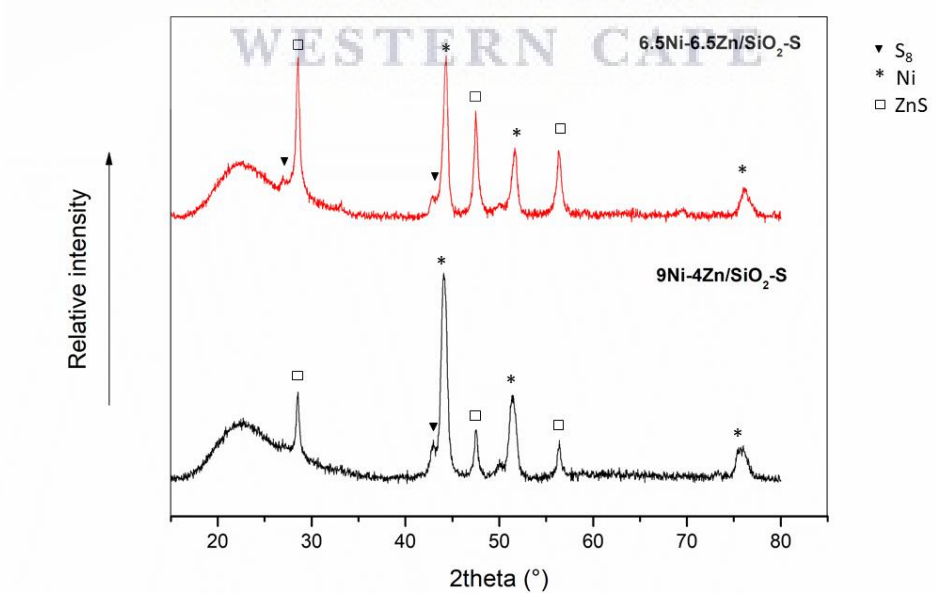

Figure 5.8. XRD pattern of sulfided bimetallic catalysts

The BET isotherms of the sulfided bimetallic catalysts are shown in **Figure 5.9**. The sulfided samples display type IV isotherms and type H_1 hysteresis loops, indicative of mesopores present in the catalysts.[32,33] Table 5.2 is a summary of the BET surface area and the crystallite size of the Ni species in the bimetallic catalysts. The 9Ni-4Zn/SiO_2-S (237 m^2/g) catalyst showed no change in the surface area compared to the unmodified catalyst 9Ni-4Zn/SiO_2 (240 m^2/g). The surface area of 6.5Ni-6.5Zn/SiO_2 increased from 200 m^2/g to 227 m^2/g for the sulfided bimetallic 6.5Ni-6.5Zn/SiO_2-S catalyst.

The introduction of sulfur to the bimetallic catalysts resulted in the appearance of a new ZnS phase as indicated by XRD analysis. The notable decrease in crystallite size of the nickel species on 9Ni-4Zn/SiO_2-S and the increase in surface area on 6.5Ni-6.5Zn/ SiO_2-S could be due to the geometric effect of both zinc and sulfur.

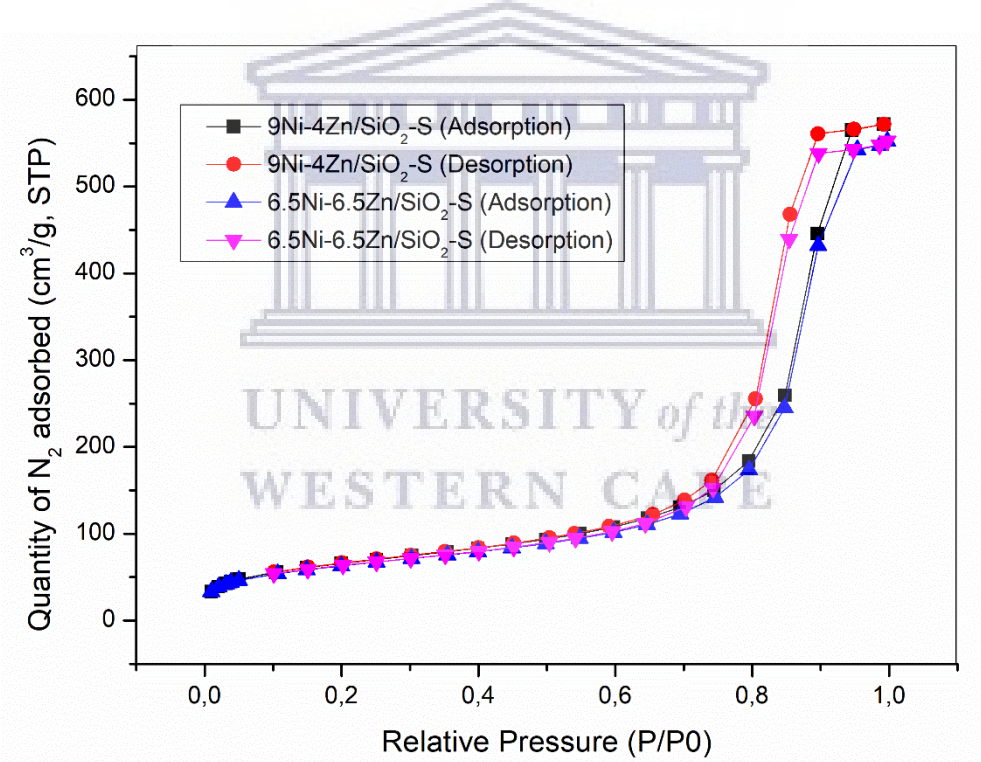

Figure 5.9. N_2 adsorption-desorption isotherms of sulfided bimetallic catalysts

Table 5.2: Surface area and crystallite size of sulfided bimetallic catalysts

Sample	S_{BET} (m^2/g)	Crystallite size Ni (nm)	Crystallite size ZnS (nm)
9Ni-4Zn/ SiO_2-S	237	11	18
6.5Ni-6.5Zn/ SiO_2-S	227	14	17

5.4.3 Morphology of sulfided bimetallic catalysts

TEM analysis was used to investigate the particle dispersion and size distribution of the sulfur modified bimetallic catalysts. Compared to the unmodified sulfur bimetallic catalysts, the 9Ni-4Zn/SiO_2-S and 6.5Ni-6.5Zn/SiO_2-S catalysts consisted of clustered particles (**Figure 5.10**). The particle size distribution of the sulfided bimetallic catalysts is shown in Figure 5.11. The average particle size for 9Ni-4Zn/SiO_2-S and 6.5Ni-6.5Zn/SiO_2-S catalysts were 13 nm and 14 nm, respectively. From TEM analysis, it was observed that the particles on the sulfided bimetallic catalysts, especially 6.5Ni-6.5Zn/SiO_2-S are more clustered.

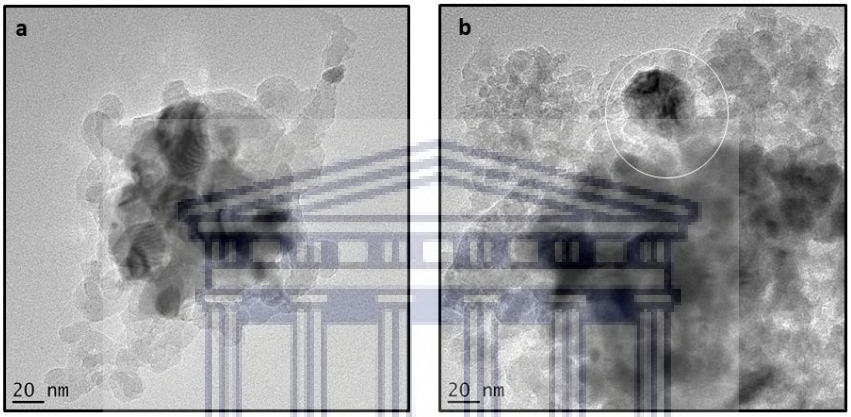

Figure 5.10. TEM images of a) 9Ni-4Zn/SiO_2-S and b) 6.5Ni-6.5Zn/SiO_2-S catalysts

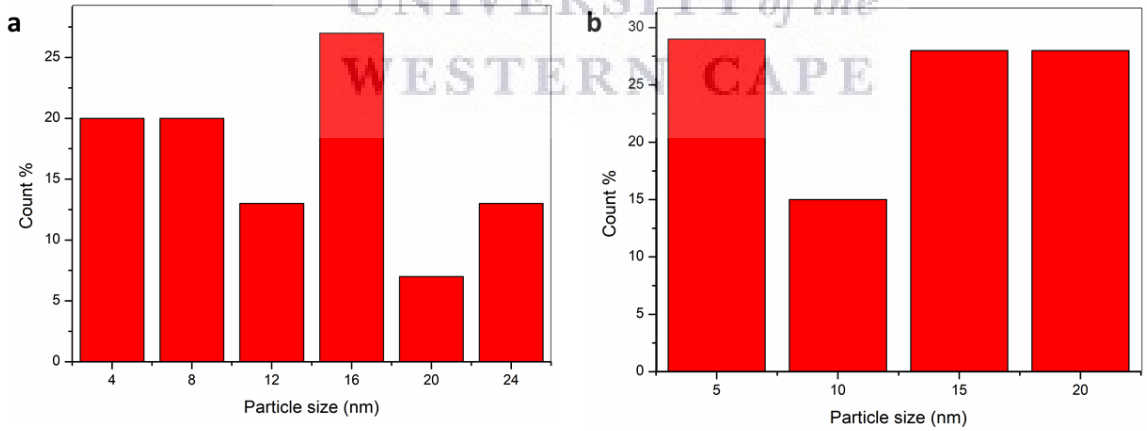

Figure 5.11. Particle size distribution of a) 9Ni-4Zn/SiO_2-S and b) 6.5Ni-6.5Zn/SiO_2-S catalysts

The dispersion of Ni and ZnS over the SiO_2 support can be seen through electron mapping images shown in **Figure 5.12** below. Visual evidence of sulfur interacting with zinc is evident for both 9Ni-4Zn/SiO_2-S (**Figure 5.12.a**) and 6.5Ni-6.5Zn/SiO_2-S (**Figure 5.12.b**) catalysts. Electron mapping imaging confirms the strong interaction between Zn and S and less

interaction between Ni-Zn when the bimetallic catalyst is sulfided. Clusters of ZnS were observed for the sulfided bimetallic catalysts, which could be the reason for the negligible change in surface area of the catalysts.

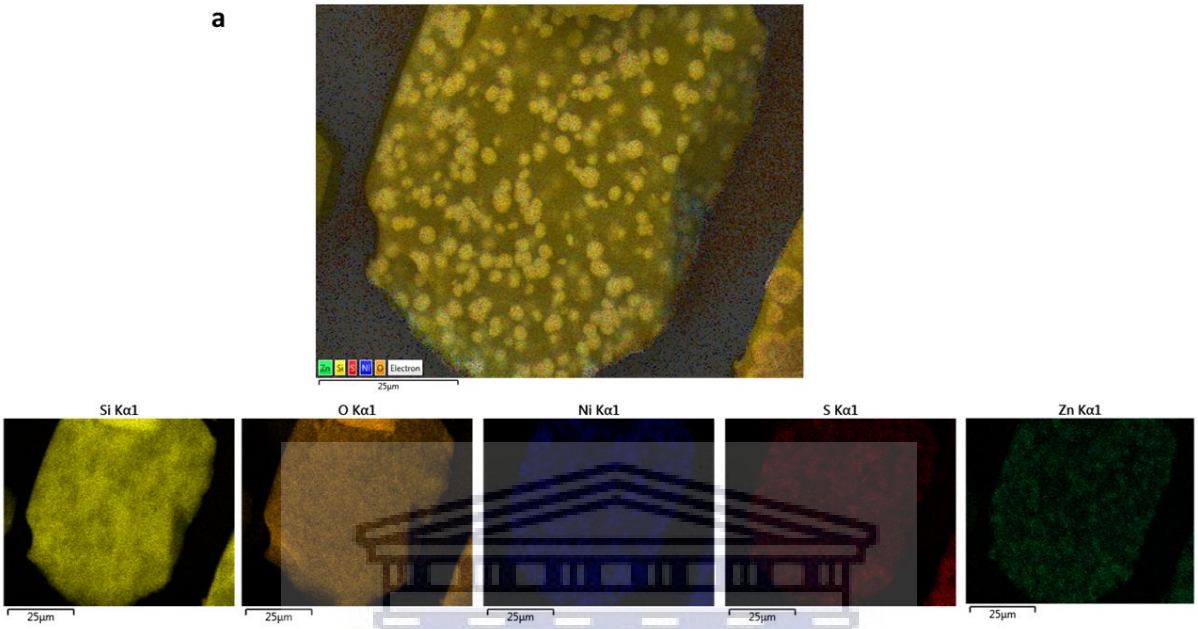

Figure 5.12. a) X-ray mapping of 9Ni-4Zn/SiO_2-S catalyst

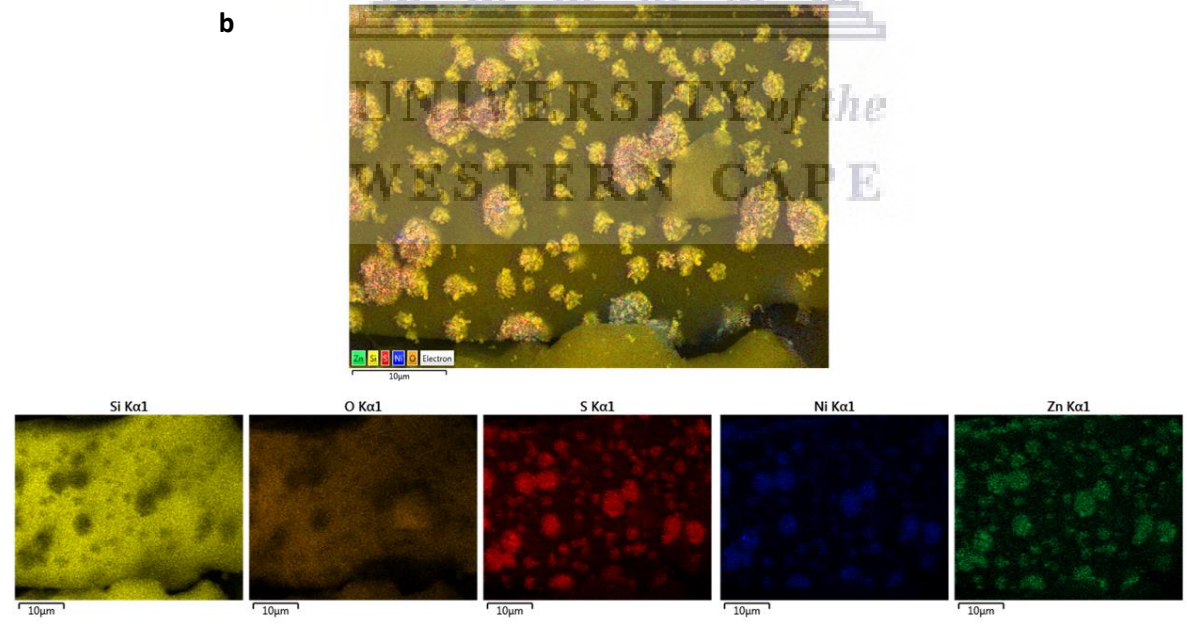

Figure 5.12. b) X-ray mapping of 6.5Ni-6.5Zn/SiO_2-S catalyst

5.4.4 Catalytic evaluation of sulfided bimetallic catalysts

The sulfided bimetallic catalysts were then evaluated for the dehydrogenation of propane. **Figure 5.13.a** shows the conversion % of propane for the sulfided bimetallic catalysts. A similar trend was observed for both 9Ni-4Zn/SiO_2-S and 6.5Ni-6.5Zn/SiO_2-S catalysts in that there was a decrease in the conversion of propane compared to the unsulfided catalysts. This could be due to dehydrogenation occurring on ZnS sites, whereas dehydrogenation occurred on NiZn in the unsulfided catalysts i.e there may be a difference in reactivity of the sulfided and unsulfided Ni-Zn catalysts. The dehydrogenation activity of ZnS has been reported in previous studies.[58,59] The conversion was 20% and 30% for 9Ni-4Zn/SiO_2-S and 6.5Ni-6.5Zn/SiO_2-S, while the unsulfided 9Ni-4Zn/SiO_2 and 6.5Ni-6.5Zn/SiO_2 catalysts had a conversion of 39% and 44%, respectively, at 3 minutes of reaction time.

The conversion of propane decreases slightly with time on stream by approximately 10% from the start of the reaction. The reason for the decline in propane conversion could be due to the loss of sulfur from the catalyst.[60] The EDS plot of the fresh and spent catalysts is shown in **Figure 5.13.b**. The %S decreased from 4.7% to 2.0% for 9Ni-4Zn/SiO_2-S and 5.2% to 2.3% for 6.5Ni-6.5Zn/SiO_2-S at the end of the 2 hour reaction time.

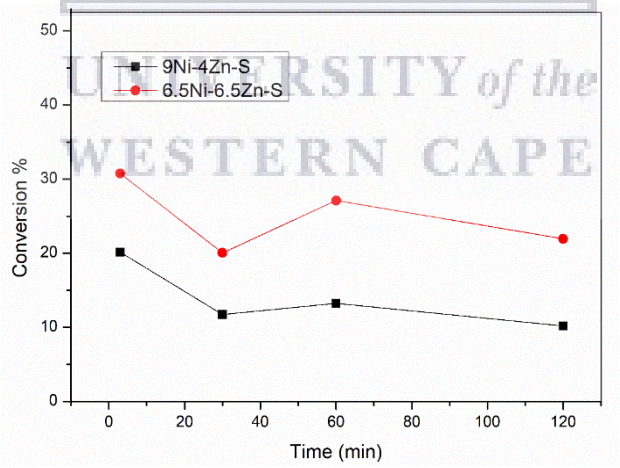

Figure 5.13. a) Conversion % of propane for 9Ni-4Zn/SiO_2-S and 6.5Ni-6.5Zn/SiO_2-S catalysts

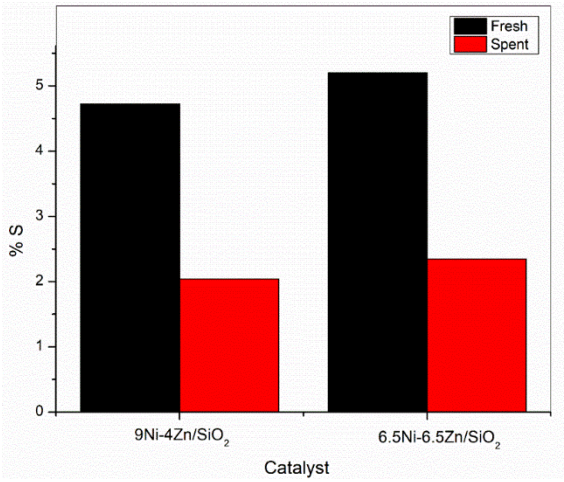

Figure 5.13. b) EDS results of fresh and spent 9Ni-4Zn/SiO_2-S and 6.5Ni-6.5Zn/SiO_2-S catalysts

The selectivity of the sulfided bimetallic catalysts toward the various products for 120 minutes on stream is shown in **Figure 5.14** below. The 9Ni-4Zn/SiO_2-S and 6.5Ni-6.5Zn/SiO_2-S catalysts both displayed high selectivity toward propene of about 67% and 60% at the end of 2 hours on stream, respectively. Interestingly, the selectivity to propene of 6.5Ni-6.5Zn/SiO_2-S was similar to the unsulfided 6.5Ni-6.5Zn/SiO_2 catalyst, showing no significant change. The activity, in terms of conversion %, of the unsulfided catalysts is slightly higher (~15%) than the sulfided catalysts, however, the selectivity remains unchanged. The improved activity may possibly be due to better reactivity of NiZn compared to ZnS.

The selectivity toward propylene for 9Ni-4Zn/SiO_2-S increased significantly compared to the unsulfided 9Ni-4Zn/SiO_2 catalyst. For example, at 3 minutes, the unsulfided 9Ni-4Zn/SiO_2 catalyst had a selectivity of 8%, while 9Ni-4Zn/SiO_2-S had a selectivity of 66 % toward propene. Methane, C2 paraffins and C2 olefins were additional products that were formed. The selectivity toward methane and that of the C2 products, suggests that cracking and hydrogenolysis secondary reactions were not completely reduced as a result of sulfur addition, although, the selectivity toward propylene increased significantly in the case of the 9Ni-4Zn/SiO_2-S catalyst. The selectivity of methane decreased from ~50% for the 9Ni-4Zn/SiO_2 catalyst to ~17% for the 9Ni-4Zn/SiO_2-S catalyst, throughout the dehydrogenation reaction.

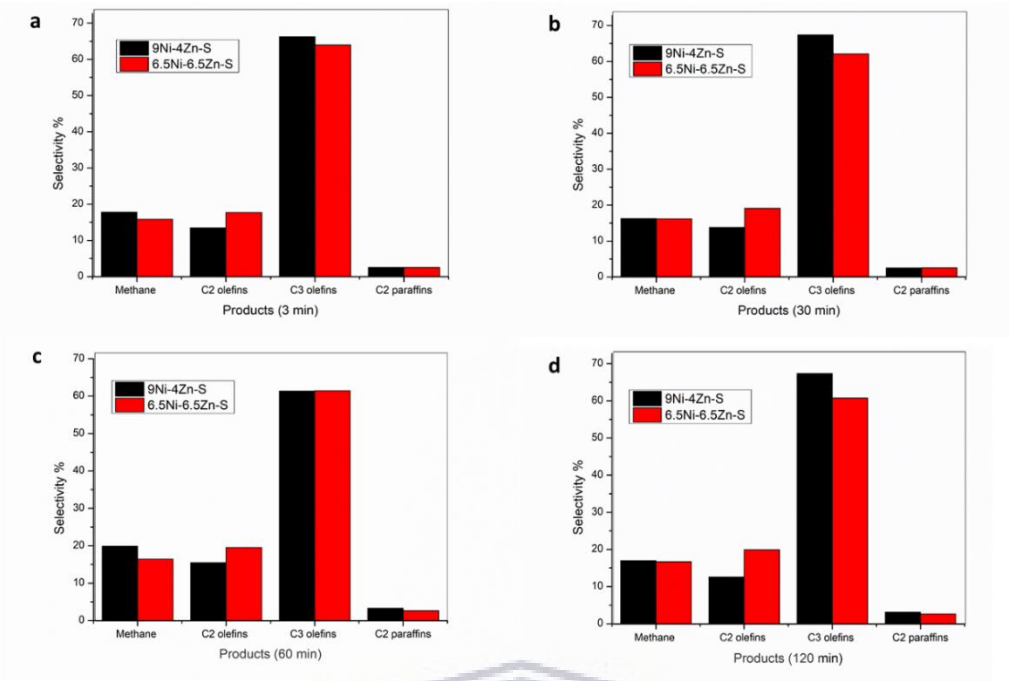

Figure 5.14. Selectivity % of sulfur modified bimetallic 9Ni-4Zn/SiO_2-S and 6.5Ni-6.5Zn/SiO_2-S catalysts at a) 3 min, b) 30 min, c)60 min and d) 120 min

The improved catalytic performance of the sulfided bimetallic catalysts is only observed for the 9Ni-4Zn/SiO_2-S catalyst whereas the 6.5Ni-6.5Zn/SiO_2-S showed no or slightly less activity than the unsulfided catalyst. The improved selectivity in the 9Ni-4Zn/SiO_2-S catalyst could be due to the geometric effects of sulfur addition, which dilutes aggregated metal particles. As discussed in XRD analysis, TEM and electron imaging, the introduction of zinc and sulfur result in better dispersion of the metals on the catalysts due to the dissociation of metal agglomerates as seen in the unmodified catalyst.

Zinc is known to act as a spacer on Pt catalysts to reduce the size of Pt particles as the role of Sn, in Pt-Sn catalysts. Similary, sulfur has been reported to have geometric effects by diluting aggregated metallic species.[6,18] The amount of Zn in the 9Ni-4Zn/SiO_2-S may be too little to block all the active sites on Ni which lead to hydrogenolysis. The addition of sulfur to 9Ni-4Zn/SiO_2 then acts as an additional site blocker leading to reduction of hydrogenolysis and further improves the desorption of olefins and dehydrogenation activity. On the other hand, the addition of sulfur, which is seen to cause segregation of the Zn and Ni metals as observed by XRD analysis of the 6.5Ni-6.5Zn/SiO_2-S and the formation of ZnS, which is also known to have dehydrogenation activity may be the reason for the slightly reduced catalytic activity of the sulfided catalyst.

The sulfur which was added to block sites active for hydrogenolysis on the bimetallic catalyst may have weakened the bonds between Ni and Zn due to its higher affinity for Zn and therefore did not improve the selectivity of the bimetallic catalyst. Addition of sulfur has been found to adjust the electronic properties on Ni atoms, facilitating the olefins and increasing product selectivity.[6,19,21] However, in this case it is possible that sulfur had much less interaction with Ni. It has been reported that in bimetallic systems where the admetal (Zn) form sulfides of higher stability than those formed by platinum, the adsorption of sulfur stops once the admetal is saturated and no PtS_x is formed.[55] It is possible that a similar effect occurs in this sample.

5.5 Conclusion

Nickel-zinc bimetallic catalysts supported on SiO_2 were successfully synthesized using the wetness impregnation method of nickel and zinc salts. The ratio of Ni:Zn was synthesized according to 13:0, 11:2, 9:4, 6.5:6.5, 4:9, 2:11 and 0:13. XRD analysis showed that for 11Ni-2Zn/SiO_2 and 9Ni-4Zn/SiO_2 catalysts, Ni peaks were present. When the ratio of Zn increased to > 4 wt% the presence of the NiZn phase was observed. A decrease in surface area was observed for 6.5Ni-6.5Zn/SiO_2 catalyst, followed by a slight increase for 4Ni-9Zn/SiO_2, 2Ni-11Zn/SiO_2 and 13Zn/SiO_2 catalysts, indicating the effects of Zn addition on particle size change and textural properties of the catalysts. Reducibility of the bimetallic catalysts were investigated by performing TPR analysis. The high temperature peaks > 550 °C appeared for the 6.5Ni-6.5Zn/SiO_2, 4Ni-9Zn/SiO_2 and 2Ni-11Zn/SiO_2 catalysts, which corresponded to the reduction of a NiZn alloy, correlating with the results obtained from XRD analysis.

The particle size of the catalysts decreased in the following order: 13Ni/SiO_2 > 11Ni-2Zn/SiO_2 > 9Ni-4Zn/SiO_2 > 6.5Ni-6.5Zn/SiO_2 > 4Ni-9Zn/SiO_2 > 2Ni-11Zn/SiO_2 > 13Zn/SiO_2. Increasing the amount of zinc on the catalyst > 4 wt% Zn resulted in smaller particles with better dispersion on the catalyst, as seen from TEM analysis.

The dehydrogenation activity of the bimetallic catalysts was shown to increase with increasing loading of Zn. Although, hydrogenolysis was the primary reaction for the 11Ni-2Zn/SiO_2 catalyst, there was a significant reduction in the formation of coke with the addition of Zn which also improved the stability and hindered deactivation.

When the ratio of Ni:Zn equalled 9:4 (9Ni-4Zn/SiO_2), the promoting effect of Zn was more evident in that dehydrogenation activity increased and hydrogenolysis was suppressed. A wider product distribution was observed with increased selectivity to propene. This was attributed the 'ensemble' effect as Zn reduced the large Ni ensembles responsible for hydrogenolysis. As the wt% of Zn increased and the particle size decreased, the selectivity to propene was improved further. Thus, highlighting the promoting effect of Zn. The improved initial activity and selectivity toward propylene for 6.5Ni-6.5Zn/SiO_2, 4Ni-9Zn/SiO_2 and 2Ni-11Zn/SiO_2 was attributed to the formation of a NiZn alloy, whereby the particle size was decreased and active sites responsible for hydrogenolysis were blocked due to enhanced interaction between Ni and Zn.

Furthermore, the transfer of electrons from Zn to Ni, may have lead to increased desorption of olefins and selectivity toward propylene equal to 49%, 59% and 63%, respectively, compared to 0% for the 13Ni-/SiO_2 catalyst.

The effect of sulfur addition to the bimetallic catalysts was then investigated. The 9Ni-4Zn/SiO_2 and 6.5Ni-6.5Zn/SiO_2 catalysts were then sulfided using DMSO as the sulfiding agent to form the corresponding sulfided 9Ni-4Zn/SiO_2-S and 6.5Ni-6.5Zn/SiO_2-S catalysts. XRD analysis indicated the presence of ZnS and Ni on the catalysts, with the absence of the NiZn alloy. TEM analysis showed that the catalysts consisted of clustered particles. Visual evidence of the ZnS clusters and the strong interaction between Zn and S were provided by electron mapping. In the Ni-Zn bimetallic system it was shown that Zn had a higher affinity for sulfur and caused a repulsive interaction between nickel and sulfur instead of promoting sulfidation of Ni. Furthermore, the addition of sulfur caused metal-metal segregation as evidenced by loss of the NiZn alloy.

The conversion % of propane on 9Ni-4Zn/SiO_2-S and 6.5Ni-6.5Zn/SiO_2-S was lower than the unmodified catalysts, which could imply that ZnS has a lower dehydrogenation activity than the NiZn alloy. There was however a significant increase in the selectivity of 9Ni-4Zn/SiO_2-S to propene compared to the unsulfided catalyst possibly due to sulfur acting as an additional site blocker thereby reducing the effects of hydrogenolysis. The selectivity toward propylene increased from 8% (9Ni-4Zn/SiO_2) to 64% for the sulfided 9Ni-4Zn/SiO_2-S catalyst in the first three minutes of reaction time. There was no significant increase in selectivity % for 6.5Ni-6.5Zn/SiO_2-S compared to the unsulfided catalyst, which could point to ZnS and NiZn perhaps having similar dehydrogenation activity at that ratio of Ni:Zn and Zn:S equal to ~ 1. Both Zn and S exhibit beneficial geometric effects and electronic effects, which affect particle size and olefin desorption. From our study, we can confirm that the molar ratio of Ni:Zn and the addition of sulfur indeed influence the structural and catalytic properties of bimetallic catalysts. Although Zn was shown to induce geometric effects which improved the catalytic performance of the bimetallic catalysts, the results of this work also leads us to investigate finding metals that will promote the sulfidation without causing metal segregation to further enhance the dehydrogenation activity of a bimetallic system.

5.6 References

1 J. Llorca, N. Homs, J. León, J. Sales, J. L. G. Fierro and P. Ramirez De La Piscina, *Appl. Catal. A Gen.*, 1999, **189**, 77–86.
2 R. A. Buyanov and N. A. Pakhomov, *Kinet. Catal.*, 2001, **42**, 64–75.
3 D. A. Nazimov, O. V. Klimov, A. V. Saiko, S. N. Trukhan, T. S. Glazneva, I. P. Prosvirin, S. V. Cherepanova and A. S. Noskov, *Catal. Today*, 2020, 1–41.
4 R. Hu, X. Li, Z. Sui, G. Ye and X. Zhou, *Chem. Eng. Process. - Process Intensif.*, 2019, **143**, 107608.
5 J. Im and M. Choi, *ACS Catal.*, 2016, **6**, 2819–2826.
6 G. Wang, C. Gao, X. Zhu, Y. Sun, C. Li and H. Shan, *ChemCatChem*, 2014, **6**, 2305–2314.
7 G. Wang, H. Zhang, H. Wang, Q. Zhu, C. Li and H. Shan, *J. Catal.*, 2016, **344**, 606–608.
8 A. H. Al-Shaikhali, A. Jedidi, L. Cavallo and K. Takanabe, *Chem. Commun.*, 2015, **51**, 12931–12934.
9 D. E. Resasco, B. K. Marcus, C. S. Huang and V. A. Durante, *J. Catal.*, 1994, **146**, 40–55.
10 G. Wang, H. Wang, H. Zhang, Q. Zhu, C. Li and H. Shan, *ChemCatChem*, 2016, **8**, 3137–3145.
11 S. De, J. Zhang, R. Luque and N. Yan, *Energy Environ. Sci.*, 2016, **9**, 3314–3347.
12 R. B. Biniwale, N. Kariya and M. Ichikawa, *Catal. Letters*, 2005, **105**, 83–87.
13 Q. Zhu, H. Zhang, S. Zhang, G. Wang, X. Zhu and C. Li, *Ind. Eng. Chem. Res.*, 2019, **58**, 7834–7843.
14 O. A. Bariås, A. Holmen and E. A. Blekkan, *Catal. Today*, 1995, **24**, 361–364.
15 J. Silvestre-Albero, J. C. Serrano-Ruiz, A. Sepúlveda-Escribano and F. Rodríguez-Reinoso, *Appl. Catal. A Gen.*, 2005, **292**, 244–251.
16 B. M. Nagaraja, C. H. Shin and K. D. Jung, *Appl. Catal. A Gen.*, 2013, **467**, 211–223.
17 X. Liu, W. Z. Lang, L. L. Long, C. L. Hu, L. F. Chu, Y. J. Guo, P. P. Li, W. Z. Lang, K. Xia, L. Luan, X. Yan and Y. J. Guo, *Chem. Eng. J.*, 2014, **247**, 183–192.
18 Y. Zhang, Y. Zhou, L. Huang, S. Zhou, X. Sheng, Q. Wang and C. Zhang, *Chem. Eng. J.*, 2015, **270**, 352–361.
19 Y. Zhang, Y. Zhou, J. Shi, X. Sheng, Y. Duan, S. Zhou and Z. Zhang, *Fuel Process. Technol.*, 2012, **96**, 220–227.
20 C. Yu, H. Xu, Q. Ge and W. Li, *J. Mol. Catal. A Chem.*, 2007, **266**, 80–87.
21 V. J. Cybulskis, B. C. Bukowski, H. T. Tseng, J. R. Gallagher, Z. Wu, E. Wegener, A. J. Kropf, B. Ravel, F. H. Ribeiro, J. Greeley and J. T. Miller, *ACS Catal.*, 2017, **7**, 4173–4181.
22 L. Rochlitz, K. Searles, J. Alfke, D. Zemlyanov, O. V. Safonova and C. Copéret, *Chem. Sci.*, 2020, **11**, 1549–1555.
23 J. A. Rodriguez, *Surf. Sci. Rep.*, 1999, **24**, 223–287.
24 G. Wang, Z. Meng, J. Liu, C. Li and H. Shan, *ACS Catal.*, 2013, **3**, 2992–3001.
25 M. J. Dees and V. Ponec, *J. Catal.*, 1989, **115**, 347–355.
26 A. H. Al-Shaikhali, A. Jedidi, D. H. Anjum, L. Cavallo and K. Takanabe, *ACS Catal.*, 2017, **7**, 1592–1600.
27 S. Musić, N. Filipović-Vinceković and L. Sekovanić, *Brazilian J. Chem. Eng.*, 2011, **28**, 89–94.
28 N. K. Gamboa-Rosales, J. L. Ayastuy, M. P. González-Marcos and M. A. Gutiérrez-Ortiz, *Int. J. Hydrogen Energy*, 2012, **37**, 7005–7016.
29 X. Yang, G. Liu, Y. Li, L. Zhang, X. Wang and Y. Liu, *Trans. Tianjin Univ.*, 2019, **25**, 245–257.
30 Y. Zhang, Y. Yang, H. Han, M. Yang, L. Wang, Y. Zhang, Z. Jiang and C. Li, *Appl. Catal. B Environ.*, 2012, **119–120**, 13–19.
31 X. Meng, H. Weng and L. Shi, *China Pet. Process. Petrochemical Technol.*, 2012, **14**, 28–32.
32 P. P. Li, W. Z. Lang, K. Xia, L. Luan, X. Yan and Y. J. Guo, *Appl. Catal. A Gen.*, 2016, **522**, 172–179.
33 S. He, C. Sun, H. Du, X. Dai and B. Wang, *Chem. Eng. J.*, 2008, **141**, 284–289.

34 Q. Wang, M. Zhu, C. Xu, H. Zhang, X. Wang, B. Dai and J. Zhang, *New J. Chem.*, 2018, **42**, 6507–6514.
35 N. Seshu Babu, N. Lingaiah and P. S. Sai Prasad, *Appl. Catal. B Environ.*, 2012, **111–112**, 309–316.
36 C. Li, Y. W. Chen and C. P. Corporation, *Thermochim. Acta*, 1995, **256**, 457–465.
37 B. Mile, D. Stirling, M. A. Zammitt, A. Lovell and M. Webb, *J. Catal.*, 1988, **114**, 217–229.
38 M. A. Martin-Luengo, P. A. Sermon and Y. Wang, *J. Catal.*, 1992, **135**, 263–268.
39 Y. Wang, J. Zhang and H. Xu, *Chinese J. Catal.*, 2006, **27**, 217–222.
40 B.-Z. Wan and H. M. Chu, *J. Chem. Soc. Faraday Trans.*, 1992, **88**, 2943–2947.
41 W. Da Oh, J. Lei, A. Veksha, A. Giannis, W. P. Chan, G. Lisak and T. T. Lim, *Chem. Eng. J.*, 2018, **351**, 230–239.
42 Y. Wang, M. Chen, Z. Yang, T. Liang, S. Liu, Z. Zhou and X. Li, *Appl. Catal. A Gen.*, 2018, **550**, 214–227.
43 J. Zhang, H. Wang and A. K. Dalai, *Appl. Catal. A Gen.*, 2008, **339**, 121–129.
44 J. Zhang, H. Wang and A. K. Dalai, *J. Catal.*, 2007, **249**, 300–310.
45 J. Xu, W. Zhou, Z. Li, J. Wang and J. Ma, *Int. J. Hydrogen Energy*, 2009, **34**, 6646–6654.
46 S. Panigrahi, A. Bera and D. Basak, *ACS Appl. Mater. Interfaces*, 2009, **1**, 2408–2411.
47 X. Yan, Y. Liu, B. Zhao, Z. Wang, Y. Wang and C. J. Liu, *Int. J. Hydrogen Energy*, 2013, **38**, 2283–2291.
48 J. Guo, H. Lou and X. Zheng, *Carbon N. Y.*, 2007, **45**, 1314–1321.
49 J. H. Sinfelt, *Bimetallic Catal.*, 1983.
50 Y. Okamoto, Y. Nitta, T. Imanaka and S. Teranishi, *J. Catal.*, 1980, **64**, 397–404.
51 J. Hornung, M. Muhr, C. Gemel and R. A. Fischer, *Dalt. Trans.*, 2019, **48**, 11743–11748.
52 Y. Okamoto, K. Nagata, T. Adachi, T. Imanaka, K. Inamura and T. Takyu, *J. Phys. Chem.*, 1991, **95**, 310–319.
53 J. C. Rodríguez, A. J. Marchi, A. Borgna and A. Monzón, *J. Catal.*, 1997, **171**, 268–278.
54 A. A. Othman, M. A. Osman, M. A. Ali, W. S. Mohamed and E. M. M. Ibrahim, *J. Mater. Sci. Mater. Electron.*, 2020, **31**, 1752–1767.
55 J. A. Rodriguez, *Prog. Surf. Sci.*, 2006, **81**, 141–189.
56 I. Bezverkhyy, O. V. Safonova, P. Afanasiev and J. P. Bellat, *J. Phys. Chem. C*, 2009, **113**, 17064–17069.
57 M. Kuhn and J. A. Rodriguez, *Catal. Letters*, 1995, **32**, 345–355.
58 J. De Andrés, A. Aguilar and J. Domenech, *J. Macromol. Sci. Part A - Chem.*, 1990, **27**, 213–223.
59 O. V. Krylov and S. Z. Roginskii, *Bull. Acad. Sci. USSR Div. Chem. Sci.*, 1959, **8**, 15–21.
60 G. Wang, C. Li and H. Shan, *ACS Catal.*, 2014, **4**, 1139–1143.

CHAPTER 6: Conclusion

This chapter provides a summary of the results obtained for this research project and recommendations for future work. Sulfided nickel catalysts were synthesized, characterised and tested for the dehydrogenation of propane to propylene.

6.1 Summary

6.1.1 Chapter 3

The objective of this study was to investigate the effect of $MgAl_2O_4$ and SiO_2 support on sulfided metal catalysts for the dehydrogenation of propane. Nickel oxide catalysts supported on $MgAl_2O_4$ and SiO_2 were sulfated using ammonium sulfate to form $NiO/MgAl_2O_4$-20wt%SO_4 and NiO/SiO_2-20wt%SO_4, with both catalysts containing the $NiSO_4$ phase. The sulfated catalysts were reduced, in separate experiments, to form $Ni/MgAl_2O_4$-20wt%SO_4 and Ni/SiO_2-20wt%SO_4, which contained the Ni_3S_2 phase. Characterisation of the catalysts (TEM and XRD analysis) showed that nickel species supported on $MgAl_2O_4$ displayed smaller particles with a higher dispersion in comparison to the particles on the SiO_2 support. STEM analysis showed localised clusters of $NiSO_4$ and Ni_3S_2 on the SiO_2 support that were absent on the $MgAl_2O_4$ support.

The bonding of sulfur varies on the two supports, which has an effect on the acidic properties of the catalyst. Sulfate is bonded as a chelating bidentate ligand on $MgAl_2O_4$ and a bridging bidentate ligand on the SiO_2 support. The metal-support interaction were stronger on the $MgAl_2O_4$ support (TPR analysis) and peaks occurring at higher temperatures on $NiO/MgAl_2O_4$-20wt%SO_4 corresponded to the decomposition of sulfur, contributing to the improved stability of the catalyst, since sulfur loss from the catalyst is associated with the deactivation.

The results obtained from catalytic testing indicated that the catalyst supported on $MgAl_2O_4$ had a higher dehydrogenation activity and that this was attributed to the smaller particle size of the active nickel-sulfided species, a stronger metal-support interaction, which resulted in a high electronic effect and facilitates the desorption of the products leading to the selectivity of above 70% toward propylene.

6.1.2 Chapter 4

The objective of this study was to investigate effect of the sulfiding agent and sulfidation temperature on the morphology, textural properties and catalytic activity of the sulfided catalysts for the dehydrogenation of propane. Nickel catalysts supported on $MgAl_2O_4$ were successfully prepared using $(NH_4)_2SO_4$ (S1), $(NH_4)_2S$ (S2) and DMSO (S3). The catalysts were sulfided at 200 °C, 400 °C and 550 °C. The sulfiding agent and sulfidation temperature was found to influence the NiS_x phase formed on the catalyst. It was noted that the increase in sulfidation temperature resulted in an increase in crystallite size of the nickel-sulfided particles, which could be due to sintering that commonly occurs at higher temperatures.

The morphology of the catalysts were distinct with respect to sulfiding agent and sulfidation temperature. The S3 catalysts catalysts had the lowest sulfur content and best dispersion compared to S1 and S2 catalysts, for Ni/$MgAl_2O_4$-S3-200, Ni/$MgAl_2O_4$-S3-400 and Ni/$MgAl_2O_4$-S3-550 catalysts indicating the type of sulfiding agent and sulfiding conditions used may influence dispersion of NiS_x species.

By sulfiding catalysts at 200 °C, 400 °C and 550 °C, the findings show that the sulfiding agent (containing the different anions) and the sulfidation conditions (temperature) has an influence on the catalyst structural and textural properties in terms of decomposition and sulfur content which affect morphology, particle size, dispersion and Ni-S interaction.

Ni/$MgAl_2O_4$-S3-550 showed the strongest interaction of nickel and sulfur, visible by clusters of Ni_3S_2 on the catalyst surface. The sulfided catalysts were then tested for the dehydrogenation of propane. The Ni/$MgAl_2O_4$-S3-550 catalyst showed the highest conversion % of propane and selectivity % toward propylene, which was attributed to the high dispersion of metal sulfide species which lead to strong Ni-S interactions and ultimately higher activity, selectivity and enhanced stability. Thus, the catalyst sulfided with DMSO at 550 °C displayed the best catalytic results.

6.1.3 Chapter 5

In this study, the effect of the Ni-Zn ratio on the structural and catalytic properties of bimetallic catalysts was studied as well as whether the effect of sulfur addition on the bimetallic catalytic system could further enhance the dehydrogenation activity of propane. Nickel-zinc bimetallic catalysts supported on SiO_2 were successfully synthesized with the ratio of Ni:Zn as 13:0, 11:2, 9:4, 6.5:6.5, 4:9, 2:11 and 0:13. XRD analysis showed the presence of Ni for the 11Ni-2Zn/SiO_2 and 9Ni-4Zn/SiO_2 catalysts.

BET analysis indicated a decrease in surface area for 6.5Ni-6.5Zn/SiO_2 catalyst, followed by a slight increase for 4Ni-9Zn/SiO_2, 2Ni-11Zn/SiO_2 and 13Zn/SiO_2 catalysts. This implies that the effects of Zn addition on particle size change and textural properties of the catalysts. Reducibility of the bimetallic catalysts by TPR analysis displayed high temperature peaks (> 550 °C) for the 6.5Ni-6.5Zn/SiO_2, 4Ni-9Zn/SiO_2 and 2Ni-11Zn/SiO_2 catalysts, corresponding to the reduction of the NiZn alloy, which correlated with the results obtained from XRD analysis. When the ratio of Zn increased to > 4 wt% for the 6.5Ni-6.5Zn/SiO_2, 4Ni-9Zn/SiO_2 and 2Ni-11Zn/SiO_2 catalysts, the presence of the NiZn phase was observed. The dehydrogenation activity of the bimetallic catalysts was shown to increase with increasing loading of Zn.

When the ratio of Ni:Zn equalled 9:4 (9Ni-4Zn/SiO_2), the promoting effect of Zn was more evident, compared to the 11Ni-2Zn/SiO_2 catalyst, in that dehydrogenation activity increased and hydrogenolysis was suppressed. The improved initial activity and selectivity toward propylene for 6.5Ni-6.5Zn/SiO_2, 4Ni-9Zn/SiO_2 and 2Ni-11Zn/SiO_2 was attributed to the formation of a NiZn alloy, whereby the particle size was decreased and active sites responsible for hydrogenolysis were blocked due to enhanced interaction between Ni and Zn. Furthermore, the transfer of electrons from Zn to Ni, may have led to increased desorption of olefins and selectivity toward propylene equal to 49%, 59% and 63%, respectively, compared to 0% for the 13Ni-/SiO_2 catalyst.

The effect of sulfur addition to the bimetallic catalysts was then investigated. The 9Ni-4Zn/SiO_2 and 6.5Ni-6.5Zn/SiO_2 catalysts were sulfided using DMSO as the sulfiding agent to form the corresponding sulfided 9Ni-4Zn/SiO_2-S and 6.5Ni-6.5Zn/SiO_2-S catalysts. In the Zn-Ni bimetallic system it was shown that Zn had a higher affinity for sulfur and inhibited the formation of a Ni-S phase and resulted in the formation of a ZnS phase. Furthermore, the addition of sulfur caused metal-metal segregation as evidenced by loss of the NiZn alloy.

The conversion % of propane on 9Ni-4Zn/SiO_2-S and 6.5Ni-6.5Zn/SiO_2-S showed that ZnS had a lower dehydrogenation activity than the NiZn alloy. There was however a significant increase in the selectivity of 9Ni-4Zn/SiO_2-S to propene compared to the unsulfided catalyst possibly due to sulfur acting as an additional site blocker thereby reducing the effects of hydrogenolysis. From our study, we can confirm that the molar ratio of Ni:Zn and the addition of sulfur indeed influence the structural and catalytic properties of bimetallic catalysts.

6.2 Recommendations

This research project showed that sulfided metal catalysts display promising results for the dehydrogenation of propane. Factors such as support, sulfiding agent, sulfidation temperature and ad metal in the case of the bimetallic system play a role in the dehydrogenation performance of the catalysts.

In chapter 5, the geometric effects of Zn admetal showed improved catalytic performance of the bimetallic catalysts. The results of this work leads to the investigation of finding metals that will promote the sulfidation without causing metal segregation to further enhance the dehydrogenation activity of a bimetallic catalytic system.

Supplementary Material A

Table S1: EDS results of sulfur modified Ni(II) catalysts supported on $MgAl_2O_4$ and SiO_2

Catalyst	Ni wt%	S wt%
$NiO/MgAl_2O_4$-20wt%SO_4	14.45	12.07
$Ni/MgAl_2O_4$-20wt%SO_4	13.25	7.51
NiO/SiO_2-20wt%SO_4	14.39	8.21
Ni/SiO_2-20wt%SO_4	14.76	5.44

Figure S1.1. Electron mapping of $NiO/MgAl_2O_4$-20wt%SO_4 showing individual elements present on the catalyst

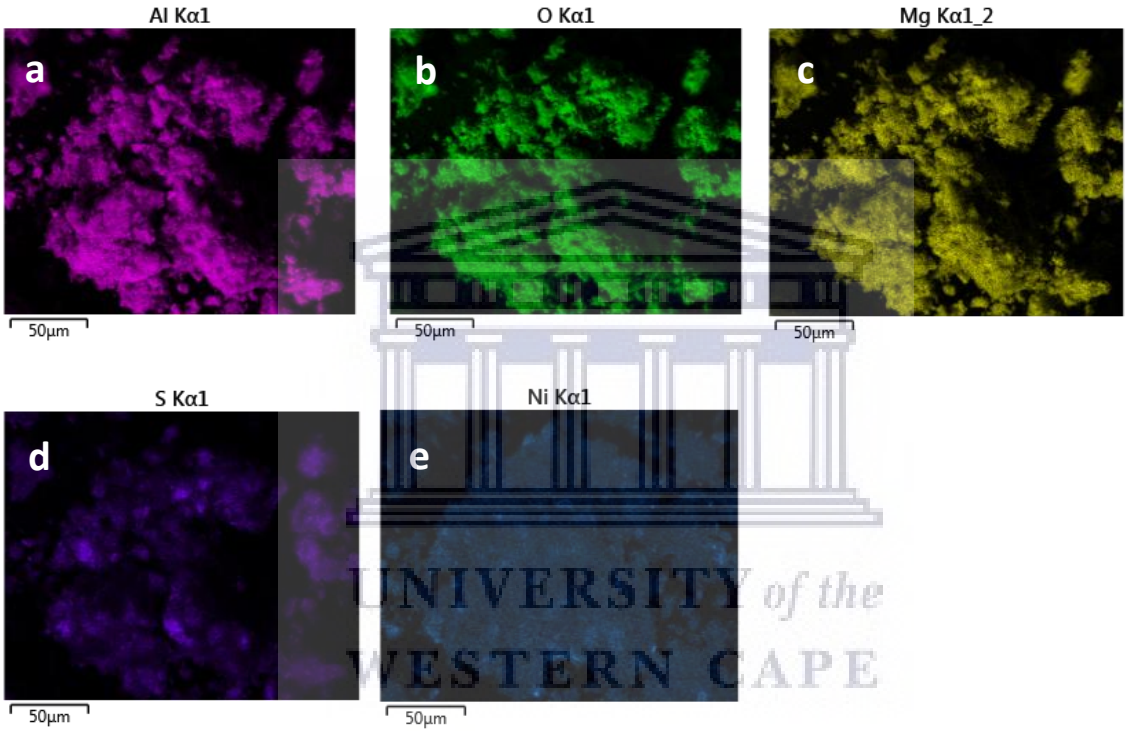

Figure S1.2. Electron mapping of NiO/SiO_2-20wt%SO_4 showing individual elements present on the catalyst

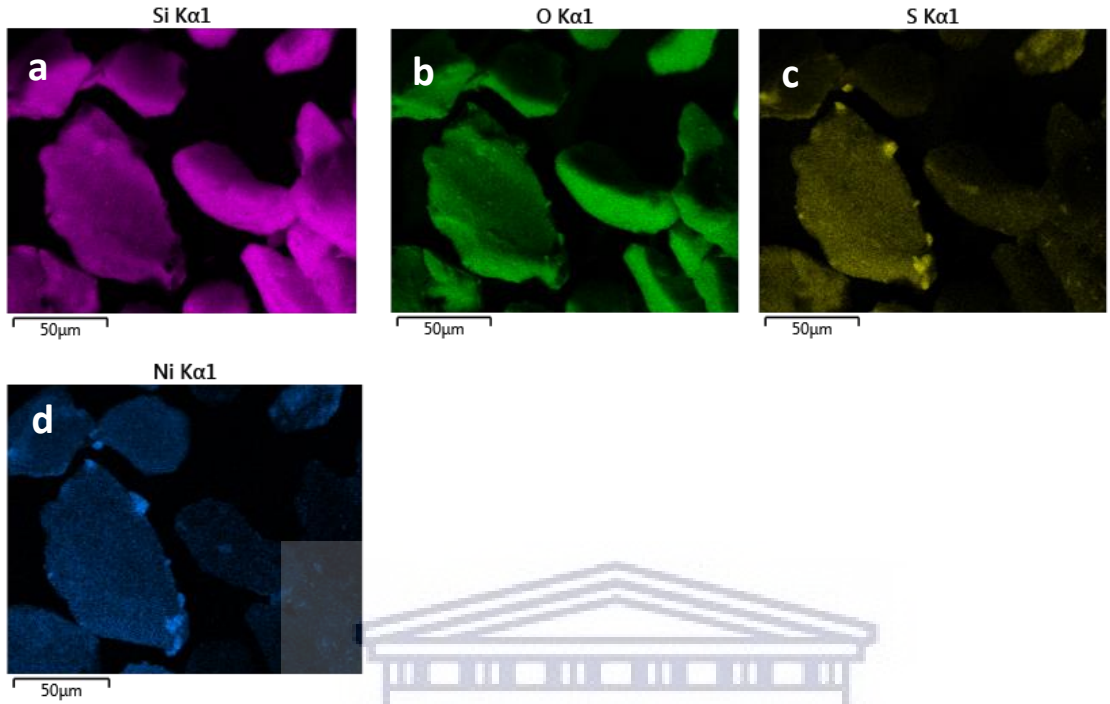

Figure S1.3. MS spectra of NiO/SiO_2-20wt%SO_4 reduced at 430 °C on TPR

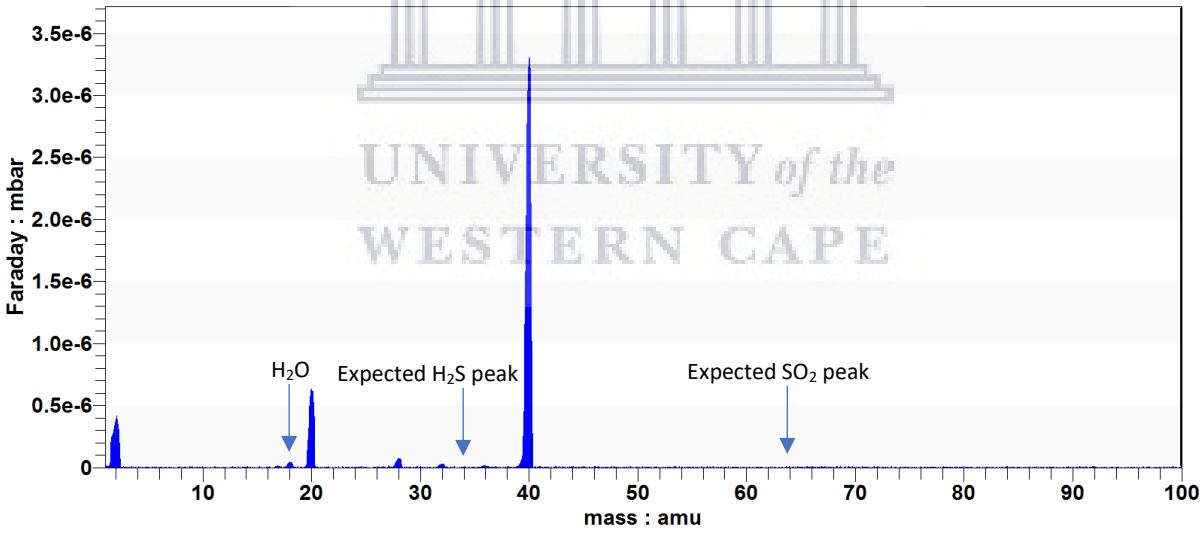

Figure S1.4. XRD pattern of NiO/SiO_2-20wt%SO_4 reduced at 435 °C

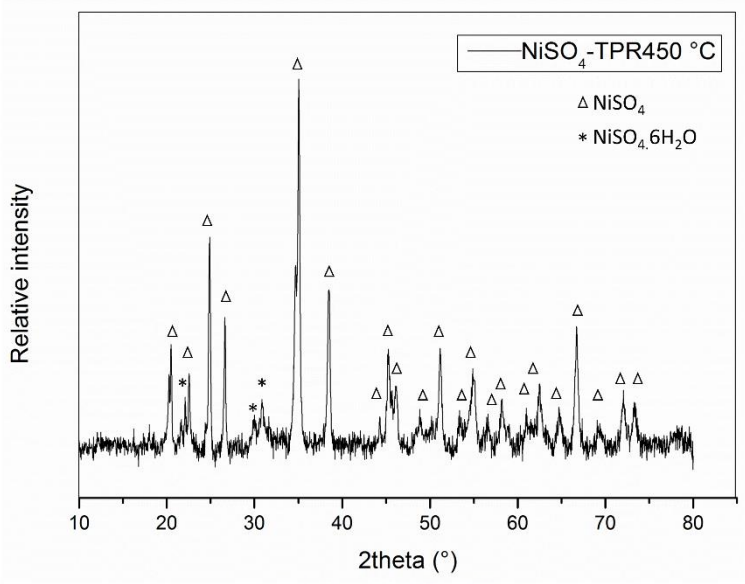

Supplementary Material B

Figure S2.1. TEM image of unmodified $Ni/MgAl_2O_4$

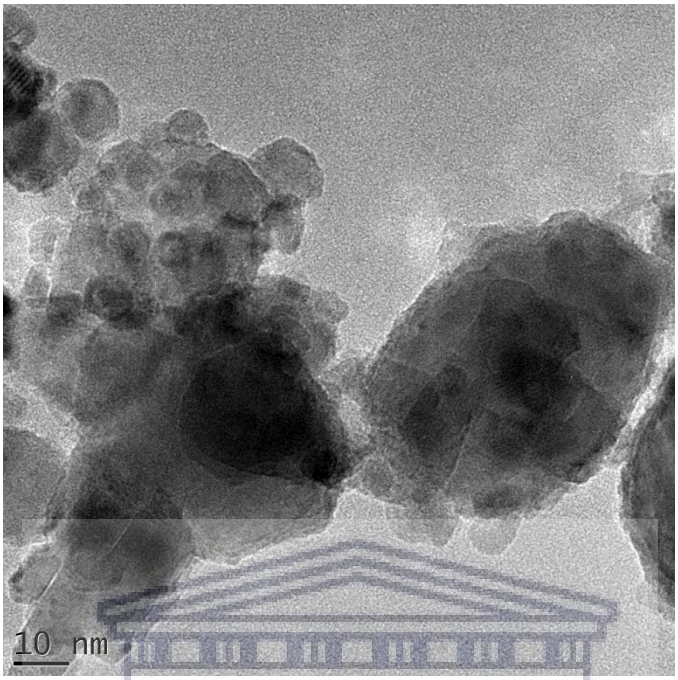

Figure S2.2. XRD analysis of spent catalysts

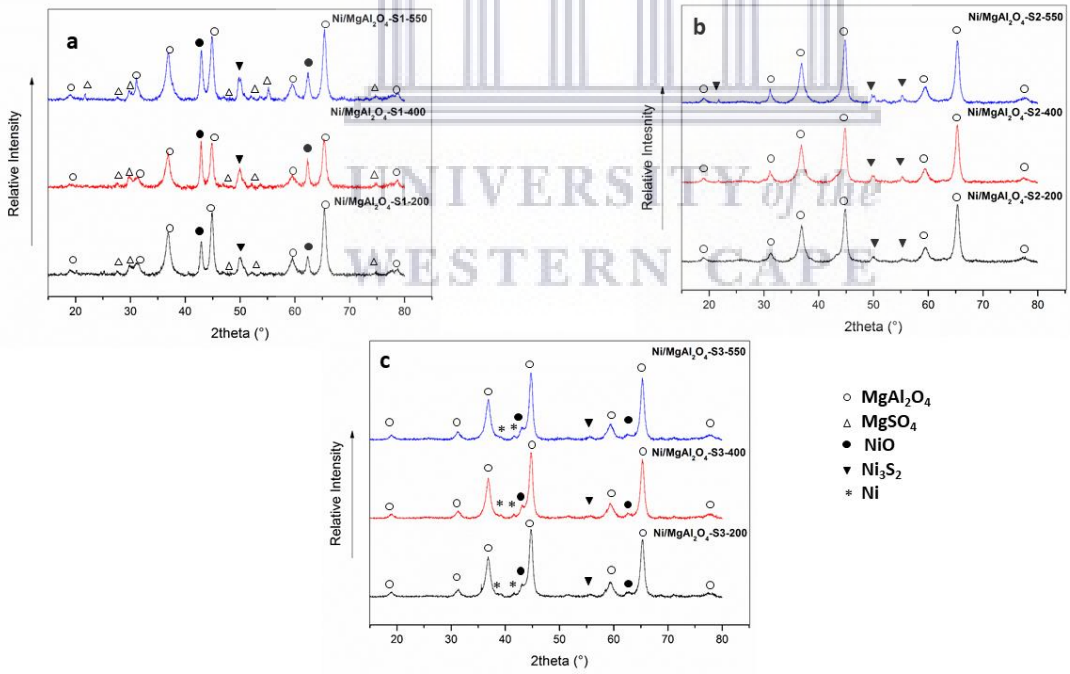

Supplementary Material C

Table S3.1. EDS data of monometallic and bimetallic catalysts

Catalyst	Wt% Ni	Wt% Zn
13Ni/ SiO_2	12	-
11Ni-2Zn/ SiO_2	9.5	2.5
9Ni-4Zn/ SiO_2	8.3	3.8
6.5Ni-6.5Zn/ SiO_2	5.2	5.4
4Ni-9Zn/ SiO_2	2.9	5.5
2Ni-11Zn/ SiO_2	1.6	10.9
13Zn/ SiO_2	-	12.5

Figure S3.1. XRD patterns of bimetallic oxide catalysts

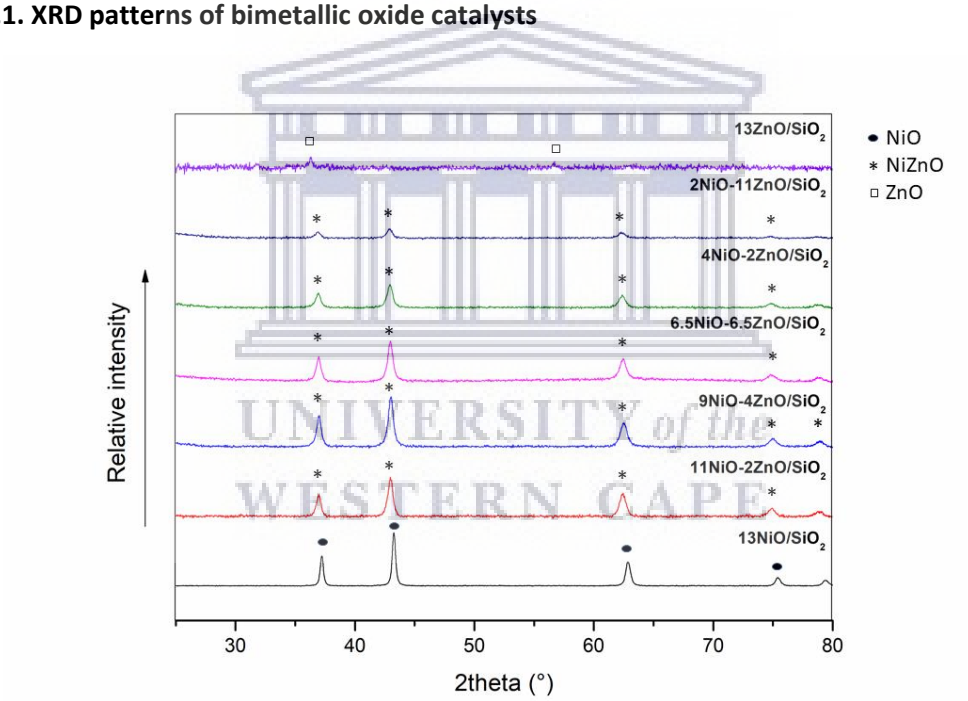

Table S3.2: EDS data of sulfur modified bimetallic catalysts

Catalyst	Wt% Ni	Wt% Zn	Wt% S
9Ni-4Zn/ SiO_2-S	15.2	6.1	4.72
6.5Ni-6.5Zn/ SiO_2-S	7.2	8.2	5.2